# Femtosecond Laser Written Lab on Chip in Glass


**Amulya Prasad**

Prof Jeroen Missinne, ir.Viktor Geudens

CMST, Technologiepark-Zwijnaarde 126, 9052 Gent


## What is the need for Point of Care?

- Growing need to provide point of care testing (poct) for prompt treatment of acute diseases
- POCT systems provide rapid diagnosis by non-trained personnel at a patient site at home, office, ambulance etc

Pros:
- Faster Diagnosis
- Low Sample Volume
- Portability

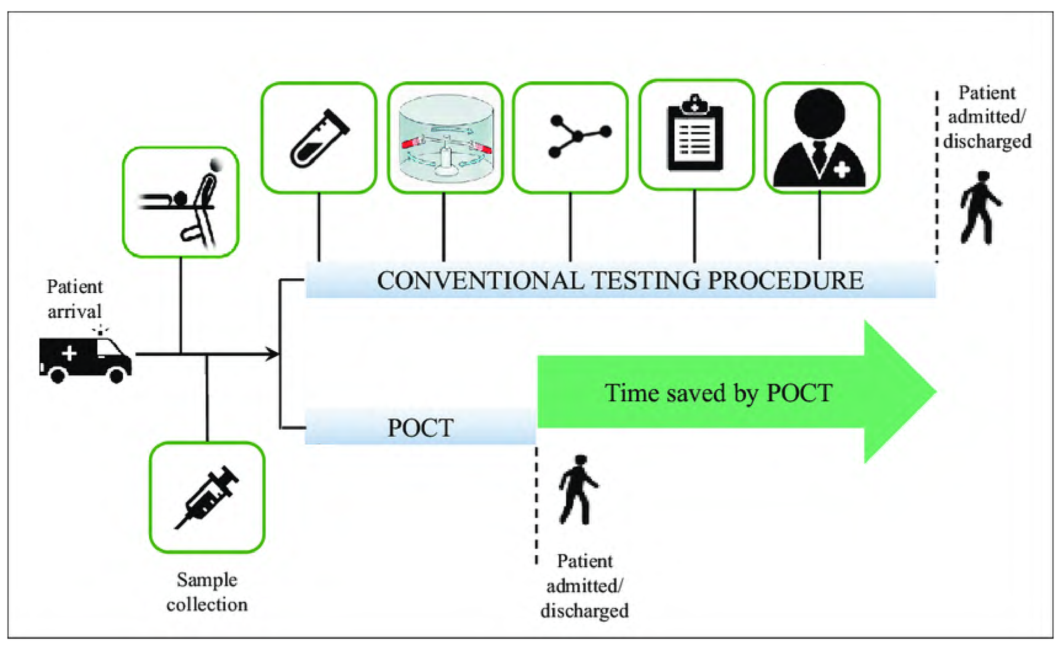


Source:[1]

**Different lab on chip materials currently in the market**

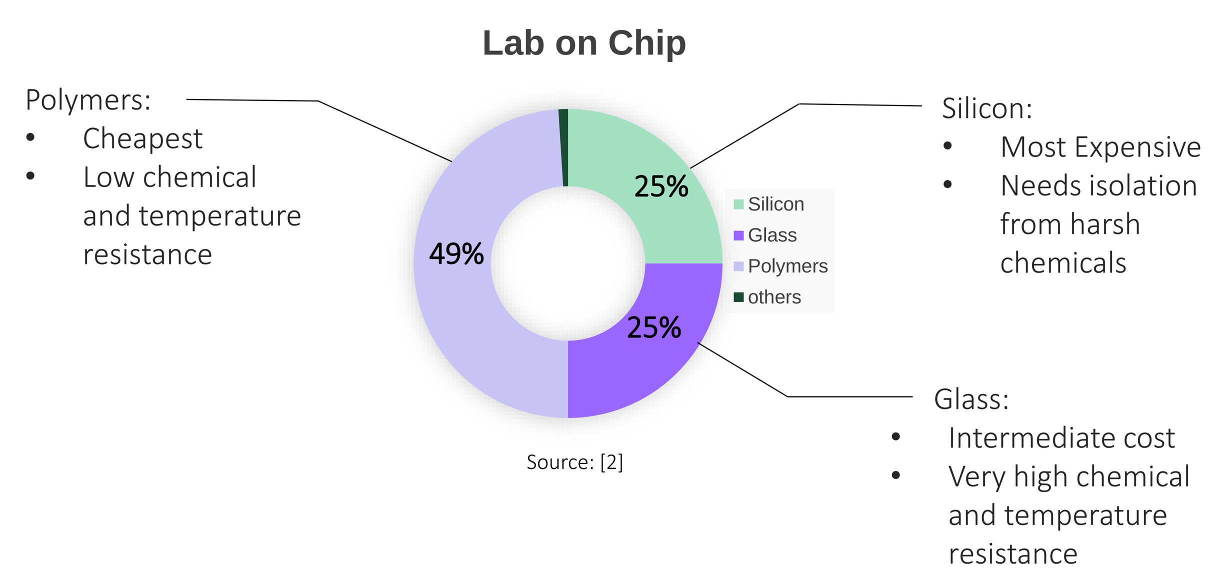


Source: [2]

In a nutshell: Aim is to fabricate a femtosecond laser written lab on chip using fused silica (glass) that can be used for POCT applications

## Design Process for the Lab On Chip

**Femtosecond Laser fabrication:**

1)

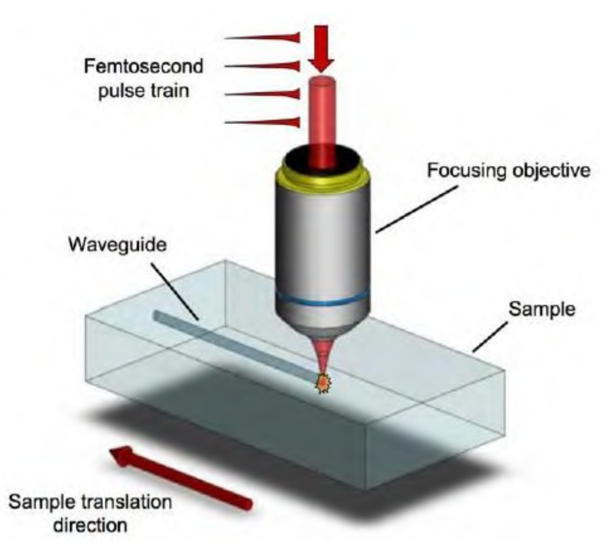


Femtosecond pulses modify the refractive index locally in the glass for that allows fabrication of waveguides

2)

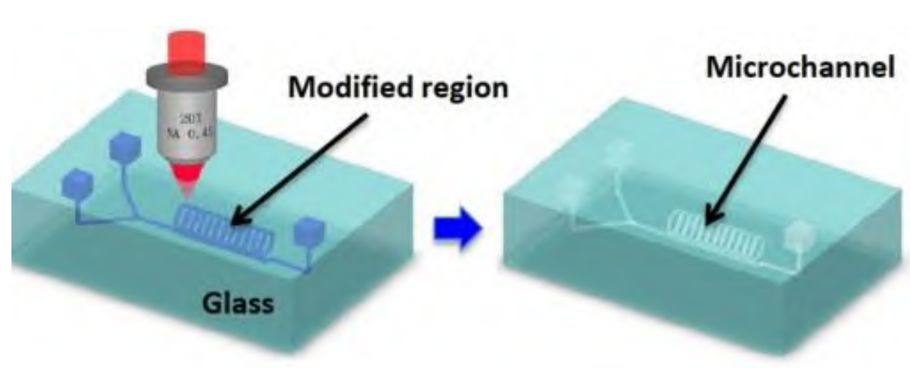


Source:[3]

Higher energy pulses form nano grating structures that helps in selective etching using HF/KOH that allows fabrication of the microchannels

**Proposed design for this thesis:**

Platform that combines waveguides and microchannels in glass that has potential for cellular level monitoring for diagnostic applications like the example given below:

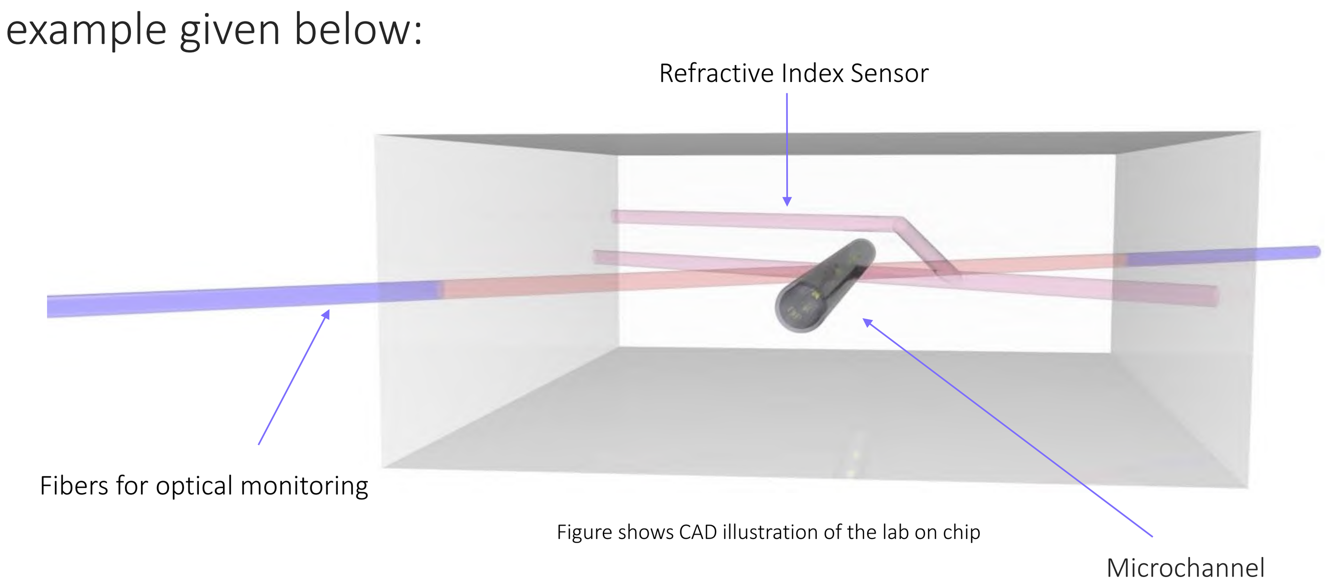


Figure shows CAD illustration of the lab on chip

## What has been done so far?

Step 1: Femtosecond Laser fabrication to write waveguides

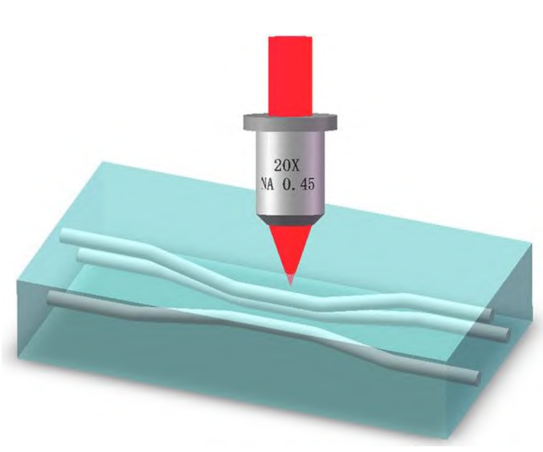

Step 2: Power measurements with laser source 850nm and 1310nm respectively

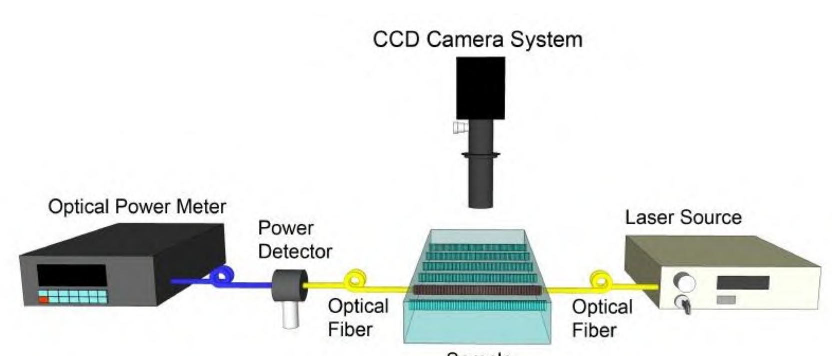


Optical Setup that measures power transmitted through waveguide

Step 3: Data Analysis

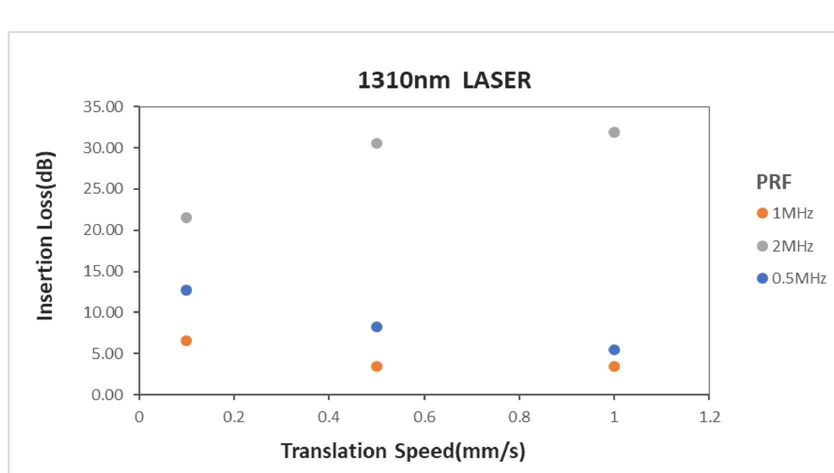


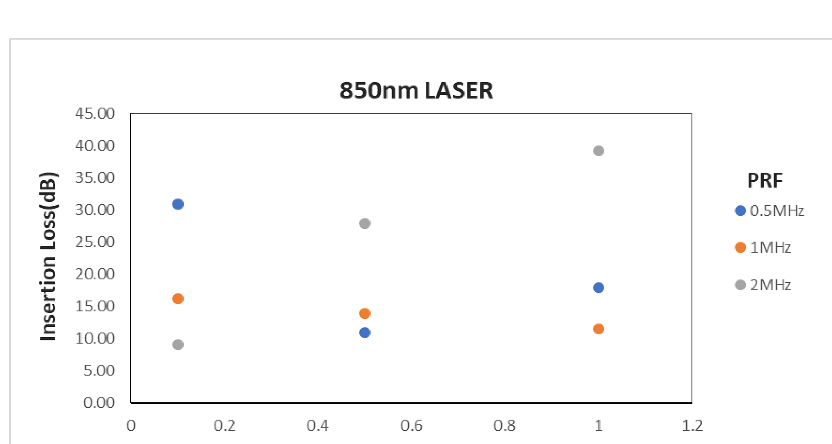


- Laser pulse energy, pulse repetition frequency (PRF) and the translation speed greatly influence the quality of the waveguide.
- Quality is greatly determined by the losses of the waveguide but for preliminary results only insertion loss has been measured. The formula is given below:

$$10 * \log(\frac{Power_{out}}{Power_{in}})$$

- **For the preliminary results the lowest loss obtained is 3dB for 25mm long waveguides which is comparable to literature review**

## Future Directions

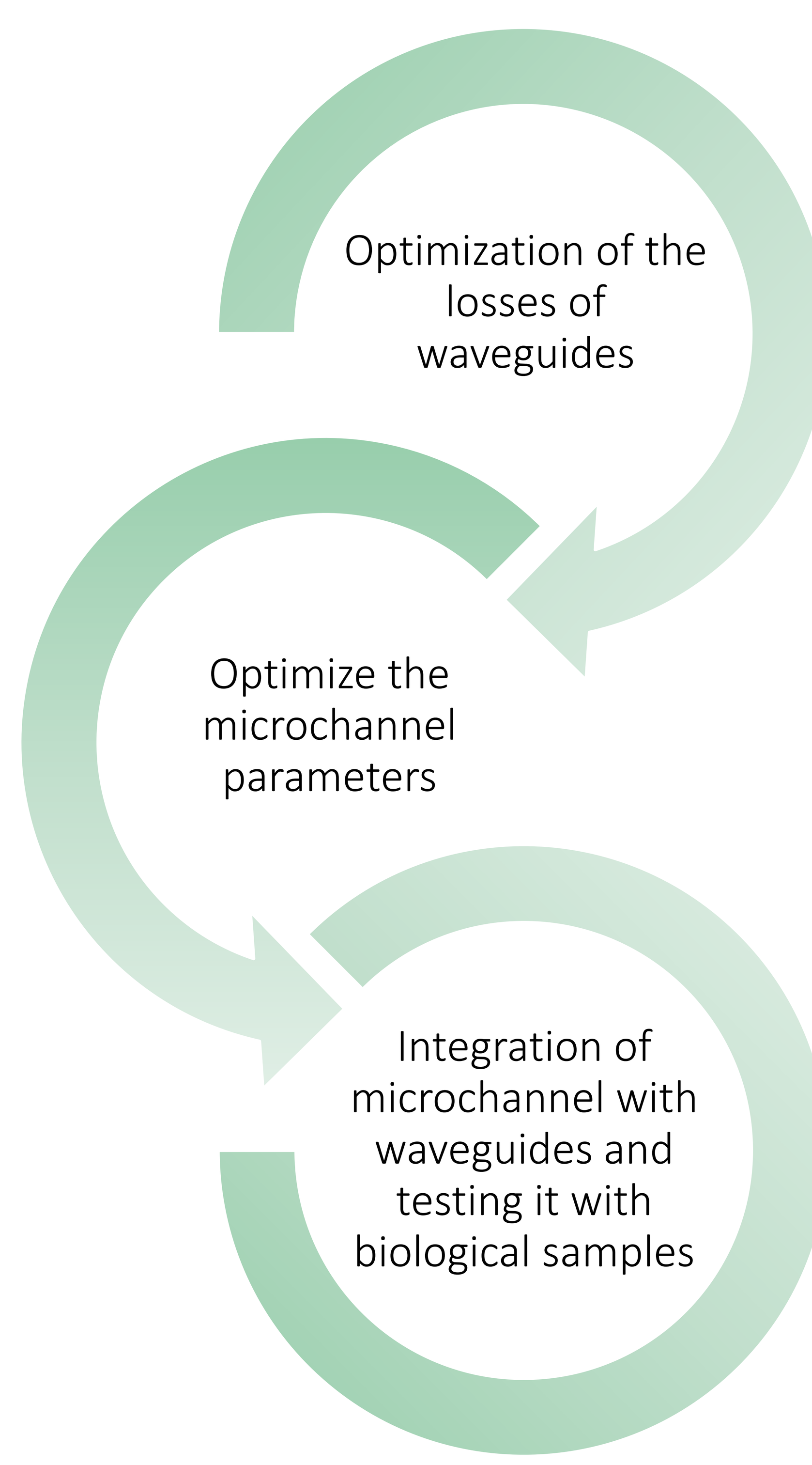


## References


[1] Srinivasan, Balaji, and Steve Tung. "Development and applications of portable biosensors." *Journal of laboratory automation* 20.4 (2015): 365-389

[2] Yole Development Micromachine Summit April 2010

[3] Sugioka, Koji. "Progress in ultrafast laser processing and future prospects." *Nanophotonics* 6.2 (2017): 393-413

[4] Ho, Stephen. Femtosecond laser microfabrication of optofluidic lab-on-a-chip with selective chemical etching



amulya.prasad@ugent.be


Master of Science in Biomedical Engineering

# Ultra-soft User Friendly Electrodes for Measurement of Human Body Bio-potential Signals

GHENT UNIVERSITY


Dipesh Sapkota

Professor Dr. Maaike Op de Beeck, Professor Dr. Jan Vanfleteren, Dr. Thomas Vervust

IMEC, CMST Lab

Ghent University, Gent, Belgium


VRIJE UNIVERSITEIT BRUSSEL

## Background

Standard Gel Electrodes

- The most common ones
- Good for short-term biopotential recording and measurements
- Drawbacks- Skin irritation and noisy behavior after long term use
- Alternative-Different forms of stiff and soft dry electrodes

## Objective of this Thesis

To design, fabricate and characterize the soft Polyurethane based electrode for bipotential measurements

## Workflow of the Thesis

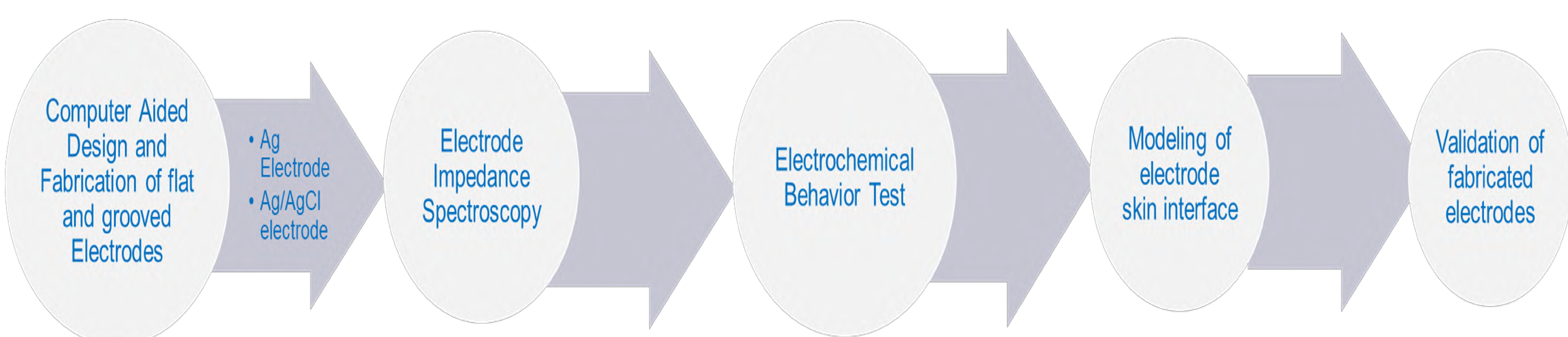


## Electrode Impedance Spectroscopy (EIS)

EIS test was done on standard gel electrodes and flat Ag electrodes

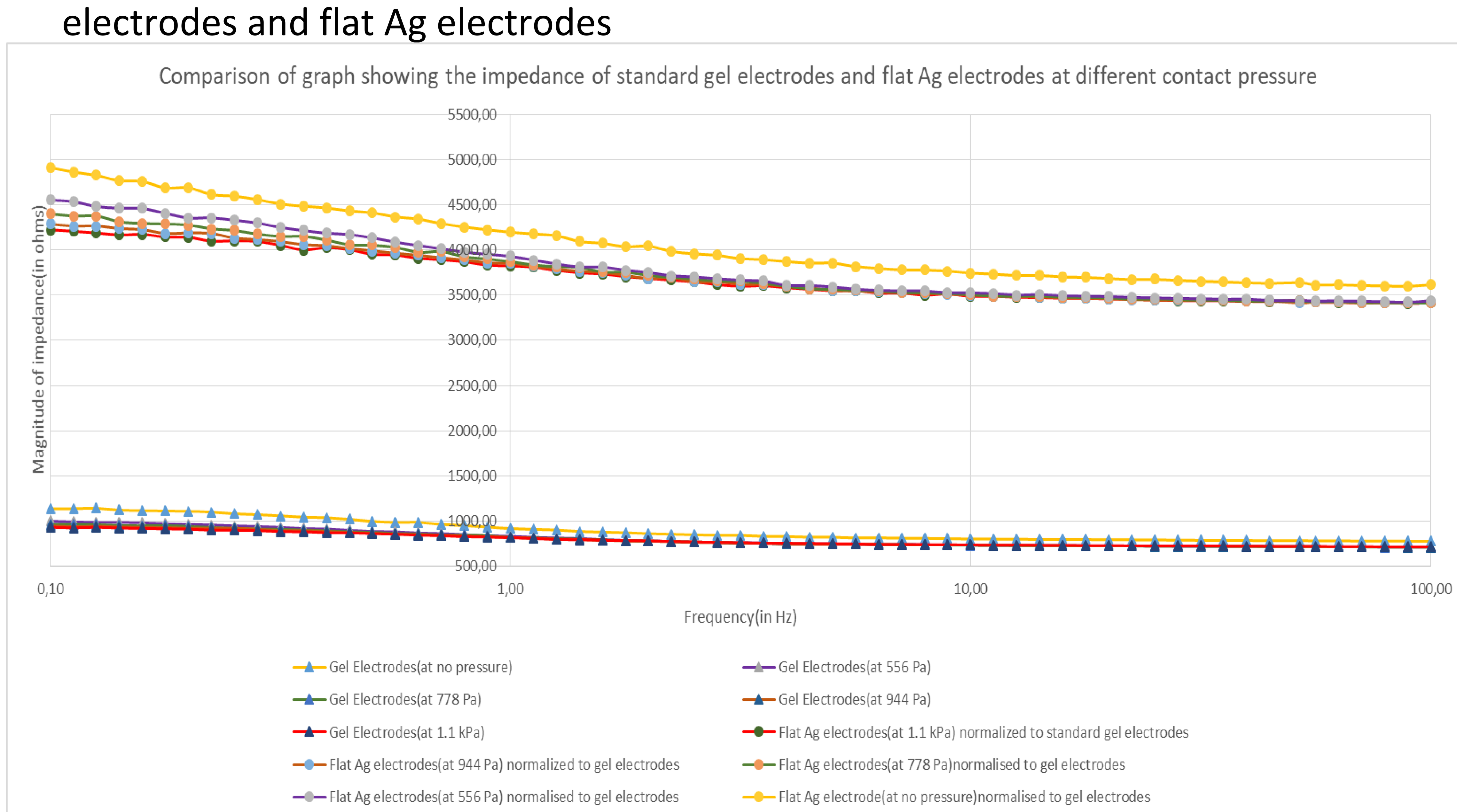


## Future Works

- Fabrication of grooved electrodes with Ag and Ag/AgCl conductive inks
- EIS tests for grooved electrodes with Ag and Ag/AgCl inks
- Electrochemical test for different electrodes
- Modeling of electrode skin interface
- Validation of electrodes by real time measurement of bio-potential signals

## Computer Aided Design of Electrodes and Stencil Printing of Electrodes

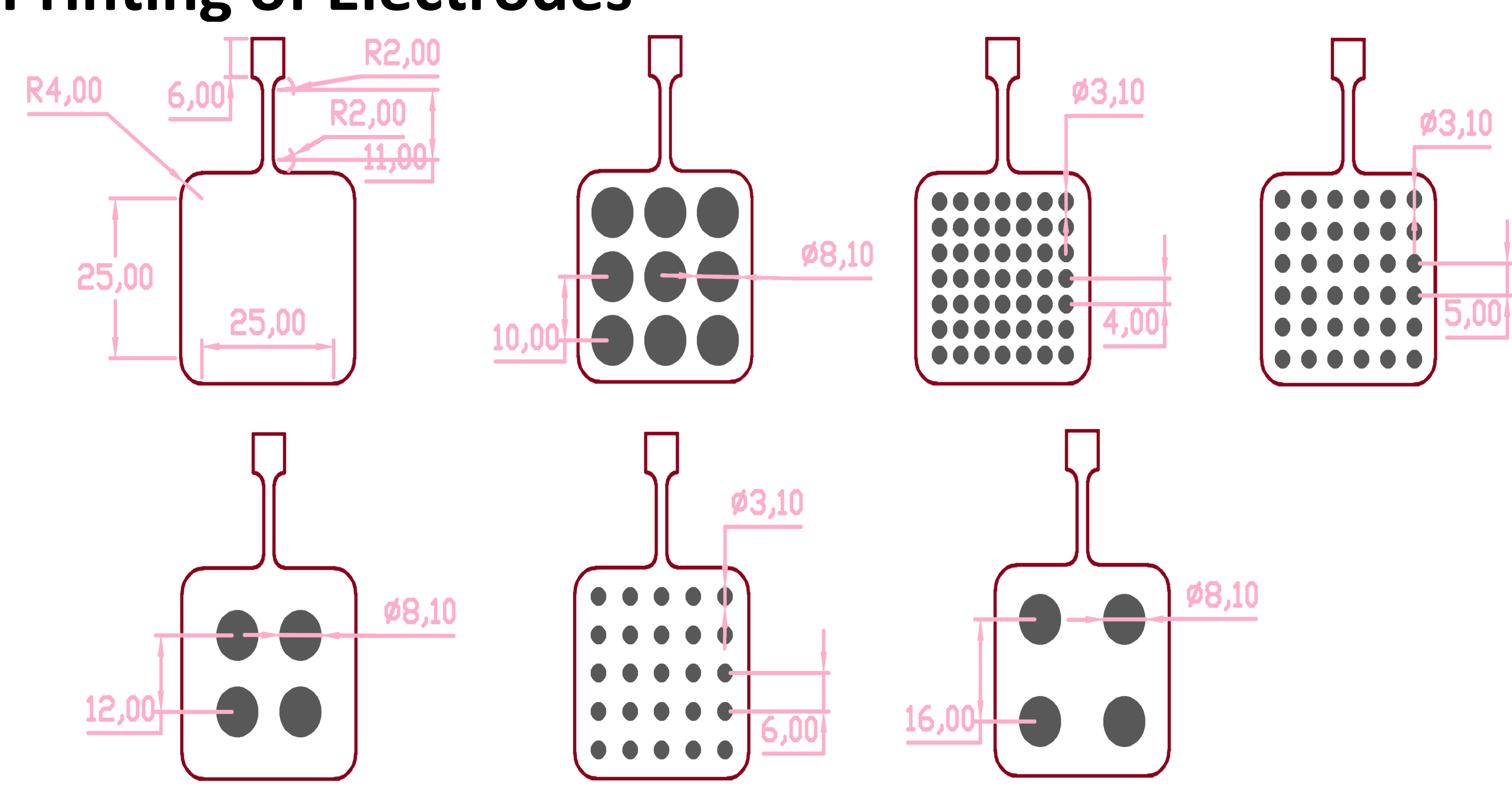


All the dimensions shown above are in mm

## References


- John G Webster. Medical instrumentation: application and design. John Wiley &Sons, 2009.
- Edward J Berbari. Principles of electro-cardiography.The Biomedical Engineering Handbook, 1:13–11, 2000.

# Chip-based Raman sensors for disease diagnosis and drug monitoring

**Francis Santos Liranzo**

Roel Baets, Haolan Zhao

imec, Ghent, Belgium

## THE AIMS

The aims of this master thesis are to **(a)** interpolate the concentration of an APP, specifically CRP, **(b)** identify the type of antibiotics and **(c)** predict the concentration of such antibiotics in plasma by using a photonic integrated chip (PIC). Raman spectroscopy, a spectroscopy technique that relies on inelastic scattering of photons, is very useful because it yields unique fingerprints of chemical compounds. Therefore, the concentrations of CRP and of antibiotics on plasma will be correlated by analysing their Raman spectra using Python and the scikit-learn library.

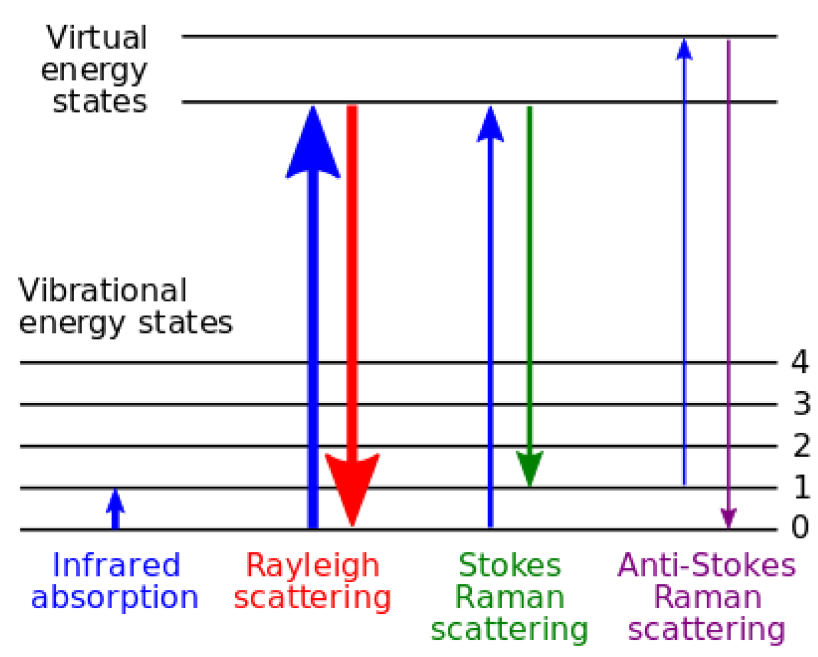


Energy-level diagram showing the states involved in Raman spectra.

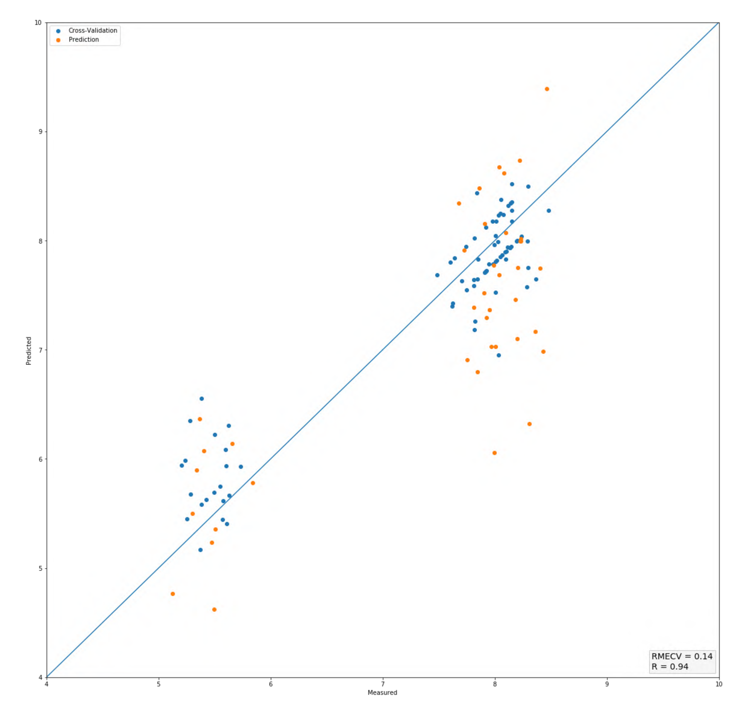


Example of output of Support Vector Regression on Python.

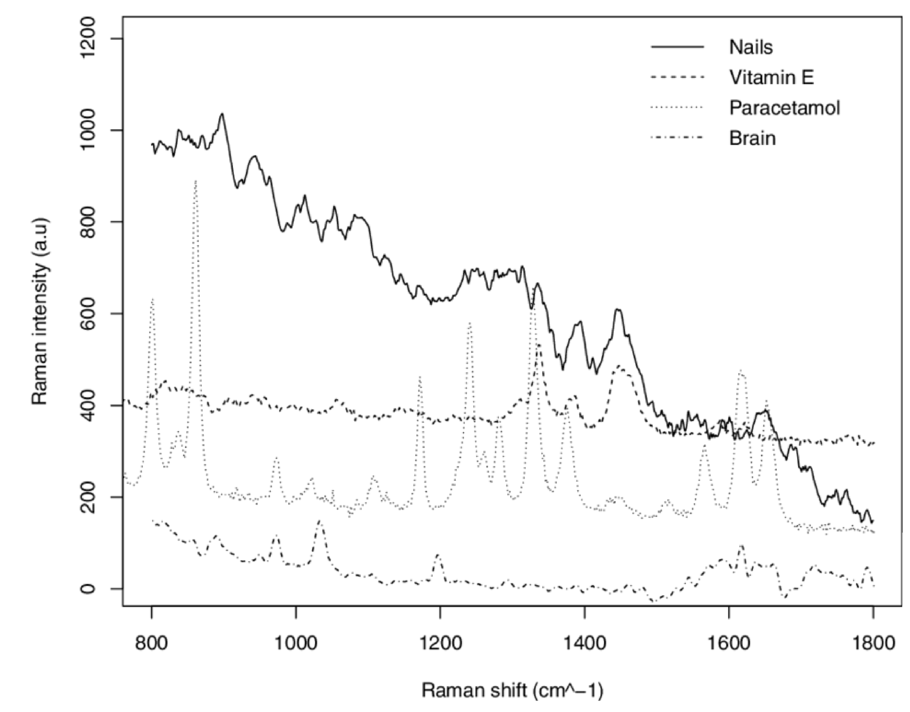


Raman spectra of different compounds (nails, vitamin E, Paracetamol and brain).

## ACUTE PHASE PROTEINS

Acute-phase proteins (APPs) are proteins that increase in concentration right after inflammation occurs, principally secreted by the liver. Four of the most important APPs are: C-Reactive Protein (CRP), serum amyloid A protein (SAA), α1-acid glycoprotein (AAG), and fibrinogen. [1]

CRP and SAA are the ones that increase the most in concentration following an inflammation episode, as much as 1000 times the normal concentration. This increase in concentration is believed to help, among other things, activate the complementary system.

Monitoring of CRP helps determine how a disease is progressing or the effectiveness of treatments (e.g. viral infections report lower CRP concentration than bacterial infections). [2]

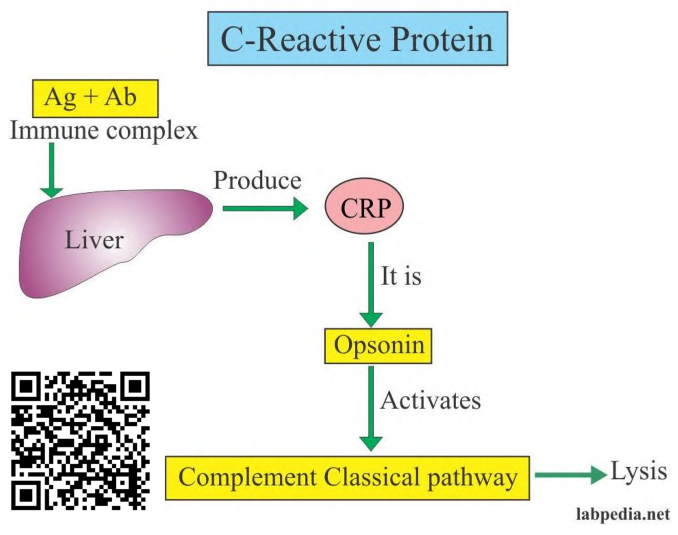


## ANTIBIOTIC RESISTANCE

Antibiotics are among the most commonly prescribed drugs for people. This and the dramatic increase of use in antibiotics for animal farming has increased the cases of antibiotic resistance. [4] [5] [6]

There's a correlation between antibiotic consumption with the development of antibiotic resistance, the higher the consumption of antibiotics, the higher the increase in bacterial resistance to antibiotics as a meta-study concluded in 2014. [3]

Therefore, it is important to monitor and provide with the strictly necessary amount of antibiotics to patients at higher risks, such as patients in the intensive care unit (ICU).

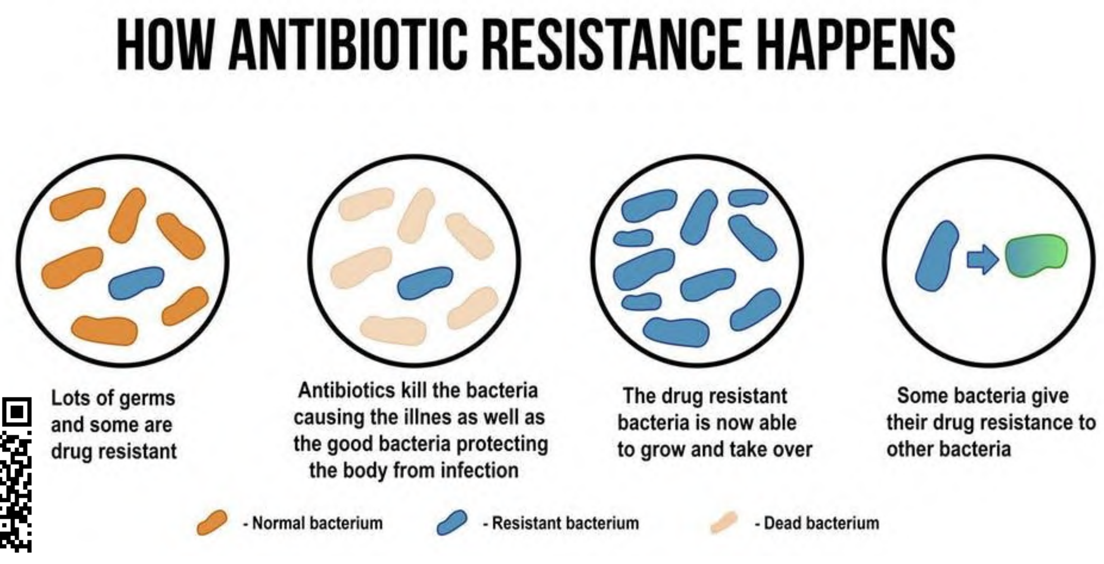


## PAST AND FUTURE STEPS + FUTURE STEPS WORKFLOW

During the first semester some experiments were conducted with the purpose of observing CRP in its raw form using spontaneous Raman spectroscopy. Unluckily the data obtained gave no useful information.

This semester will start off by measuring the Raman spectra of different antibiotics, alone and mixed with different specimens of human blood plasma in varying concentrations.

Soon after all samples' signals will be pre-processed, as machine learning algorithms, like Support Vector Regression that is the algorithm of choice, won't report good results from them in their noisy state.

Finally, the model will be trained, tested and tweaked to obtain the most accurate results.

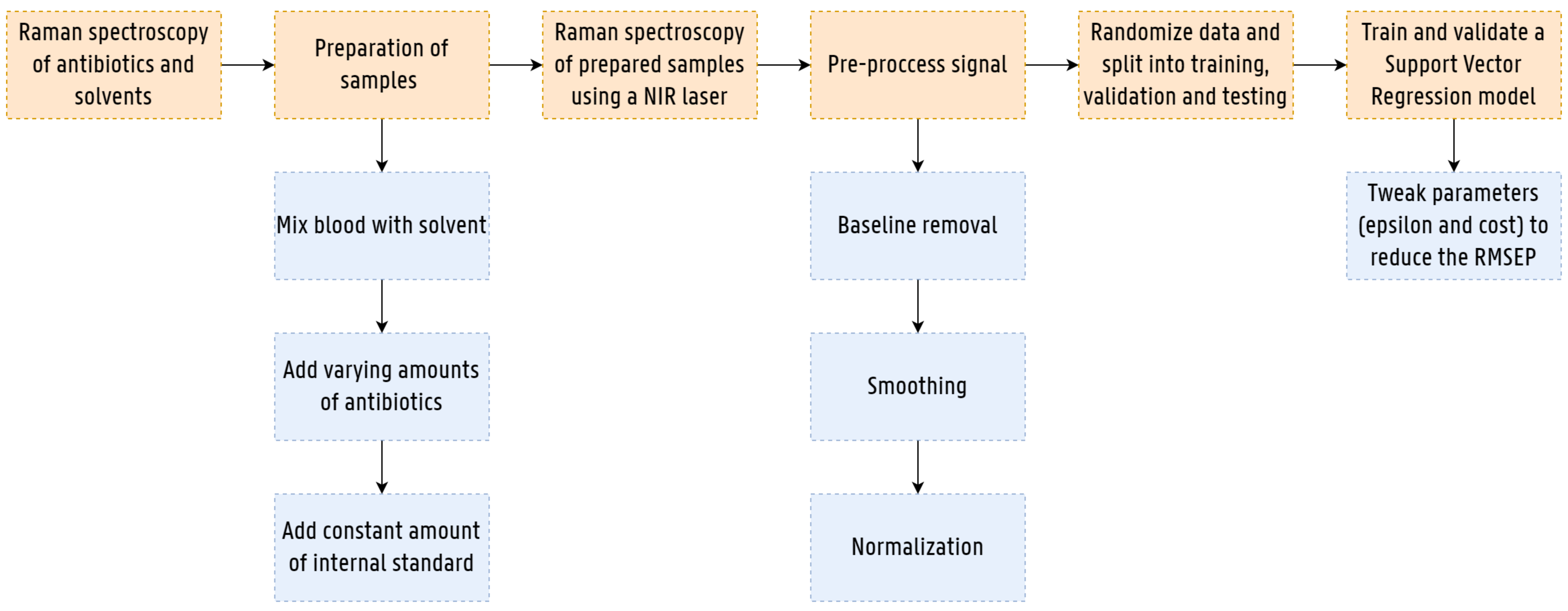


## REFERENCES

**[1]** Schultz, D. R., & Arnold, P. I. (1990, December). Properties of four acute phase proteins: C-reactive protein, serum amyloid A protein, α1-acid glycoprotein, and fibrinogen. In *Seminars in arthritis and rheumatism* (Vol. 20, No. 3, pp. 129-147). WB Saunders. **[2]** Jain, S., Gautam, V., & Naseem, S. (2011). Acute-phase proteins: As diagnostic tool. Journal of Pharmacy and Bioallied Sciences, 3(1), 118. **[3]** Bell, B. G., Schellevis, F., Stobberingh, E., Goossens, H., & Pringle, M. (2014). A systematic review and meta-analysis of the effects of antibiotic consumption on antibiotic resistance. BMC infectious diseases, 14(1), 13. **[4]** Shah, S. Q., Colquhoun, D. J., Nikuli, H. L., & Sørum, H. (2012). Prevalence of antibiotic resistance genes in the bacterial flora of integrated fish farming environments of Pakistan and Tanzania. Environmental science & technology, 46(16), 8672-8679. **[5]** Le, T. X., Munekage, Y., & Kato, S. I. (2005). Antibiotic resistance in bacteria from shrimp farming in mangrove areas. Science of the Total Environment, 349(1-3), 95-105. **[6]** Österberg, J., Wingstrand, A., Jensen, A. N., Kerouanton, A., Cibin, V., Barco, L., … & Bengtsson, B. (2016). Antibiotic resistance in Escherichia coli from pigs in organic and conventional farming in four European countries. PloS one, 11(6).

francis.santos.liranzo@vub.be

Master of Science in Biomedical Engineering

# A computational biomechanics study of the Chiari-Syringomyelia complex -Mechanics of Spinal Cord

GHENT UNIVERSITY

VRIJE UNIVERSITEIT BRUSSEL

**Asawari Pratiksha Ashok Kumbhar**

Prof. dr. ir Patrick Segers[1], dr. MD. Frank Dewaele[2]

ir. Sarah Vandenbulcke[1], MD. Tim De Pauw[2]

[1]IBiTech-bioMMeda, Ghent University, Gent, Belgium

[2]Department of neurosurgery, UZ Ghent, Ghent, Belgium

## What is Syringomyelia?

- Neurological disease as a consequence of Chiari type 1 malformation or traumatic spinal injury
- Obstruction to free-flow of CSF in the spinal subarachnoid space
- Mechanically driven by abnormal fluid flow and significant pressure dissociation
- One or more macroscopic fluid filled cavities

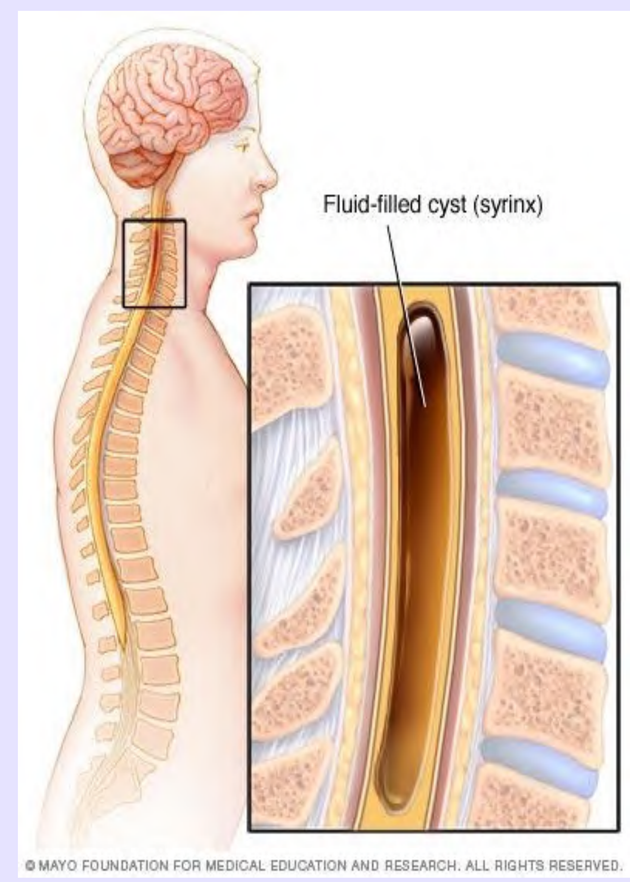


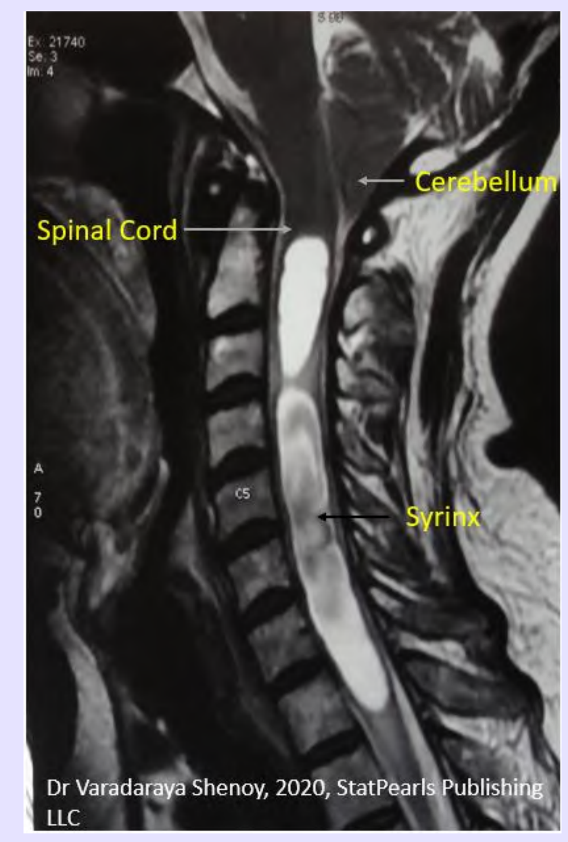


## Objective

Construction and simulation of a patient-specific 3-D model of spinal cord including properties such as poro-elasticity and anisotropy.

## Fluid-Structure interactions-models

### Linear elastic model (Bertram C.D. 2006)

- Capture the pressure wave propagation
- Do not explain the accumulation of fluid in syrinx

### Poro-elastic model (Støverud 2015)

- Hydraulic connection between syrinx and CSF
- Cavities within the cord cause axial pressure gradients
- Idealized geometry do not specifically define the actual results

**Aim of this study**: To simulate the behavior of patient specific spinal cord model with the syrinx

### Poro-elastic model with patient-specific geometry including syrinx:

To investigate whether complex geometry plays significant role in formation in syrinx.

### Characteristics of model:

- Anisotropic gray and white mater
- Poro-elastic pia membrane
- Elastic dura membrane

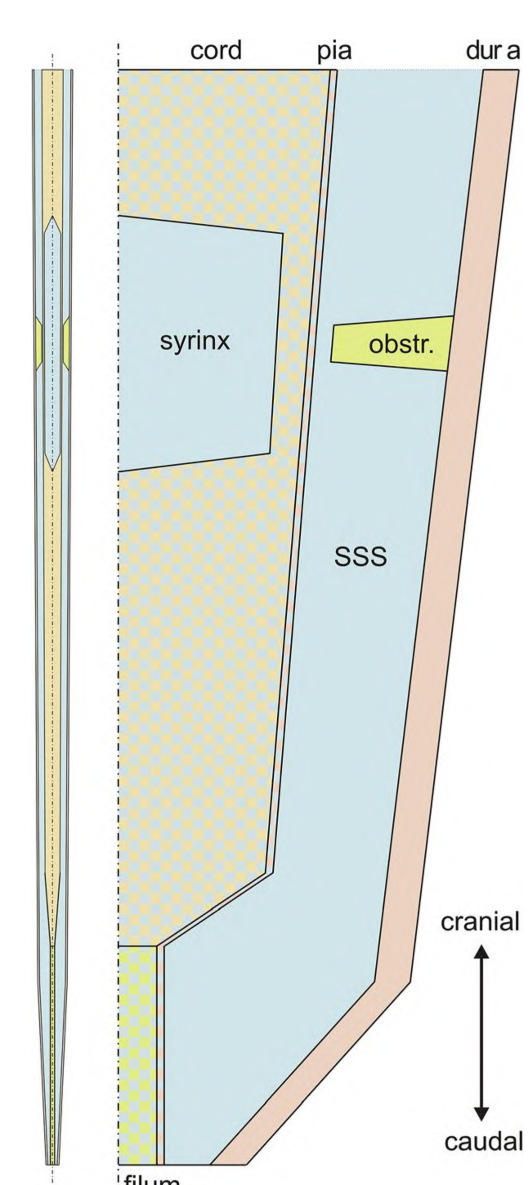


C. D. Bertram-2017, Journal of Biomechanical Engineering, Vol. 139

## Workflow

Extracting the geometry from MRI → Software: MIMICS 3-Matic

Specifying boundary conditions → High Pressure gradient and pulsatile CSF Flow

Simulation → Software: COMSOL Multiphysics

AsawariPratiksha.Kumbhar@UGent.be

Master of Science in Biomedical Engineering

# Detecting the type of dementia using EEG measurements and machine learning

UNIVERSITEIT GENT

**Bavo Derijcke**

Supervisor: Ir. Jolan Heyse

Promotors: Prof. Dr. Ir. Pieter van Mierlo

Prof. Dr. Ir. Tijl De Bie

Epilog & Ghent University, Gent, Belgium

VUB VRIJE UNIVERSITEIT BRUSSEL

## Dementia

Dementia is an overall term for a list of brain diseases that are characterized by a declined ability to think or remember. Alzheimer's disease is the most famous form of dementia. However, there are many more diseases that cause dementia.

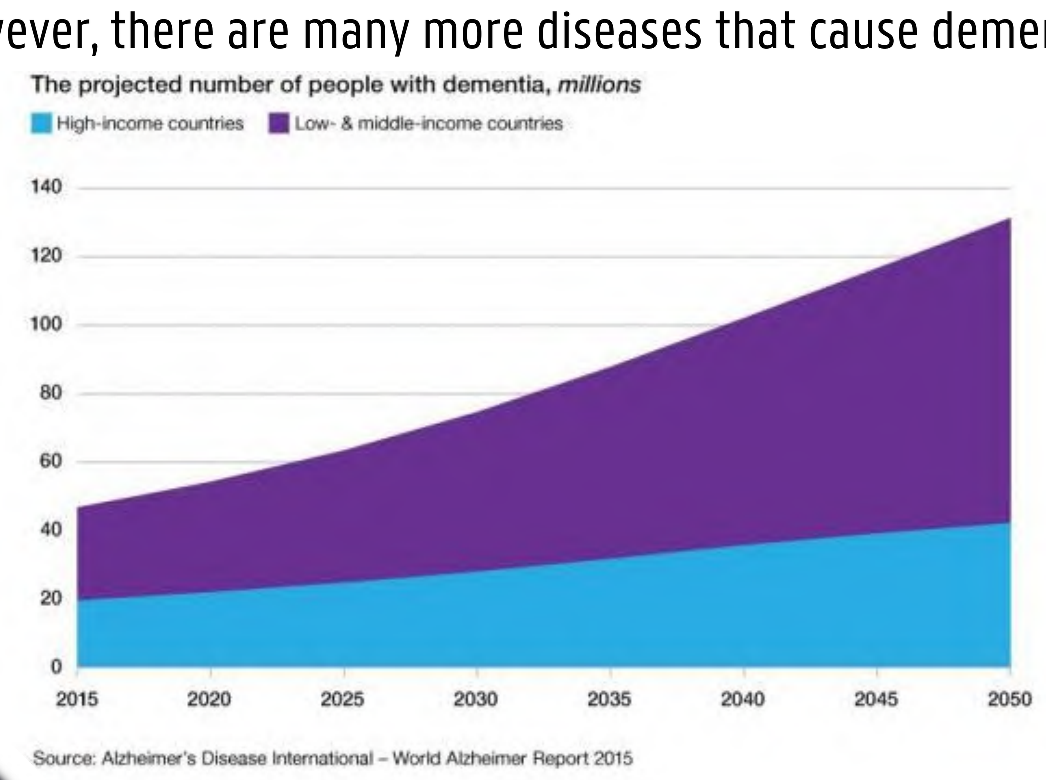



More than 10 % of all people byond the age of 80 have some form of dementia.

Due to the aging wold population, dementia cases are expected to triple in the next 30 years.

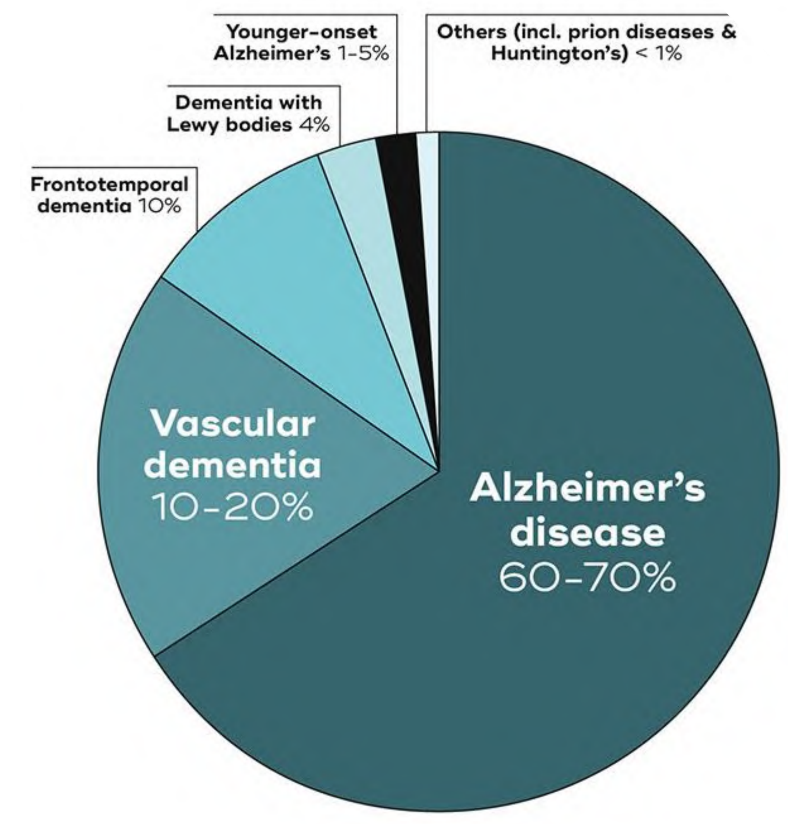


(The University Of Queensland - Queensland Brain Institute)

## EEG

Electroencephalography (EEG) is a method to monitor the electrical activity of the brain. Electrodes are placed along the scalp that measure voltage fluctuations resulting from the firing of hundreds of thousands up to millions of neurons in the brain.

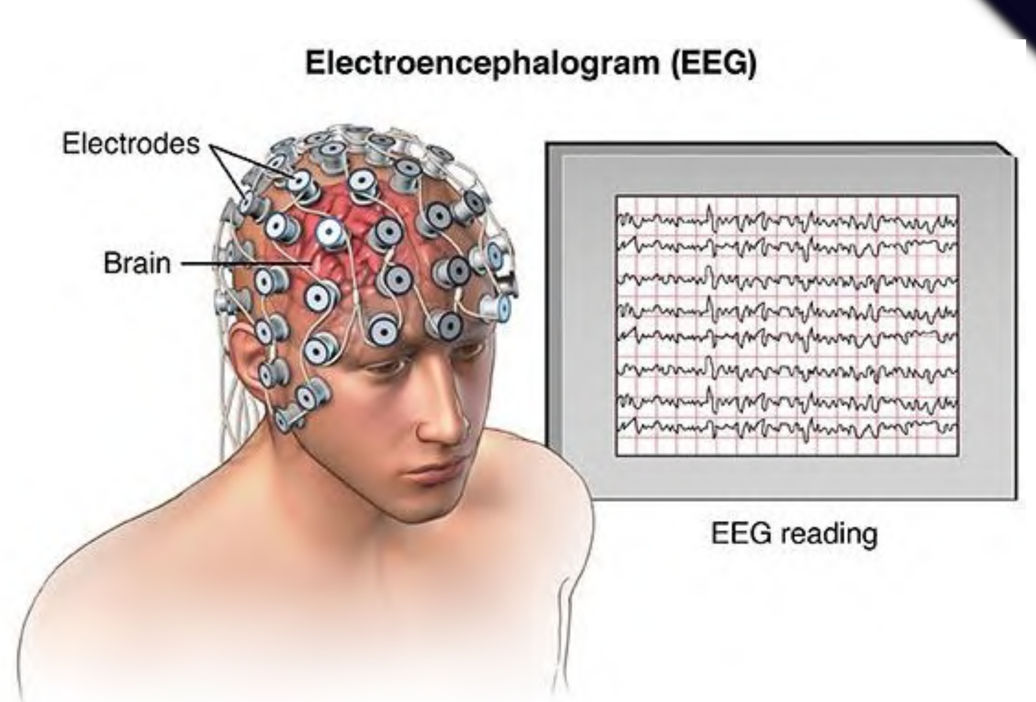


(Electro-Encefalografie – O.L.V. van Lourdes Ziekenhuis Waregem)

## Problem statement

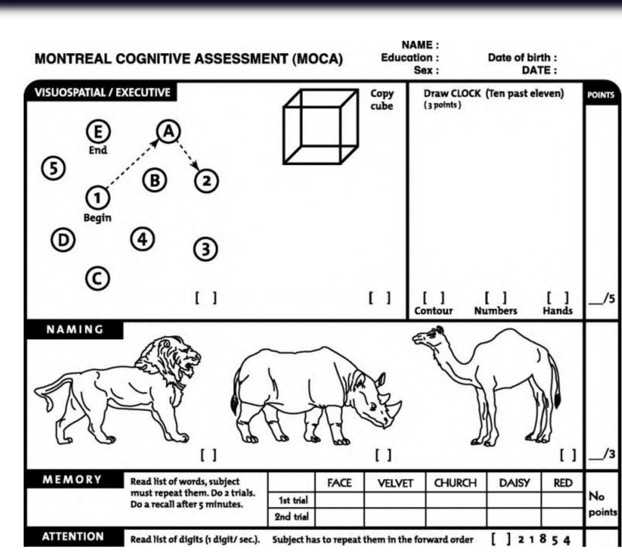


Montreal Cognitive Assessment – R. Mahendran

Current ways to diagnose the type of dementia include

- Medical history
- Cognitive tests
- Imaging
  - CT, MRI → brain structures
  - SPECT, PET → functional neuroimaging

These diagnostic tests lack the ability to differentiate between the different types of dementia. The **goal** of the thesis is to **diagnose the type of dementia through EEG measurements.**

## Method

### Preprocessing

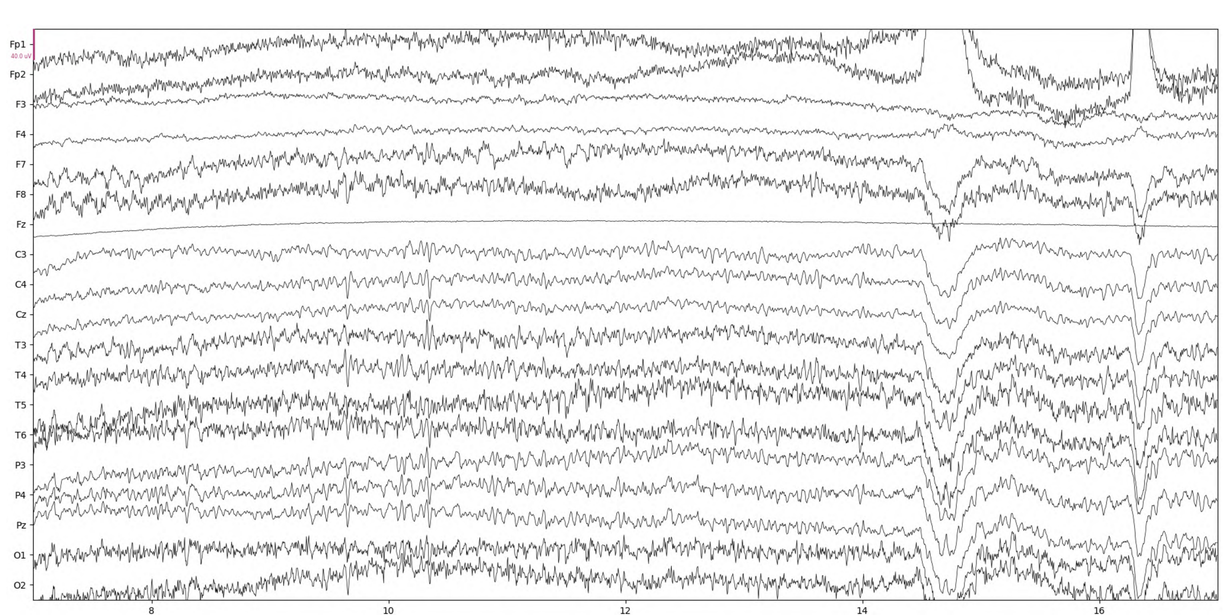

→

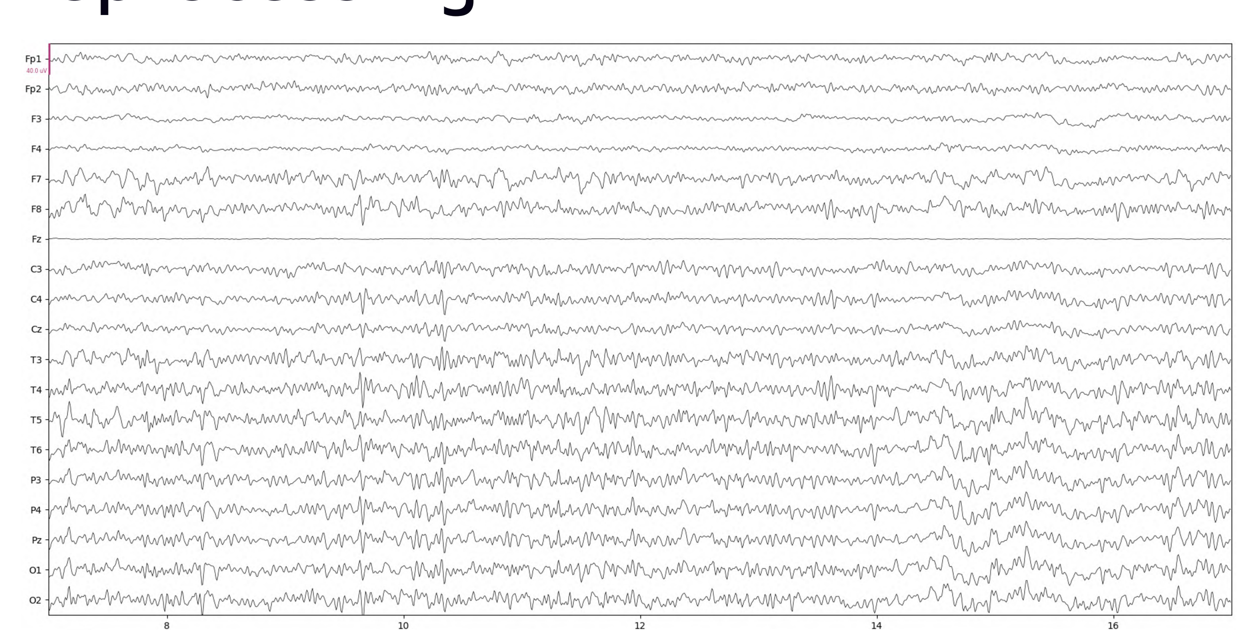

EEG signals are filtered with high and low pass filters (cut-off frequencies 1Hz and 30Hz resp.), EOG artifacts are removed using ICA. The cleaned signals are then divided into epochs and bad epochs are rejected.

### Feature extraction

#### Spectral analysis

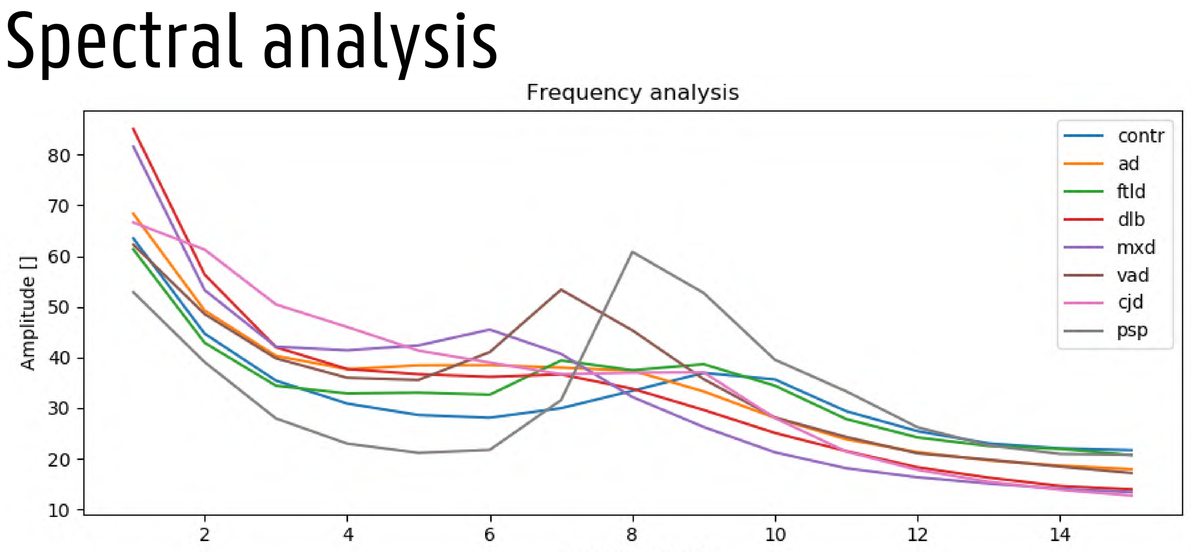


Spectral analysis used to describe the properties of the EEG signals for the different dementia types in the frequency domain.

#### Functional connectivity analysis

Functional connectivity analysis assesses the information transfer between regions in the brain. Here we used conherence, mutual information and PDI [1].

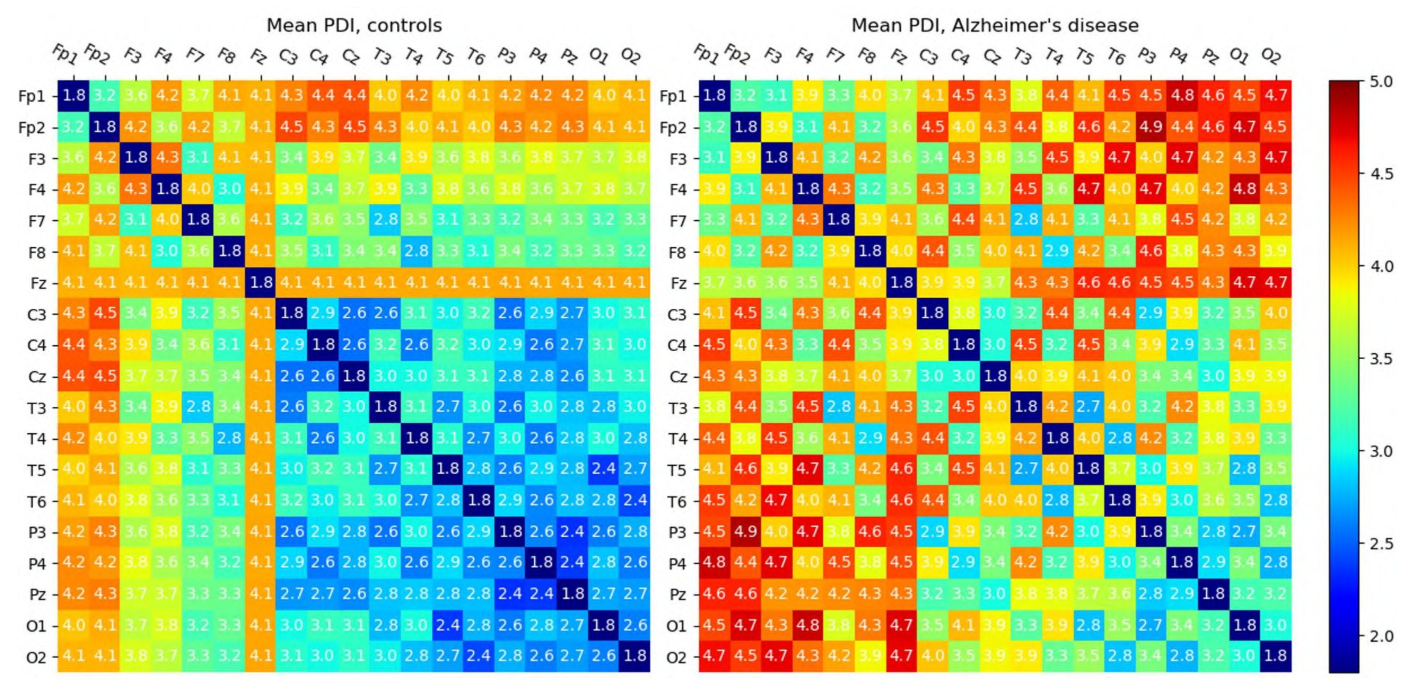


### Machine learning

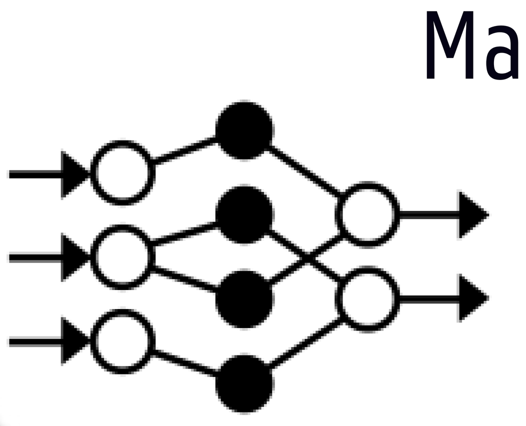

Features are given to a machine learning algorithm that tries to find recurring patterns among the features, which will be used for future classifications.

## Preliminary results

For now, only a handful of features were used to train an artificial neural network (multilayer perceptron). This results in an ability to differenciate healthy people from Alzheimers disease patients with 87% precision, 88% recall and 87% f1-score. (12/2019).

References:

[1] Mammone, N. a. (2017). Permutation Disalignment Index as an Indirect, EEG-Based, Measure of Brain Connectivity in MCI and AD Patients. *International Journal of Neural Systems*, 1750020.

[2] S. Yang, J. M.-L. (2019). M/EEG-Based Bio-Markers to Predict the MCI and Alzheimer's Disease: A Review From the ML Perspective. *IEEE Transactions on Biomedical Engineering*, 2924-2935

bavo.derijcke@ugent.be

Master of Science in Biomedical Engineering

# Monte Carlo simulations on dosimetry and image quality for pediatric imaging in Total Body PET

**Jeff Rutten**

Prof. Dr. Ir. Stefaan Vandenberghe & Prof. Dr. Ir. Klaus Bacher

Ir. Charlotte Thyssen

MEDISIP, Ghent University, Ghent, Belgium

GHENT UNIVERSITY

VUB VRIJE UNIVERSITEIT BRUSSEL

## IMPORTANCE OF LOW PEDIATRIC RADIATION DOSE

- Pediatric patients are more sensitive for radiation dose than adults.
- The dose can be lowered with a new design of a PET scanner, namely the total-body PET system.
- However, the dose-image quality relationship is still unknown for a total-body PET system.

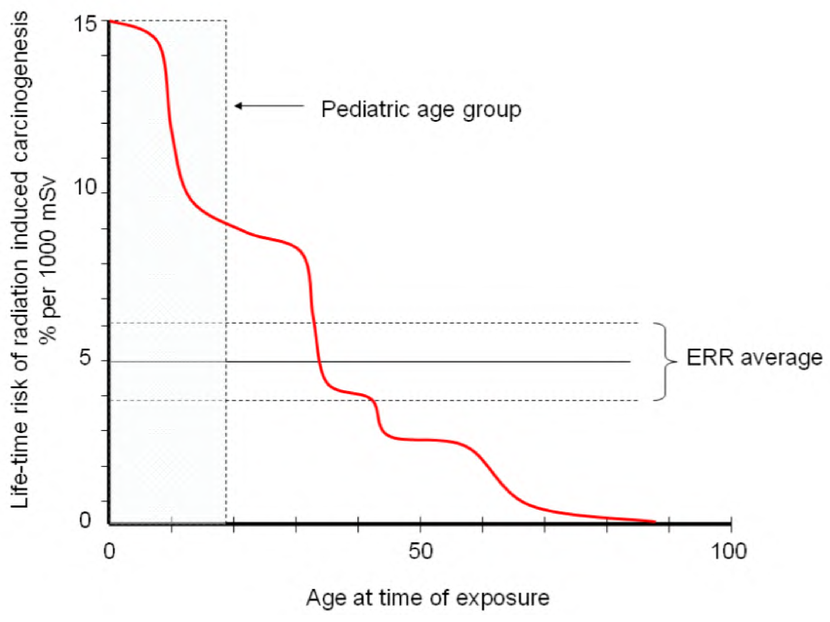


Life-time risk of a radiation induced cancer as a function of age [1]

## GOAL OF THE THESIS

To determine the dose-image quality relationship for a total-body PET system compared to a current PET system using pediatric phantoms.

## TOTAL-BODY PET

- Current clinical PET systems detect 1% of all the decays that occur inside the patient.
- Increase the axial length of the system → detect additional annihilation photons.

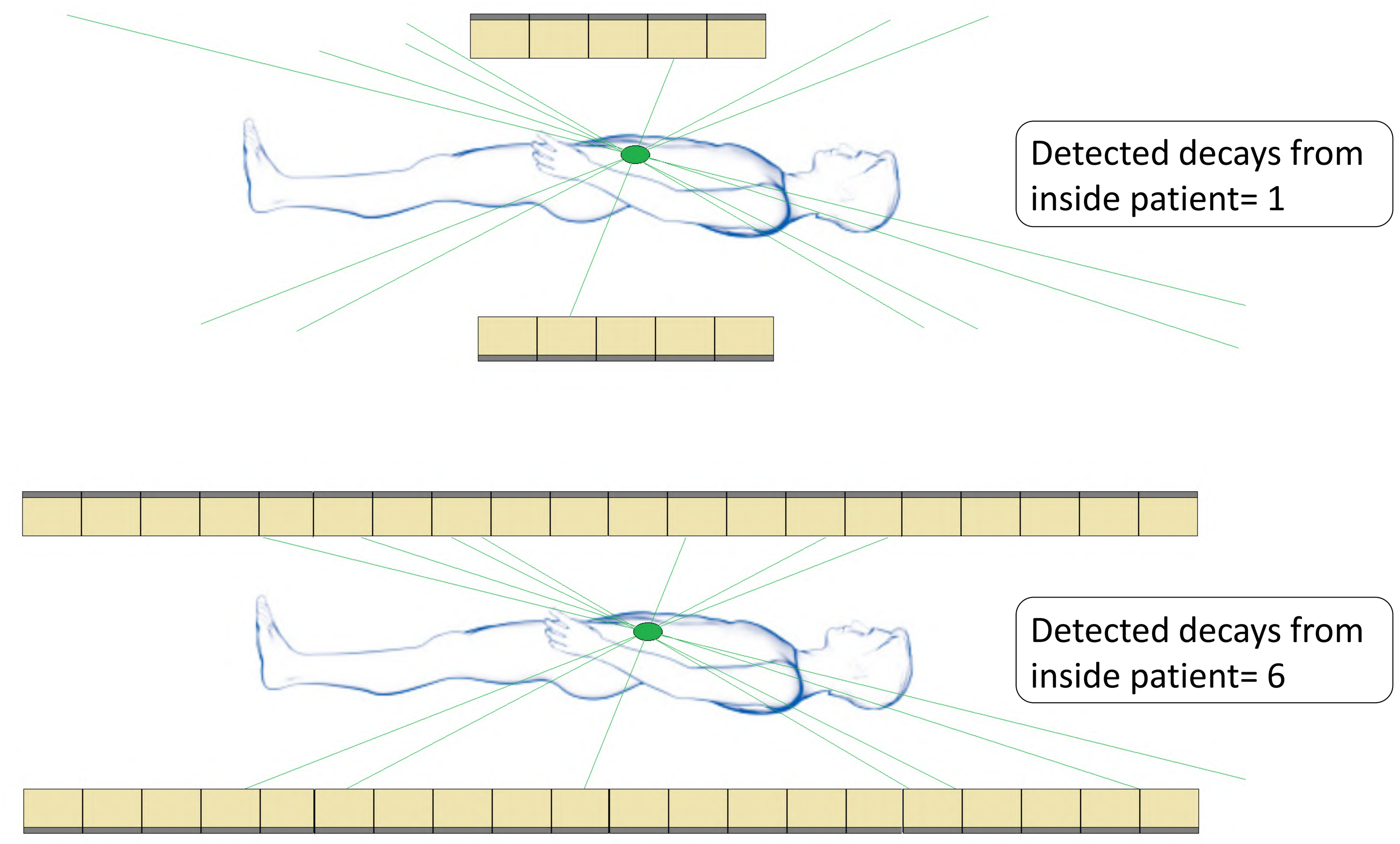


Each green line is a detectable photon pair originating from within the patient. Due to the increased length, the total body-PET detects more photon pairs

## MATERIALS & METHODS

### GATE MONTE CARLO SIMULATIONS

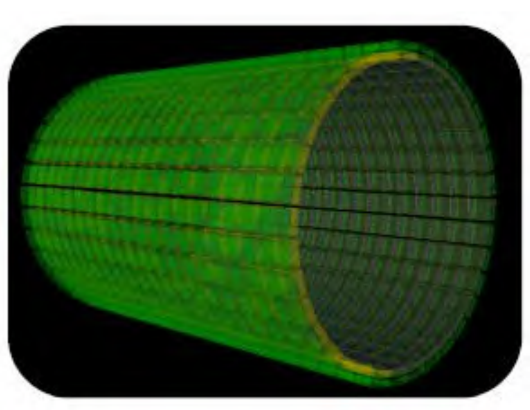

**Total-body PET**
- Axial length = 104 cm
- 20 detector rings [2]

**GE discovery MI PET**
- Axial length = 20 cm
- 5 detector rings [2]

### MATHEMATICAL PHANTOMS BASED ON REFERENCE DATA

**Pediatric phantom: 1 year old boy**

- ➢ Height and organ weight based on literature [3]
- ➢ 6 organs are included
- ➢ Organ FDG activity based on adult pharmacokinetics

| Organ | Organ mass (g) |
|---|---|
| Heart | 97.4 |
| Stomach | 85.8 |
| Bladder | 19.8 |
| Brain | 945.2 |
| Liver | 327.1 |
| Lungs | 149.3 |

### DATA PROCESSING

- Radiation dose assessment with the use of actors (built-in tool)
- Post-processing with Python and C code to evaluate image quality

## DOSE ACTOR VERIFICATION

- Homogenous FDG distribution in a sphere
- Python script extracts radiation dose per slice
- Simulated radiation dose in sphere = 0.634 Gy
- Theoretical calculated dose in sphere = 0.636 Gy

ASSUMPTIONS FOR THE THEORETICAL CALCULATION
- ✓ Average positron energy of 0.25 MeV
- ✓ Positron range << 1 cm, so all the energy is deposited in the tumor
- ✓ Time frame of 2.5 hours

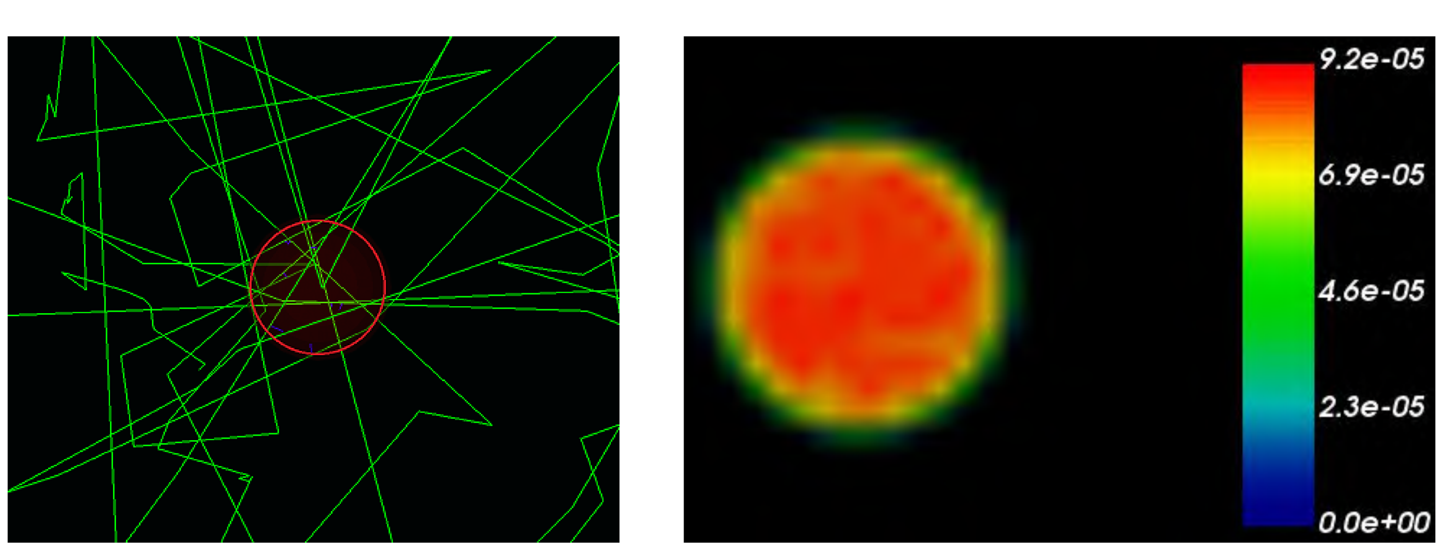


Spherical tumor, each green line is a photon (left) and the dose distribution of the tumor obtained by dose actor (right)

## FUTURE WORKPLAN

- Dose distribution of mathematical phantoms of 5, 10 and 15 year old children
- Evaluation of image quality based on signal to noise
- Determine the correlation between dose and image-quality for a total-body PET
- Additionally, the effect of pediatric obesity on the resulting image can be explored

## REFERENCES

[1]"How to Understand and Communicate Radiation Risk", *Imagewisely.org*, 2017. [Online]. Available: https://www.imagewisely.org/-/media/Image-Wisely/ Files /CT/IW-Peck-Samei-Radiation-Risk.pdf?la=en.

[2]C. Thyssen, "Monte Carlo simulations of total-body PET systems", Master, Ugent, 2018.

[3]T. Xie and H. Zaidi, "Evaluation of radiation dose to anthropomorphic paediatric models from positron-emitting labelled tracers", *Physics in Medicine and Biology*, vol. 59, no. 5, pp. 1165-1187, 2014. Available: 10.1088/0031-9155/59/5/1165.

jeff.rutten@ugent.be

Master of Science in Biomedical Engineering

# Detecting the cause of dementia using EEG measurements and machine learning

**Emma Depuydt**

prof. dr. ir. Tom Dhaene, prof. dr. ir. Pieter van Mierlo,
ir. Tom Van Steenkiste and prof. dr. ir. Dirk Deschrijver

**Epilog** and **IDLab**, Ghent University – imec, Ghent, Belgium

GHENT UNIVERSITY

VUB VRIJE UNIVERSITEIT BRUSSEL

## 1 Dementia

- **Dementia** is a chronic neurocognitive syndrome that affects:
  - Memory
  - Language
  - Thinking and comprehension
  - Planning
- It can be caused by a **variety of diseases** and injuries that affect the brain

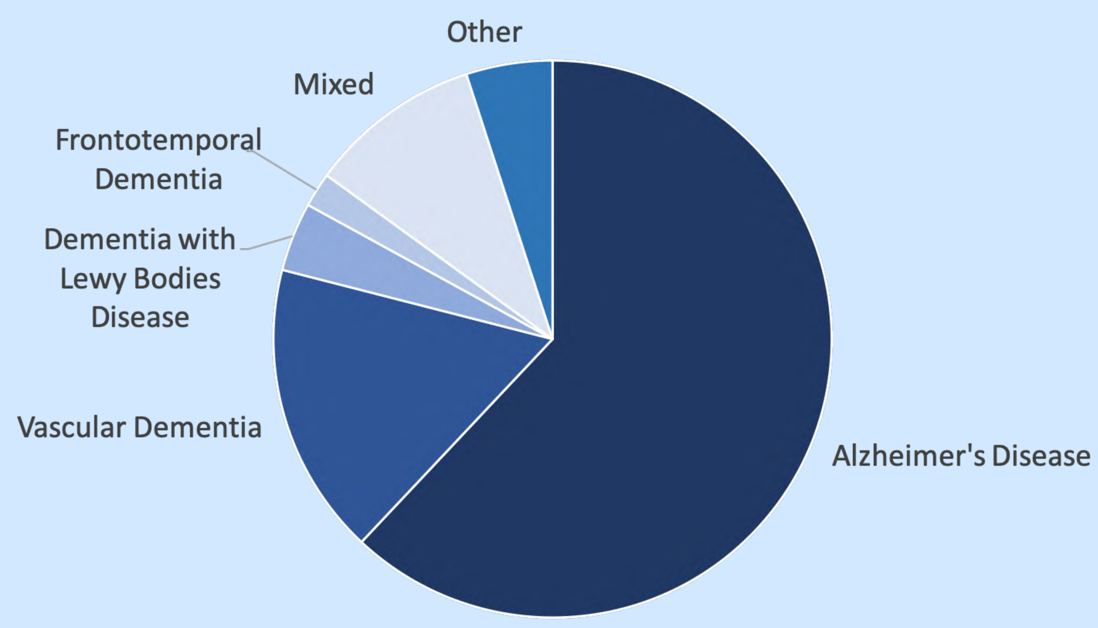


- **Diagnosis** often at a relatively **late stage** of the disease
- Current diagnosis based on:
  - **Cognitive testing**
  - **History of the illness**
  - **Imaging**

**Can EEG measurements help in the diagnosis and classification of dementia?**

## 2 Data analysis

- Resting state **EEG** recordings
- 19 channels
- Diagnosis confirmed post-mortem
- Large **class imbalance**

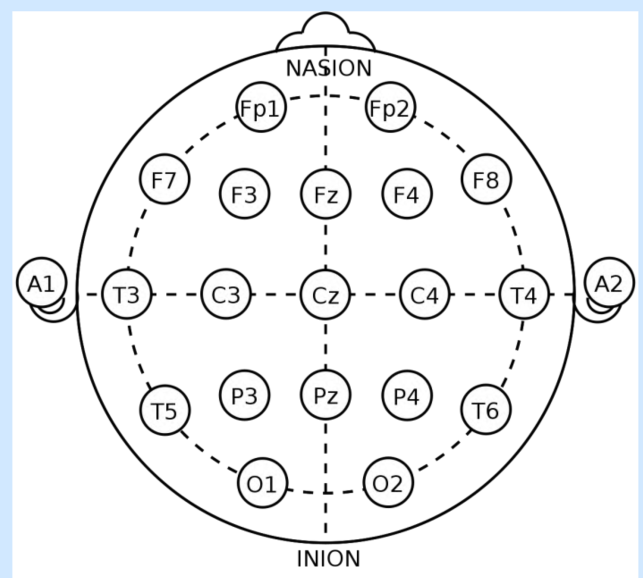


Source: https://bio-medical.com/electro-caps.html

| Class | # patients |
|---|---|
| **Dementia** | **102** |
| Alzheimer's disease | 53 |
| Fronto-temporal dementia | 19 |
| Diffuse Lewy-body disease | 11 |
| Creutzfeldt-Jakob disease | 4 |
| Progressive supranuclear palsy | 2 |
| Vascular Dementia | 6 |
| Mixed Dementia | 7 |
| **Controles with other disorder** | **40** |
| **Controles asymptomatic** | **43** |

## 3 Preprocessing

- **Filtering**
  - Bandfilter: 0.5Hz – 100 Hz
  - Notch filter: 50 Hz
- **Rereferencing**
  - Based on the average
- **Removal of eyeblinks**
  - Using **ICA**, code provided by Epilog
- Epoch selection of 3s
- **Artefact detection** and removal of bad epochs
  - Peak2peak > 150 µV
  - Flat segments > 20ms
  - Absolute minimum/maximum > 85 µV

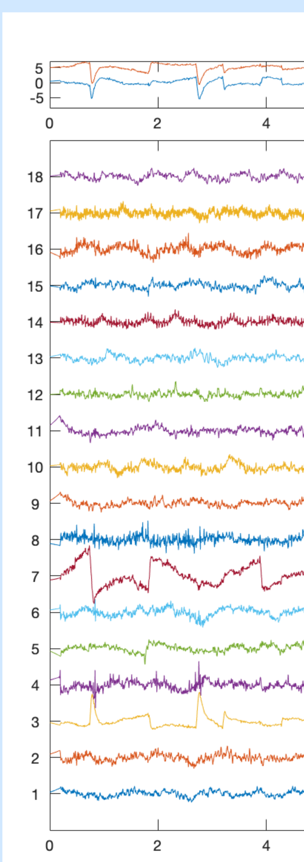

Fp1 and Fp2 channels

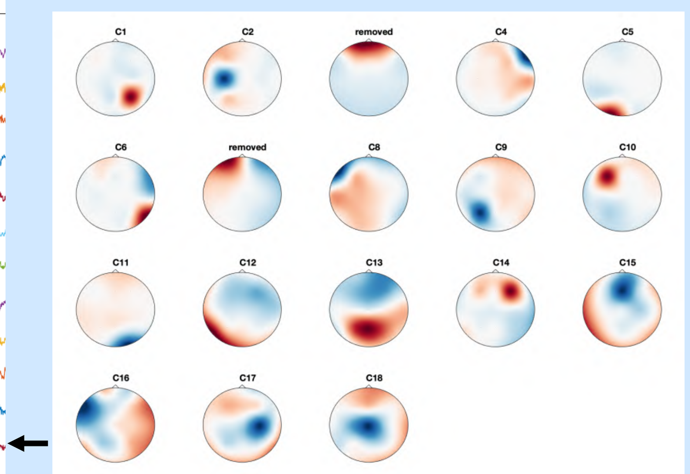

ICA component 3 contains the eye blinks, component 7 are left-right eye movements

## 4 Feature extraction

### Spectral Features

- **Peak frequency**
  - Global
  - For each frequency band
- **Mean power** for each frequency band

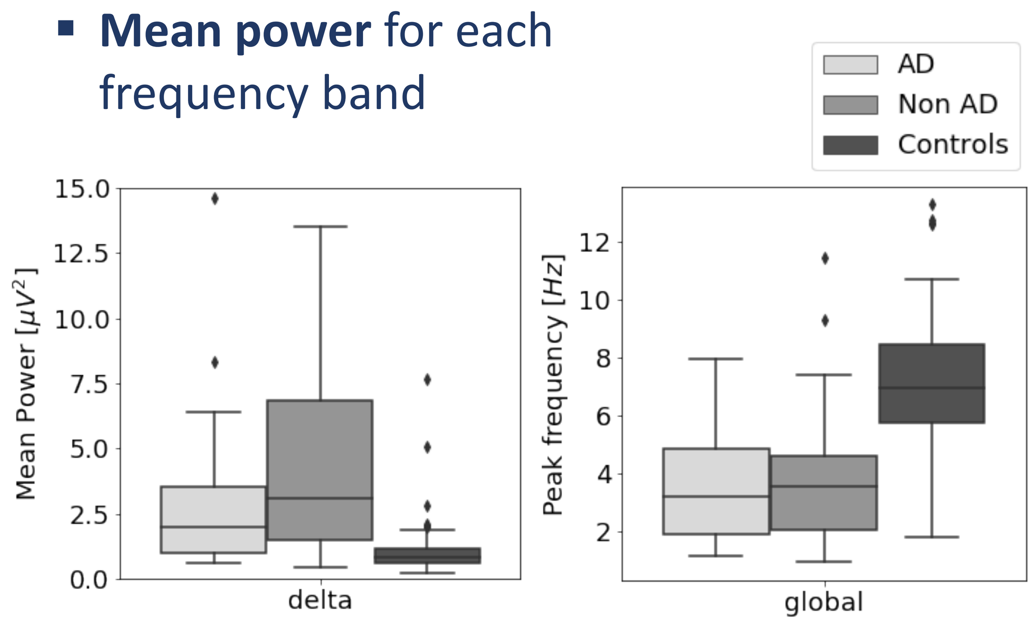


### Information measures

- **Mutual Information**

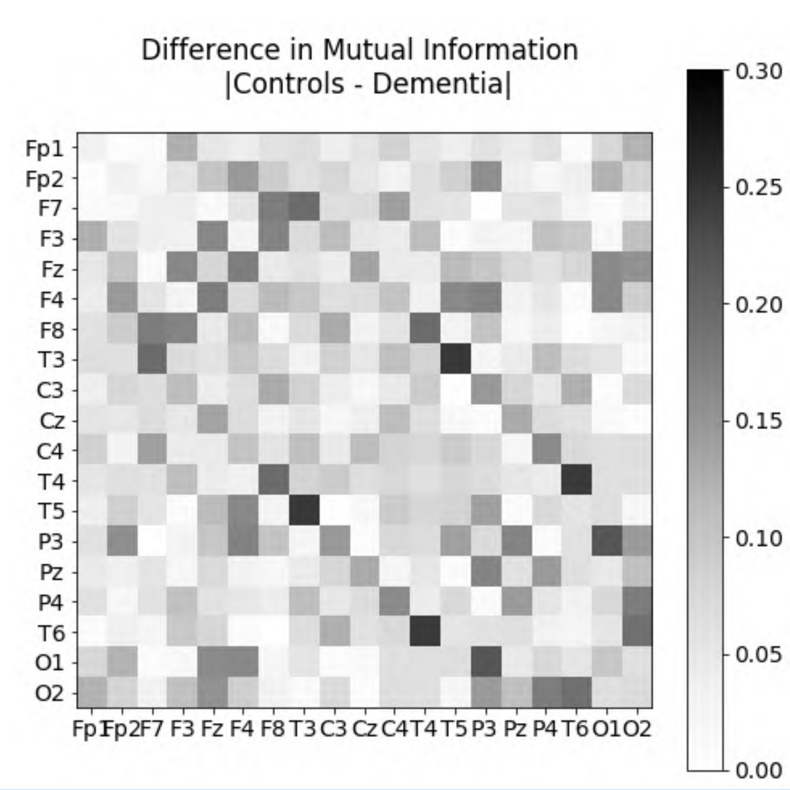


### Functional Connectivity

- Functional connectome calculated using:
  - **Directed transfer function (DTF)**
  - **Partial directed coherence (PDC)**
- **Graph analysis** on the connectomes:
  - In- and out-degree

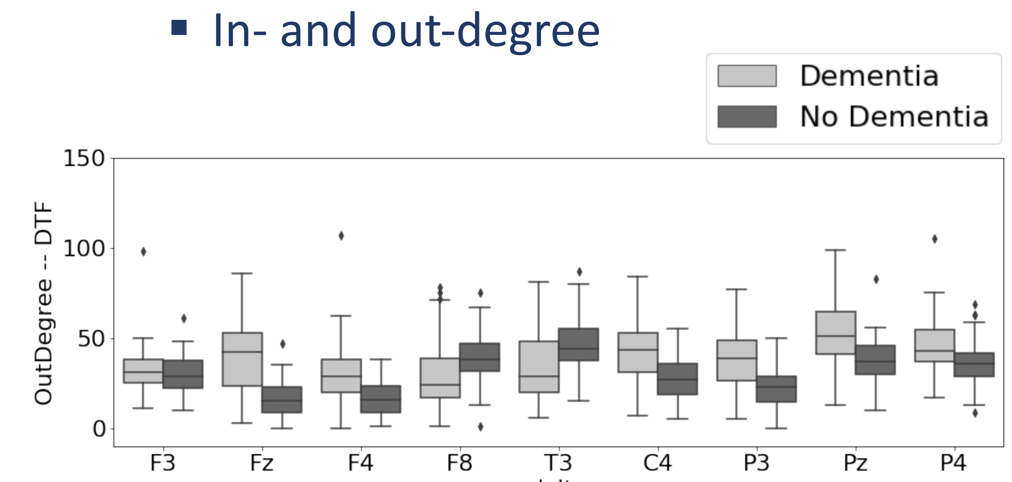


## 5 Classification Models: initial results and discussion

- Data split into **training** set and **test** set
- **Leave One Out cross validation** on the training set to optimize hyperparameters by maximizing the **Area Under the Precision Recall Curve (AUPRC)**
- The features allow to **discriminate patients** with dementia **from the control group** (92% accuracy)
- **Extra features** and **more complex models** might be needed to distinguish patients with Alzheimer's Disease from patients with a different disorder causing dementia

### Logistic Regression

| Metric | Dementia vs No Dementia | AD vs Non AD vs Controls |
|---|---|---|
| **AUPRC** | 0.984 | 0.672 |
| **Accuracy** | 0.916 | 0.701 |
| **F1-score** | 0.915 | 0.650 |
| **Recall** | 0.915 | 0.653 |

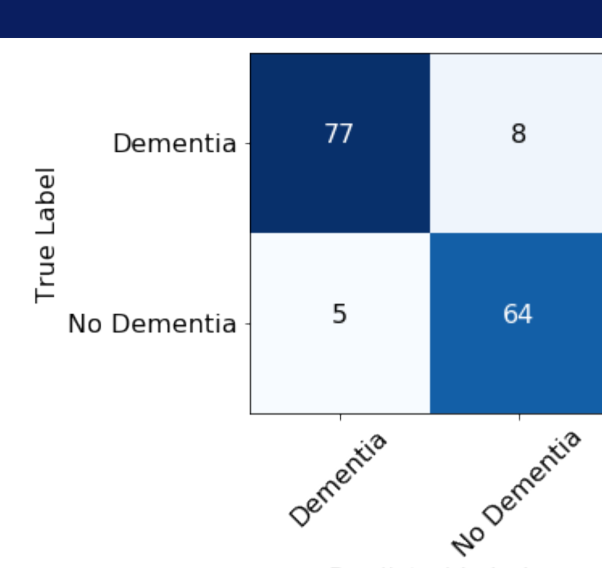


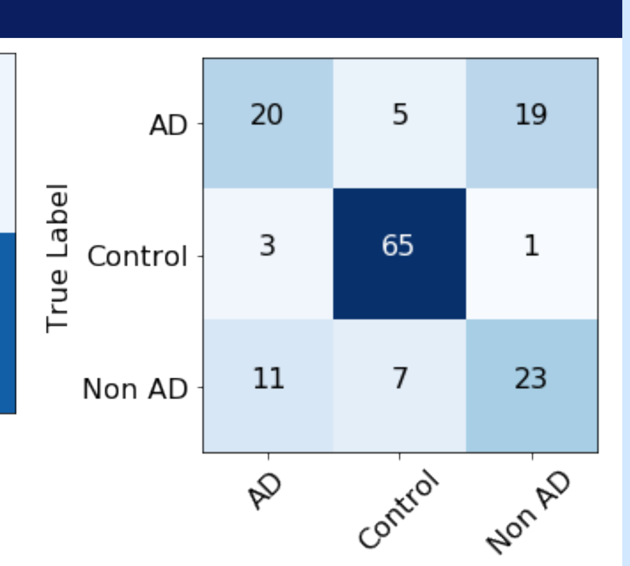


emma.depuydt@ugent.be

Master of Science in Biomedical Engineering

# LOW IMPACT RUNNING

**Guylian Stevens**

Prof. Dr. V. Segers, Prof. M. Forward, PhD R. Derie

Department of Movement and Sports Sciences - Ugent, Department of Electronics and Information systems, Ugent

GHENT UNIVERSITY

VRIJE UNIVERSITEIT BRUSSEL

## On your marks

I ❤ Running

**200** milj.
People run, worldwide

**35%**
Reduction of all cause mortality rate

Up to **79%**
Sustain an injury within a given year

Up to **14%**
Injuries are due to stress fractures


Treadmill gait retraining reduces impact and thus injuries. Can outdoor gait retraining acquire similar results?

## Running track

**Initial screening**
150 screened subjects
150 runners at initial screening, screened on vertical instantaneous loading rate and peak tibial acceleration with inclusion of 30% subjects with highest peak impact

**Pre-gait retraing**
Motion capture system
Control and experimental group
20 people included in study
Full motion capture of ten motion files

**Gait-retraining**
Over-ground retraining
Auditive faded feedback system
Noise extrapolation on music based on tibial acceleration

**Post-gait retraing**
Motion capture system
Full motion capture of ten motion files
Similar to the pre-gait retraining test

**Segmented model**
Visual 3D
Eleven segment model
Calculation of ground reaction force, joint angles, moments and power

## Split time

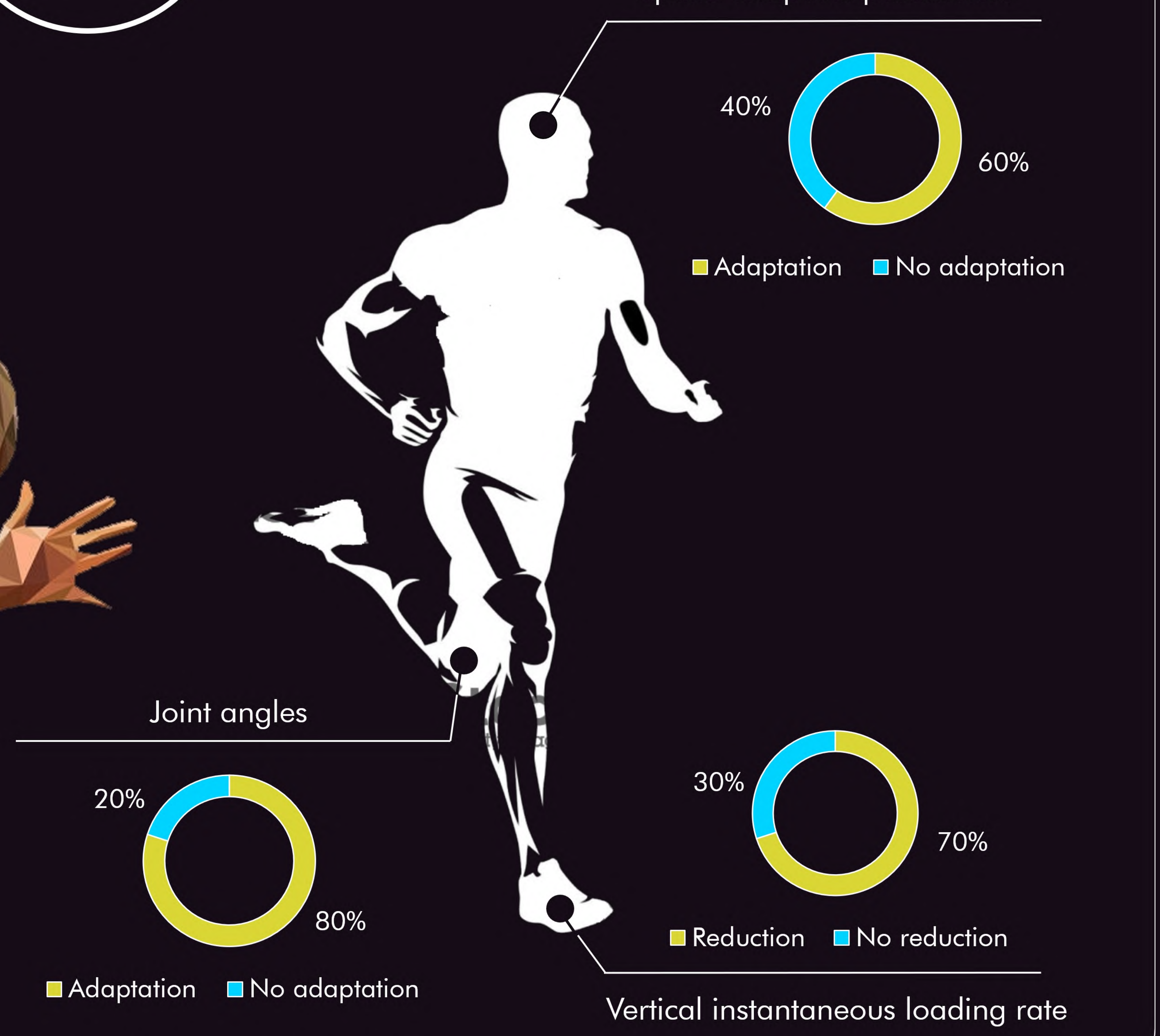


Preliminary results based on visual comparisson (25-feb-2020)

Guylian.stevens@ ugent.be

Master of Science in Biomedical Engineering

# Draining the brain: a computational biomechanics study of the Chiari-Syringomyelia Complex: mechanics of brain tonsils

GHENT UNIVERSITY

**Jana Bovyn**

Supervisors: prof. dr. ir. Patrick Segers[1], dr. MD. Frank Dewaele[2]
Counsellors: ir. Sarah Vandenbulcke[1], MD. Tim De Pauw[2]

VUB VRIJE UNIVERSITEIT BRUSSEL

[1]IBiTech-bioMMeda, Ghent University, Ghent, Belgium
[2]Neurology department, UZ Gent, Ghent, Belgium

## Chiari-Syringomyelia Complex

- **Chiari malformation type I** (CMI) is a condition in which the cerebellar tonsils extend 5 mm or more below the foramen magnum.
- 65% of people with CMI develop a **syrinx** (fluid filled cavity in spinal cord) → **Chiari-Syringomyelia Complex**.
- The link between CMI and syrinx formation is not fully understood yet.

Isu et al. (1990). Hydrosyringomyelia associated with a Chiari I malformation in children and adolescents. Neurosurgery, Vol. 26, pp. 591–597.

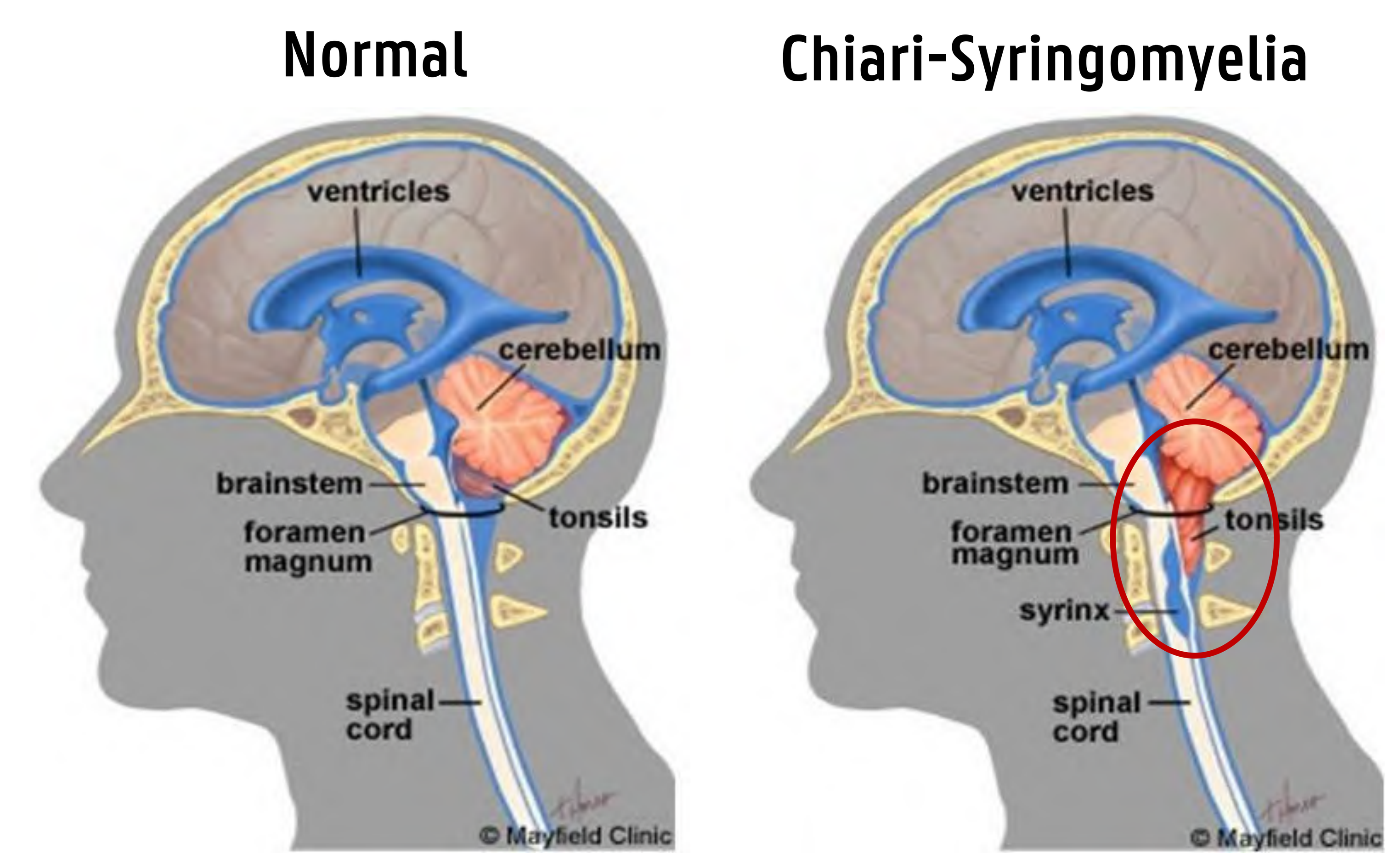


Mayfield Clinic, 2018

## Hypothesis

CMI: tonsils cause obstruction at level of foramen magnum
↓
Disturbed cerebrospinal fluid (CSF) flow
↓
Large pressure gradients
↓
Syrinx formation

## Objective: a computational biomechanics study

The hypothesis will be tested in silico from a **biomechanical** point of view.

A **computational Finite Element (FE) model** will be set up for the neurological tissues involved in this disease.

This thesis focusses on the biomechanics of the **tonsils**, which cause the obstruction.

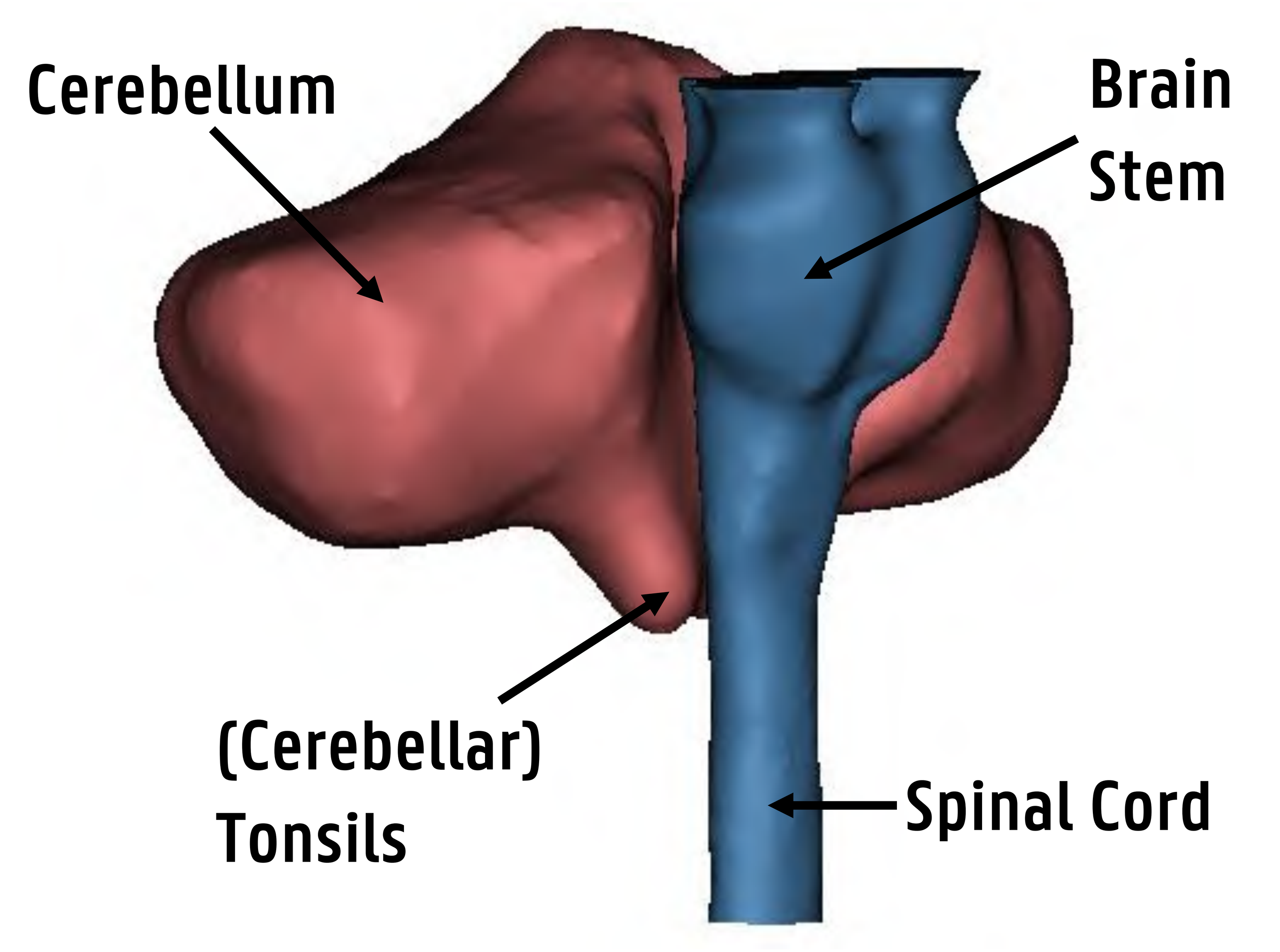


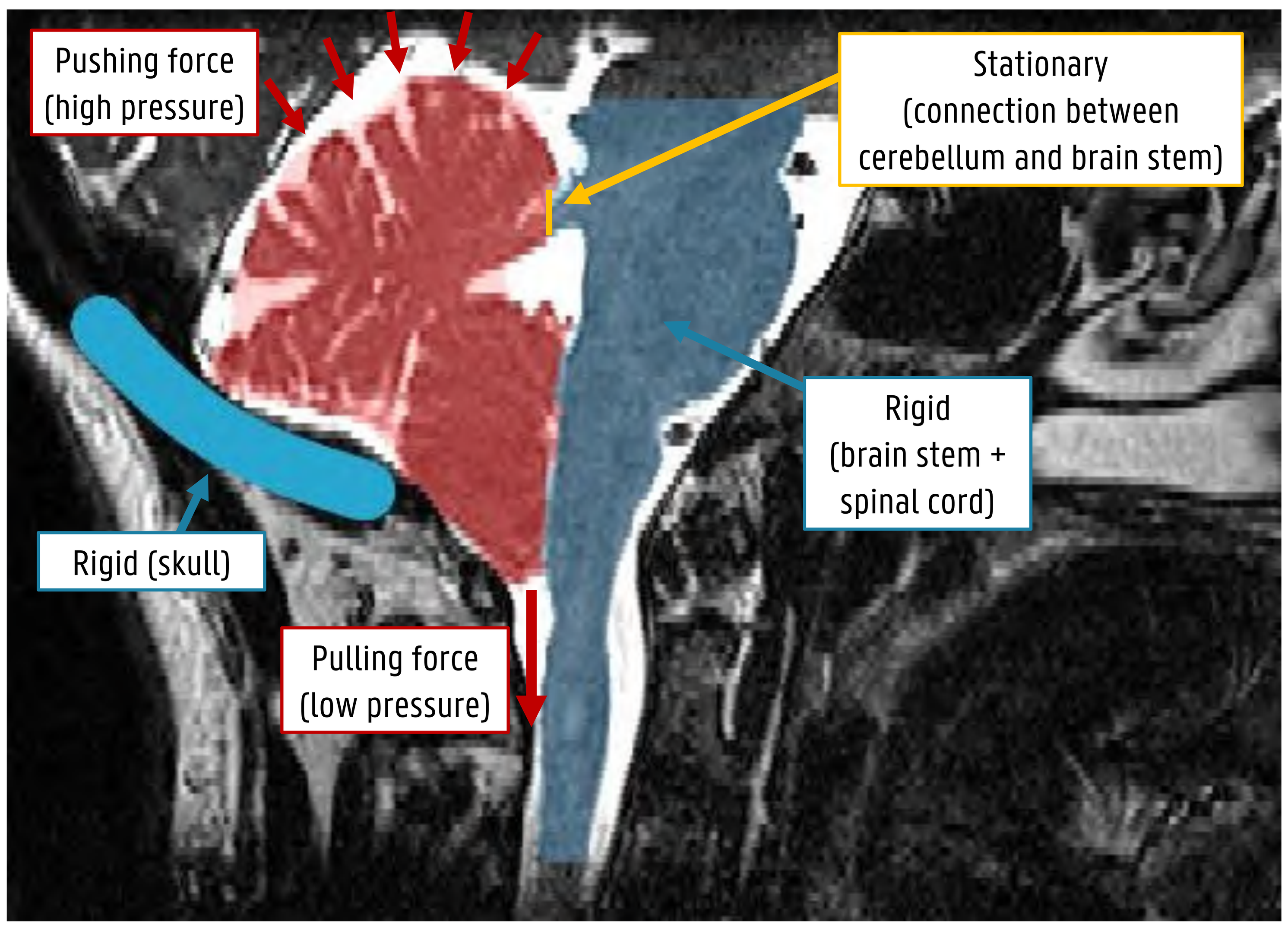


Head MRI, UZ Gent, 2020

## Mechanics of brain tonsils: workflow

1) Construction of **3D geometry** of the cerebellum based on MRI scans of patients with CM1 (Mimics)

2) **Meshing** the geometry (ICEM)

3) Assigning **material properties** to the cerebellum
   - Grey and white matter: viscoelastic[3]
   - Pia mater (membrane): linear elastic[4]

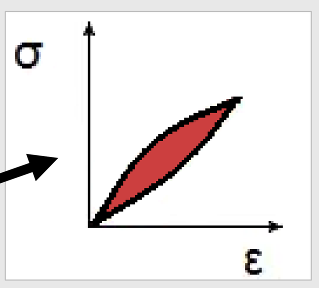


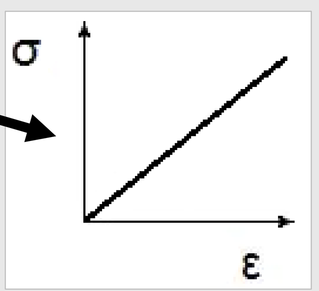


4) Define **boundary conditions** and perform **FE simulations** (Abaqus)

5) **Validate** results experimentally

[3] John Zhang et al., Journal of Biomechanics (2011)
[4]Carolyn J. Sparreye et al., Journal of Neurotrauma (2009)

# Knee sounds: a model

**Kate Duquesne**

prof. dr. ir. Dick Botteldooren[a], dr. ir. Edouard Auvinet[b] & prof. dr. Catherine Van Der Straeten[b]

[a]Waves-INTEC, Ghent University, Gent, Belgium

[b]HIRUZ, UZ Ghent, Gent, Belgium

## Introduction

Noise around the knee is common, especially when performing repetitive knee extension and flexion or squats. This noise may be physiological or pathological. Many authors have tried to measure these sounds to use as a biomarker for evaluating disorders of the knee joint [1-2]. Measuring the sound is often performed using contact microphones. The purpose of the thesis is to model the sound propagation in a knee to get a better understanding of the phenomenon. First, a forward model is created. Next, using the obtained transfer function, a backward model will be created.

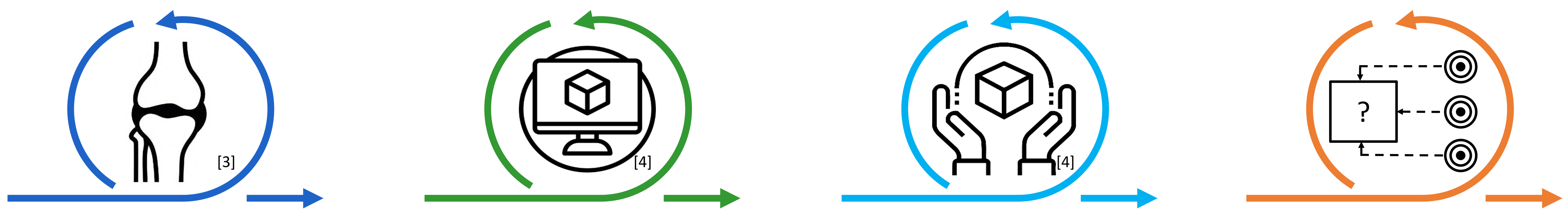


Anatomy — Modelling software — Forward model — Backward model

## Anatomy

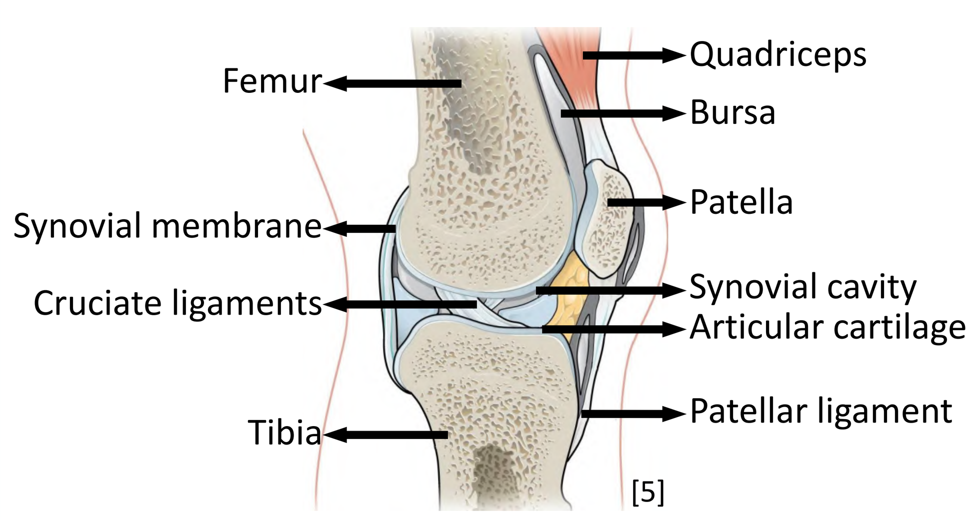


The knee is a complex joint

Bones provide structure

Ligaments and muscles provide stabilization

The joint cavity provides lubrication and supplies nutrients and oxygen to the cartilage

Bursae facilitate movement of the tendons and skin over joints

## Modelling software

Selection of a modelling software based on:

- Audible frequencies
- Viscoelastic properties
- Anisotropy
- Time/frequency domain
- Link with DICOM files
- Postprocessing
- Documentation

COMSOL MULTIPHYSICS® [6]

## Forward model

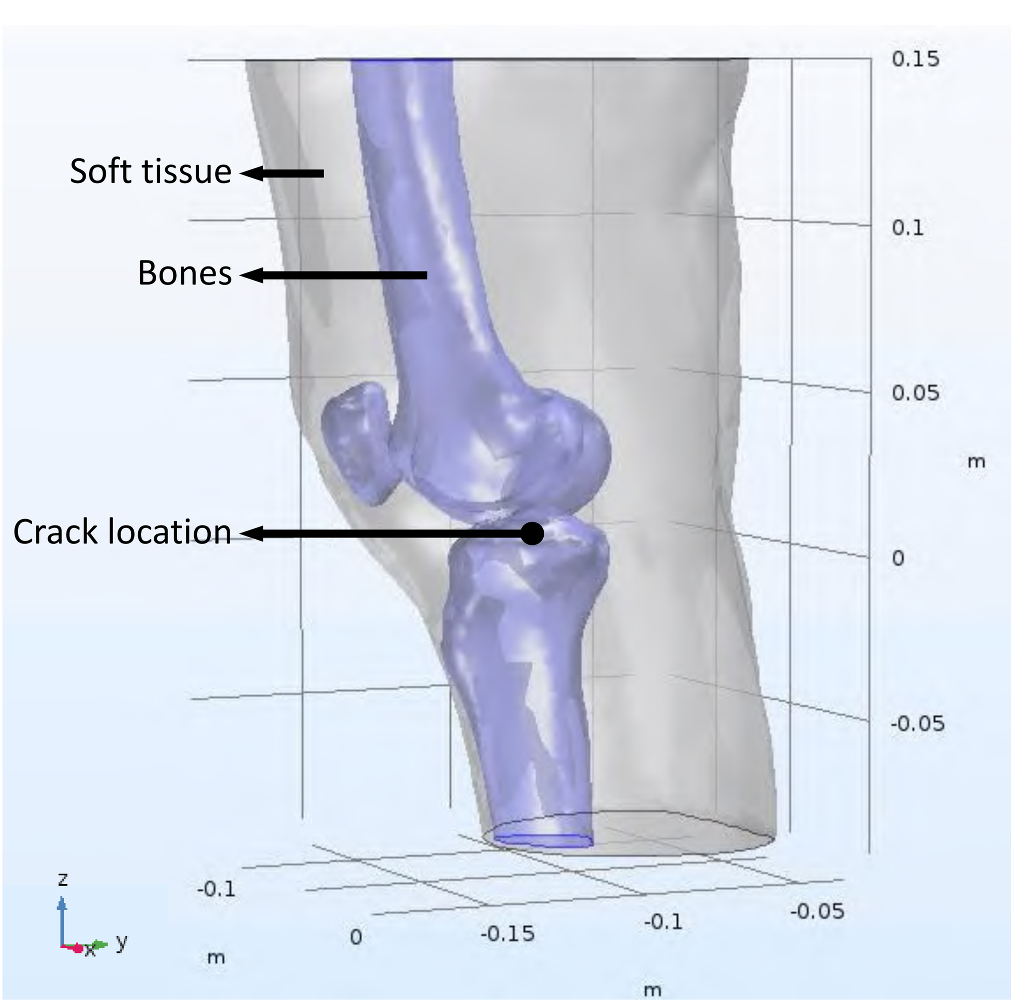


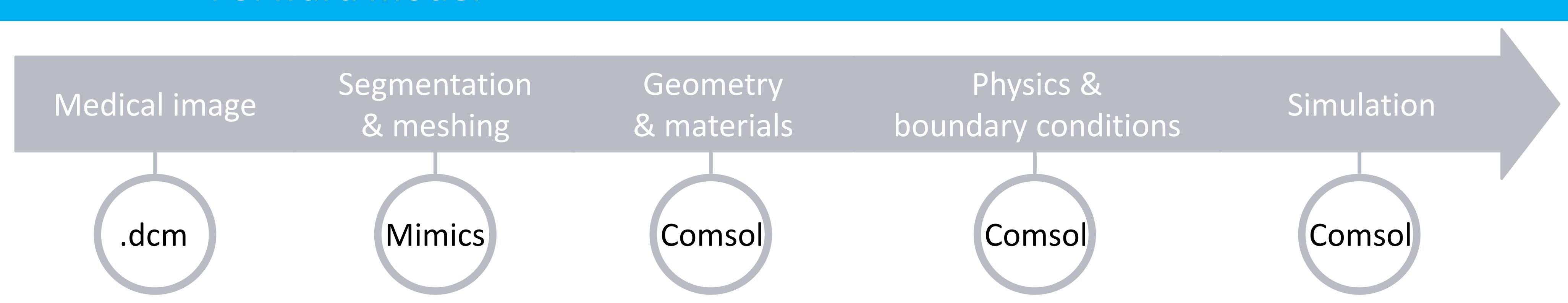


| | | |
|---|---|---|
| Geometry: | Soft tissue<br>Bones: femur, tibia and patella | |
| Material properties: | Linear elastic with viscoelastic properties | |
| Physics: | Solid mechanics | |
| Boundary conditions: | Crack location:<br>Surface of soft tissue:<br>Top and bottom surface:<br>Interface between soft tissue and bones: | Applied force<br>Free<br>Low reflecting boundary<br>Two options: No/Thin elastic layer |
| Applied force: | Gaussian pulse with frequency content until 10 000Hz | |

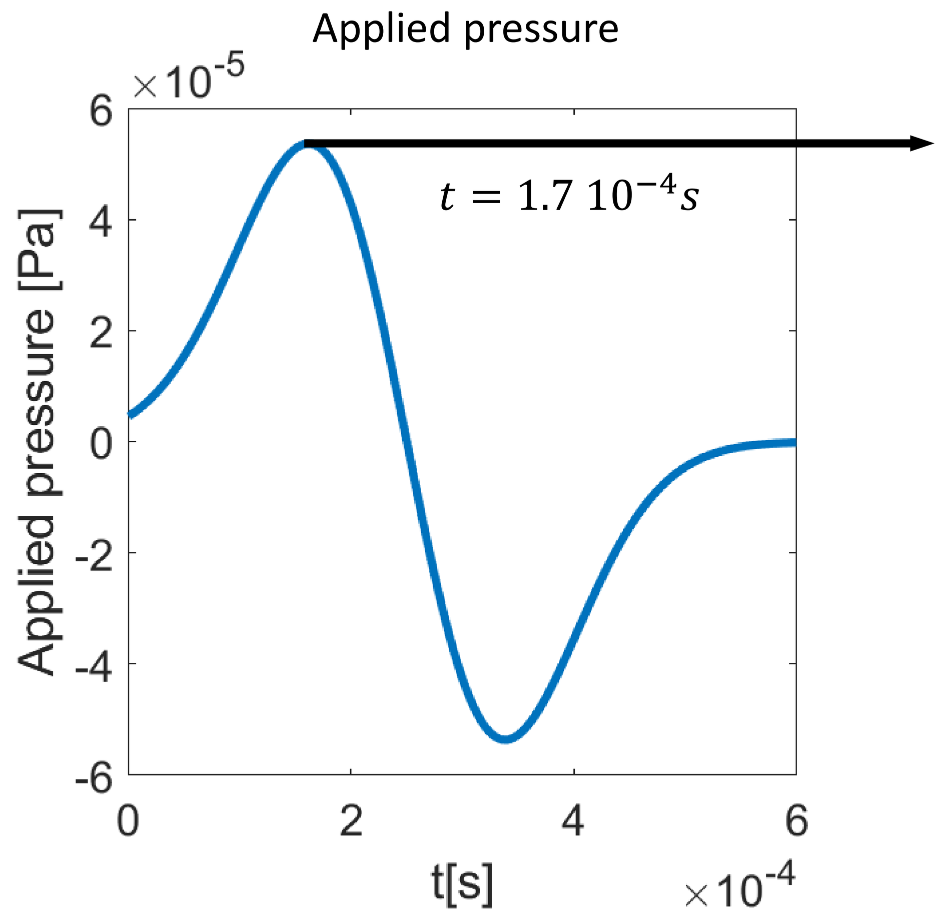


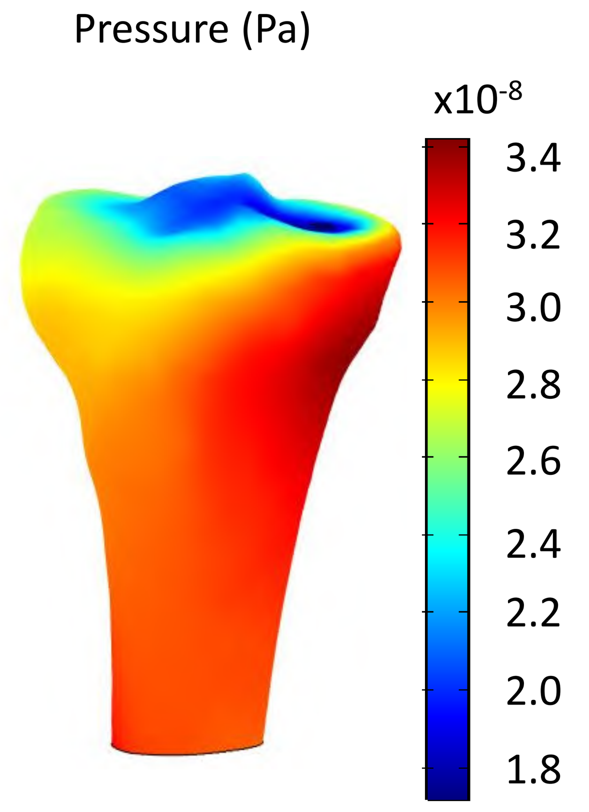


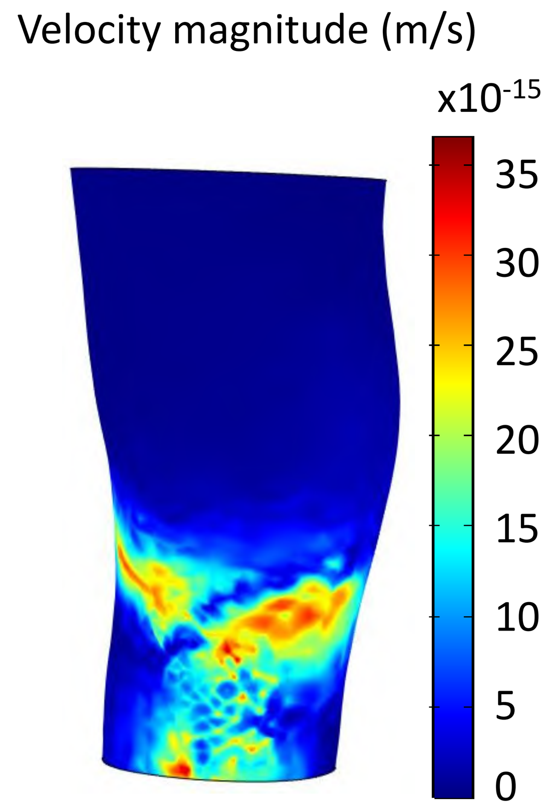


The simulation is time dependent study.

A snapshot of the output of the model at timepoint 0.17ms is given on the left. At the surface of the tibia the propagation of the stress (using pressure as a measure) can be studied. At the surface of the soft tissue the velocity profile can be studied, which is related to what a contact microphone measures.

The interface between the soft tissue and the bones is currently modelled in two different ways namely via direct coupling of the displacement and via a thin elastic layer. Here, the result of the model with direct coupling of displacements is shown. During future experimentation, it will be determined which model is more appropriate.

## Backward model

Future work includes producing a backward model. Based on the determined transfer functions in the forward model, the source of the sounds might be determined. Furthermore, the location where the source emits might be determined using time reversal.

## References

[1] T. I. Khan, M. Kusumoto, Y. Nakamura, S. Ide, and T. Yoshimura, "Acoustic emission technique as an adaptive biomarker in integrity analysis of knee joint," *J. Phys. Conf. Ser.*, vol. 1075, no. 1, 2018.
[2] I. Vatolik, G. Hunter, M. Everington, and A. Augousti, "Monitoring and analysis of acoustic emissions from knee joints," *Proc. Inst. Acoust.*, vol. 38, no. June 2019, pp. 133–138, 2016.
[3] https://www.gettyimages.be/illustraties/joint-pain?excludenudity=false&sort=mostpopular&mediatype=illustration&family=creative&phrase=joint%20pain
[4] https://www.flaticon.com/free-icon/
[5] J. G. Betts *et al.*, "Joints -Anatomy and Physiology - OpenStax College," in *Human Anatomy and Physiology*, BCcampus.
[6] https://www.comsol.com/

kate.duquesne@ugent.be

Master of Science in Biomedical Engineering

# Segmentation of Cerebral Arteriovenous Malformations in Digital Subtraction Angiography and 3D Rotational Angiography Images


**Kilian Adriaenssens**

prof. dr. ir. Charlotte Debbaut, dr. Ir. Danilo Babin,
prof. Ir. Vincent Keereman

TELIN, Ghent University, Gent, Belgium


GHENT UNIVERSITY

VRIJE UNIVERSITEIT BRUSSEL

## Goal of this research

The purpose of this research is to find an efficient method that projects the 2D digital subtraction images (DSA) onto the segmented 3D vascular tree of the brain. This would allow for the blood flow of the arteries and veins to be visualised in a more clear way for the surgeon, such that these images can be included in the workflow and decision-making of the treatment of Arteriovenous Malformation.

## What is cerebral arteriovenous malformation and what are the risks of leaving it untreated?

**Cerebral Arteriovenous Malformation (AVM):**

A congenital disorder of blood vessels characterized by a complex tangled web of abnormal arteries and veins connected by one or more fistulas: abnormal connections between arteries and veins without passing through a capillary bed.

→ **AVM affects 1 in every 10.000 humans [1]**

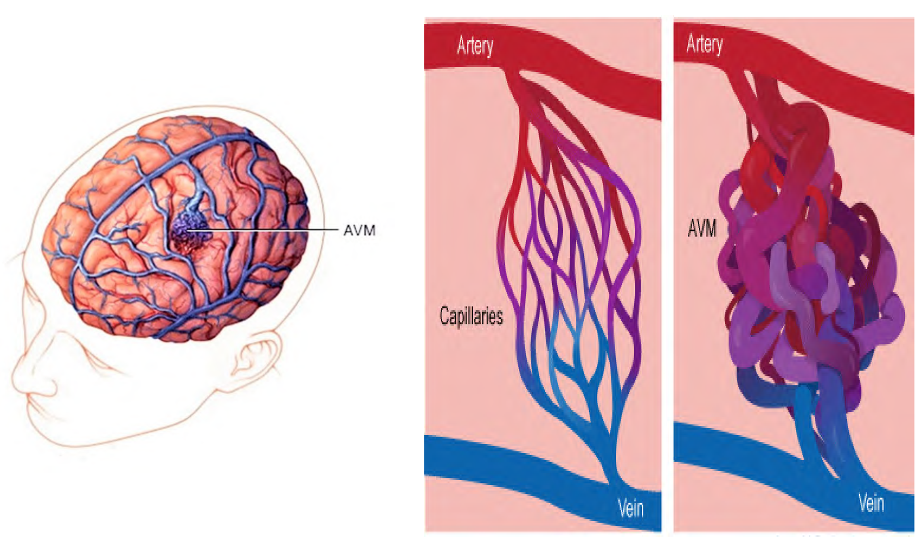


[2]

**Risks of leaving AVM untreated:**

→ Risk of hemorrhage increases by 2% to 4% each year
→ Reduced oxygen to parts os the brain
→ Brain damage because of growing AVM

[2]

10% - 50% of patients are at risk of neurological disability [3]

5% - 25% of patients are at risk of death [3]

## Treatment of AVM: (micro)surgery

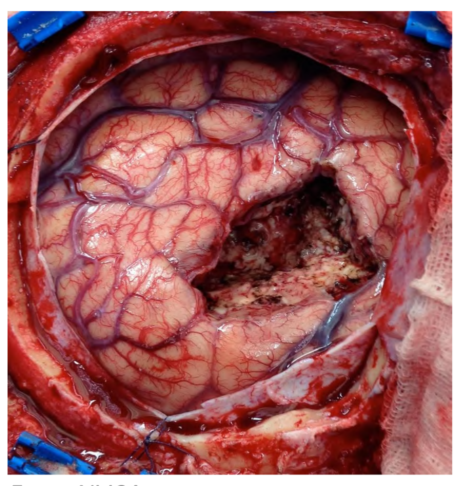

From NVCA

Tying off or clipping feeding arterial veins, obliterating draining veins and removing the nidus or nest of the AVM.

→ Minimal morbidity & high efficacy after surgery.
→ Best-known and longest standing treatment.

→ **The technique is highly invasive and can be very challenging for high grade malformations.**

## Treatment of AVM: endovascular occlusion

A catheter delivers material like balloons, sclerosing drugs or embolization glue to block connection between arteries and veins.

→ Less efficacy after operation.
→ Procedure is safer and less invasive.

→ **Doctors need clear information on blood flow for accurate planning and treatment.**

## Desired workflow: combining 2D DSA and 3D RA for 3D blood flow analysis


**2D Digital Subtracted Angiography (DSA)**

→ Visualizes blood vessels and blood flow.
→ AVM appears tightly packed with enlarged feeding arteries that supply a central nidus.
→ DSA is performed on a bi-plane system.

**3D Rotational Angiography (RA)**

→ Produces a sequence of DSA-type images while rotating around the subject.
→ Creates a 3D image of high quality.
→ Segmentation gives vascular tree.

**Goal: projection of 2D DSA on vascular tree**

→ Using both planes of the DSA image to project the blood flow on the vascular tree.
→ No extra imaging needed: DSA & RA are already acquired in the current workflow

## First steps in image registration

**2D DSA** **MIP of vascular tree** **Projection DSA on vascular tree**

1. Select easily recognizable anatomical landmarks in the DSA image.
2. Select the same anatomical landmarks in the maximal intensity projection (MIP) of the vascular tree.
3. Adjust DSA to match with MIP
4. Project DSA value on all the corresponding voxels of the MIP along the axis of projection.

## References


[1] Fleetwood, Ian G., and Gary K. Steinberg. "Arteriovenous malformations." The Lancet 359.9309 (2002): 863-873.
[2] Mayo Clinic Staff. "Brain AVM (arteriovenous malformation)."Mayoclinic, Mayo Foundation for Medical Education and Research (MFMER), 17 May 2019, mayoclinic.org/diseases-conditions/
[3] Ellis, Jason A., and Sean D. Lavine. "Role of embolization for cerebral arteriovenous malformations." *Methodist DeBakey cardiovascular journal* 10.4 (2014): 234.



Kilian.Chris.Adriaenssens@vub.be


Master of Science in Biomedical Engineering

# Using diffusion MRI and tractography to investigate changes in white matter tracts in a rat model of temporal lobe epilepsy


**Marjoleen Wouters**

Supervisor: Emma Christiaen

Promotors: Prof. dr. Christian Vanhove and Prof. dr. Robrecht Raedt

IBiTech-MEDISIP, Ghent University, Gent, Belgium


## Temporal lobe epilepsy

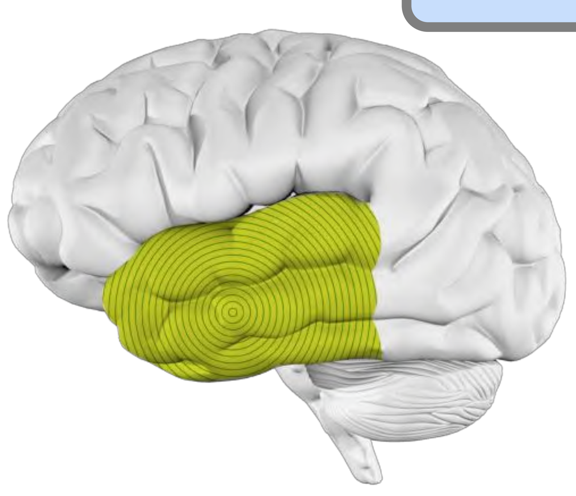

Human temporal lobe

(YorkPsych, 2019) (Epilepsie Liga)

**Epilepsy**

1/100 people worldwide

Abnormal neuronal activity in brain

→ Epileptic seizure: shaking, lower consciousness and awareness

**Temporal lobe epilepsy (TLE)**

Seizure origin in temporal lobe

## Kainic acid rat model

(Charles river)

**Kainic acid = neuro-excitatory amino acid**

⇩

Intraperitoneal injection in rat

⇩

Binding + activation glutamate receptors

⇩

Status epilepticus induced in rat

⇩

Model for **chronic epilepsy**

## Diffusion MRI

Diffusion of **water** molecules within **voxel** = contrast in dMRI

→ Diffusion Tensor Imaging (DTI): Free diffusion

→ Diffusion Kurtosis Imaging (DKI): Hindered/restricted diffusion

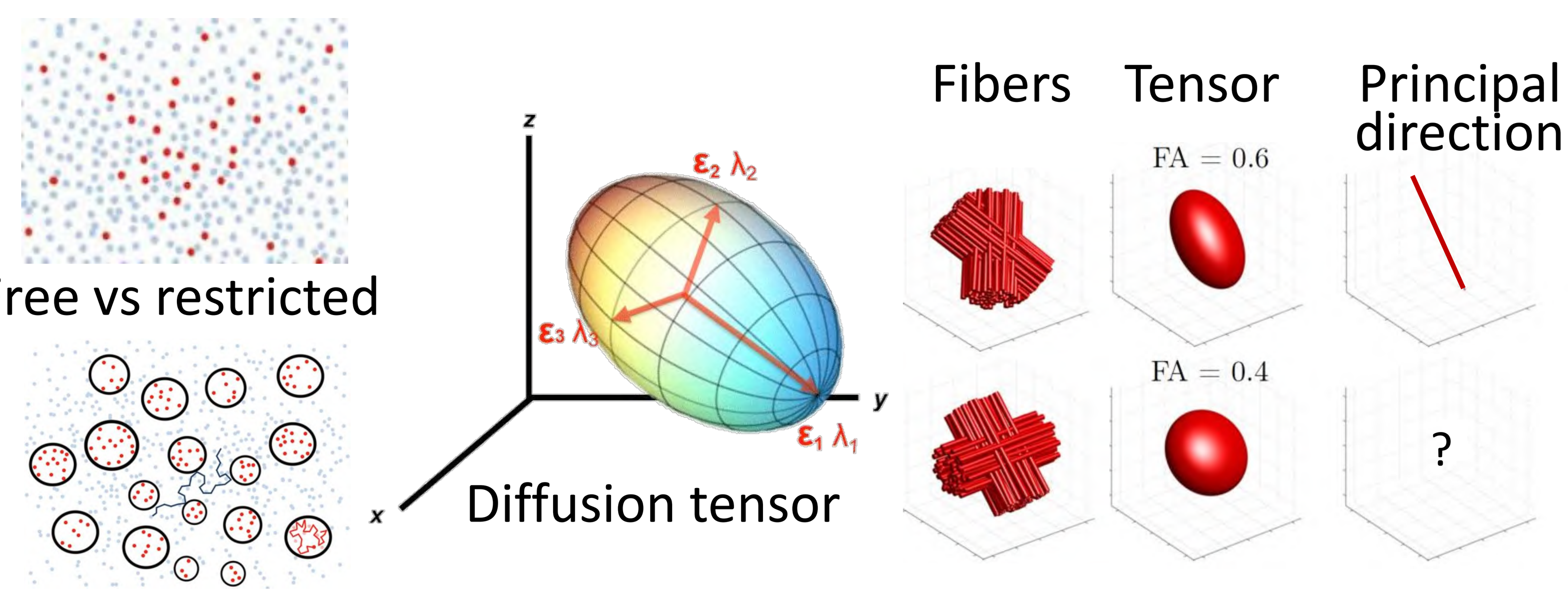


Limitation DTI/DKI: **crossing fibers** in voxel not distinguished

→ Fixel-based analysis: Fiber Orientation Distribution (FOD)

(Van Hecke, 2016) (Jeurissen, 2012)

## Tractography

**Tractography**

Visualization of white matter tracts, calculated from dMRI data

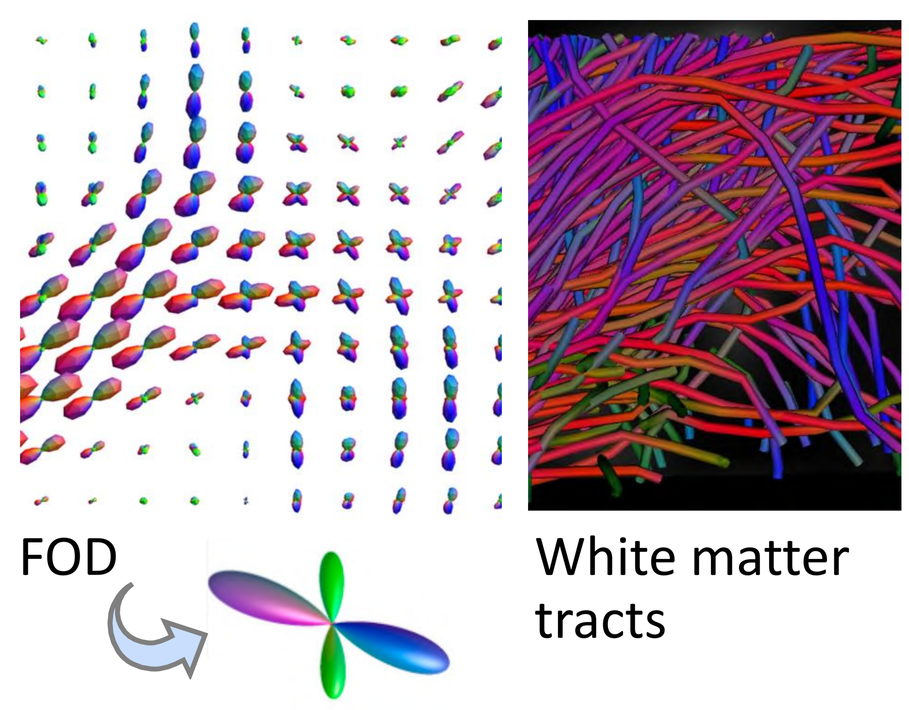


**Parameters**

\# streamlines

fractional anisotropy (FA)

axial diffusivity (AD)

radial diffusivity (RD)

mean diffusivity (MD)

(Portegies J.M. et al., 2015)

## MRI acquisition and data analysis

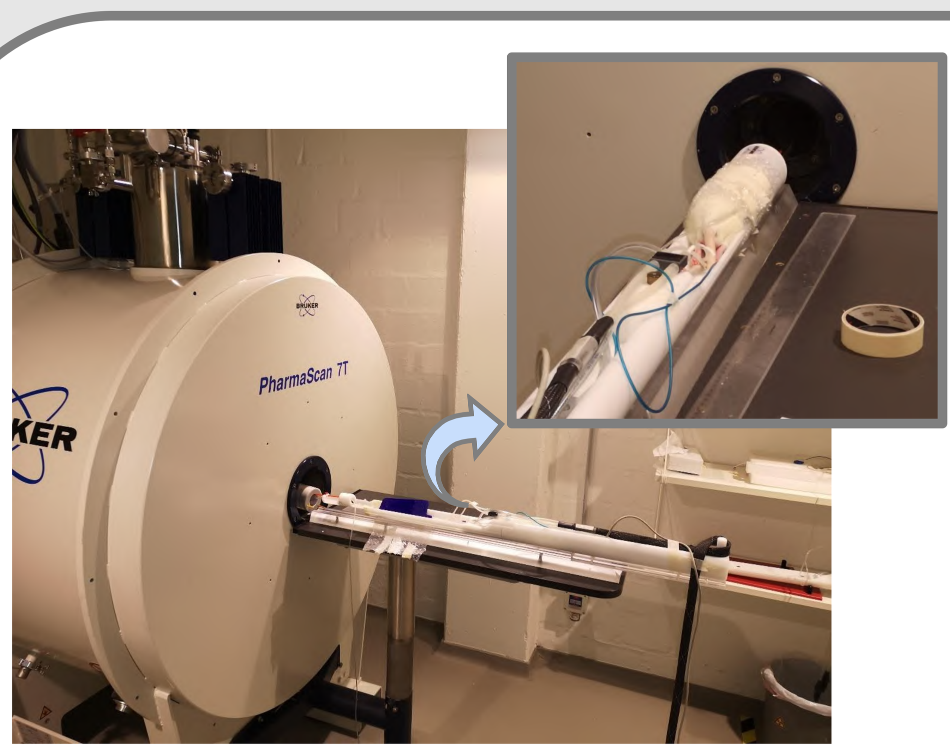

**7 Tesla Bruker BioSpin PharmaScan**

- 7 rats in TLE group, 7 in control group
- 2% isoflurane anesthesia + heating pad
- MRI at **baseline** and **16 weeks** post-injection

**T2-MRI scan**: RARE sequence

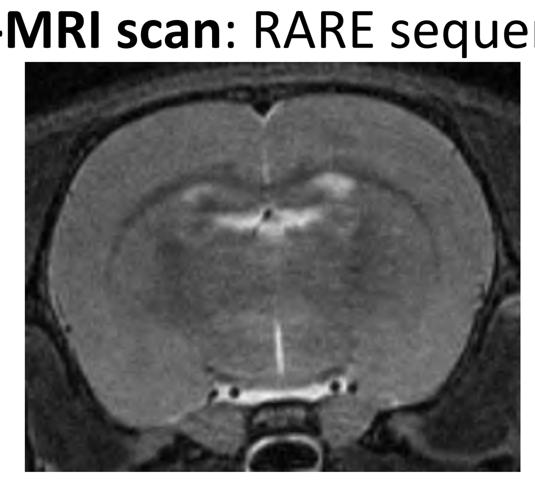

**dMRI scan**: SE EPI sequence

3 DWI scans: b-values 800, 1500, 2000 s/mm²

MRtrix3

ExploreDTI

**Preprocessing**

- Raw data DWI scan per rat
- Denoising and Gibbs ringing correction
- Extract bval/bvec
- Calculate DTI file
- Motion/distortion correction
- Calculate FOD template

**Tractography**

- Calculate white matter tracts on FOD template

## Changes in white matter tracts

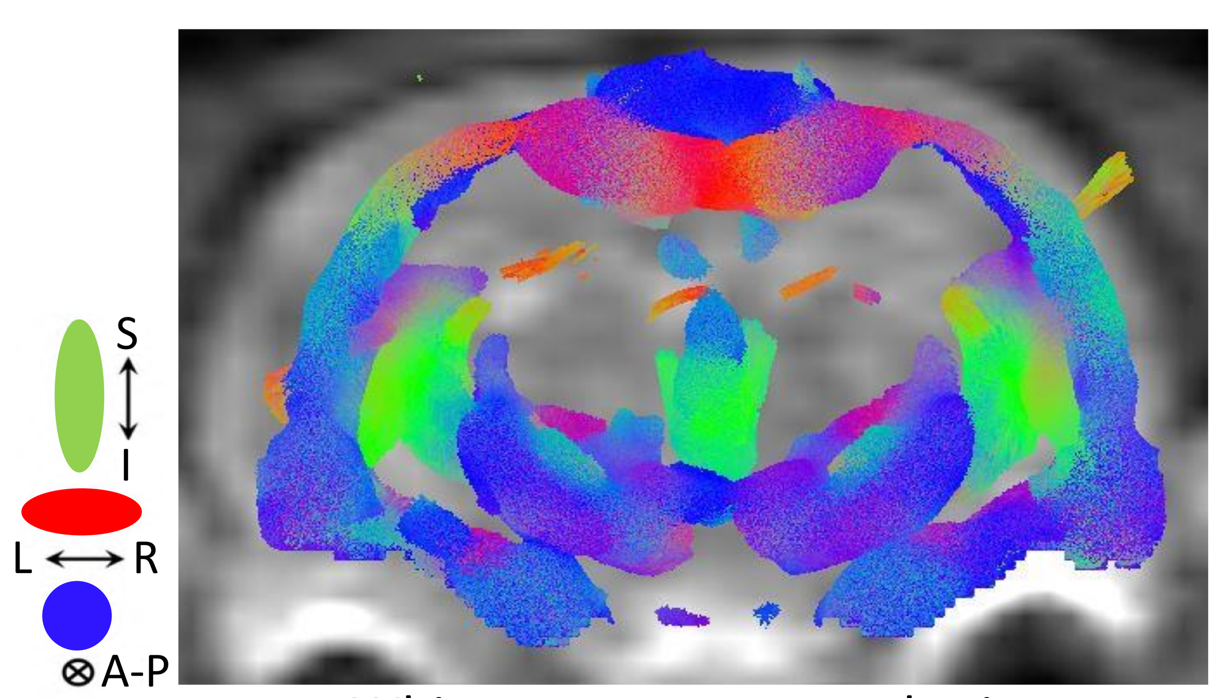


White matter tracts rat brain

**Development TLE: changes in white matter tracts**

Compare parameters white matter tracts for TLE and control group

## Biomarker for epilepsy therapies

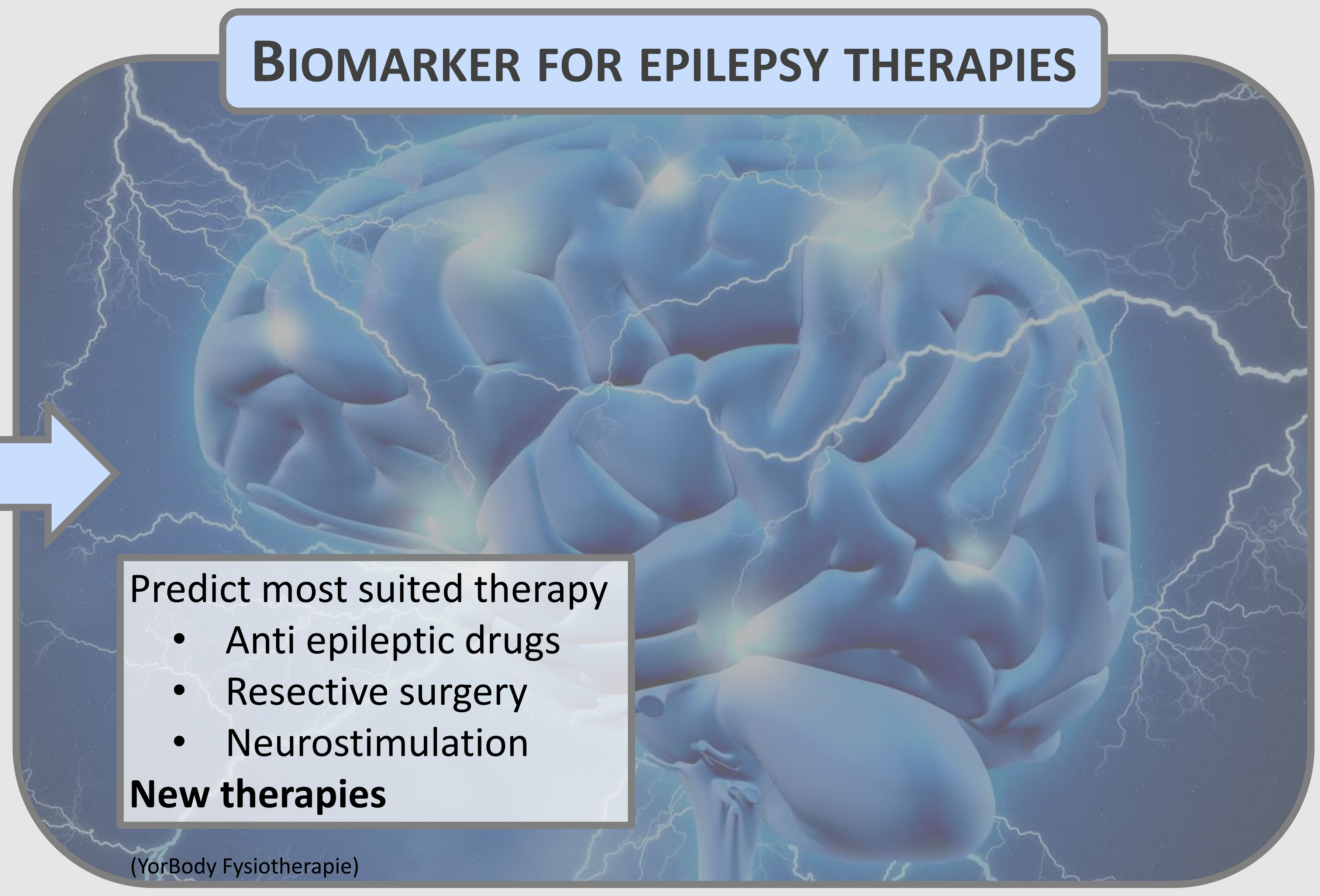

Predict most suited therapy

- Anti epileptic drugs
- Resective surgery
- Neurostimulation

**New therapies**

(YorBody Fysiotherapie)


marjoleen.wouters@ugent.be

# F-18 labeling of microspheres to enable Interventional PET for liver radio-embolisation

GHENT UNIVERSITY

VUB VRIJE UNIVERSITEIT BRUSSEL

**Caroline De Bock**

prof. dr. ir. Stefaan Vandenberghe, dr. ir. Christian Vanhove, dr. Ken Kersemans

IBiTech-Medisip, Ghent University, Gent, Belgium

University Hospital Ghent; Department of Nuclear Medicine, Gent, Belgium

## Liver radio-embolisation

**Radio-isotope treatment with $^{90}$Y SIR-Spheres for liver tumors**

- Prediction of the patient response → $^{99m}$Tc-MAA microspheres

➢ Personalize treatment by using dosimetry

➢ Interventional PET camera: real-time feedback

➢ More accurate surrogate

⟶ **$^{18}$F labeled microspheres**

**Objectives**

- Investigate labeling strategies ✓
- Optimise process
- First preclinial trials

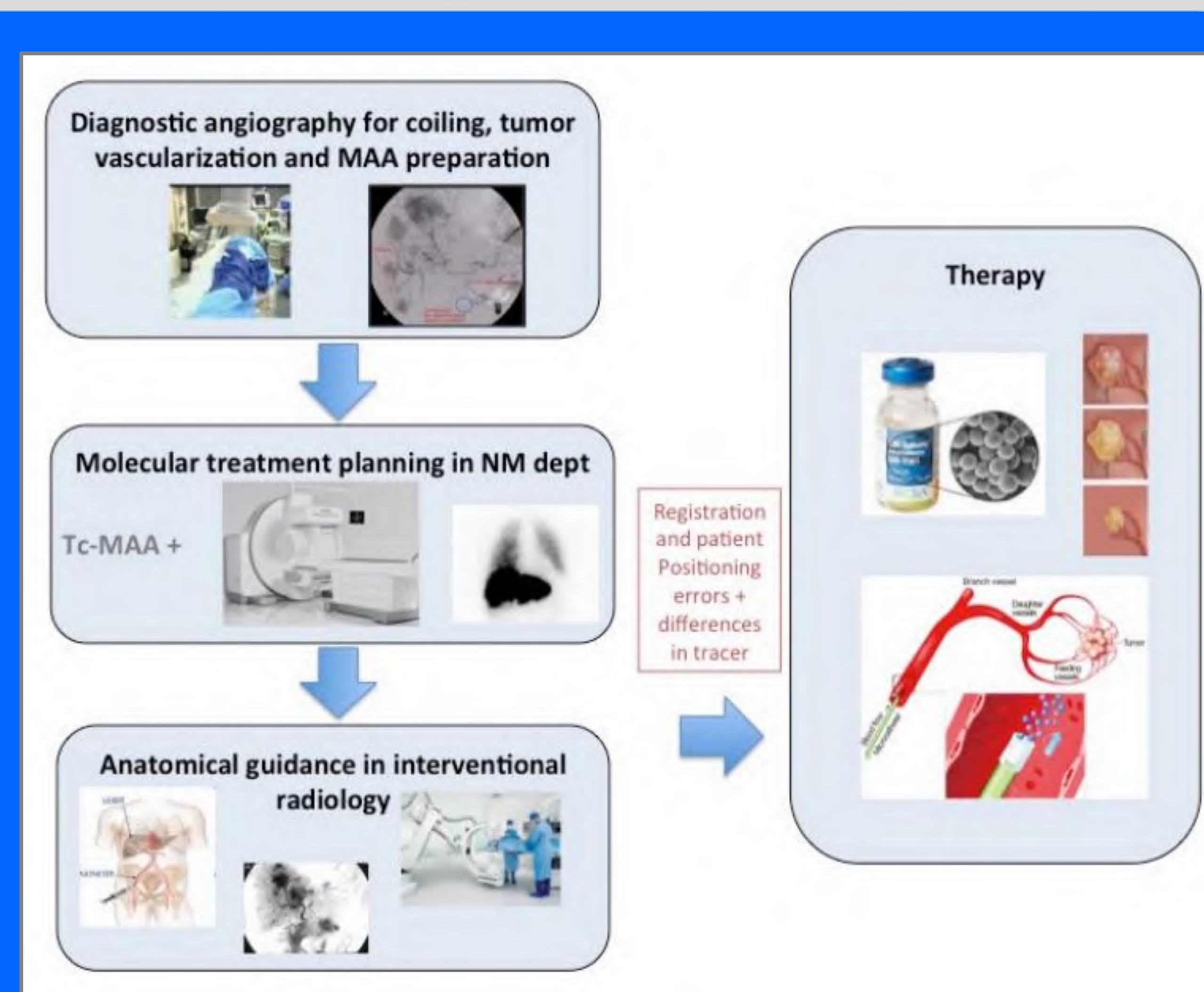


Fig 1: Current workflow for liver radio-embolisation

## Strategy 1: Chelation with p-SCN-NOTA and amino-functionalized silica gel

- Produce $^{18}$F in cyclotron
- Complexation of Al$^{18}$F from $^{18}$F and $AlCl_3$
- P-SCN-NOTA binds to “Amino-Silica”
- Al$^{18}$F binds to chelator on functionalised silica


Fig 2: Used products for chelation

## Strategy 2: $^{18}$F-FDG labeling

- Produce $^{18}$F in cyclotron
- Radiosynthesis of $^{18}$F-FDG
- DOWEX microspheres react with $SOCl_2$
- $^{18}$F-FDG binds to activated DOWEX

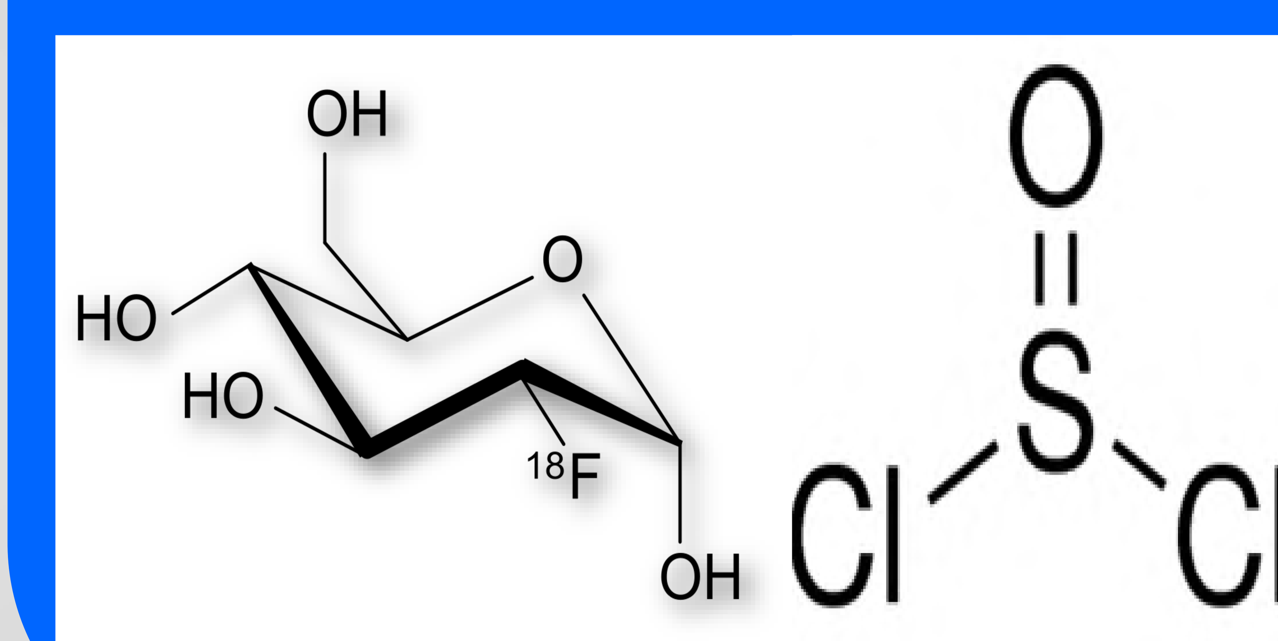


Fig 3: Chemical formulas for FDG labeling

## Purification protocol

- Wash spheres with acetonitrile (min. 3 times)
- Centrifugation + Decantation
- Test stability radiopharmaceutical in NaCl

**Conclusions**

Both labeling strategies resulted in labeled microspheres. The yield of $^{18}$F-FDG is quite low, lower than 20%. To achieve a feasable radiation dose, the amount of needed microspheres is too high. Chelation with p-SCN- NOTA is a more promising technique with initial yields up to 85%. Future plans involve the optimisation of the chelation strategy and starting preclinical trials.

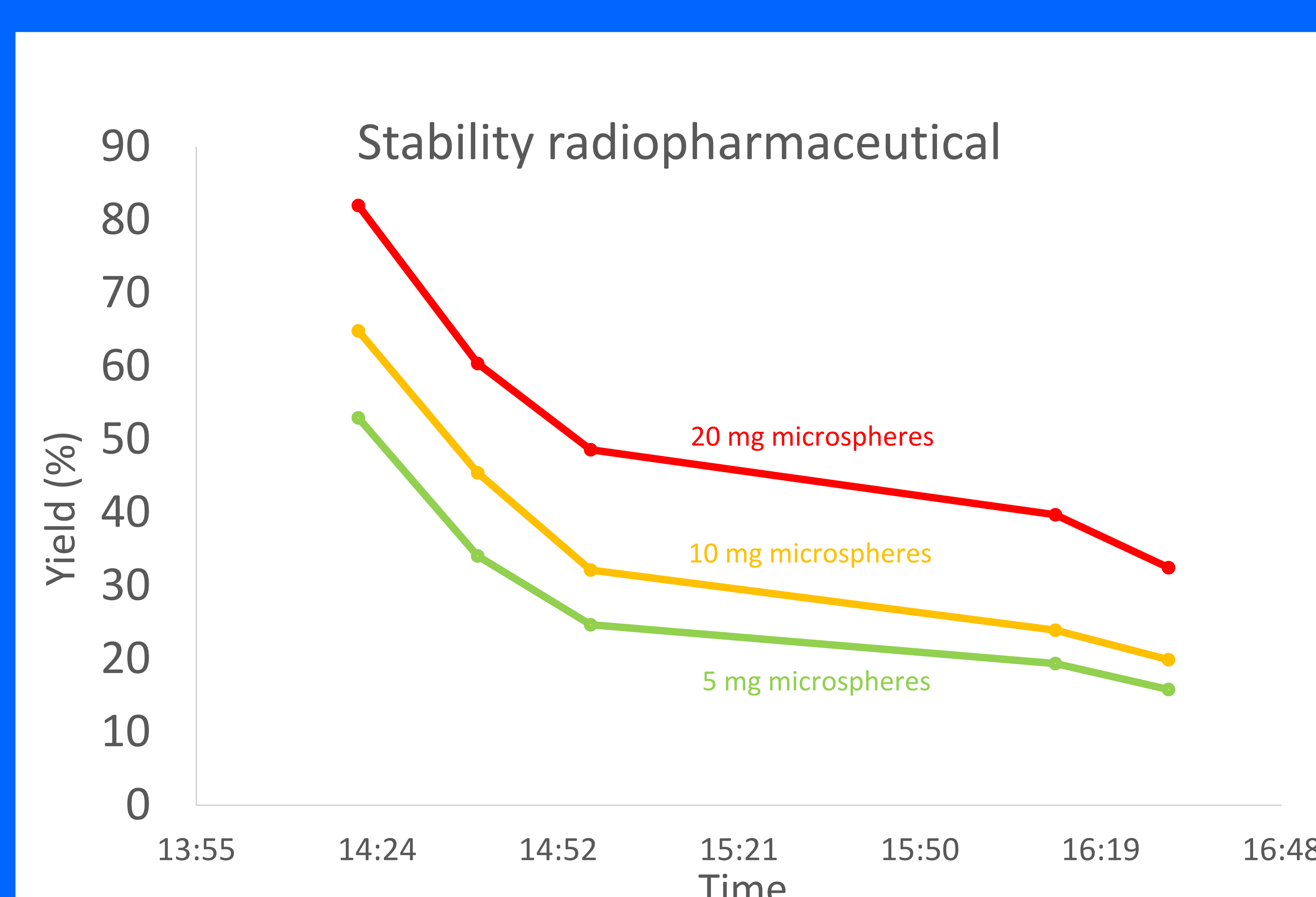


Fig 4: Stability radiopharmaceutical

caroline.debock@ugent.be

Master of Science in Biomedical Engineering

# Non-invasive Measurement of Intra-abdominal Pressure

**Salar Tayebi**
Prof. Dr. Ir. Johan Stiens
Prof. Dr. Manu Malbrain
Department of Electronics and Informatics, Vrije Universiteit Brussel, Brussels, Belgium
Faculty of Medicine and Pharmacy, Vrije Universiteit Brussel, Brussels, Belgium

## Intra-abdominal Pressure

Around 25% of critically ill patients suffer from intra-abdominal hypertension (IAH), defined as a sustained increase in intra-abdominal pressure (IAP) equal to or above 12 mmHg and more than half of the patients hospitalized in the ICU will develop IAH within their first week of stay. The presence of IAH can result in diminished organ perfusion, organ dysfunction, and finally, multiple organ failure and death depending on the IAP value inside the abdominal compartment. As a result, IAP monitoring is another vital sign for patients hospitalized in the ICU. Furthermore, late detection of IAH can result in abdominal compartment syndrome (ACS), a fatal condition characterized by a sustained increase in IAP above 20 mmHg with a new onset of organ failure.

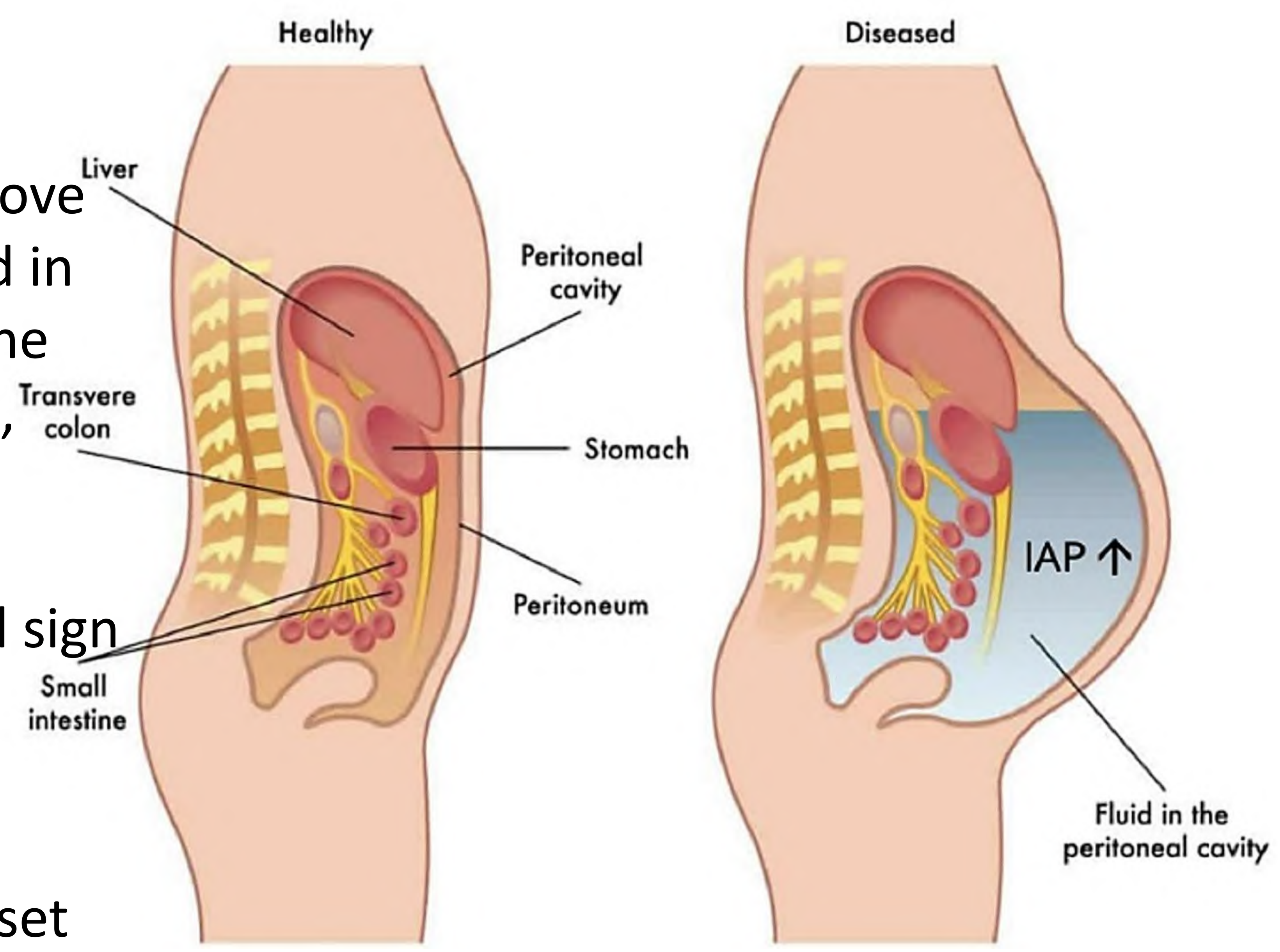


Malbrain et al., ISICEM 2019

## Abdominal Wall

Abdominal wall is a multilayer structure that its electromagnetic properties depends on the thickness of each layer. On the other hand, The thickness of each layer, highly depends on IAP. Thus, IAP changes can result in different electromagnetic properties (for instance reflection response).

Artificial abdominal wall manufactured by "The Chamberlain Group", MA, USA

## Microwave Reflectometry

The (microwave) reflection response is an electromagnetic property that can be modeled as:

$$\boldsymbol{\Gamma_i} = \frac{\boldsymbol{\rho_i} + \boldsymbol{\Gamma_{i+1}} \boldsymbol{e}^{-2jk_i l_i}}{1 + \boldsymbol{\rho_i} \boldsymbol{\Gamma_{i+1}} \boldsymbol{e}^{-2jk_i l_i}}$$

Where $\Gamma_i$, $\rho_i$, $\eta_i$, $k_i$ and $l_i$ are the layer reflection response, primary interface reflection coefficient, characteristic impedance, angular wavenumber and the **thickness** of the $i^{th}$ slab, respectively.

## IAP measurement by Microwave Reflectometry

The main concept of this measurement technique is to monitor the reflection response of abdominal wall. Since the reflection response is a function of abdominal wall thickness and, the thickness of abdominal wall is a function of IAP, microwave reflectometry can be used to measure IAP in a non-invasive, continuous way.

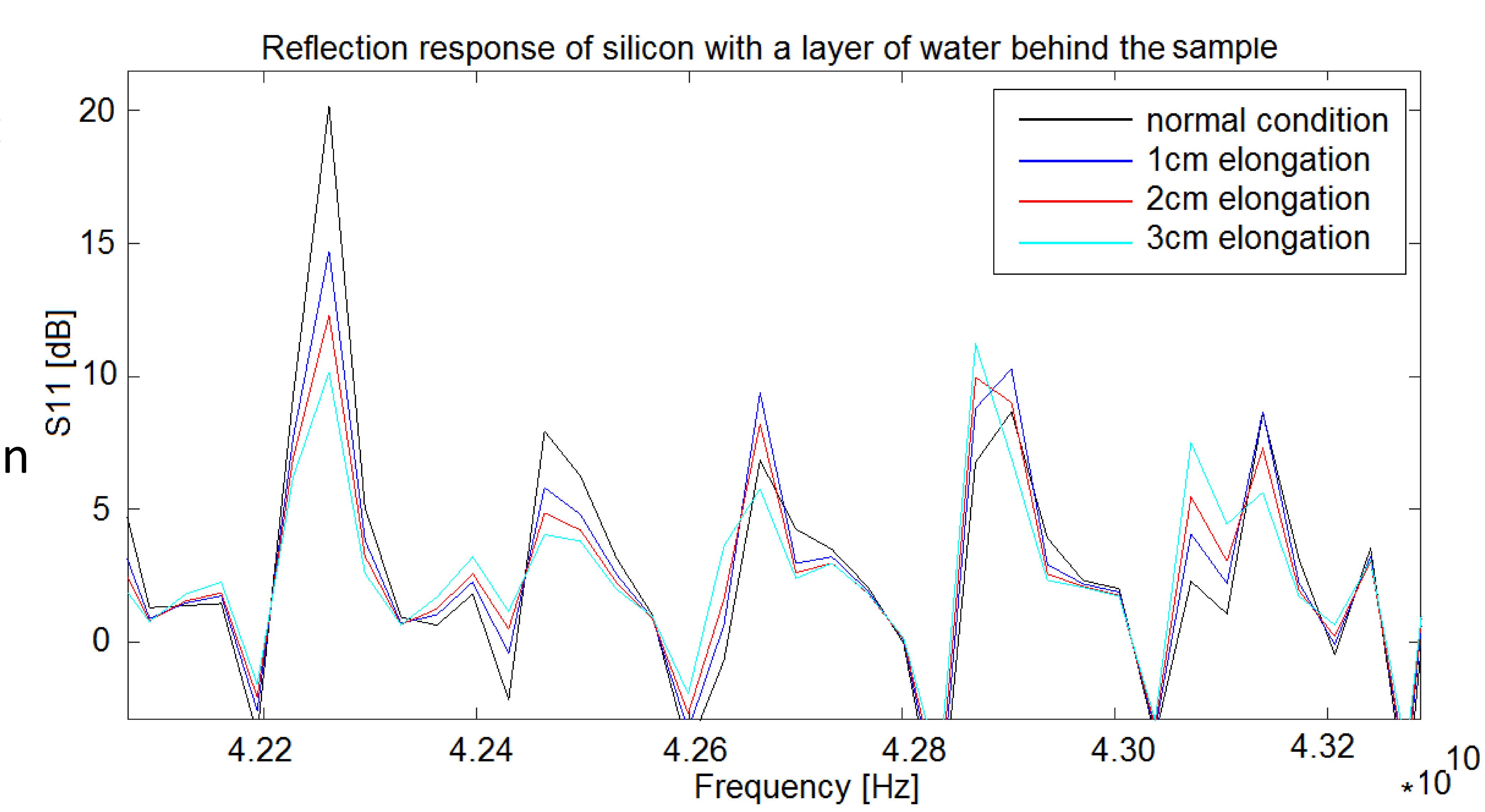

# Deep Learning for Computer-Aided Diagnosis of Lung Nodules in low-dose CT scans

GHENT UNIVERSITY

Nathan Sennesael

Supervisor: Milan Decuyper Promotor: prof. dr. Roel Van Holen

Research group: Medical Imaging and Signal Processiong (MEDISIP)
IBiTech, ELIS, FEA, UGent, Ghent, Belgium

VUB VRIJE UNIVERSITEIT BRUSSEL

## Motivation

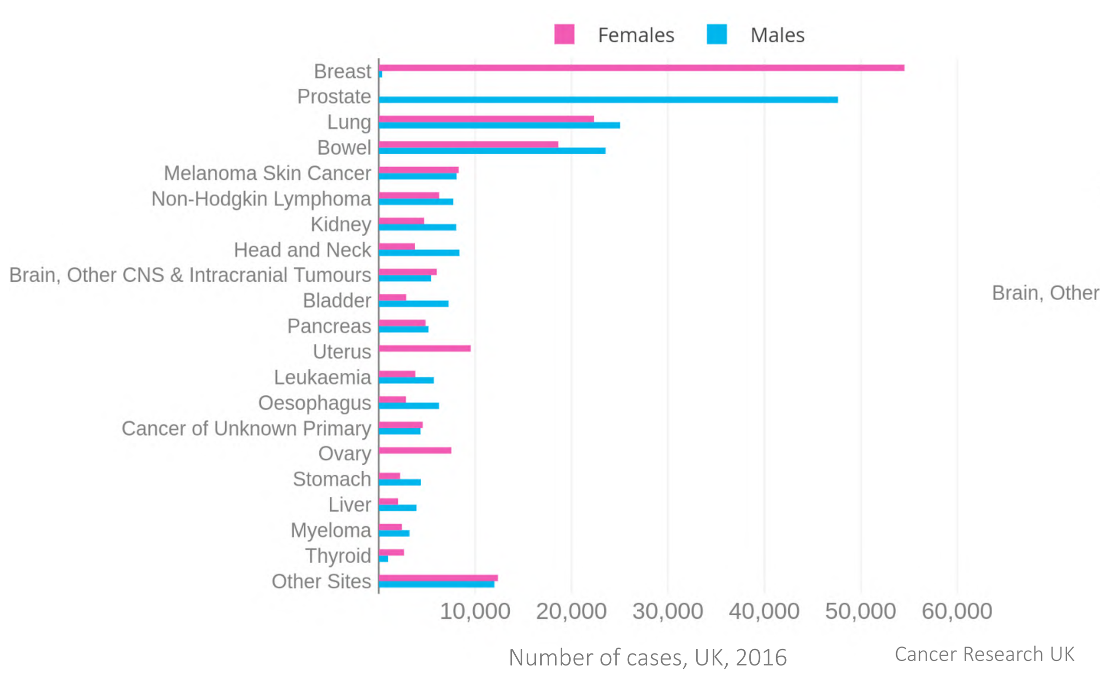


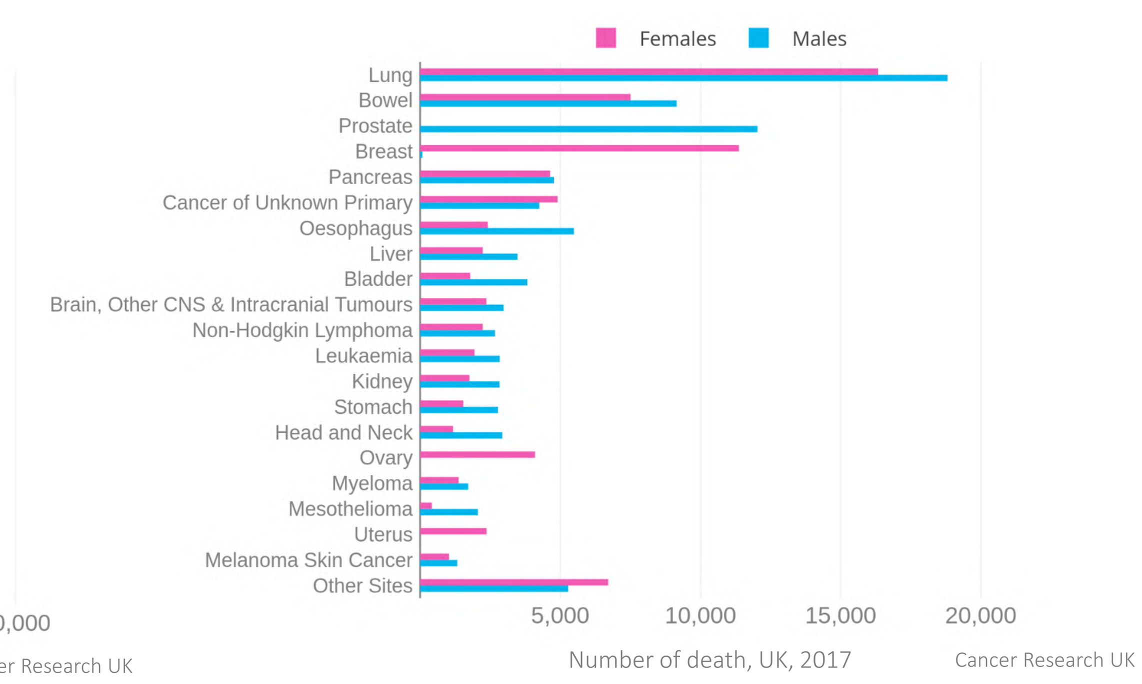


- Cancer is globally the second most common cause of death next to cardiovascular disease.
- Lung cancer is the most mortal form of cancer as a result of its high prevelance and low survival rates.
- Lung cancer (stages 1-4) has a 5-year survival rate of only 15% in developed countries.
- If lung cancer is detected at an early stage (stage 1), the 5-year survival rate increases to 55%.
- Therefore, screening for lung cancer in high-risk population groups is increasingly becoming routine practice.

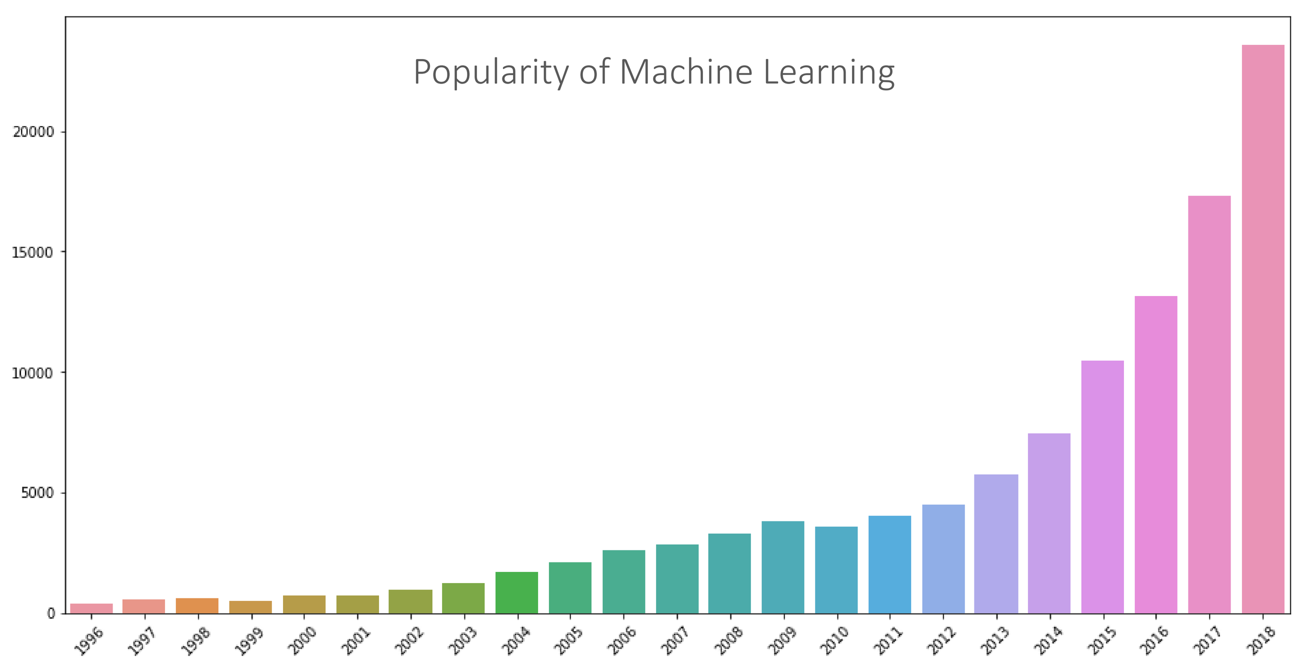


- The popularity of Machine Learning techniques has been on a tremendous surge in recent years.
- New advances in Machine Learning methods have shown to match and even out-perform human intelligence for particular tasks.
- Neural Networks and Deep Learning in specific have become computationally feasible thanks to the improvements in computational power (Moore's law) as well as larger quantities of data, data accessibility and cheaper data storage.
- the only recommended method for lung cancer screening as of today is low-dose Computed Tomography (CT) scans. These scans have to be low-dose because the epithelial lung tissue is extremely sensitive to ionizing radiation.
- This causes the scans to have a low resolution making manual interpretation prone to error, time consuming and costly. The hope is that deep learning algorithms can cope with this lower resolution.

The goal of this thesis is to use recent advances in Deep Learning to detect/diagnose lung nodules in low dose CT scans to ultimately reduce human workload, reduce medical costs and increase accuracy of diagnosis.

## LIDC-IDRI dataset

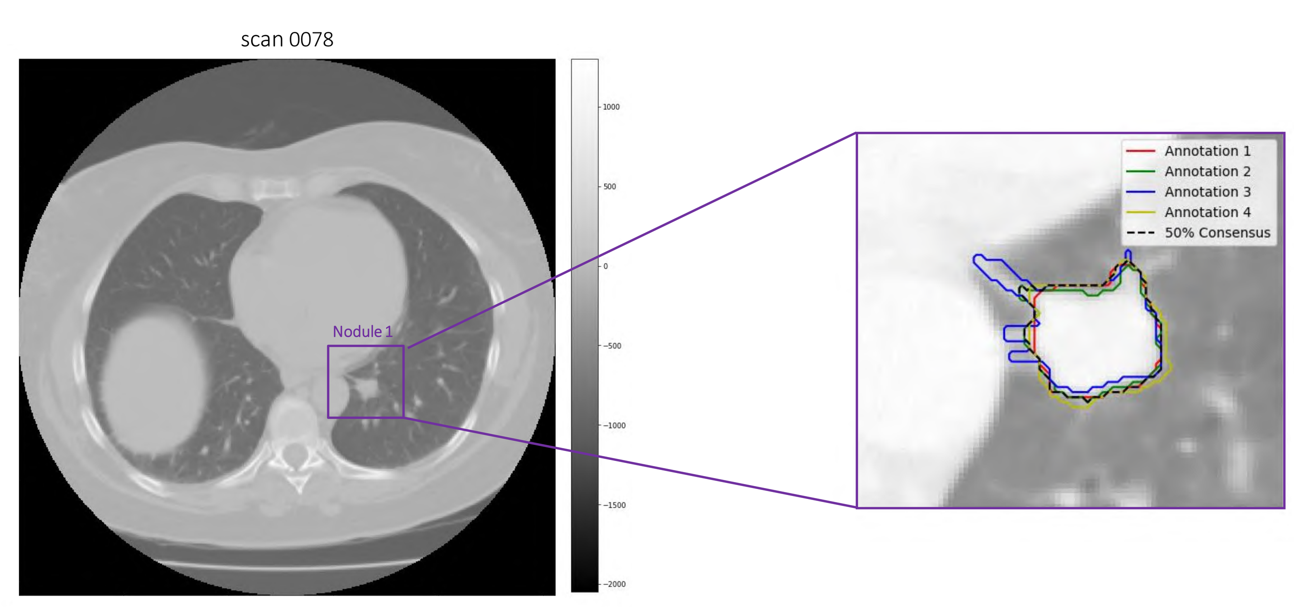


- The public LIDC-IDRI dataset from The Cancer Imaging Archive (TCIA) contains 1018 low-dose CT scans used in lung cancer screening.
- These scans were annotated by 4 radiologists independently and classified into 3 categories:
  → Nodules > 3 mm
  → Nodules < 3 mm
  → Non-nodules

## Preprocessing

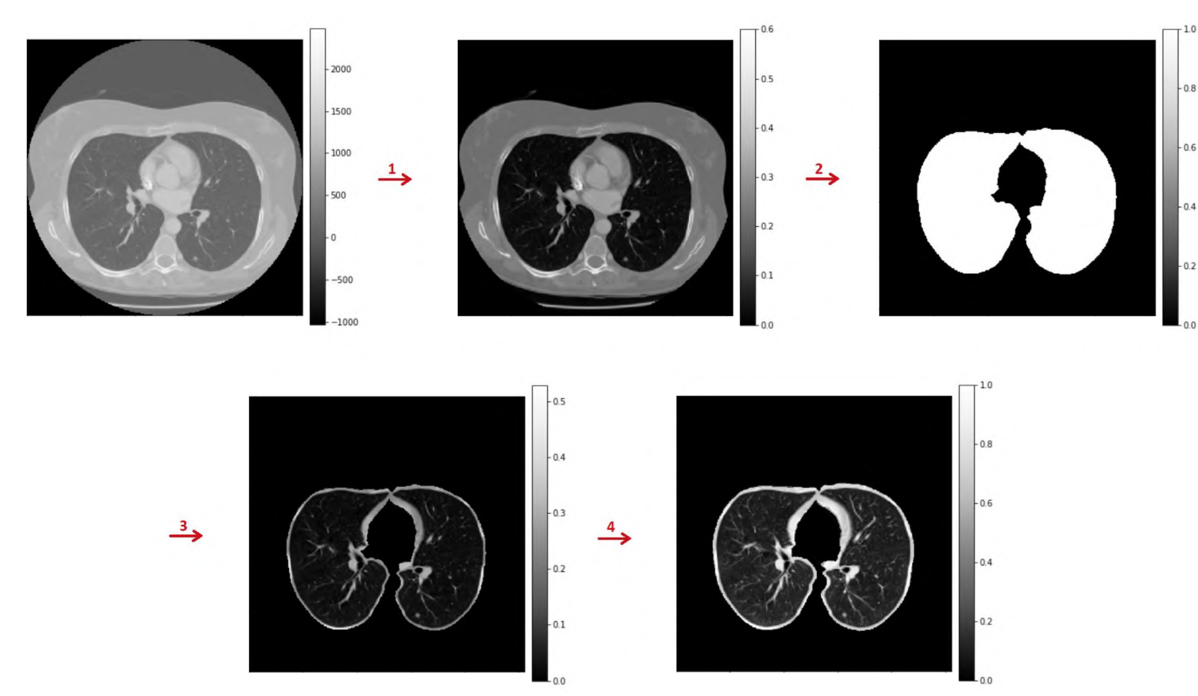


- Original scans are expressed in Hounsfield units and must be normalized.
- Lungs are segmented using an intensity-based segmentation algorithm as this is the only important structure for the Neural Network.
- Intensity is normalized and contrast is improved by rescaling outlier intensity values from the histogram of the scan.

## Detection & segmentation of nodules

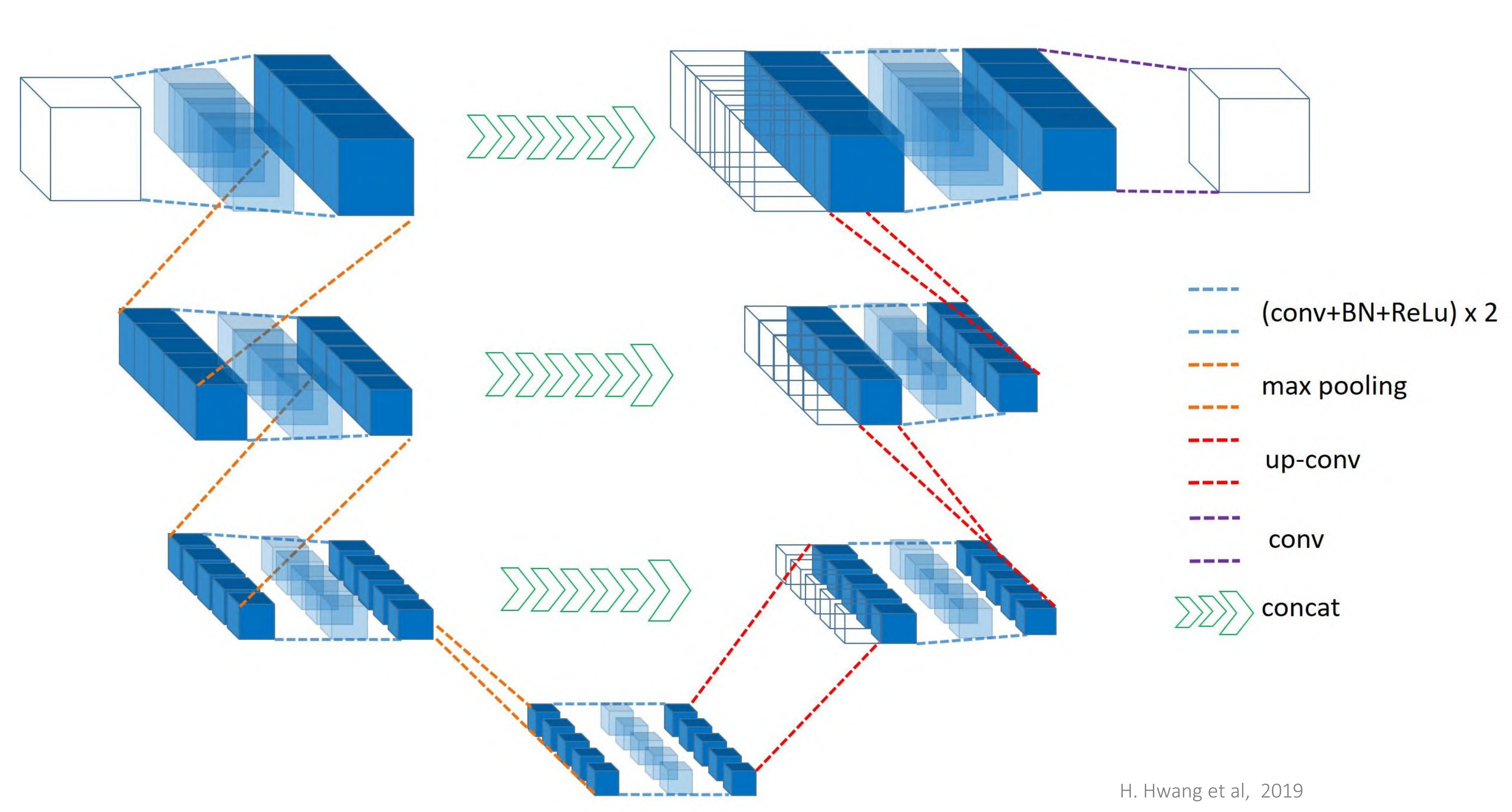


- Convolutional Neural Network (ConvNet) : 3D U-Net ⇒ detection & segmentation of nodules
- Can capture both large structures in medical images as well as high spatial accuracy on small scales due to the skip connections between layers (concat).

## Classification of nodules

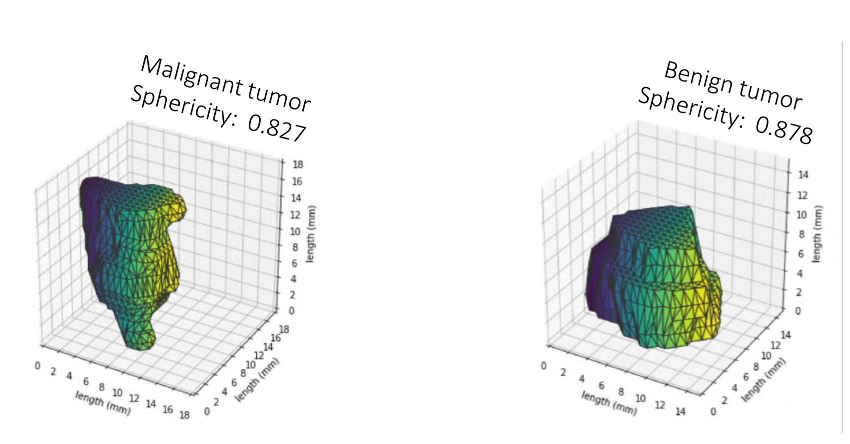


- Classification of the individual nodules based on their radiomic features.
  ⇒ Diagnosis: malignant/benign

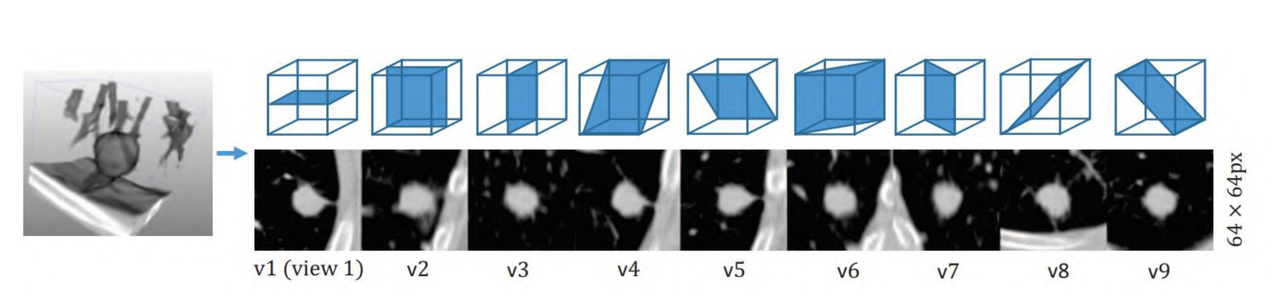


- Extract 2D patched from 9 different viewing angles from each nodules.
  ⇒ Separate ConvNet that can also learn from the features surrounding the tumor (e.g. angiogenesis) for classification of the nodules.

nathan.sennesael@ugent.be

Master of Science in Biomedical Engineering

# 4D-CT for in-vivo assessment of trapezio-metacarpal joint kinematics in osteoarthritis patients

**Adrián Gutiérrez**

Prof. Nico Buls, Prof. Erik Cattrysse, Prof. Dr. Jean Goubau, Ir. Benyameen Keelson

UZ Brussel, Faculty of Medicine and Pharmacy, Research Cluster Biomedical Imaging and Medical Physics,
Faculty of Physical Education and Physiotherapy, Research Group ARKI, Department of Orthopedic Surgery and Traumatology.

UNIVERSITEIT GENT

VUB VRIJE UNIVERSITEIT BRUSSEL

## PURPOSE OF THIS STUDY

This study aims to investigate the kinematics of the trapezio-metacarpal joint when affected by osteoarthritis, using dynamic 4D radiographic acquisition (4D-CT) during real-time in-vivo motion of the thumb. Image processing is implemented in order to analyse the kinematics of the joint and assess the effects of osteoarthritis and its therapy.

## TRAPEZIO-METACARPAL OSTEOARTHRITIS

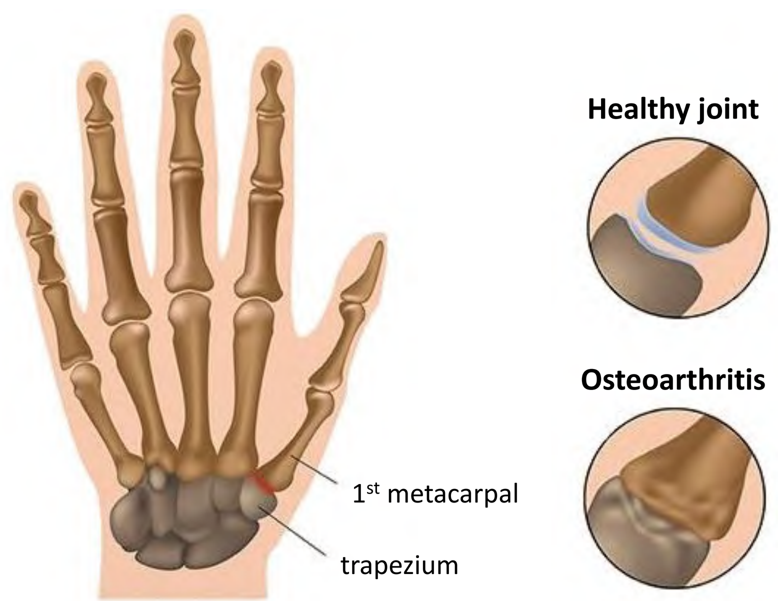


From Boulder Center for Orthopedics and Spine

-The trapezio-metacarpal joint allows us to perform a wide range of complex functions such as writing and grasping objects.

-Unfortunately, the high physical demand predisposes the joint to degenerative osteoarthritis.

-In osteoarthritis, cartilage wears down causing pain and decreasing joint function.

-Specially prevalent in post-menopausal women [1]

-Also caused by inflammatory diseases (rheumatoid arthritis) or past trauma (e.g. intra-articular fracture).

**40%** of women

**25%** of men

Prevalence after 75 years old [2]

## 4D-CT TO ASSESS JOINT KINEMATICS

From General Electric (GE) Healthcare

-With 4D-CT, several 3D reconstructions of the joint can be recorded over time

-Performing movements of the thumb during the scan, the motion of the different bones in the field of view can be recorded and analyzed.

**AIMS OF IN-VIVO MEASUREMENT OF JOINT MOTION**

-Understand kinematics of joint pathology.

-Quantify changes induced by therapy.

-Evaluate outcome of clinical treatment

## WORKFLOW: FROM 4D-CT TO KINEMATICS ANALYSIS

### Acquisition

-Static CT acquisition.

-Dynamic 4D-CT acquisition, during thumb opposition and retropulsion motion.

-Goal: scan 30 patients with different degrees of osteoarthritis, including pre- and post-treatment acquisitions. Healthy, asymptomatic volunteers are also included for comparisons.

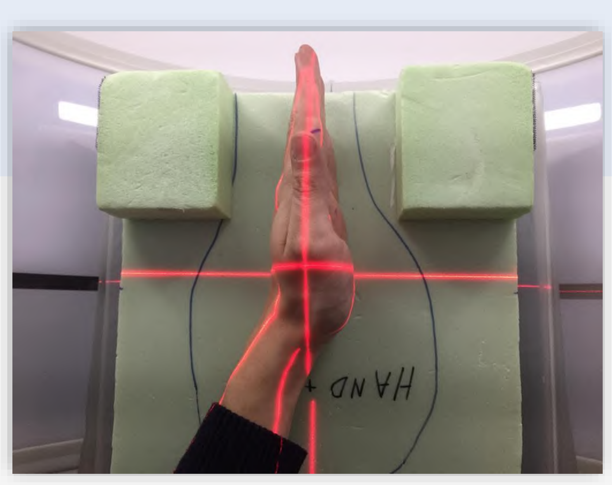


### Image processing

-Segmentation of static image to obtain anatomy. Partial segmentation of bones of interest in dynamic images.

-Rigid registration of dynamic images onto static image using Simple ITK in Python.

-Transformation matrices are calculated from rigid registration.

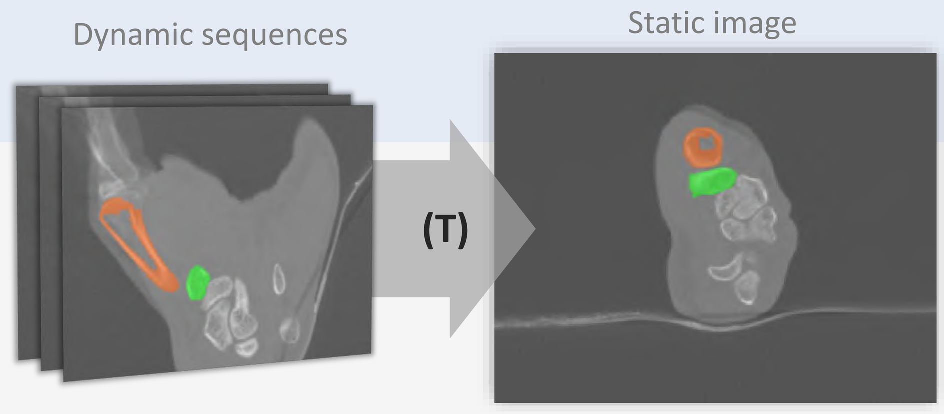


### Kinematics analysis

-Definition of system of coordinates from anatomical landmarks.

-Calculation of relative motion between trapezium and first metacarpal.

-Calculation of helical axes and joint proximities.

-Intra-subject and inter-subject comparisons.

From Kerkhof F. et al. [3]

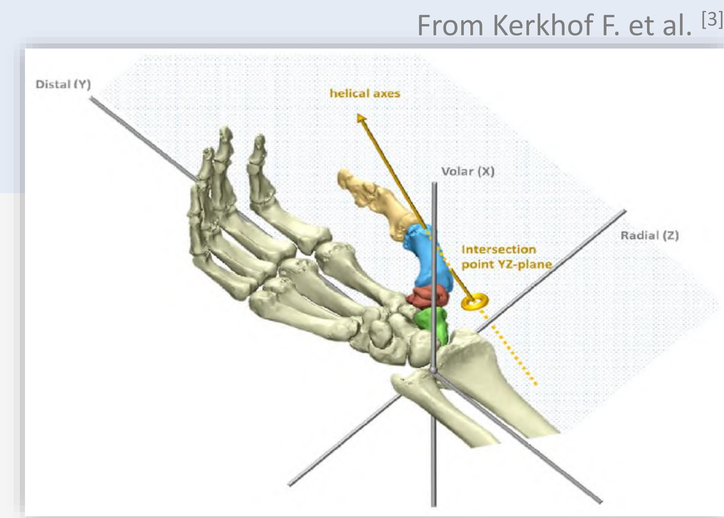

## WHAT HAS BEEN DONE SO FAR?

**CLINICAL STUDY**

-Approval of Ethical Committee of UZ Brussel in order to include patients in the study.

-Elaboration of protocols, documentation and design of the study workflow, which involves hand surgeons, physiotherapists, radiologists, nurses and technicians.

-Currently waiting for patients to participate in the study.

**FIRST ACQUISITIONS**

-From healthy subjects (volunteers).

-After validation of scan protocol the modality chosen is Cine, a continuous acquisition without table movement and tube rotation time 0.28s.

-Segmentation of 4D-CT sequences has been performed with ITK SNAP.

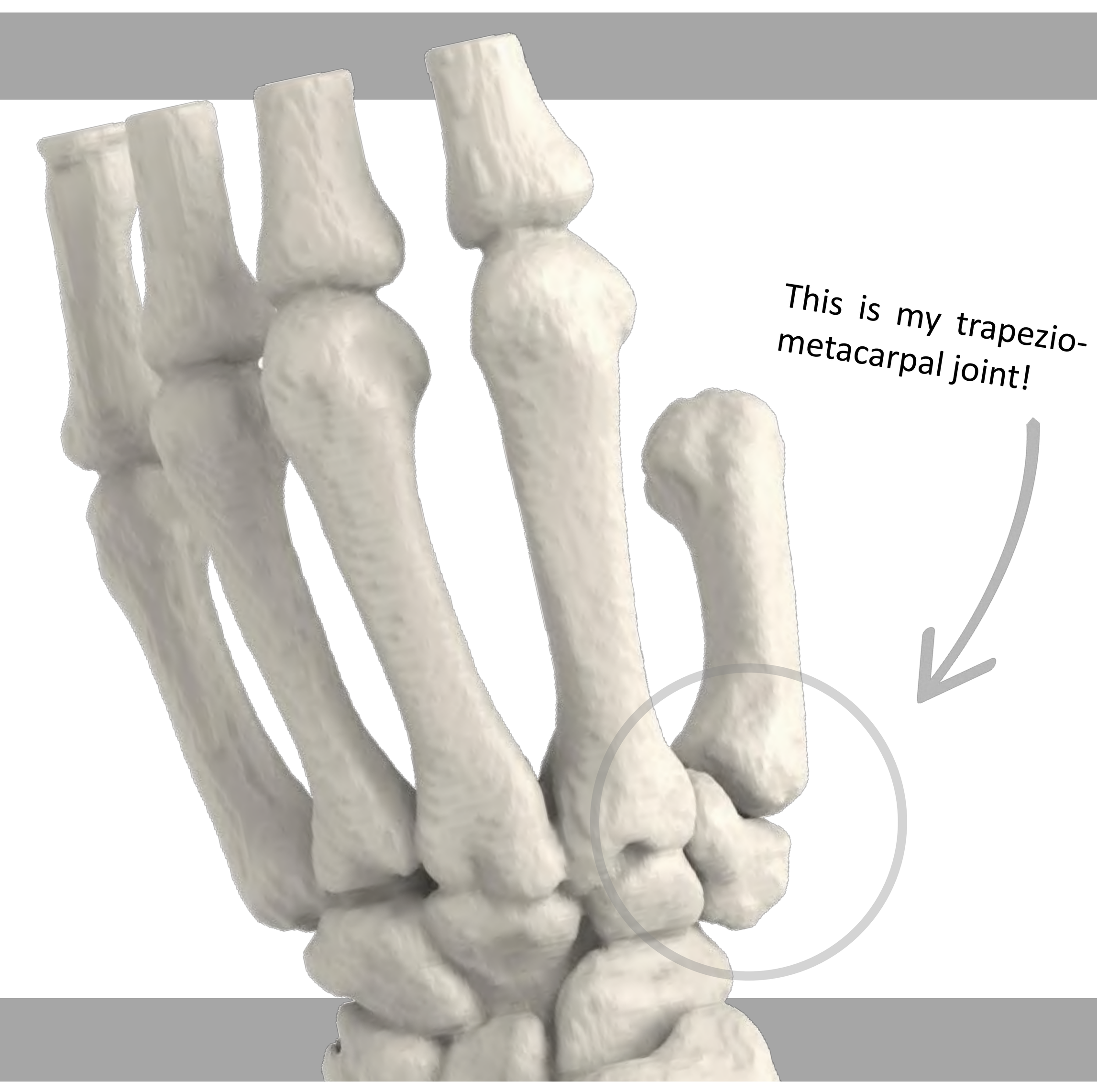


## REFERENCES

[1] Armstrong, A. L., Hunter, J. B., & Davis, T. R. C. (1994). The prevalence of degenerative arthritis of the base of the thumb in post-menopausal women. *Journal of hand surgery*, *19*(3), 340-341.

[2] Becker, S. J., Briet, J. P., Hageman, M. G., & Ring, D. (2013). Death, taxes, and trapeziometacarpal arthrosis. *Clinical Orthopaedics and Related Research*, *471*(12), 3738-3744.

[3] Kerkhof, F., Brugman, E., D'Agostino, P., Stockmans, F., Jonkers, I., & Vereecke, E. (2013). Determining thumb opposition kinematics using dynamic CT: Opportunities and challenges for musculoskeletal modelling. In *Congress of the International Society of Biomechanics, Date: 2013/08/04-2013/08/09, Location: Natal, Brazil*.

adrian.ruiz.gutierrez@vub.be

Master of Science in Biomedical Engineering

# Dynamic dual energy CT for simultaneous ventilation and perfusion imaging

**Arwen Van Wittenberghe**

Prof. Nico Buls, Dr. Gert Van Gompel

Department of Radiology, UZ Brussel, VUB
Laarbeeklaan 101, 1090 Brussels, Belgium

## Lungs: Our natural filter

Particles
Chemicals
Infectious organisms

Lungs → Diseases

- Chronic Obstructive Pulmonary Disease
- Astma
- Respiratory Tract Infections
- Tuberculosis
- Lung Cancer

1 billion people
All in top 30 most common causes of death

Diagnosis + Monitoring

Lungs

## Dual energy CT

X ray attenuation → image contrast
depends on Compton scatter and photoelectric effect
depends on atomic number and energy

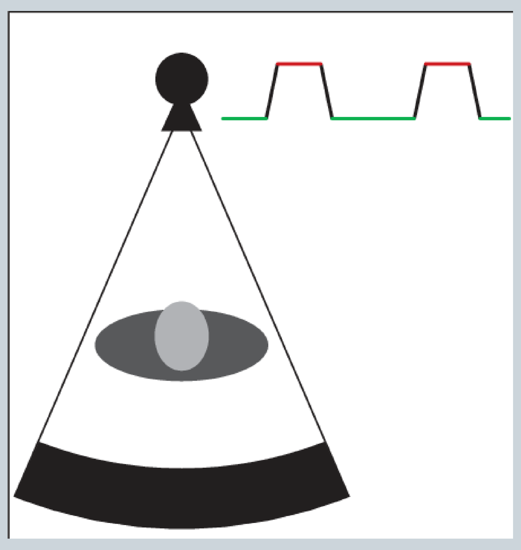

DECT

Rapid kilovoltage switching
One tube
Switch tube voltages
One detector

→ Determine tissue composition
Better contrast
Reduced artifacts

## Ideas are like rabbits…

… you get a couple and learn how to handle them, and pretty soon you have a dozen

Rabbit

A preclinical animal experiment [1] was performed with six rabbits, to investigate the functionality of the lungs in normal conditions and in provoked bronchoconstriction.

## Perfusion vs ventilation

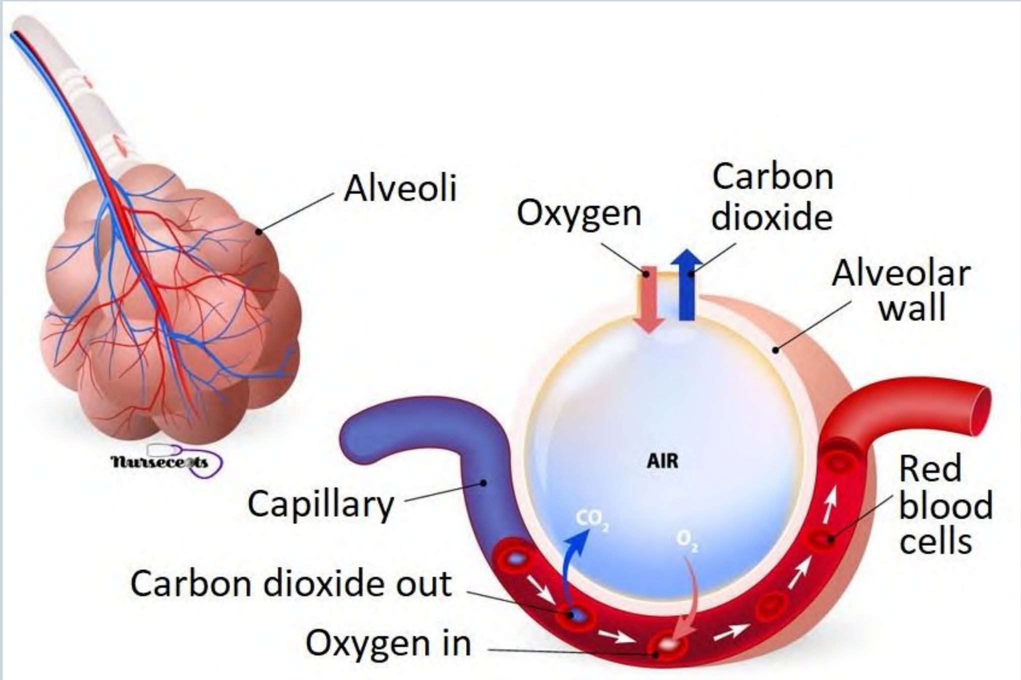


Alveolar gas exchange

**Ventilation**
= transport of air

Visualized by inhalation of Xenon gas

**Perfusion**
= transport of blood through capillaries

Visualized by IV administration of Iodine or Gadolinium

### Regional lung ventilation by Xenon enhanced imaging

| Contrast agent | Atomic number | K edge (keV) |
|---|---|---|
| Xenon | 54 | 34,6 |
| Iodine | 53 | 33,2 |
| Gadolinium | 64 | 34,6 |

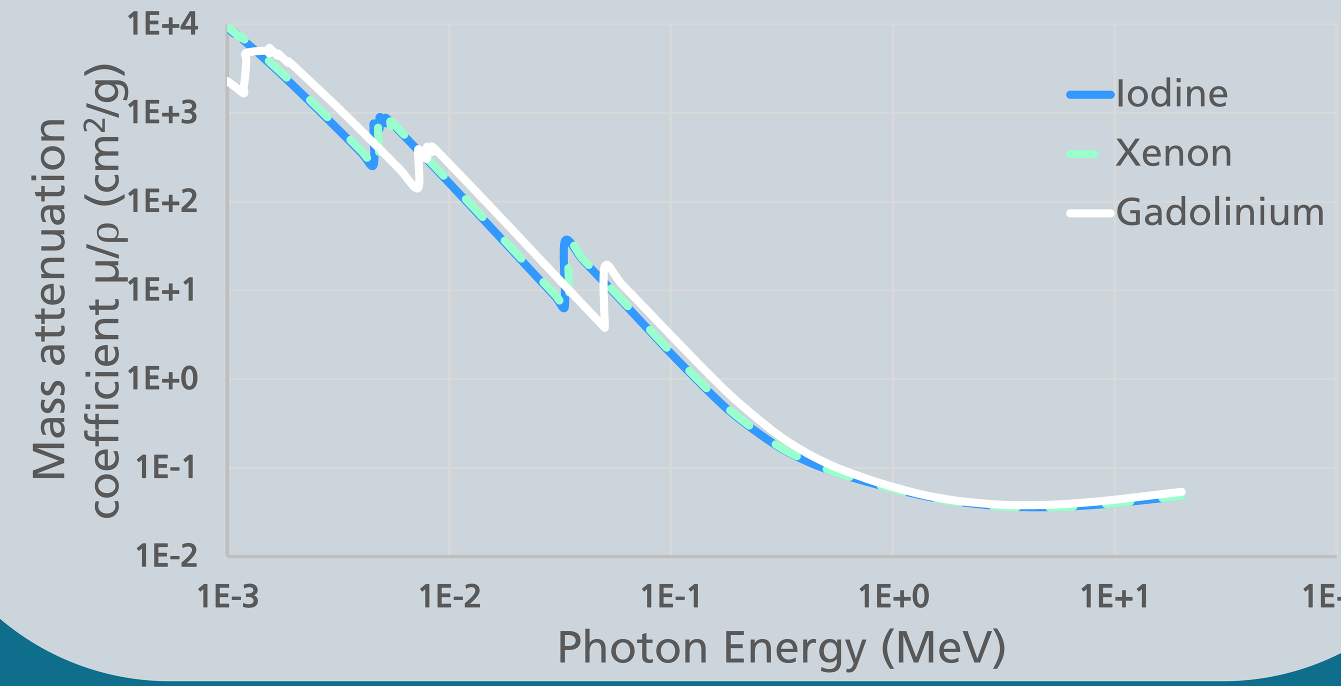


## Benefits

| | | | Information: | | lung function: |
|---|---|---|---|---|---|
| Current techniques | ⇒ | Spirometry<br>Plethysmography<br>Pulmonary function tests | = Quantitative | + | Global |
| VS | | | | | |
| Dual Energy CT imaging | ⇒ | Simultaneous ventilation and perfusion | = Quantitative and **Qualitative** | + | Global and **Regional** |

### References

Lungs: Dalley A, Your lungs are really amazing. An anatomy professor explains why, *The conversation, March 2019*
DECT: Johnson, T. R. (2012). Dual-energy CT: general principles. *American Journal of Roentgenology, 199*
Rabbit: IXXI Print 315 Rabbit
[1] described in Rubio, E.I. Quantification of regional and temporal lung ventilation properties in xenon enhanced dual energy CT imaging, 2019
Alveolar gas exchange: Nursecepts, 9 Facts About The Respiratory System Every Nursing Student Should Know
NIST Standard Reference Database 126
Forum of International Respiratory Societies. The Global Impact of Respiratory Disease – Second Edition. Sheffi eld, European Respiratory Society, 2017

Arwen.Van.Wittenberghe@vub.be

Master of Science in Biomedical Engineering

# Finite element modeling and design optimization of 3D printed scoliosis braces for patient specific healthcare

**Caydie Van Brabant**

Prof Wim Van Paepegem, Dr. M. Cristiana Costa

Mechanics of Materials and Structures, Ghent University, Gent , Belgium

GHENT UNIVERSITY

VUB VRIJE UNIVERSITEIT BRUSSEL

Interreg 2 Seas Mers Zeeën 3DMed

VIGO helping people move on

## ADOLESCENT IDIOPATHIC SCIOLIOSIS

Adolescent idiopathic scoliosis is a complex **three dimensional deformity of the spine and trunk** with the onset before skeletal maturation. Although the 3D aspect of the deformity, it is generally defined as a lateral deviation of more than 10° in the frontal plane. It is a highly prevalent disease, affecting 2-4% of children between the age of 10-18 years old [1]. **Brace treatment** is prescribed in case of mild deformities, i.e. Cobb angle below 40°. The treatment consists of wearing a rigid brace around the trunk ranging from 14h to 24h a day [1]. The brace stabilizes the spine via a **3 point pressure system**, which consists of a main force acting on the convex side of the curvature, and a proximally and distally applied counterforce. One of the main limitations of brace treatment is the discomfort (e.g. sweating, pressure points, etc.), resulting in **low patient compliance** [2].

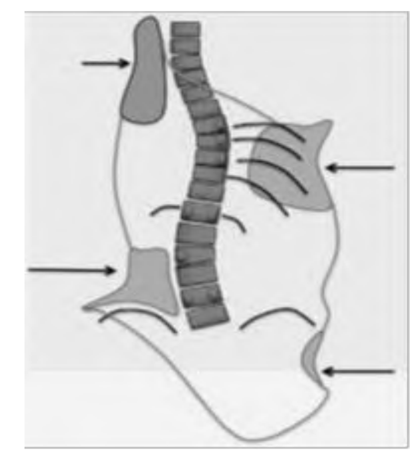

3 point pressure system [2]

**References** [1]Jada A. et al. 2017, [2]Stokes I. 1994

**Acknowledgments** The authors gratefully acknowledge the support of the European Regional Development Fund from Interreg 2 Seas (contract nr. 2S04-014_3DMed) of the 3DMed project and the technical orthopedics company VIGO

## PATIENT SPECIFIC FEM BRACE - TRUNK

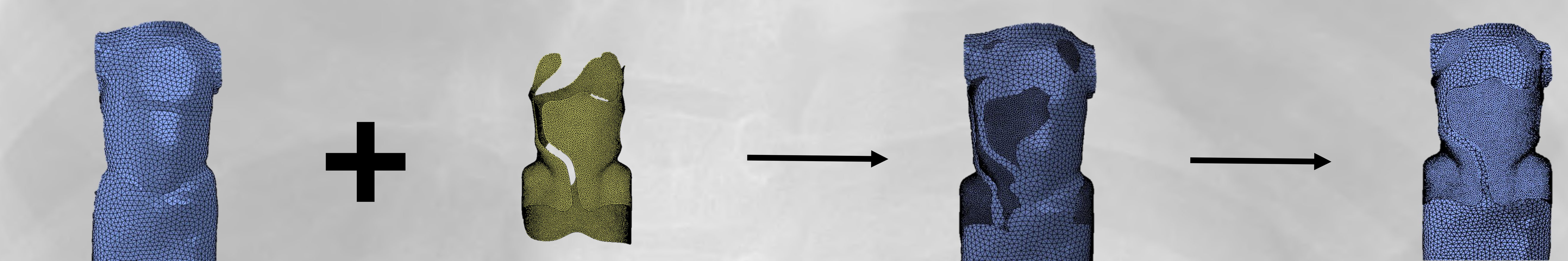

**External geometry**
3D surface scan

**Reference brace**
CPO Vigo

**Alignment brace - trunk**

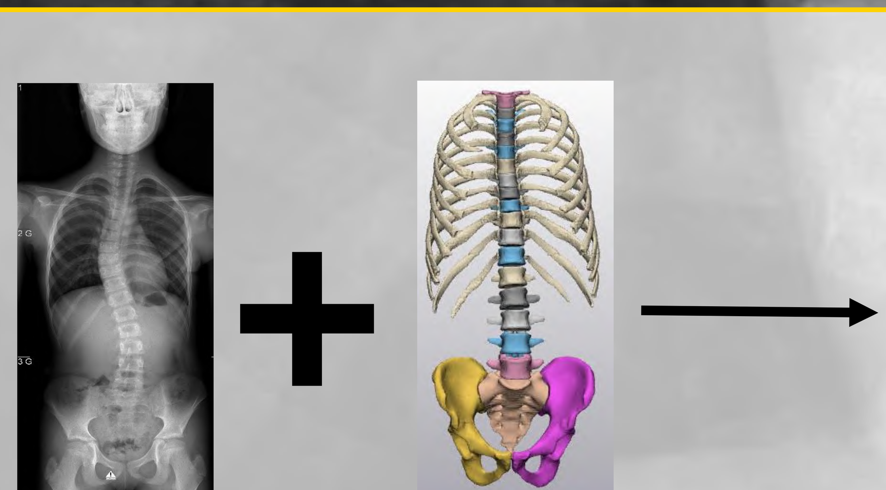

**Internal Geometry**

**X-ray** **VHP**

Inclusion internal geometry in FEM trunk by deforming segmented spine of Visible Human Project (VHP) data according to patient specific measures from the X-ray and alignment with external geometry.

**Parts and mesh**
- Brace: shell with 34637 3-noded triangular elem.
- Trunk: solid with 643522 4-noded triangular elem.

**Boundary conditions**
- Top nodes: U1 = U2 = UR1 = UR2 = 0
- Bottom nodes: ENCASTRE

**Contact**
- Surface to surface with friction

**Method**
- Nodal displacement
- Force displacement
- Interference fit via general contact

## DESIGN OPTIMIZATION

**Requirements**
- Breathability
- Stiffness gradient
- Weight reduction

**Strategies**
- Hole pattern
- Thickness gradient

## OPTIMAL DESIGN?

**Post-processing**
**Reference vs new brace**
- Pressure distribution trunk
- Distance map at brace-trunk interface
- Spinal correction
- Weight reduction

NO

YES

## 3D PRINTING

Caydie.vanbrabant@ugent.be

# Development of polymer membranes to function in in-vitro models to evaluate ocular drugs

**Dilna Varghese**

Prof. Sandra Van Vlierberghe

Prof. Katrien Remaut

Laboratory of Polymer Chemistry, Laboratory of General Biochemistry and Physical Pharmacy, Ghent University, Gent, Belgium

## 1 What is hindering IVT drug administration?

- ❑ 2.2 billion people worldwide suffer from vision impairment
- ❑ Retinal diseases continue to be leading causes
- ❑ Intravitreal (IVT) injection is a safe and minimally invasive treatment
- ❑ Success of IVT injection hindered by physical barriers
- ❑ Inner limiting membrane (ILM) obstructs the transfer of drug carriers to the retina

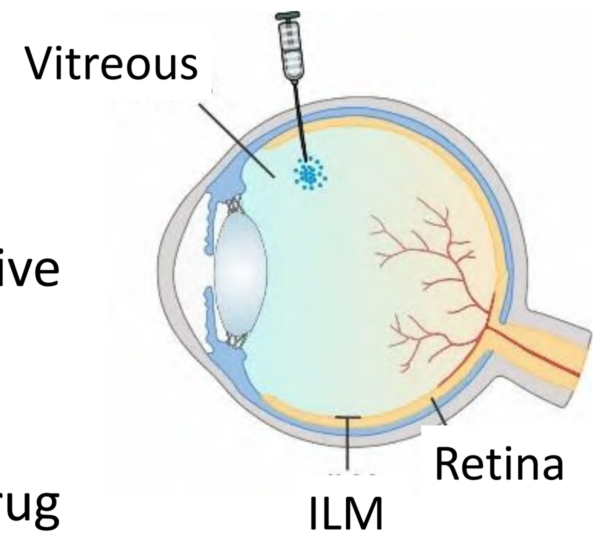


(Peynshaert et al., 2017)

## 2 Overcoming this barrier

**Use of photoporation:**

- ❑ ILM is stained with Indocyanine green (ICG), a photothermal dye
- ❑ Laser pulses induce vapor nanobubbles (VNBs) in the membrane
- ❑ These VNBs collapse to form pores, disrupting the ILM surface

## 3 Representing this concept in an in-vitro model

- ❑ Bovine retinas are physiologically similar to human retinas but their ILMs lack thickness
- ❑ This raises the need to develop an artificial ILM from polymers to accurately represent the human ILM
- ❑ Polymer membranes + ICG stain + bovine retinal explants + (high-energy) short laser pulses → local pore formation

## 4 Developing the in-vitro model

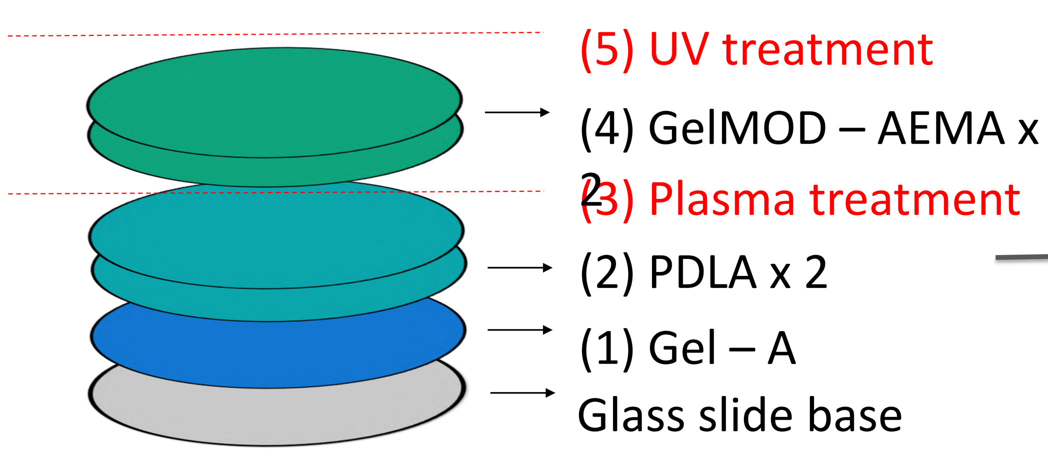


(a) Artificial ILM preparation by spin-coating

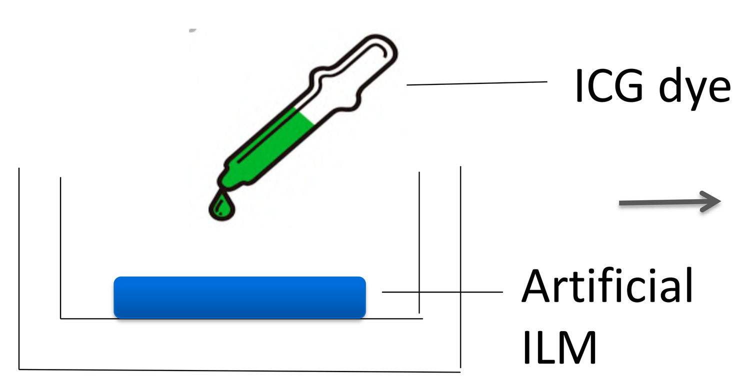


(b) ICG-staining of ILM

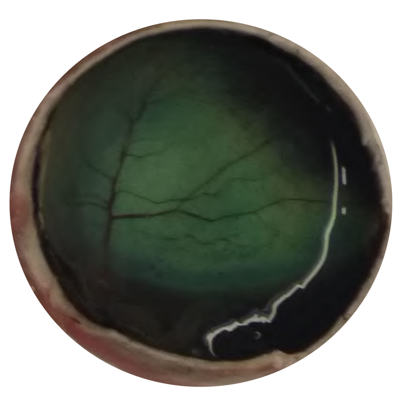

(c) Bovine retinal dissection

**ICG-stained ILM + retina**

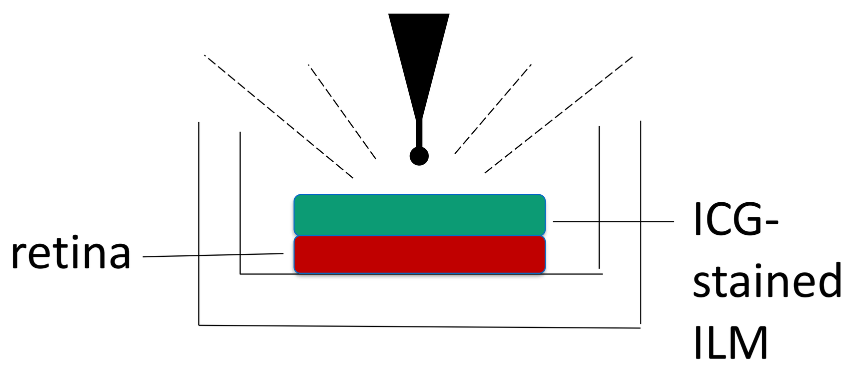


(d) Laser photoporation

(e) Scanning electron microscopy (SEM)

**SEM of artificial ILM + retina**:

- ❑ Numerous pores scattered across the artificial ILM surface
- ❑ Further optimization necessary to tell us whether the pores are indeed from the laser treatment or from the preparation

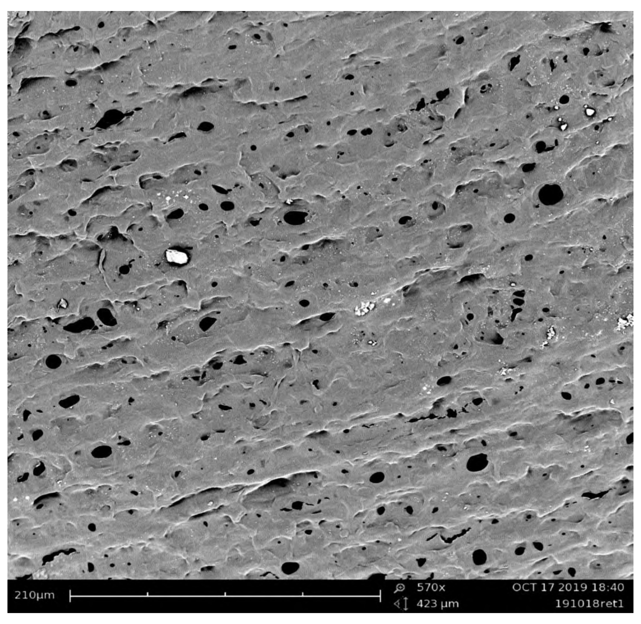

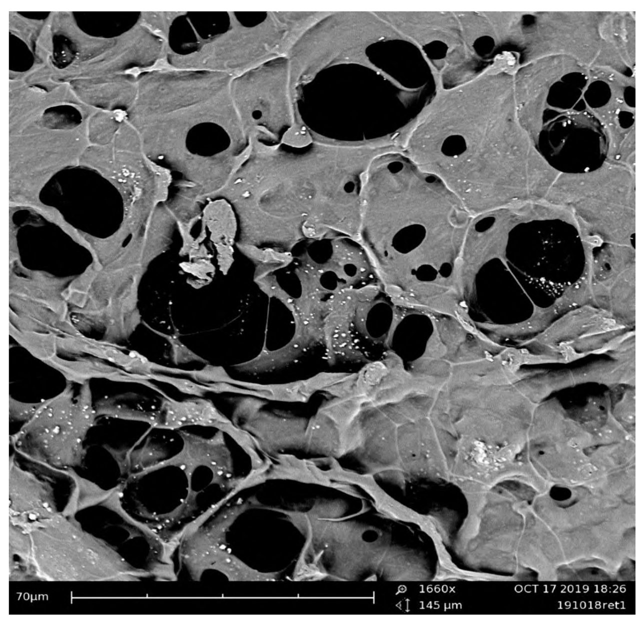

## 5 Future perspectives

- ❑ Doctor-blading is being explored as an alternative for spin-coating
- ❑ Characterizing the membrane thickness and transparency
- ❑ Optimizing membrane thickness, ICG concentration and laser power to form pores of optimal sizes

## 6 Reference

K. Peynshaert, J. Devoldere, V. Fradot, S. Picaud, S.C. De Smedt, K. Remaut, Toward smart design of retinal drug carriers: a novel bovine retinal explant model to study the barrier role of the vitreoretinal interface, Drug Deliv. 24 (2017) 1384–1394.

# Exploring deep-learning-based tracking algorithms for real-time tumour tracking on 2D radiography

**Evelien Smets**, Ir. Jennifer Dhont, Prof. Dr. Ir. Jef Vandemeulebroucke
Vrije Universiteit Brussel, Department of Electronics and Informatics, Belgium

## Radiotherapy

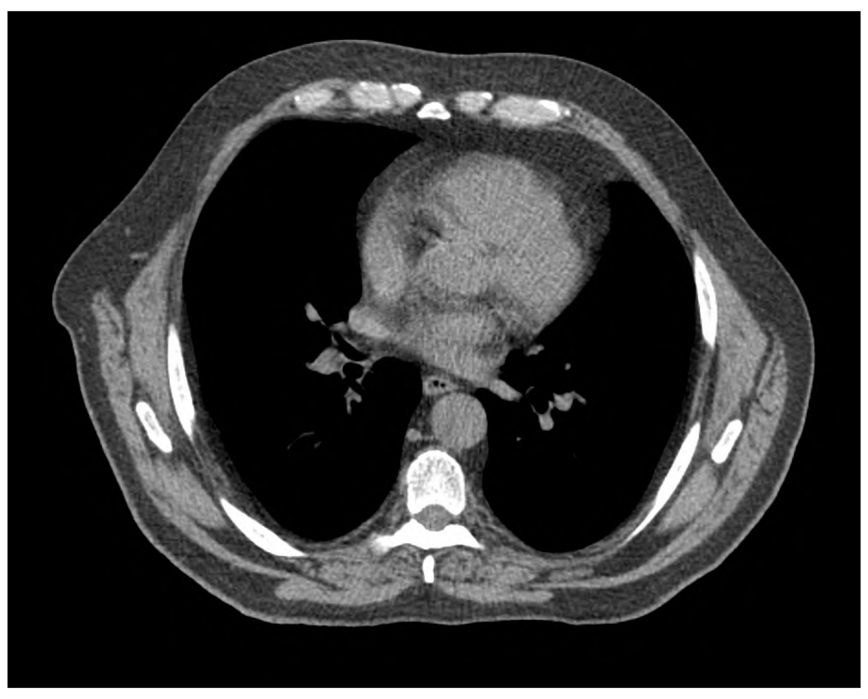

Axial view of 1 phase of the 4DCT

### Imaging

Image guided radiotherapy uses advanced imaging and image registration. This improves target definition, patient setup and intra-fraction monitoring, resulting in conformal doses and smaller high-dose volumes.

Conventional radiotherapy limits the pre-treatment imaging to a 3D-CT image.

### Respiratory induced motion

Due to respiration the internal organs and structures can move up to several centimetres. This requires the use of a pre-treatment 4D-CT (3D + time).

### Motion management

A passive technique is motion encompassing. This causes more healthy tissue to be irradiated.
Active techniques include respiratory gating, breath holding and tumour tracking.
Tumour tracking does not elongate the treatment time and is therefore the most promising active technique.
But it requires real-time tumour localization:

- Directly
- Via an internal surrogate
- Via an external surrogate and correlation model

Direct tracking is challenging but has no disadvantage of needing to verify the correlation and has higher geometrical accuracy.

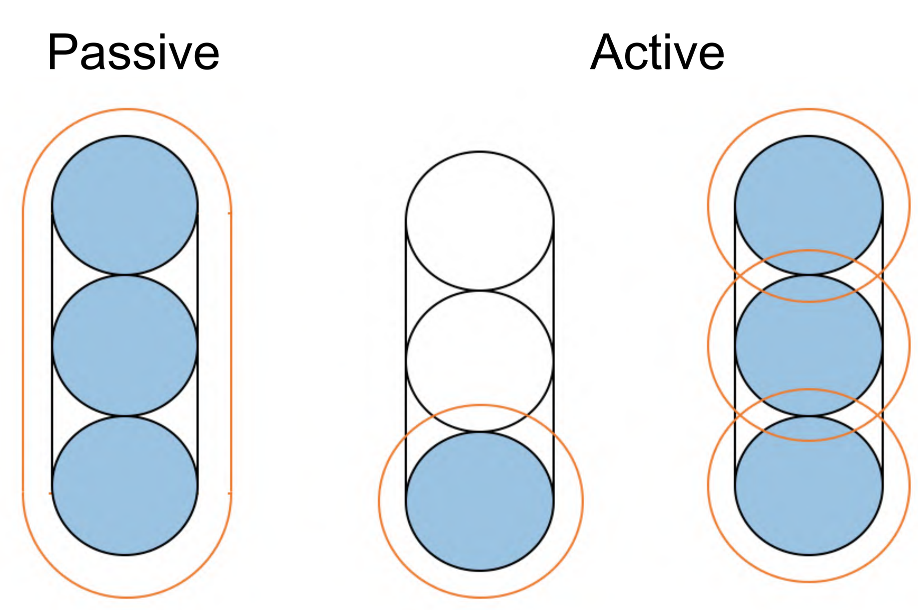


Visual representation of motion management techniques

## Goal 1: Finding a way to generate training data

Tracking is done in real-time on 2D radiographs of the patient, taken during the treatment fraction.

However to train the deep-learning network a sufficient number of radiographs are needed.
Therefore, a trick is needed to go from a pre-treatment CT volume to a 2D radiograph.
This step is realized by the use of the DeepDRR framework:

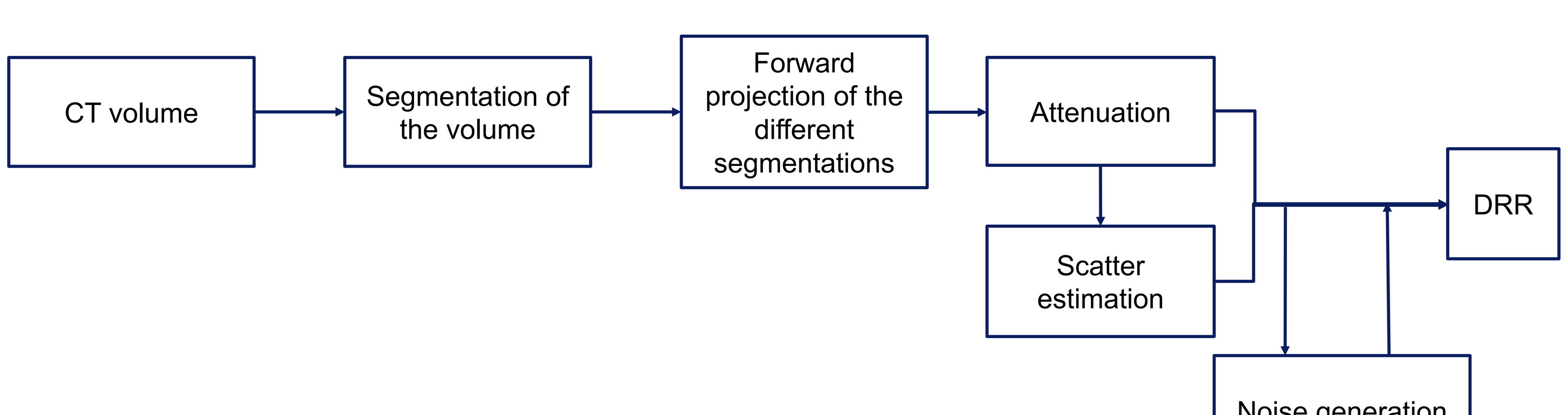


Schematic overview of DeepDRR

A 4D-CT is limited to 10 phases in the breathing cycle, but to get enough training data an interpolation has to be done. This results in a representation of the complete respiration cycle.

## Goal 2: Evaluate which deep-learning methods perform on medical images

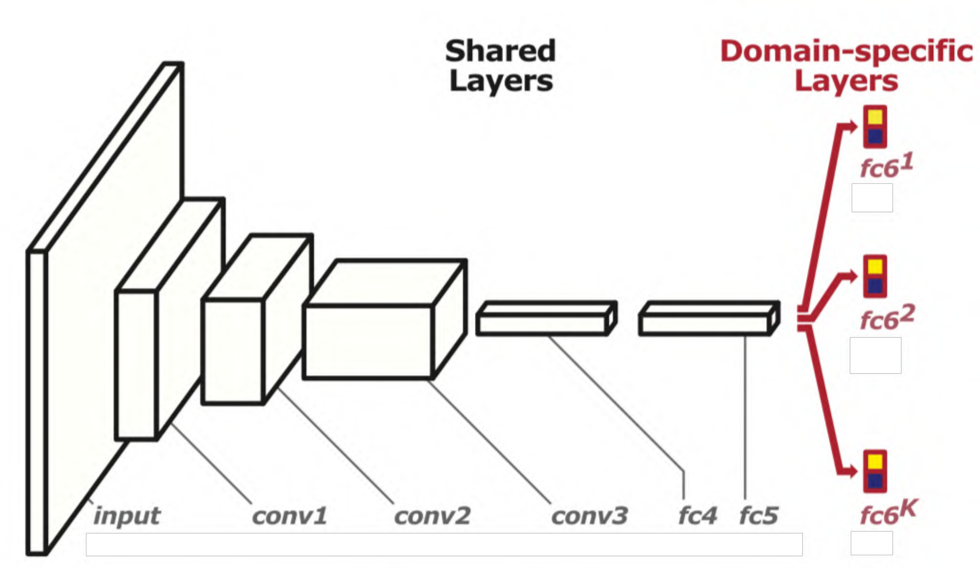


Visual representation of the MDNet, conv stands for convulutional layer, fc for fully connected layer

Deep-learning (DL) is a subfield of machine learning. It tries to imitate the brain by creating patterns.

Object tracking is currently done in the field of computer science.
In this work, multiple promising DL networks are adapted to work on DRRs
Proposed networks are

- ROLO: recurrent YOLO
- MDNet
- DeepSORT

### References:

P J Keall, et al. "The management of respiratory motion in radiation oncology report of AAPM Task Group 76 a"
M Unberath, et al. "Deepdrr–a catalyst for machine learning in fluoroscopy-guided procedures"
P Meyer, et al. "Survey on deep learning for radiotherapy".
A Sachan. Zero to Hero: Guide to Object Detection using Deep Learning: Faster R- CNN, YOLO, SSD. 2017.
Hyeonseob Nam and Bohyung Han. "Learning Multi-domain Convolutional Neural Networks for Visual Tracking".

# Surface properties and surface treatments of Additive Manufactured Titanium alloy for biomedical applications


GHENT UNIVERSITY

**Farah Ibrahim**

Iris Degraeve

VUB VRIJE UNIVERSITEIT BRUSSEL


## Additive Manufactured Ti6Al4V in biomedical applications

**What is additive manufacturing (AM)?**
A technique that produces objects at their near-net shape structures by adding one layer at a time

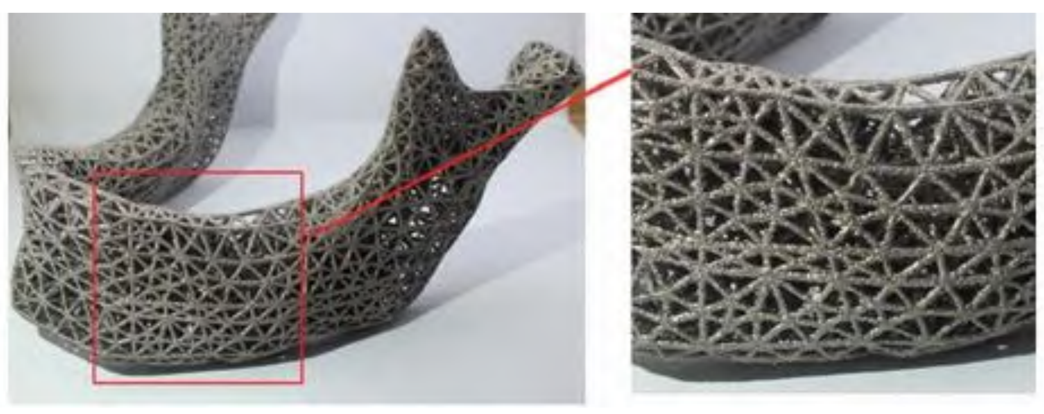

Liu et al (2019) additive manufacturing of Ti6Al4V. Prothesis scaffold

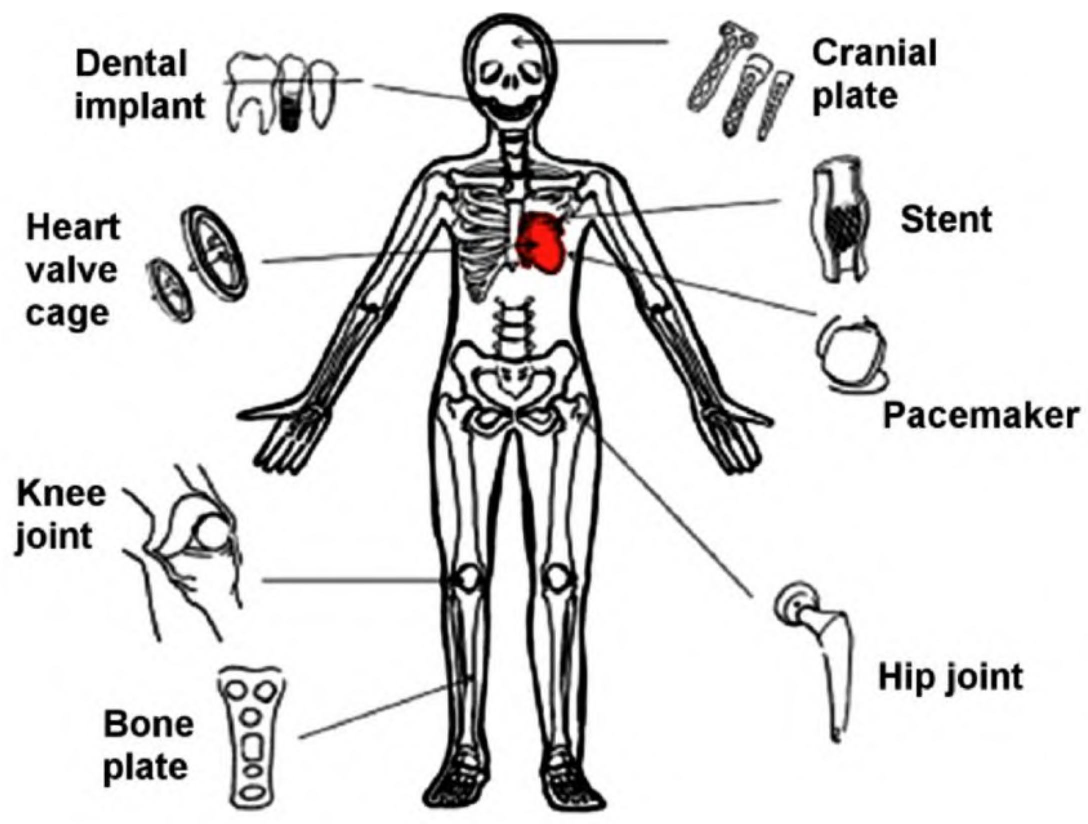


Stróż et al. (2018) electrochemical formation of oxide layers

Titanium alloy (Ti6Al4V) is one of the most used metals in biomedical applications

**Why Ti6Al4V?**

- high strength to weight ratio
- Bio-compatible
- Corossion resistance

**Investigation and research of the properties of AM Ti6Al4V is of great importance for the development of new generation of implants.**

## Microstructure and corrosion behaviour

**Microstructure**

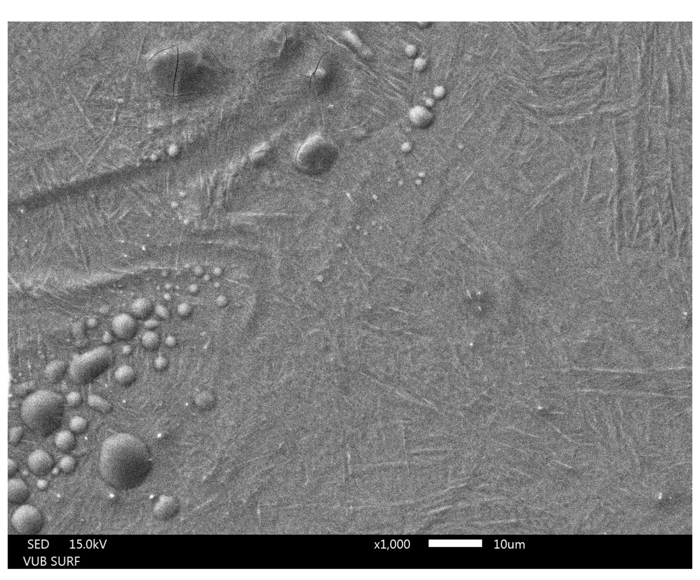

Fine needle alpha prime martensite

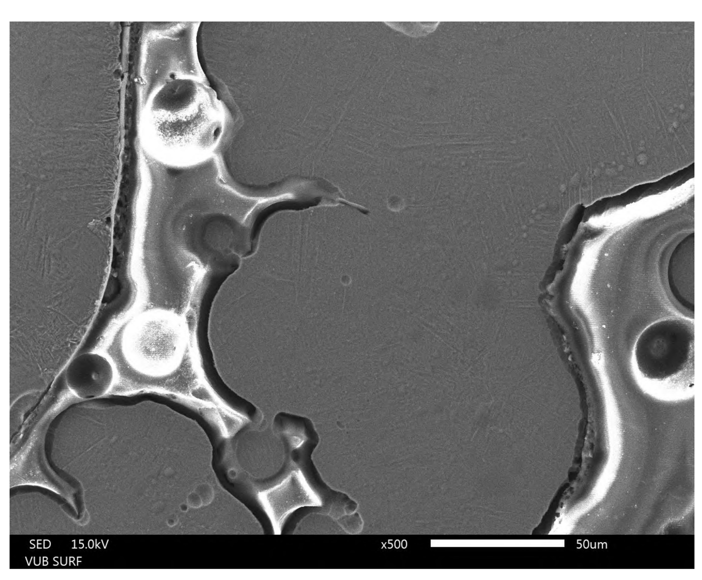

Existance of lack-of-diffusion pores across the surface

**Corrosion behaviour**

Corrosion experiments are performed in an electrochemical cell using 3,5wt% Nacl

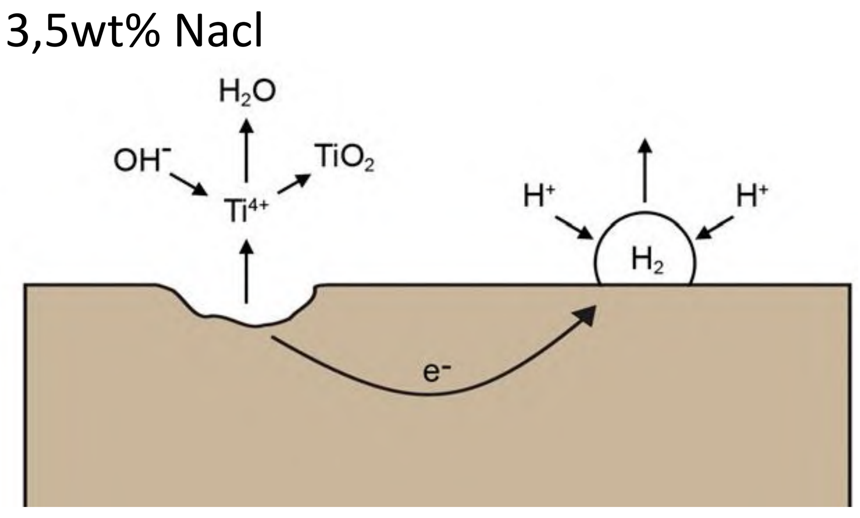


$Ti \rightarrow Ti^{4+} + 4e^-$
$4H^+ + 4e^- \rightarrow 2H_2$
$Ti^{4+} + 4OH^- \rightarrow TiO_2 + 2H_2O$

Bajat et al.(2014)

**Experimental results**

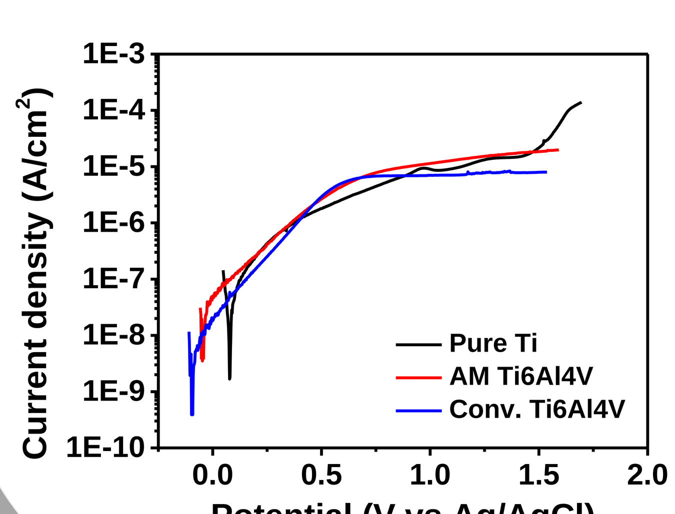


**Observations**

- $Ecorr_{pure\_Ti} > Ecorr_{AM}$
- $Ecorr_{AM} \approx Ecorr_{conventional}$

## Anodization experiments

L:

**Anodization**
An electrochemical process that consists in the formation of an oxide layer, which protect the material against corrosion.

**Anodizing technique**
The metal is placed in the anode and embedded in $H_2SO_4$.

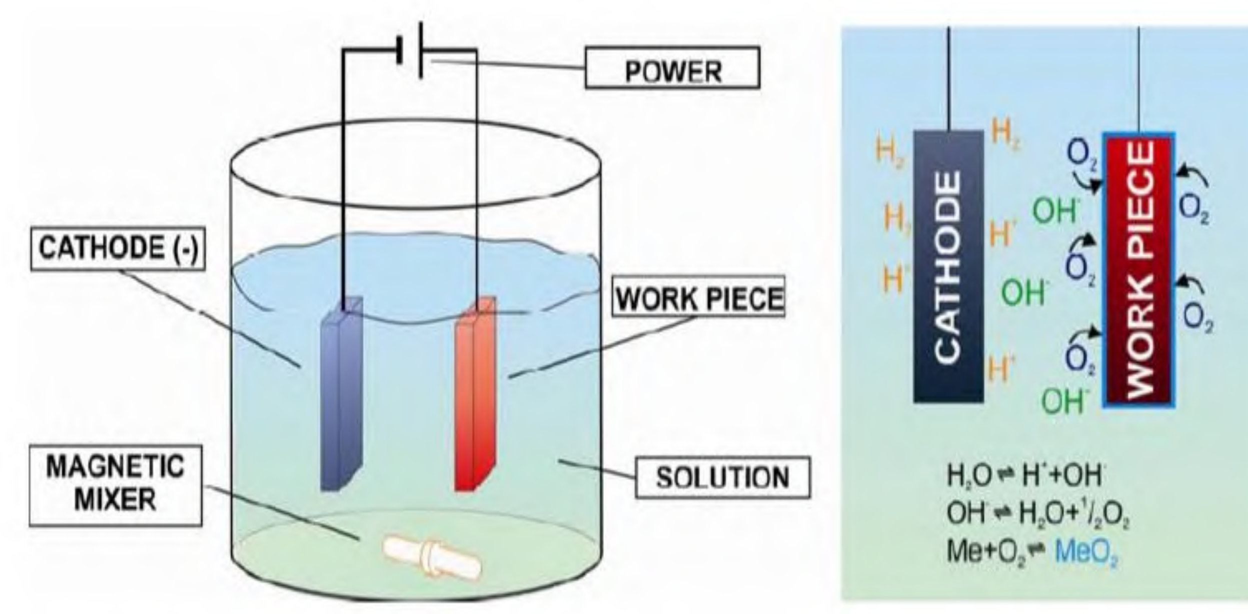


Katona et al. Anodization of medical grade titanium

$Ti \rightarrow Ti^{4+} + 4e$
$Ti^{4+} + 2H_2SO_4 \rightarrow TiO_2 + 4H^+$

**Experimental results**

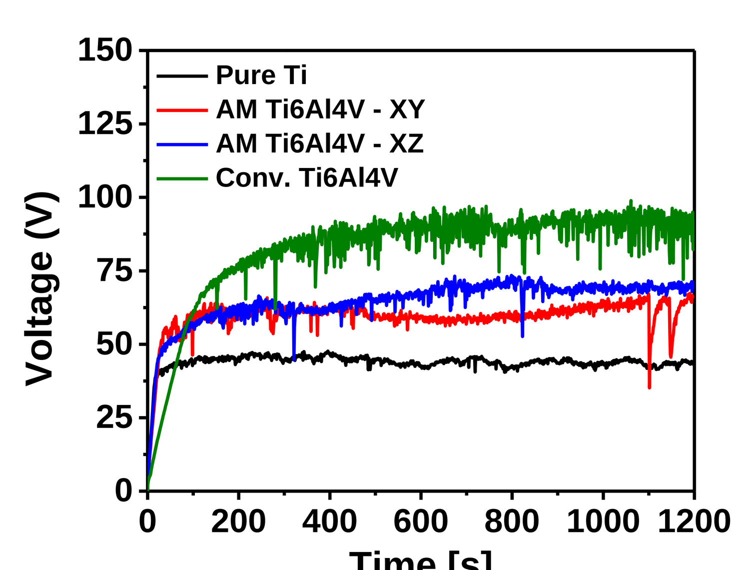


**Observations**

- $V_{conventional} > V_{AM} > V_{pure\_Ti}$
- $V_{AM\_xy} \approx V_{AM\_xz}$

## What have we learned?

1. The oxide layer of the AM Ti6Al4V is thicker than the oxide layer of the pure Titanium, indicating a better corrosion resistance.
2. The conventional manufactured Ti6Al4V shows the thickest oxide layer.
3. The conventional manufactured Ti6Al4V and the AM Ti6Al4V exhibit a high resistance against pitting.


Farah.falih.ibrahim@vub.be


Master of Science in Biomedical Engineering

# Multi-material 3D printing of self-healing soft robots

GHENT UNIVERSITY

**Ikram Mohout**

prof. dr. ir. Bram Vanderborght, dr. ir. Seppe Terryn

VRIJE UNIVERSITEIT BRUSSEL

Department of Robotics and Multibody Mechanics (R&MM) & Physical Chemistry and Polymer Science (FYSC), Vrije Universiteit Brussel (VUB) , Brussels, Belgium

## The need for self-healing soft robotics in healthcare

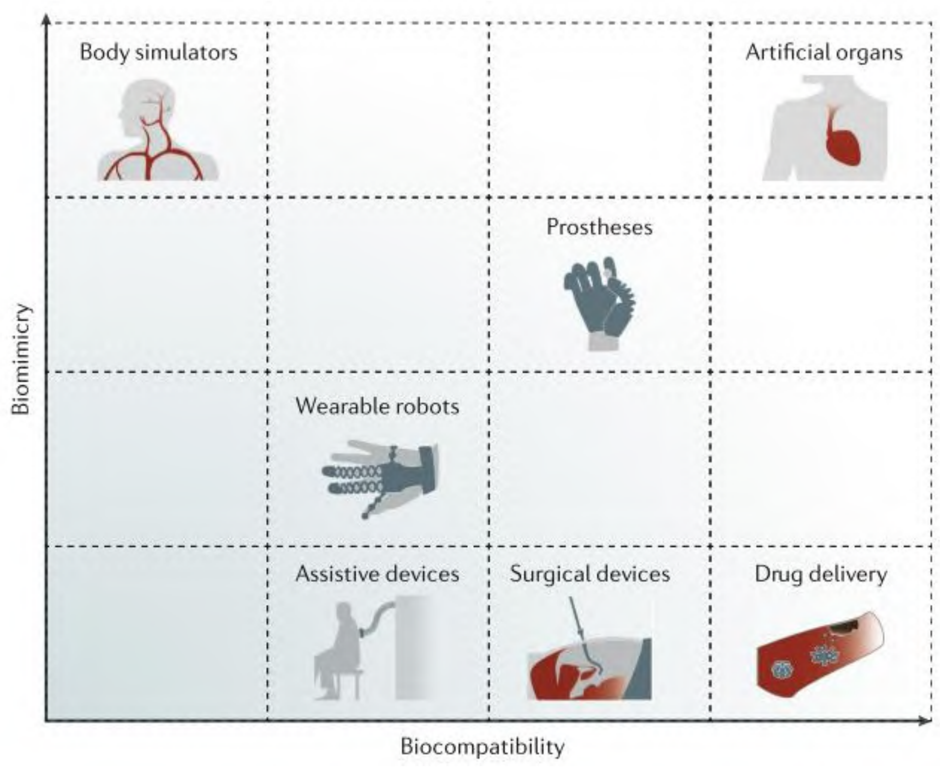


M.Cianchetti, C.Laschi, Cecilia, A.Menciassi, P.Dario, 2018

Robotics and healthcare are fast evolving fields where innovation thrives. More specifically, soft robotics introduces a new bioinspired perspective within the field of robotics. The inherent compliance of the soft robots gives rise to a wide range of novel applications. The soft materials used provides safety for humans who come in contact or share the same environment with the robot. This safety aspect allows a closer connection between robots and humans. This is certainly interesting in the context of healthcare.

With the focus on biomimicry and biocompatibility, soft robots can be implemented for numerous tasks within the biomedical field. For example in surgery, rehabilitation or any other medical procedure where there is physical contact between a robot and a patient.

## Material characterisation of self-healing Diels-Alder polymers

- Diels-Alder reaction between furan and maleimide functional groups

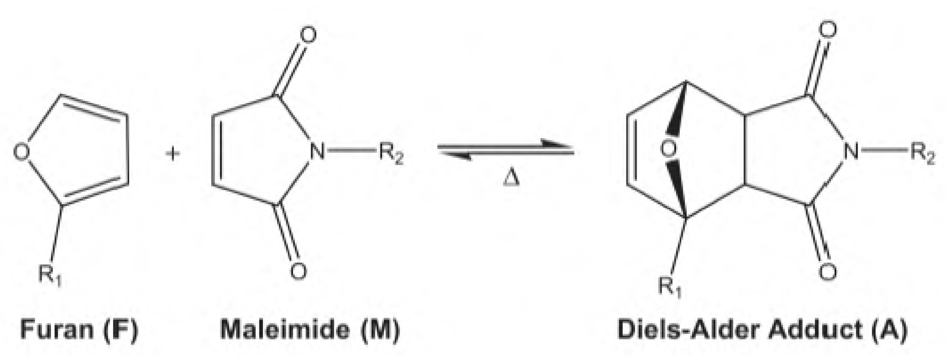


G. Scheltjens, M. M. Diaz, J. Brancart, G. Van Assche, and B. Van Mele, 2012

- Stress-strain curves of four 3D printed samples with nozzle temperature respectively 116 °C and 118°C

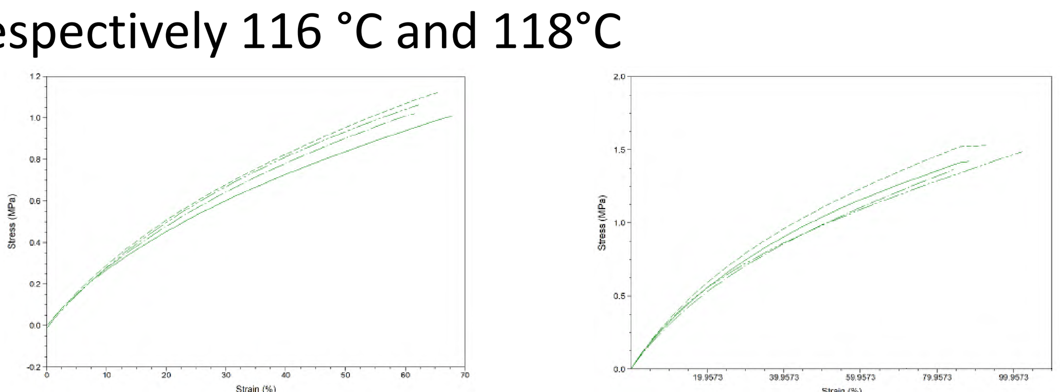

- Material analysis with Dynamic Mechanic Analyser

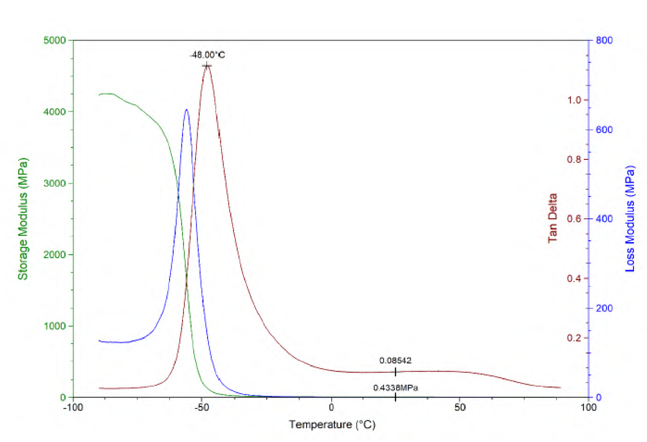

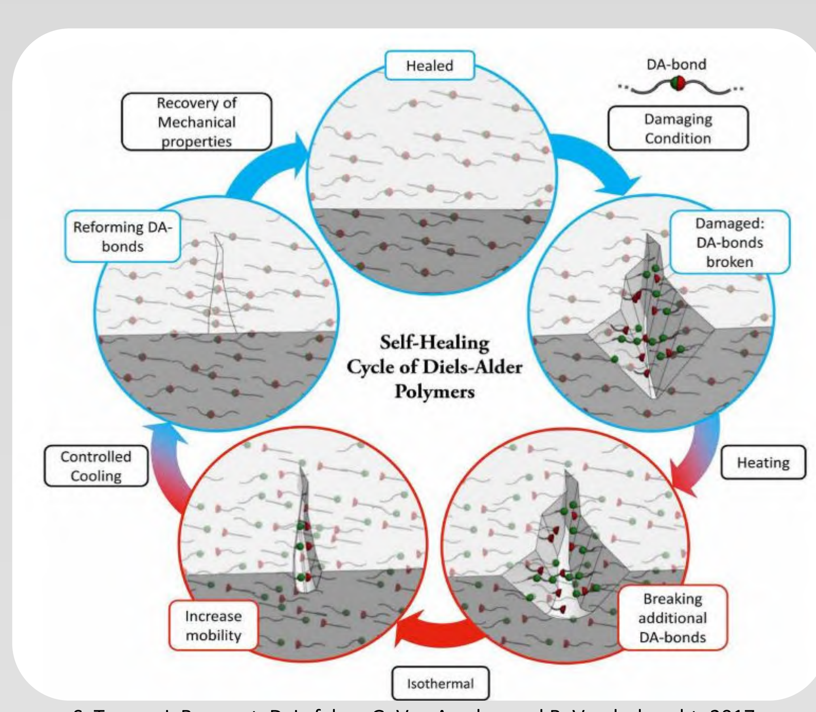


S. Terryn, J. Brancart, D. Lefeber, G. Van Assche, and B. Vanderborght, 2017

## Manufacturing techniques for self-healing Diels-Alder polymers

- The manufacturing process allows for efficient recycling of the material

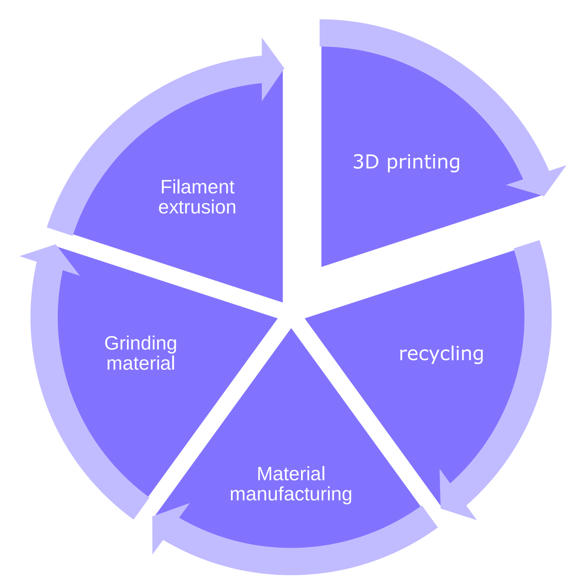


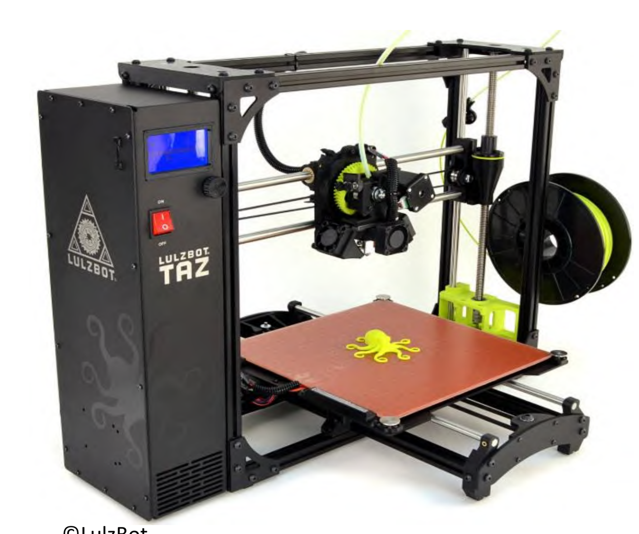

©LulzBot

- Multiple manufacturing techniques can be considered for self-healing Diels Alder elastomers

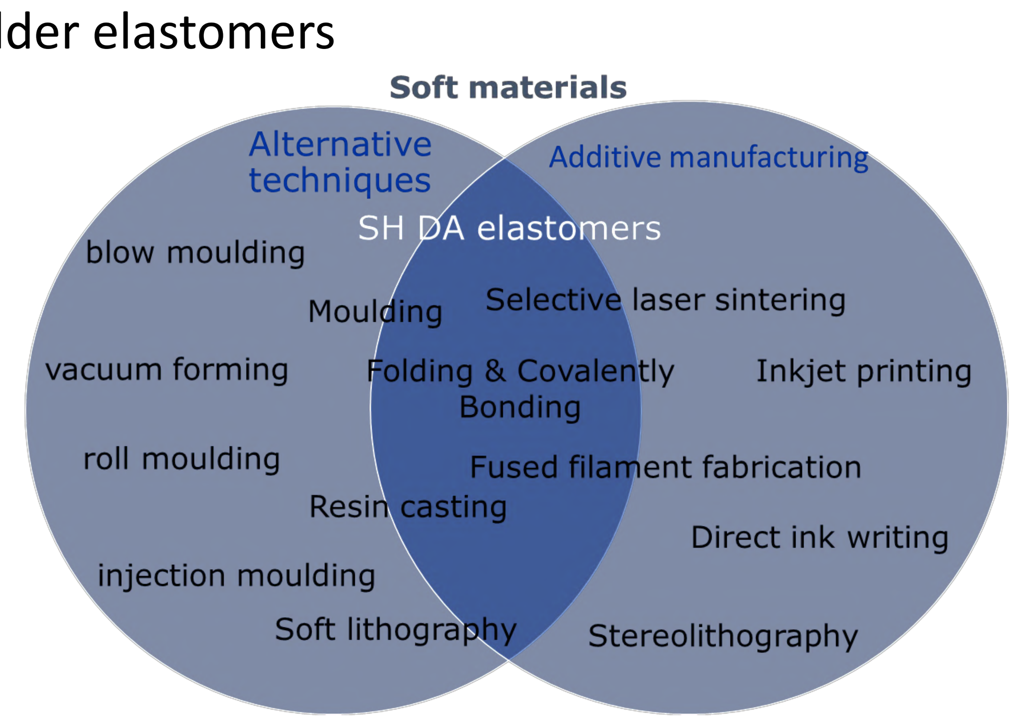


## Biomedical application: soft robotic glove for rehabilitation

The goal of a soft robotic glove is to augment the quality of life for patients who suffer from a (partially) paralyzed hand, this is done by applying external forces onto the hand in order to achieve movement. The glove depicted in the image is the ‘Exo-Glove Poly’, it consists out of silicone base material and is tendon driven. Powering is done by actuator units that allow flexion and extension of the fingers. Such a wearable soft robotic device could augment safety, comfort and usability among other things. However, bringing soft material in such close contact with humans and the surrounding, makes the robot vulnerable to cuts, scratches, punctures, etc. A prominent solution to this problem is the use of self-healing material. When damage occurs, the material can be triggered, in this case by heat, to start the self-healing process in the form of the Diels-Alder chemical reaction.

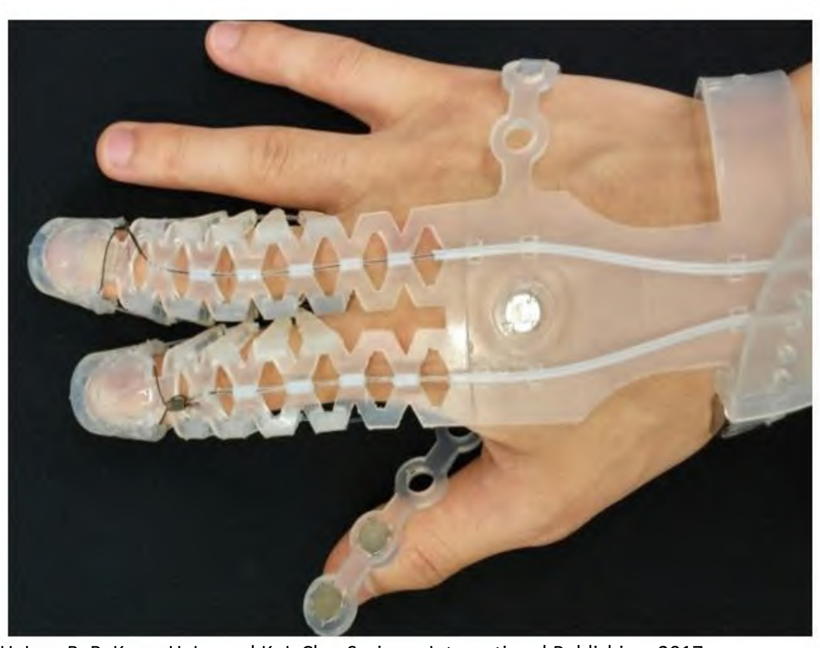

H. Lee, B. B. Kang, H. In, and K. J. Cho, Springer International Publishing, 2017

## Progress and continuation of the project

Diels-Alder polymers have been successfully extruded and 3D printed using the fused filament fabrication manufacturing technique.
Remaining challenges:

- Using fused filament fabrication technique to perform multi-material 3D printing of Diels-Alder polymers
- Finding solutions to 3D print inner air chambers in soft robotic components
- Exploiting multi-material fused filament fabrication for biomedical applications

Ikram.Mohout@vub.be

Master of Science in Biomedical Engineering

# Spike Sorting of Subthalamic Single Neuron Recordings in Parkinson Patients

GHENT UNIVERSITY

**Lien Gemmel**

prof. dr. ir. Pieter van Mierlo
prof. dr. Patrick Santens

VUB VRIJE UNIVERSITEIT BRUSSEL

## Introduction: Parkinson Disease

The **pathology** of PD is complex and not completely understood yet. Loss of dopamine-producing cells in the pars compacta of the substantia nigra in the mesencephalon leads to a deficiency of dopamine in the striatum.

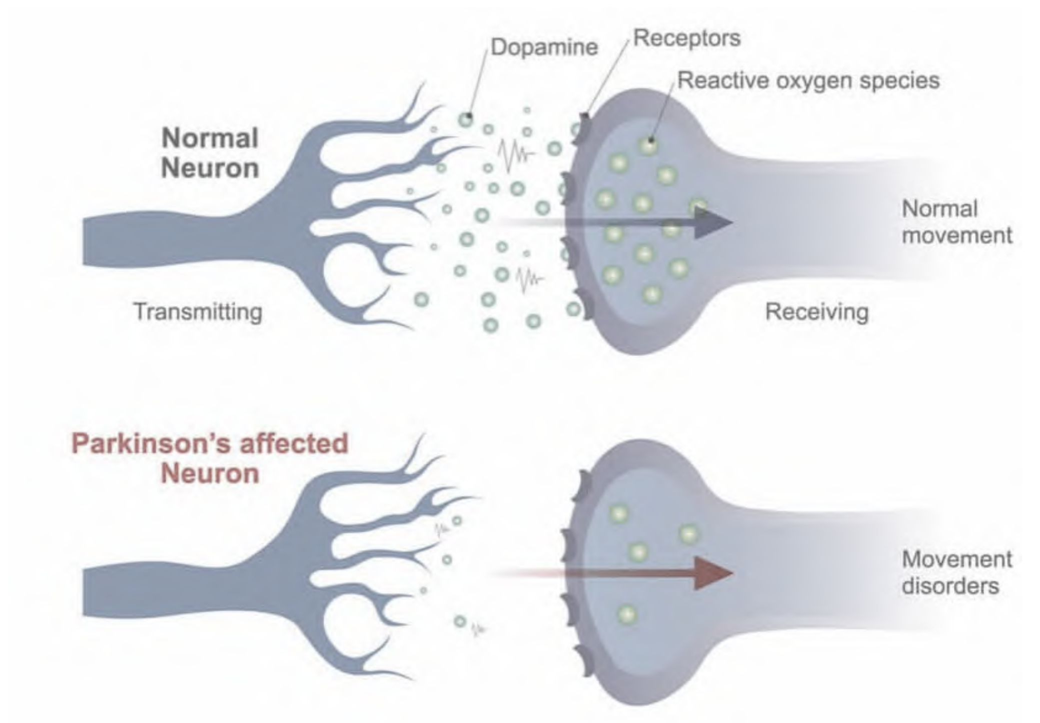


source:. labiotech.eu

A result of dopamine deficiency is the disturbance in the electrical activity of the subcortical circuits. This gives rise to a problem with controlling the motor cortex. The cardinal motor **symptoms** are: tremor, rigidity, akinesia and posture instability.

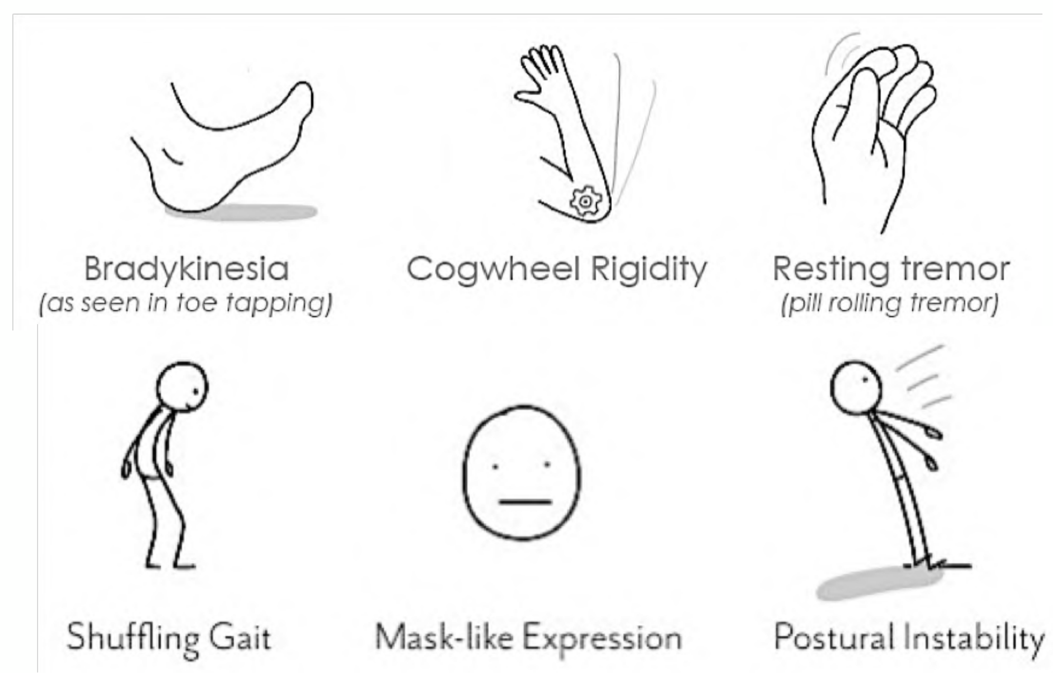


source: Advancells

The motor symptoms can be kept under control by implanting electrodes in the subthalamic nucleus. Deep brain stimulation has been established as a highly-effective **therapy** for advanced PD patients.

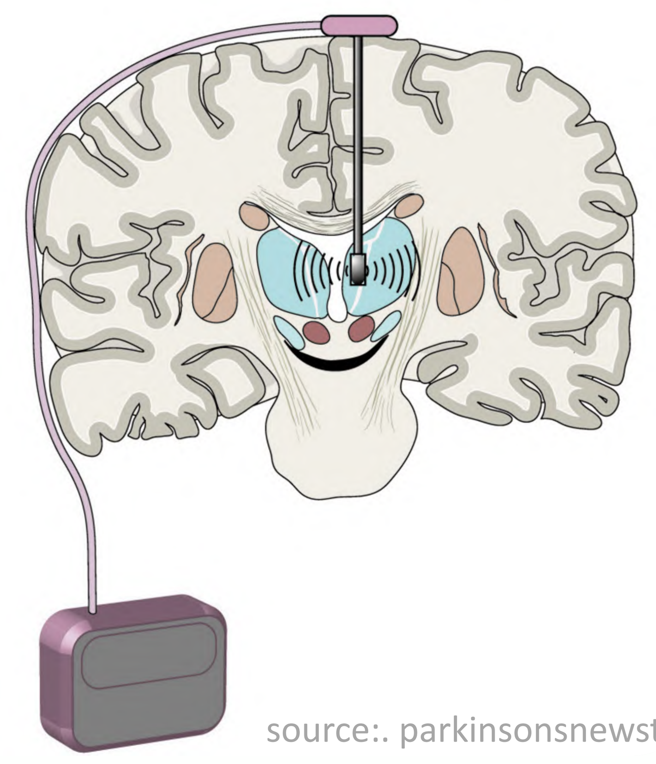

source:. parkinsonsnewstoday

## Data: Subthalamic Single Neuron Recordings

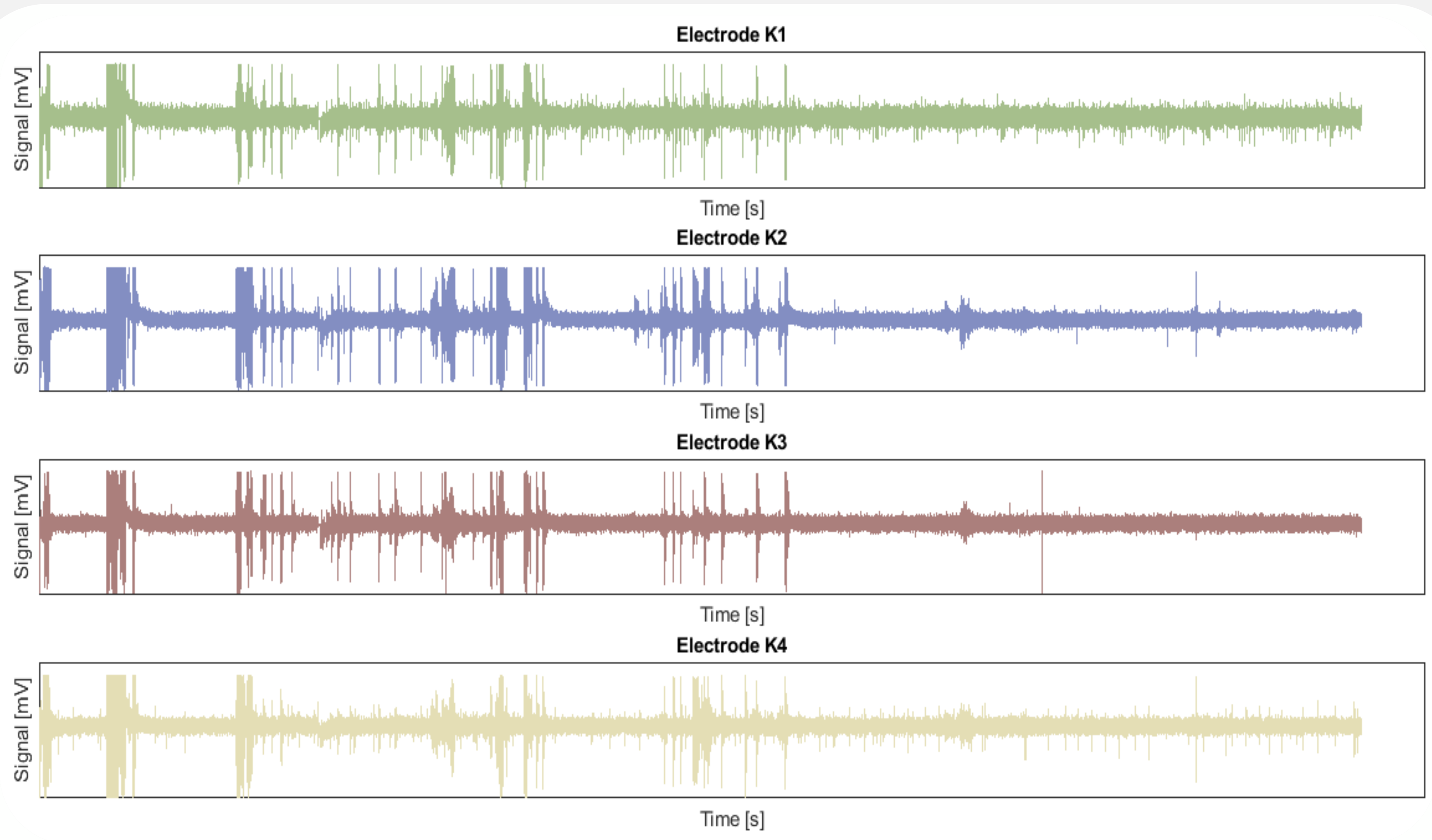


During the operation, the location of the subthalamic nucleus is estimated by making intraoperative **microrecordings**. This figure shows the neuronal activity at a certain depth in the brain picked up by four electrodes. The neurosurgeon can recognize the STN based on increased spiking activity.
(Data obtained from the University Hospital in Ghent)

## Future: Results

Identifying the best spike sorting algorithm:

- Neuronal correlations
- Spike-LFP coupling
- laterality

Automization and optimization in clinical practice:

- Automatic spike detection during surgery
- On demand deep brain stimulation

## Goal: Spike Sorting

Spike sorting is the seperation of activity produced by different neurons by grouping the detected spikes into clusters based on their waveform.

The process of spike sorting:

(a) A raw neural signal is recorded by the electrode.

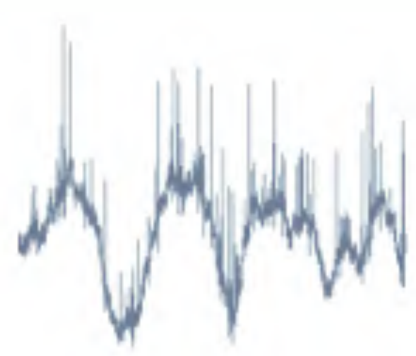

(b) The signal is bandpass filtered to remove high frequency interference.

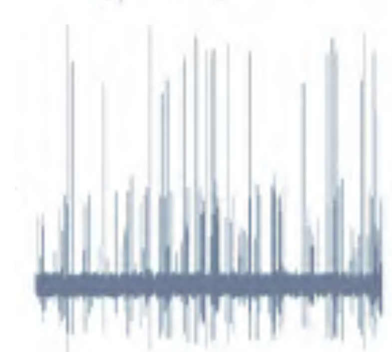

(c) Spikes in the signal are detected and aligned by their peak.

(d) The spikes are compared against templates to determine which neuron fired.

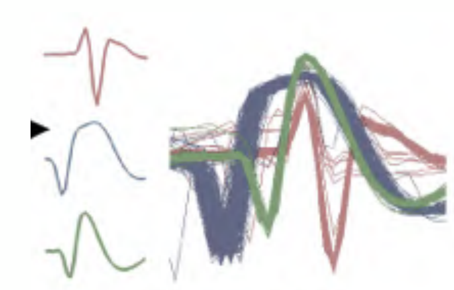

source:http://www.senseback.com/spike-sorting/

### Spike Sorting Algorithms

SPYKING CIRCUS — semi automatic, smart clustering, template matching, overlapping spikes, cross-validated, in vivo & in vitro...

PLEXON — (semi) automatic, overlapping spikes, waveform matching, density plots...

Wave clus — automatic, wavelets clustering, fast, unsupervised...

# 3D CFD modelling of kidney perfusion in support of robot assisted partial nephrectomy procedures

GHENT UNIVERSITY

**Lieve ten Vergert**

Supervisors: Prof. dr. ir. P. Segers & Prof dr. ir. C. Debbaut
Counsellor: ir. Tim Bomberna

VUB VRIJE UNIVERSITEIT BRUSSEL

e.g. IBiTech-bioMMeda, Ghent University, Gent, Belgium

## Robot assisted partial nephrectomy

Renal Cell Carcinoma (RCC) is a common type of kidney cancer with a high global incidence rate, in 2018 there were 403,000 new cases. How can the treatment of RCC be improved?

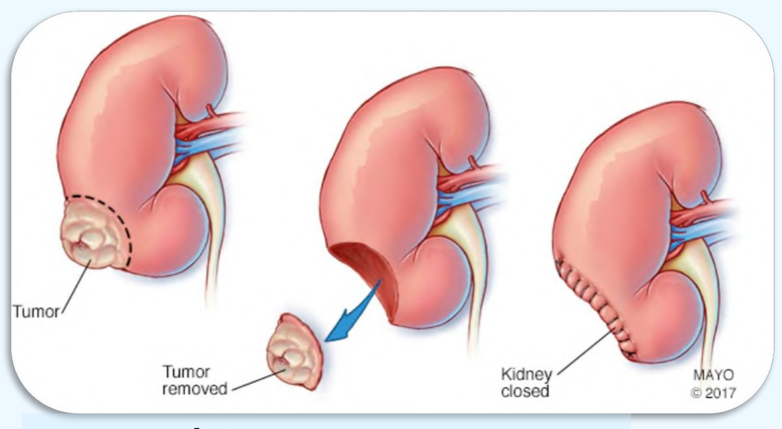


www.mayoclinic.org

- Clamp the main renal artery
- Remove the tumor
- Close the kidney

GOAL ➡

- Clamp one or more smaller arteries, closer to the tumor to avoid ischemia of healthy tissue
- Study the influence of this clamping on the renal bloodflow (CFD)
- Perform an uncertainty analysis on the results.

## Computational Fluid Dynamics (CFD) Workflow

*1. Segmentation of the arterial tree from medical images in Mimics (Materialise, Leuven)*

*2. Mesh generation (Ansys ICEM)*

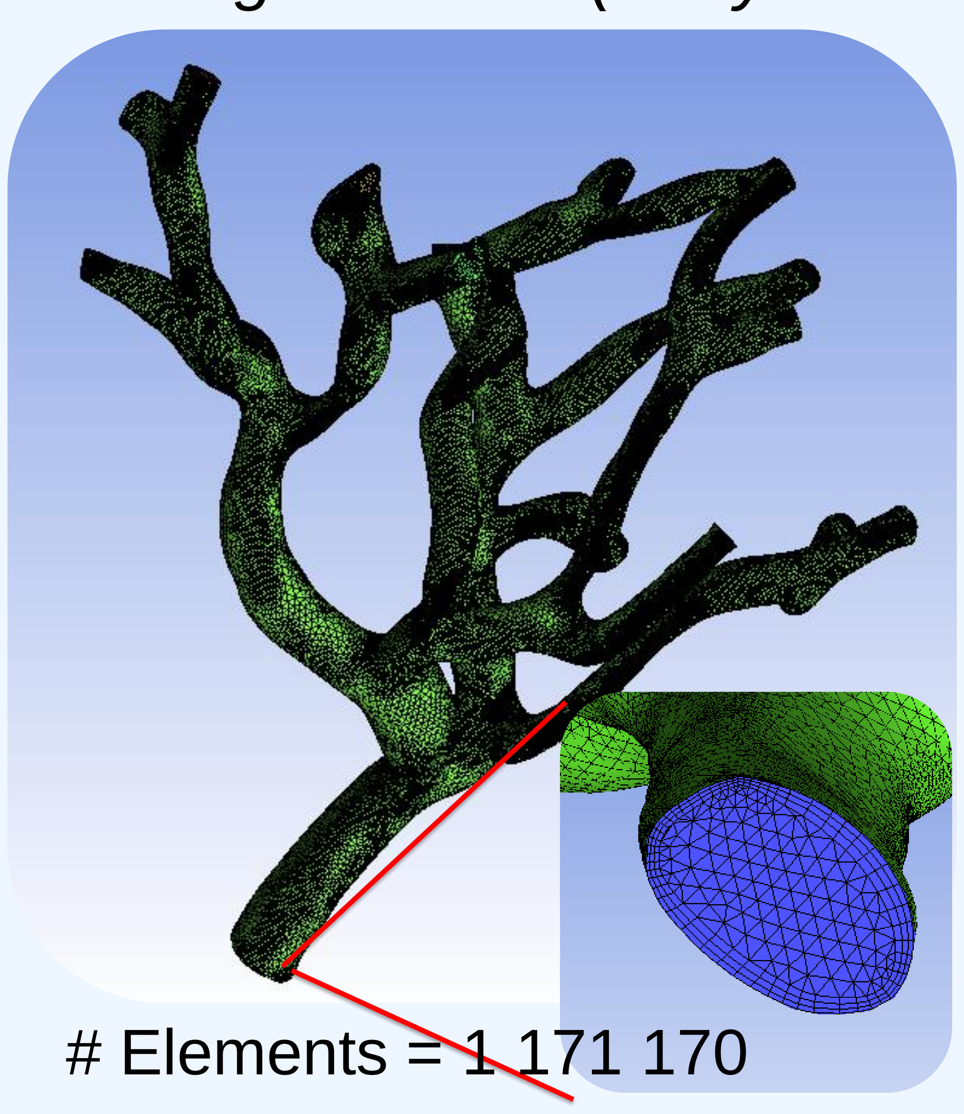


*3. Search appropriate Boundary conditions*

| | |
|---|---|
| Inlet | Patient specific |
| Outlet | Murray's law/Alternatives? |
| Wall | Rigid walls + no slip |
| Blood | non-newtonian (Quemada) |

*4. Run simulation with Ansys Fluent*

*5. Interpret the results + determine uncertainty on the results (Statistical analysis)*

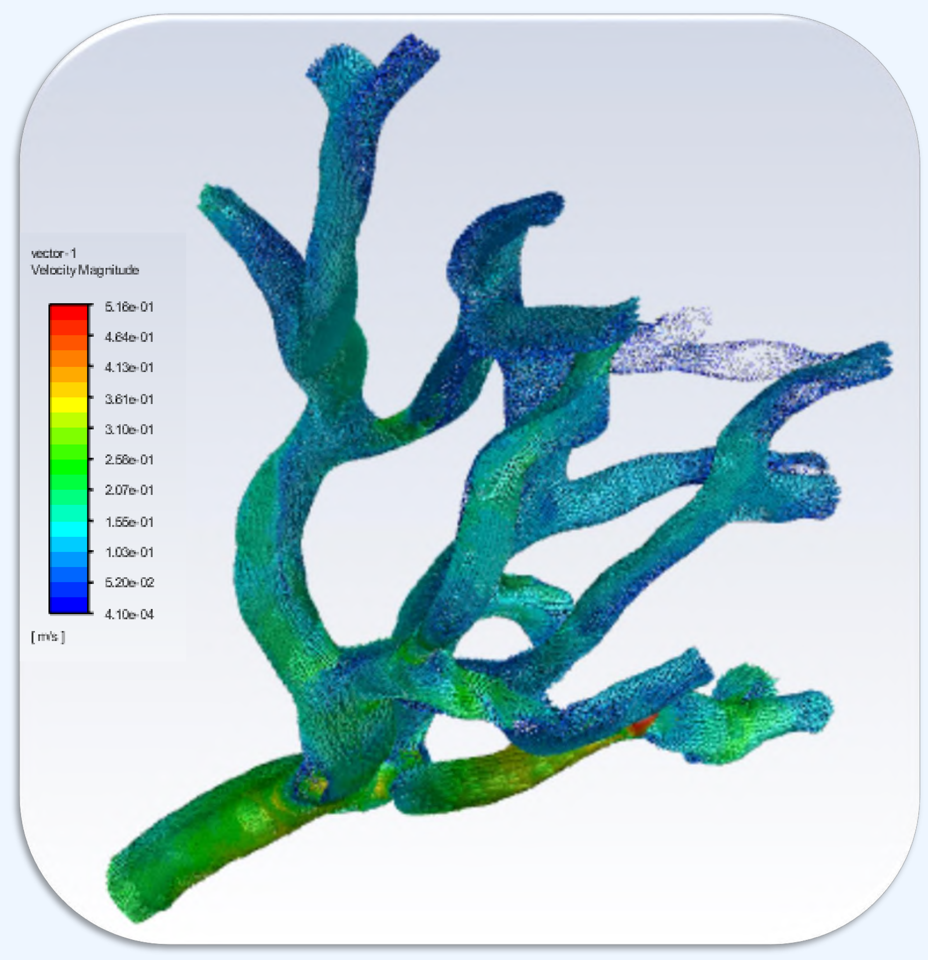

Steady Simulation
Inlet velocity = 0.22m/s
Outlets = fractional outflow

## The possibilities of PC-MRI

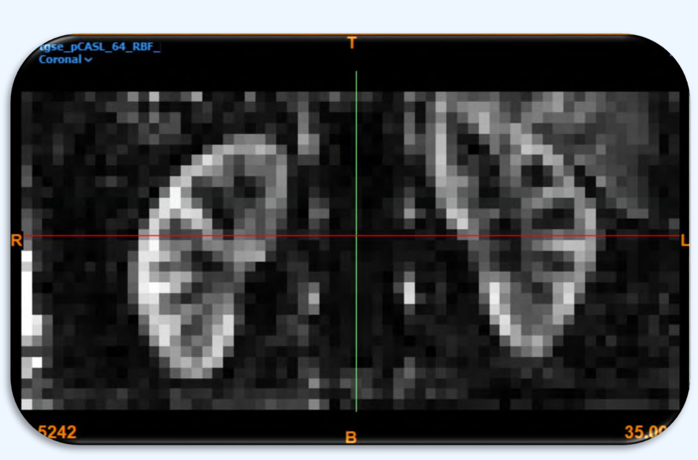

Phase-contrast MRI
Patient-specific bloodflows
⬇
Test-scan PC-MRI on own kidneys
(05/03/2020)
⬇
Personalized boundary conditions

## Statistical Analysis

Study the influence of several parameters on the CFD-results:

- The segmentation quality (erode/dilate)
- The inlet BC
- The outlet BC's

## The influence of clamping

Validation in the operation room (OR)

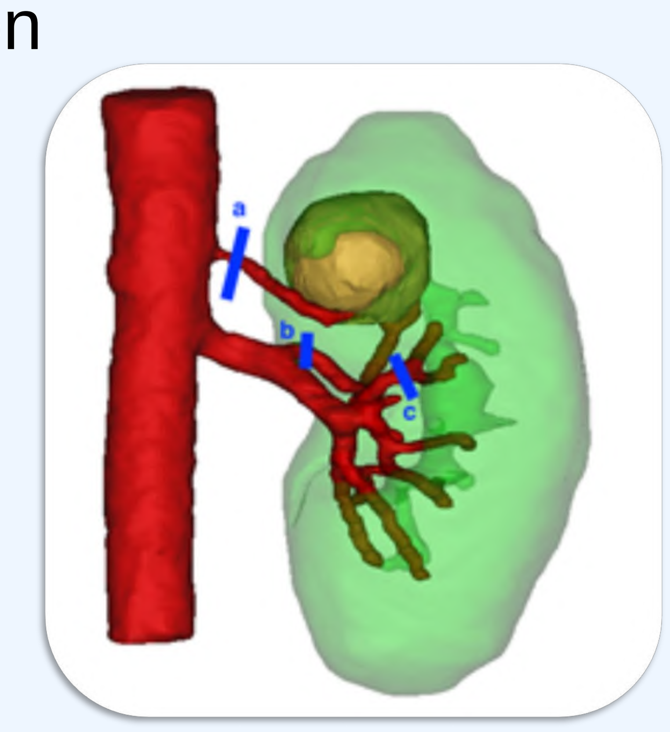


Only artery a was accessible for clamping during surgery

Not clamping of artery b and c resulted in some **bloodloss** during surgery. This might be **quantified** by using CFD simulations.

Although some excessive bleeding the surgery was succeeded succesfully

Lieve.tenVergert@UGent.be

Master of Science in Biomedical Engineering

# Photoacoustic spectroscopy with a laser Doppler microphone for non-invasive glucose sensing


GHENT UNIVERSITY

VRIJE UNIVERSITEIT BRUSSEL

**Maxim Meersman**

Colleague: Julia Böke

Promotor: Roel Baets, Supervisor: Yanlu Li

Photonics Research Group, Ghent University, Gent, Belgium


## Diabetes worldwide

| | 2019 | | 2030 | | 2045 | |
|---|---|---|---|---|---|---|
| | Number of people with diabetes (millions) | Prevalence (%) | Number of people with diabetes (millions) | Prevalence (%) | Number of people with diabetes (millions) | Prevalence (%) |
| Men | 240.1 | 9.6 | 296.7 | 10.4 | 357.7 | 11.1 |
| Women | 222.9 | 9.0 | 281.8 | 10.0 | 342.5 | 10.8 |



- Ever increasing number of diabetes patients who need regular glucose measurement
- Current standard practice is mainly done invasively with lancing system
- There are alternatives, but still not fully non-invasive
- Risk of infection + unpleasant for patient
- Even with multiple daily finger pricks, highs and lows can go undetected



## Need for non-invasive glucose sensing

## Photo Acoustic Effect

Pulsed laser with energy E hits specimen where $E_a$ is absorbed locally, this causes a local temperature increase with $C_p$ the specific heat and ρ the density of the absorbing volume V:

$$\Delta T = \frac{E_a}{C_p \rho V}$$

1. <u>Thermal confinement</u>:

   If the laser pulse is short enough so there is no thermal diffusion, the temperature increase will cause thermal expansion and generate a local pressure increase in the irradiated volume with β the thermal expansion coefficient and v the speed of sound in the irradiated volume:

2. <u>Stress confinement</u>:

   To get a good SNR it is important that the induced stress is limited to the thermal elastic expansion volume and has no time to relax during irradiation.

$$\Delta P = \rho v^2 \cdot \beta \Delta T = \left(\frac{\beta v^2}{C_P}\right) \cdot \left(\frac{E_a}{V}\right) = \Gamma H \mu_a$$

This ΔP will then propagate outside the irradiated volume as an acoustic wave and can be detected at the surface of the specimen.

→
- Generated Acoustic wave ~ $\mu_a$
- By varying frequency of stimulating laser several absorption peaks of sample can be determined

## Laser Doppler Vibrometry

To detect the vibrations generated on the surface by the PA effect, a homodyne LDV is used. The measurement beam will hit the vibrating surface and will undergo a Doppler phase change $\theta(t)$:

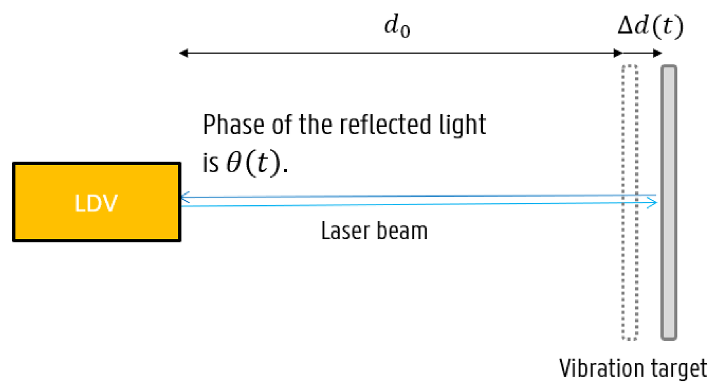


$$\theta(t) = \frac{2\pi}{\lambda_0}.(2\Delta d(t) + 2d_0)$$

$$\Delta f(t) = \frac{1}{2\pi}.\frac{d\theta(t)}{dt} = \frac{2v(t)}{\lambda_0}$$

From the related frequency shift the instantaneous out-of-plane velocity v(t) of the surface can be determined.

Polytec OFV-534 LDV sensor head.


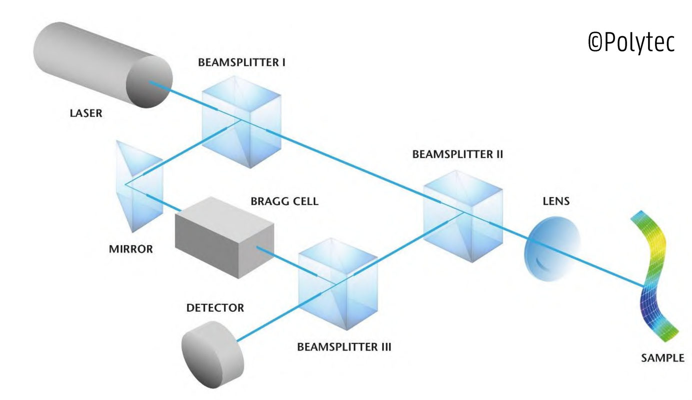




The $\Delta f(t)$ and d(t) can be recovered by analyzing the interference between the reflected beam and the reference beam.

.

→
- High resolution: up to femtometer ($10^{-15}$ m)
- Noncontact

## Proof of concept experiment

### Set-up:

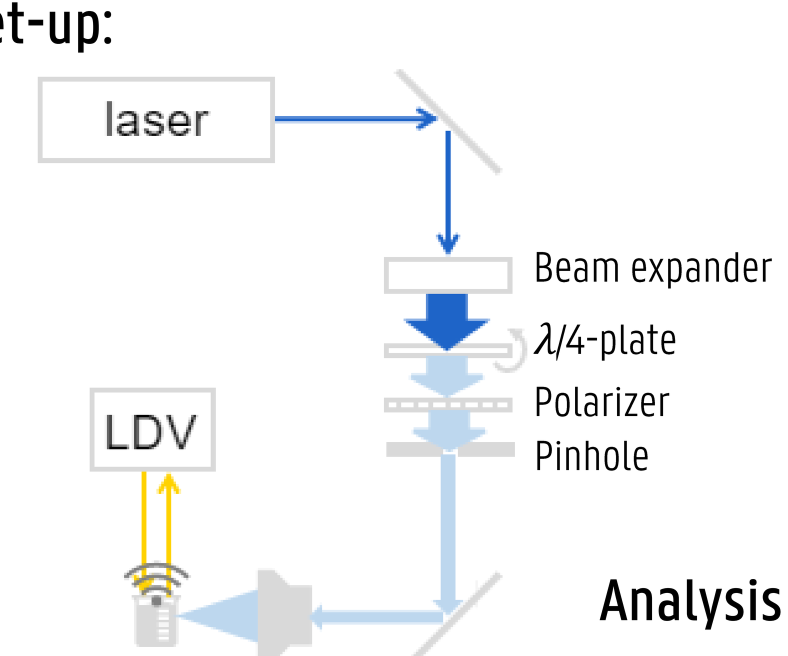


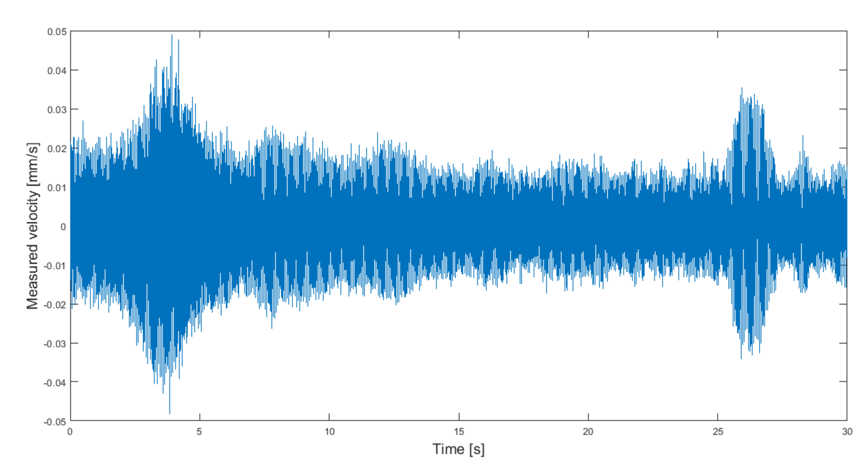

**Measured velocity signal from LDV:**

Transform to frequency domain →

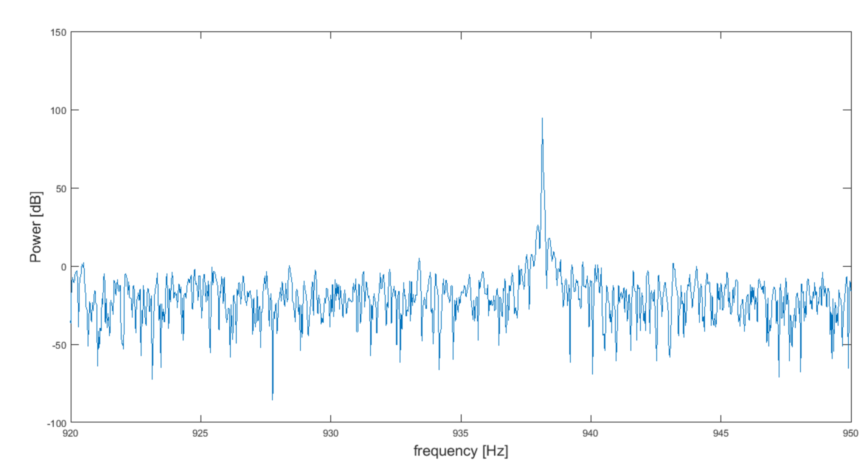

**Measured velocity signal in frequency domain:**

### Analysis of velocity component at the pulse frequency:

- Test specimen was placed in optical set up
- Laser of 532 nm was pulsed at 938,1 Hz and sent through a λ/4-plate to control the input power before it hit the specimen.
- Polytec LDV was focused on back side of specimen
- Velocity signal was acquired with sample frequency of 4000 Hz for average input powers varying from 0 to 140 mW .
- Acquired signal (30 second recordings) was analyzed in MATLAB

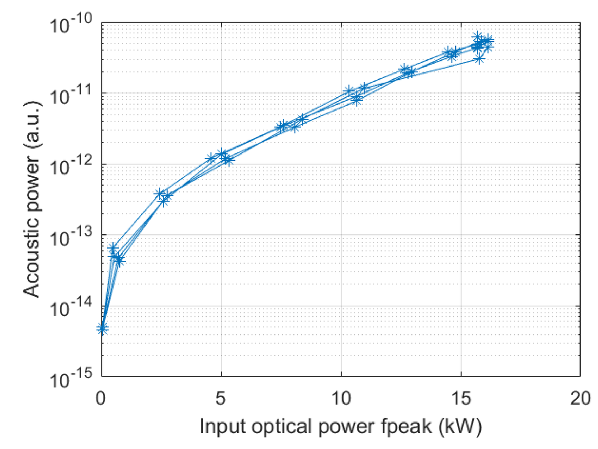


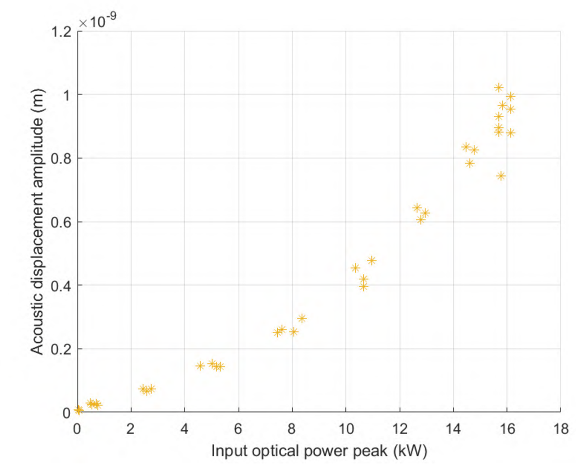


## What's next?

Combination of both techniques is possible, but will it show comparable results to golden standard?

- Compare absorption peaks of different specimens at 532 nm and 1064 nm
- Relate PA signal with glucose concentration
- Determine accuracy of measurement system

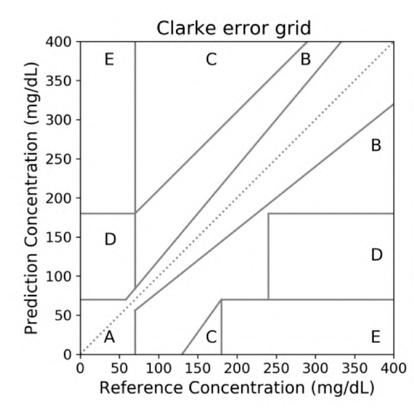


A. Clinically Accurate
B. Benign Errors, Clinically Acceptable
C. Overcorrection
D. Dangerous Failure to Detect and Treat
E. Erroneous Treatment, Serious Errors

Maxim.Meersman@UGent.be

# Computational Modelling of Dorsal Root Ganglion Stimulation for Pain Relief

GHENT UNIVERSITY

**Sebastiaan Priem**

prof. dr. ir. Emmeric Tanghe, prof. ir. Vincent Keereman,

Tom Van de Steene, Thomas Tarnaud

UGent-WAVES, Ghent University, Gent, Belgium

VUB VRIJE UNIVERSITEIT BRUSSEL

## Overview of chronic pain

The International Association for the Study of Pain defines pain as “an unpleasant sensory and emotional experience associated with actual or potential tissue damage, or described in terms of such damage”. Pain becomes chronic pain if it lasts longer than 3 months. According to B. McCarberg and S. Passik, 20-25% of the population suffers from chronic regional pain and 10% suffers from chronic widespread pain. Chronic pain has more implications than only the physical pain as can be seen in Figure 1.


Figure 1 – Implications of chronic pain

https://www.mychronicpainteam.com/resources/chronic-pain-what-people-dont-see-infographic

## The dorsal root ganglion

The dorsal root ganglion (DRG) is a cluster of neurons in the dorsal root of the spinal nerve. This ganglion plays a major role in experiencing  pain and temperature. It contains the cell bodies of all primary sensory neurons (PSN) innervating the dermatome governed by its spinal segmental level.

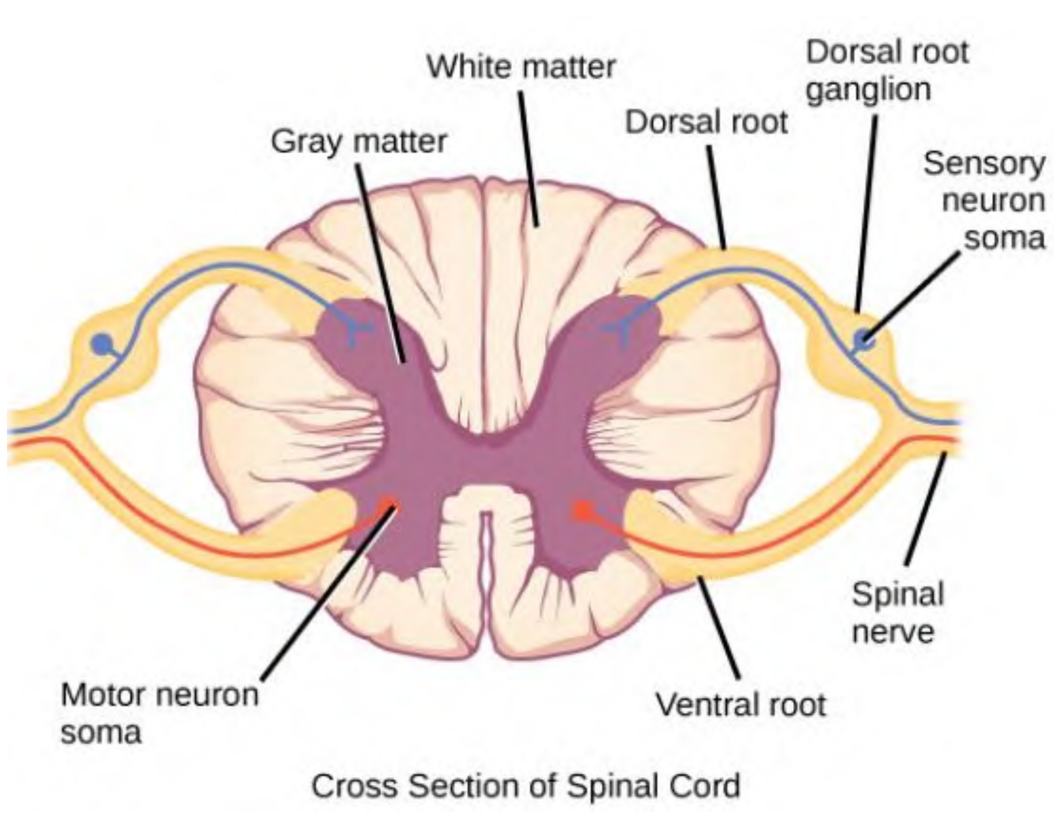


Figure 2 – The dorsal root ganglion

https://embryology.med.unsw.edu.au/embryology/index.php/2018_Group_Project_5

## Computational modeling: electromagnetic model

An electromagnetic model of the DRG is build by combining information from literature (Figure 3) and using the software Sim4Life. An electrode is placed above the ganglion to stimulate it. In this way electromagnetic fields can be generated and the effect on the structure as well as the surrounding structures can be examined.

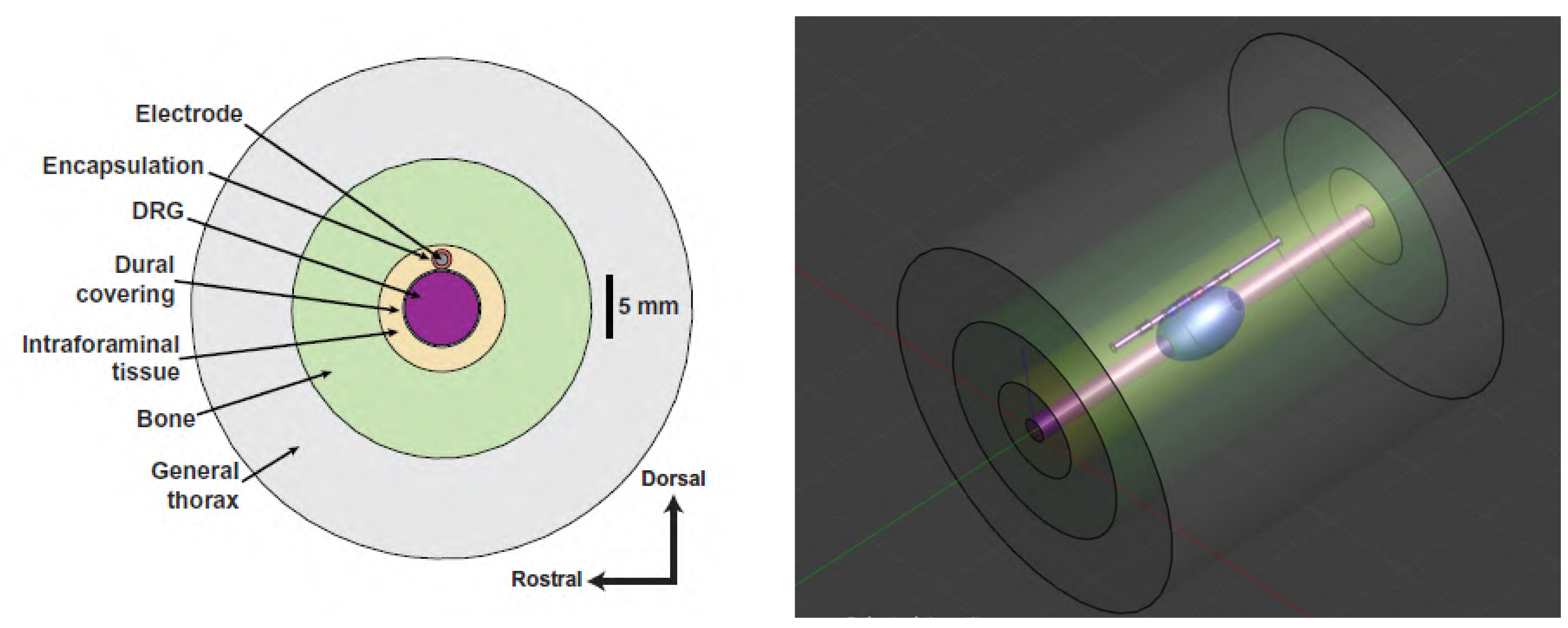


Figure 3 – EM model of the DRG

Dorsal root ganglion stimulation for chronic pain modulates Ab-fiber activity but not C-fiber activity: A computational modeling study

## Computational modeling: neuron model

The next step is to create a neuron model to examine the effect of the generated electromagnetic fields on the PSNs. This model will mostly consist of Aβ-fibers because it is shown that these play a major role in other chronic pain models.

## Analysis of stimulation of the DRG

The final step in the thesis is to use the two models to analyse the following aspects:

- Activation threshholds of action potentials
- Influence of the position of the electrode relative to the DRG
- Effect of different current densities
- More efficient way like a patch electrode?

Sebastiaan.priem@ugent.be

# Wireless control of a 3D-printed prosthetic arm

**Simeon Beeckman**
Prof. Dr. Ir. Arno Thielens
Prof. Dr. Ir. Wout Joseph
Matthias Van Den Bossche
imec - waves, Ghent University, Gent, Belgium

## Introduction

Quality of life for amputees tends to be significantly lower than that of a normal person. This can be improved however with the rise of new technology allowing for increasingly robust and accurately controlled prosthetics. [1] These bionic limbs can be controlled via sEMG signals. Since these are biological signals they tend to be somewhat complex and difficult to extract. A lot of research has been done already in the field of accurate pattern recognition of e.g. different hand movements. [2] [3]

The goal of this master thesis is to optimize the wireless link between a 3D-printed prosthetic arm and wireless nodes located on the same arm.

- Why wireless?

Obviously it is a lot less practical to walk and move around with a plethora of cables and connections placed on the body. Also the processor of the measured signals e.g. laptop, smartphone benefits from wireless control.

- Surface EMG vs inplanted EMG

The sensors used are sEMG sensors again because of the ease of use. A less invasive setup will always be preferable to an invasive one. The latest sensors are capable of accurate muscle activity measurements.

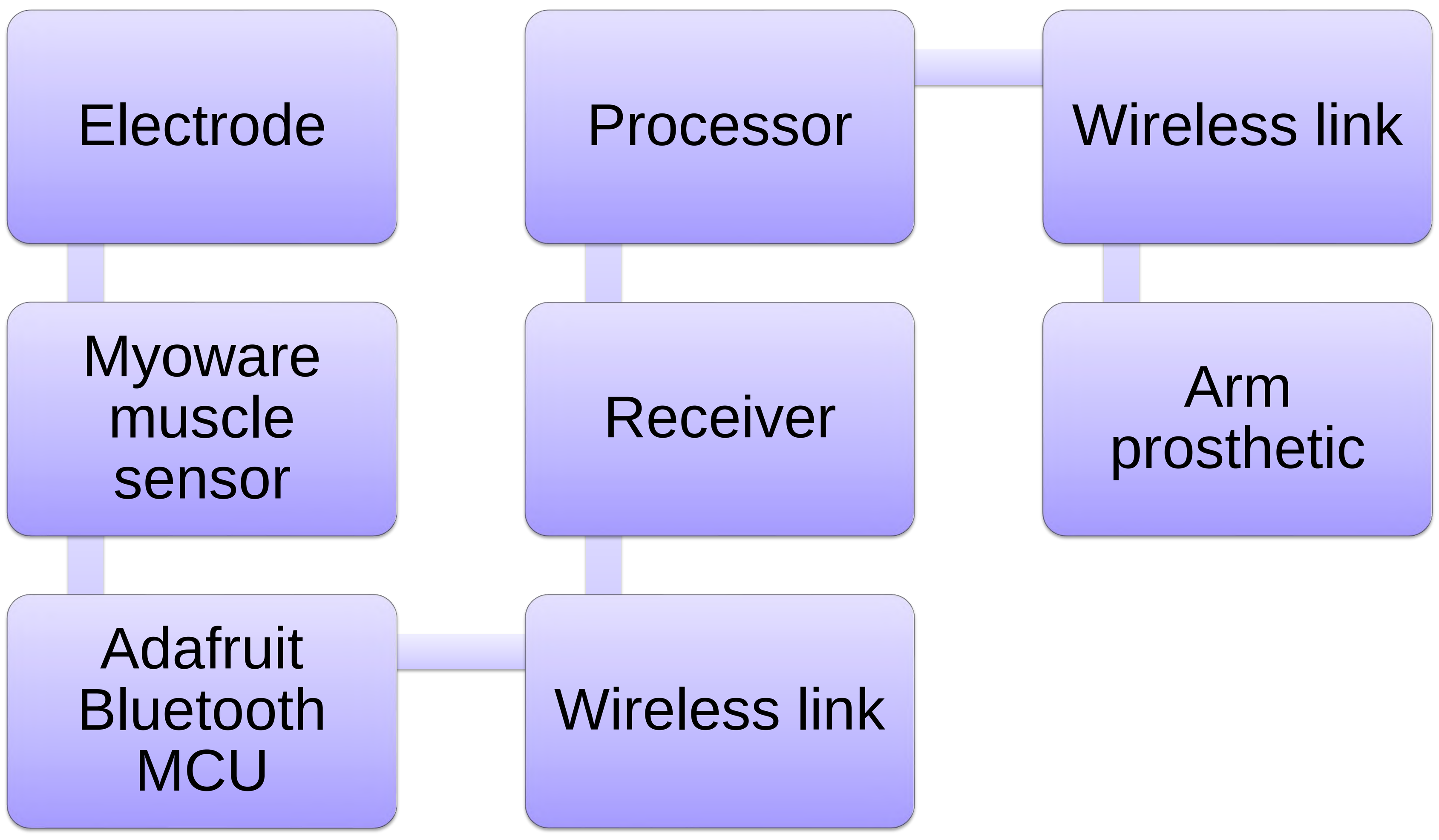


## Parts of the circuit

- The arm that is used is the HACKberry model founded by exiii inc. This is an open-source 3D-printable bionic arm, which can be controlled wirelessly via Bluetooth. The parts of this arm are downloaded and 3D-printed at the imec – waves workfloor in the iGent building at Zwijnaarde.
- The MCU used is an adafruit feather nrf52840.
- The sEMG sensor used is the Myoware muscle sensor.

## Muscle activity

A first experiment was to conduct 20 test readings of muscle sensor. The sensor is placed on the flexor carpi radialis. This way a signal can be read when those muscles flex and the fist is clenched. The setup can be seen on the figure below.

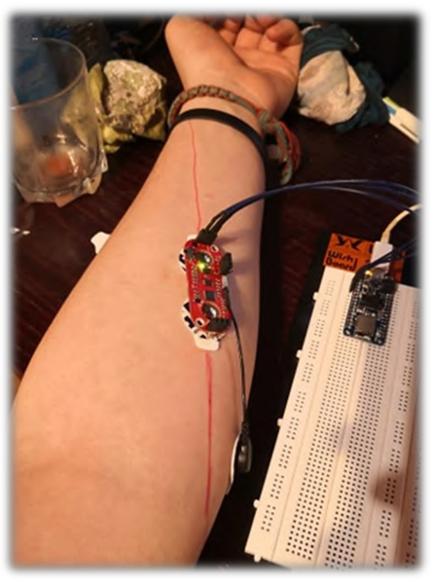

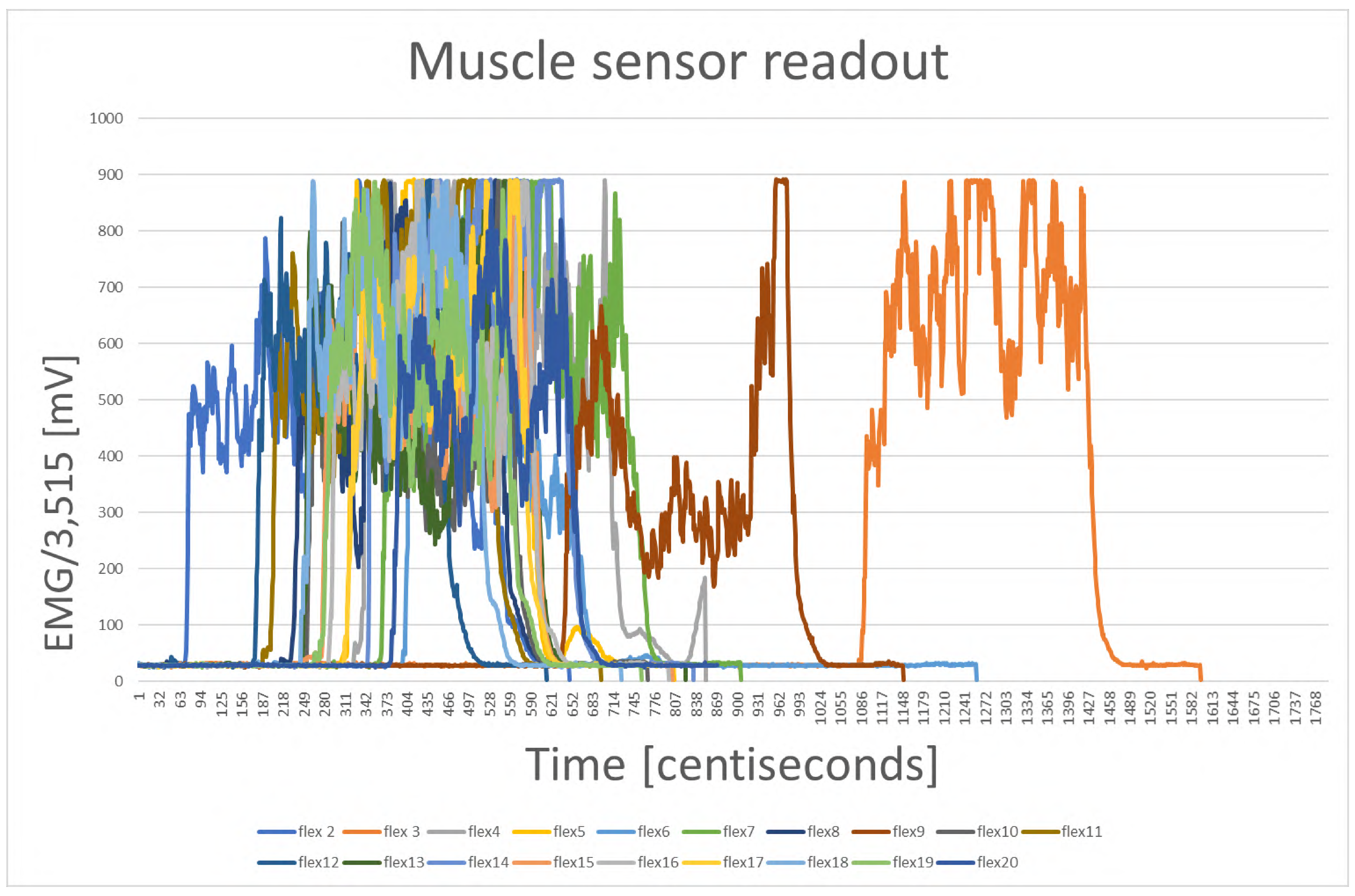


Figure 3: 20 Unprocessed sEMG signals read during a first experiment.

## Future work

- Preprocessing of EMG signals
- Statistical analysis on these signals
- Determining the optimal bandpassfilter to be applied.
- Constructing a decision tree to recognize future flexes.
- Repeat experiments with wireless connections.
- Optimize sensor and MCU placement.

## References

1. Moin Ali, Thielens Arno, Araujo Alvaro, Rabaey Jan M., Adaptivity to Enable an Efficient and Robust Human Intranet, 2018
2. A. Moin et al., A wearable electromyography-based hand gesture recognition system with real-time on-board incremental learning and classification, 2019
3. S. Benatti et al., A prosthetic hand body area controller based on efficient pattern recognition control strategies, 2017

Simeon.Beeckman@ugent.be

# Introduction of MedTech innovations in different health systems

**Olsi Kamami**

Prof. Dr. Ir. Pascal Verdonck

Prof. Dr. Ir. Jef Vandemeulebroucke

GHENT UNIVERSITY

VRIJE UNIVERSITEIT BRUSSEL

## Healthcare systems: Albania, Belgium, Italy, Switzerland

When introducing a new ***MedTech innovation (European Medical Device Regulation) in a single health system*** there are several factors that need to be taken into account.

### Countries under investigations [1]

Albania

Belgium

Italy

Switzerland

1. Description of the socio-political aspects of health in each country (focus on Albania).
2. Health economics and market description.
3. The impact of innovation: why some countries are more innovative than others?

### Why compare different health systems? [2]

| Country | Model | Role of government | Providers | Position in Euro Health Consumer Index (2018) |
|---|---|---|---|---|
| Switzerland | NHIM | Federal, cantonal and municipal | Public and private | 1st |
| Italy | Beveridge | Central | Public | 20th |
| Belgium | Bismarck | Federal/Regional | Public and private | 5th |
| Albania | Bismarck/NHIM | Central | Public and private | 35th |

1. Understand the health indicators that determine the performance of a health system.
2. Quality of care and costs?
3. Investigate why they differ and how to reduce the gap (focus on Albania).

## Methodology: an engineering approach

**Why innovation?**
Innovation is considered to be a key parameter to introduce value based healthcare in a future proof health system.

**How to trigger and enable innovation?**
Innovation must be facilitated in between the triangle of the government, the industry and the health care sector with as point of gravity: "the patient first"

**How to introduce it in the market?**
After understanding the technical and functional features of the new technology (product or service) , the benefits and the costs to society are investigated (health economics before market access).

**Description of the innovation process**
From the generation of ideas, the clinical evaluation and the planning of the technology, the prototype testing up to the creation of a home market with/without reimbursement.

## Case-study: moveUP (mHealth)

### 1. Patient cycle

[3]

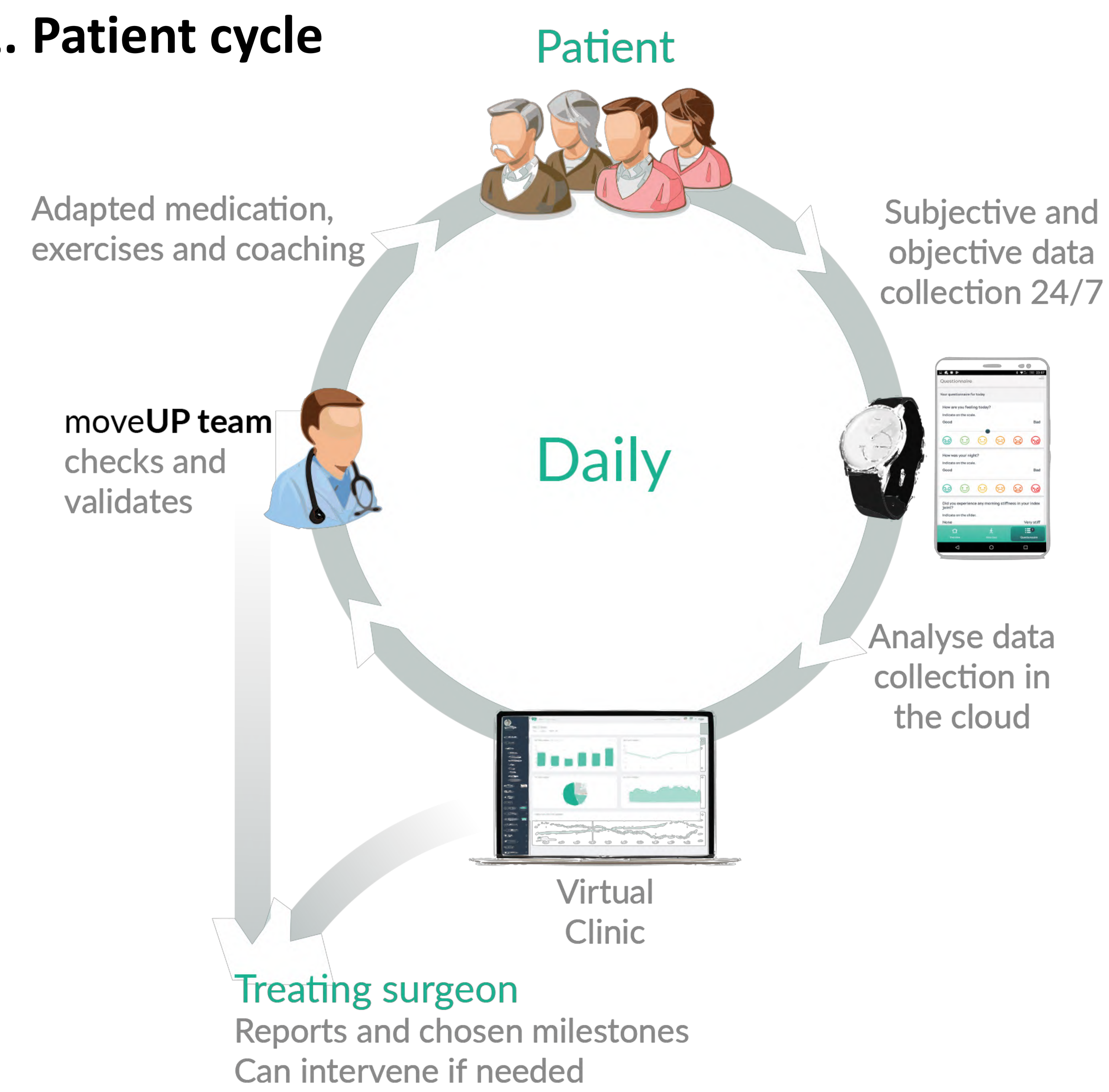


### 2. Real world evidence

| | Standard of care | moveUP |
|---|---|---|
| **Readmission rate** | 5-10% | 1.5% |
| **Unplanned consultations** | 10-20% | 3.8% |
| **Chronic post-surgical pain** | 15-30% | 0% |

## Results and future perspectives

1. The differences between health systems are mainly a result of distinct socio-political and cultural backgrounds.
2. The innovation process is an efficient instrument to investigate different health systems and markets for MedTech with the new MDR.
3. The case-study (moveUP) in mobile health will help to understand why and how some countries have a future proof health system.
4. The focus on Albania will hopefully pave the way to improve the country's health(care).

***References:***
[1]. Mossialos, Elias, et al. *2015 international profiles of health care systems*. Canadian Agency for Drugs and Technologies in Health, 2016; [2] Bjornberg, A. "2017 Euro Health Consumer Index." *PharmacoEconomics & Outcomes News* 796 (2018): 31-10; [3]. https://moveup.com

Olsi.Kamami@vub.be

# Developing a magnetic nanoparticle targeting platform


**Robbe Landuyt**

Promotors: prof. dr. ir. Guillaume Crevecoeur, prof. dr. ir. Luc Dupré

Supervisors: dr. ir. Annelies Coene, ir. Rikkert Van Durme, ir. Matthias Vandeputte

Department of Electromechanical, Systems and Metal Engineering, UGent


## Magnetic nanoparticle properties

- Magnetic core: Ni, Fe or Co
- Coating to obtain biocompatibility
- Functional/therapeutic coating

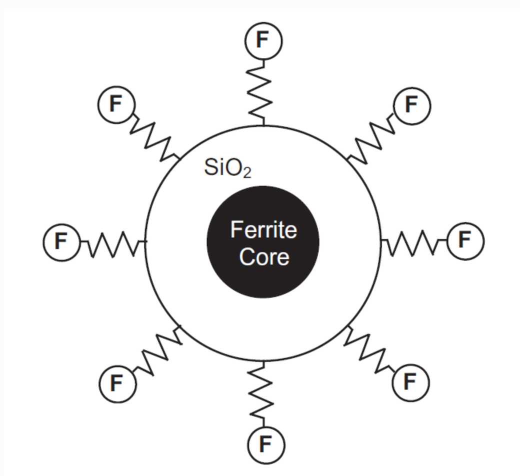


- Mostly superparamagnetic and single domain

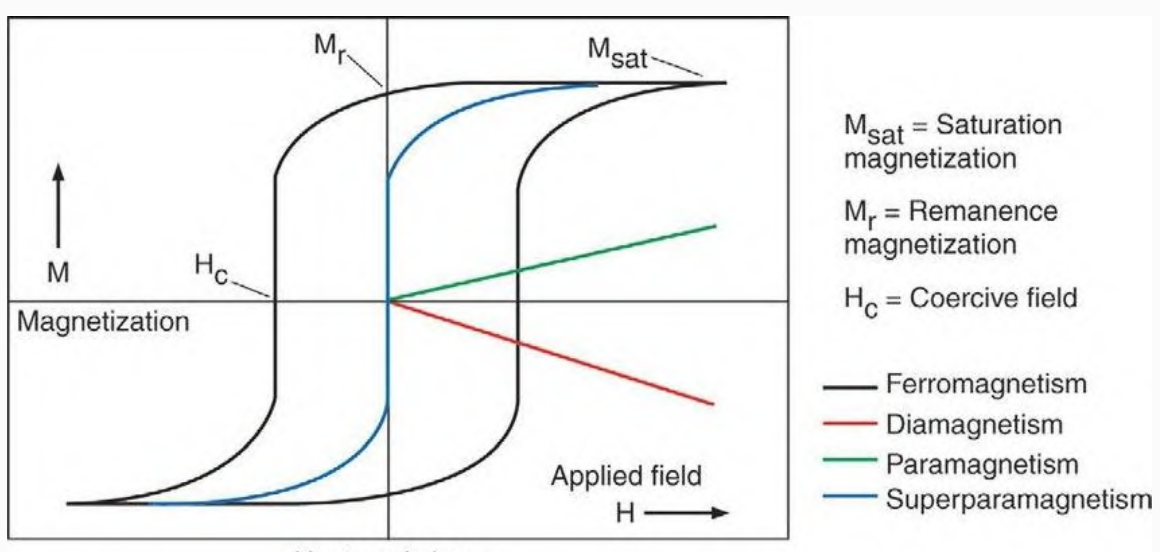


Hysteresis loop

*Namdeo, Mini et al (2008). "Magnetic Nanoparticles for Drug Delivery Applications." Journal of nanoscience and nanotechnology. 8. 3247-71*

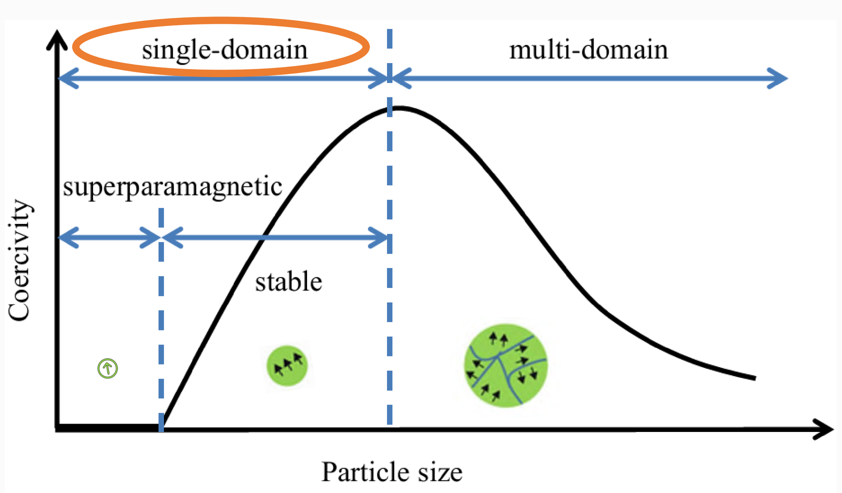


*A. Feoktystov, 2012, "Magnetic nanoparticles", Jülich Centre for Neutron Science*

## Application examples

### Drug delivery

Delivering cytotoxic drugs to specific target tissue (e.g. tumour)
⇒ Reduce systemic distribution of drug
⇒ Reduce dosage

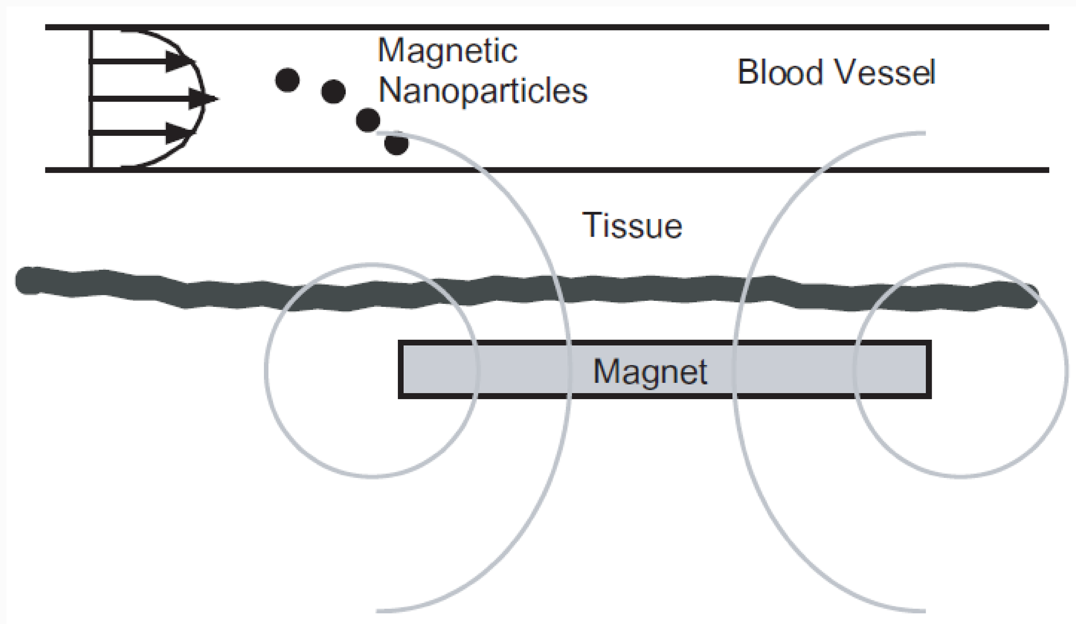


*Q A Pankhurst et al 2003, Applications of magnetic nanoparticles in biomedicine, J. Phys. D: Appl. Phys.*

### MRI contrast enhancement

Protons in cells tagged by magnetic particles have a shorter T2* relaxation time than those in untagged cells

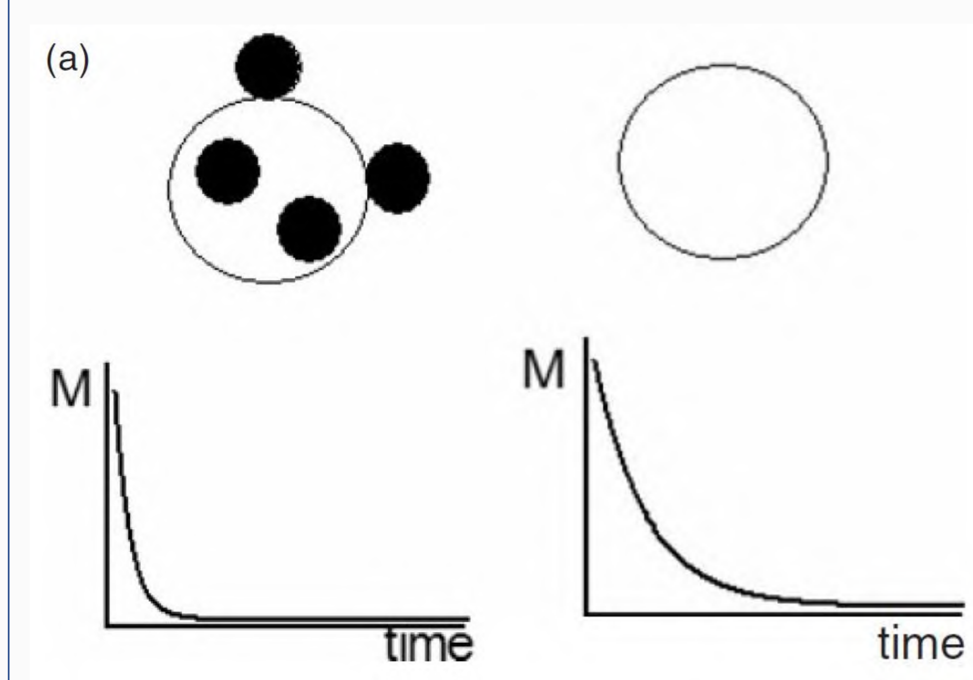


*Q A Pankhurst et al 2003, Applications of magnetic nanoparticles in biomedicine, J. Phys. D: Appl. Phys.*

### Hyperthermia

Treating cancer by heating malignant cells while sparing surrounding healthy tissue. Magnetic particles are dispersed throughout the target tissue and an external AC magnetic field is applied to heat up the particles.

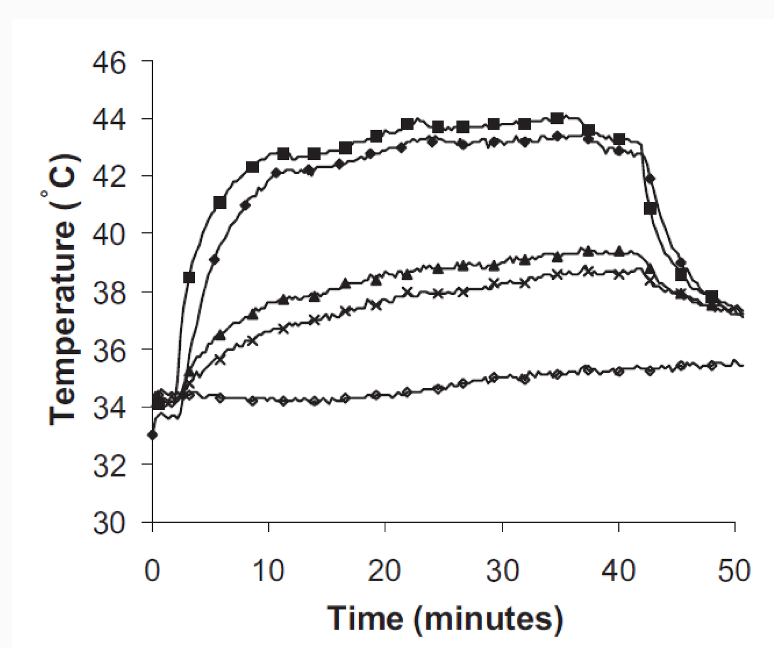


(■) tumour edge, (◆) tumour centre, (Δ) normal liver 1–2 cm from tumour, (×) alternative lobe, and (◊) core body temperature.

*Q A Pankhurst et al 2003, Applications of magnetic nanoparticles in biomedicine, J. Phys. D: Appl. Phys.*

### Magnetic separation

Removing specific biological entities from their environment into concentrated samples

1. Labelling biological entity with nanoparticles (● in figure)
2. Separating

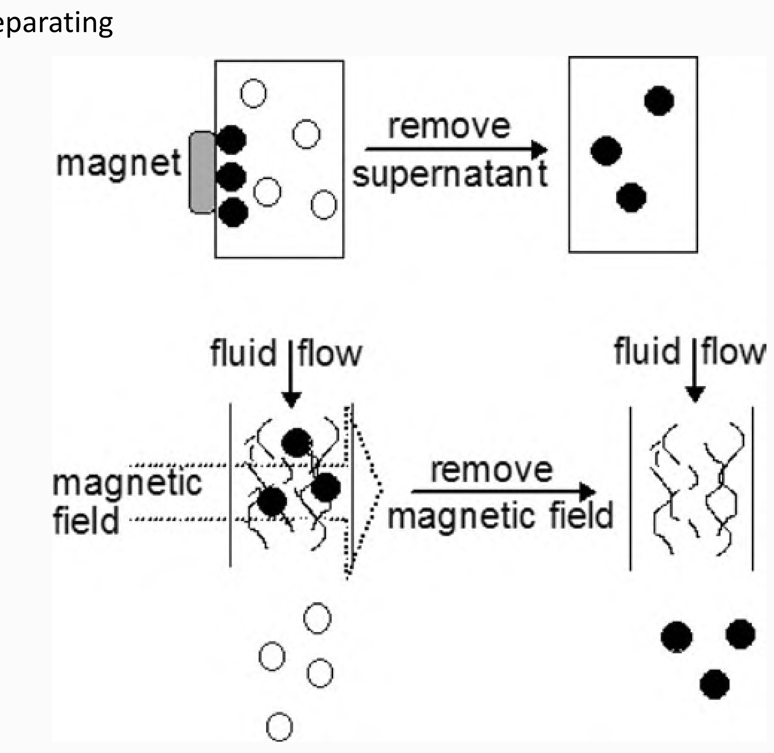


*Q A Pankhurst et al 2003, Applications of magnetic nanoparticles in biomedicine, J. Phys. D: Appl. Phys.*

## Ongoing research in magnetic targeting

**Physics and chemistry**

- Magnetic carriers
- Liquids

**Magnet design**

- Electromagnetic coils
- Permanent magnets

**Guiding**

- Dynamics
- Control

## Objective of this thesis

Design magnet set-up to be able to efficiently move the nanoparticles in a desired direction

$$\sum F = ma$$

Magnetic - and drag force dominate

Implement control to be able to react on changes in the nanoparticle's path and guide it towards the target

## Experiment

Building magnet and camera set-up to move particles in 1 dimension

Testing and validating the simulations in Matlab

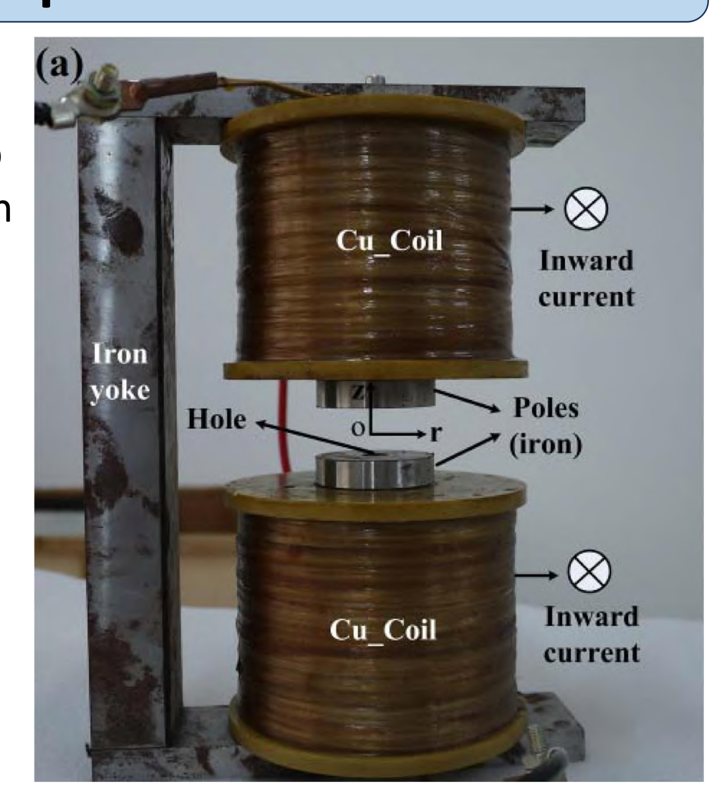


*Weizhong Wei & Zhen Wang, 2018, Investigation of Magnetic Nanoparticle Motion under a Gradient Magnetic Field by an Electromagnet*

## Results: simulations so far

$$F_m = (m.\nabla)B$$

Proportional to gradient of magnetic field

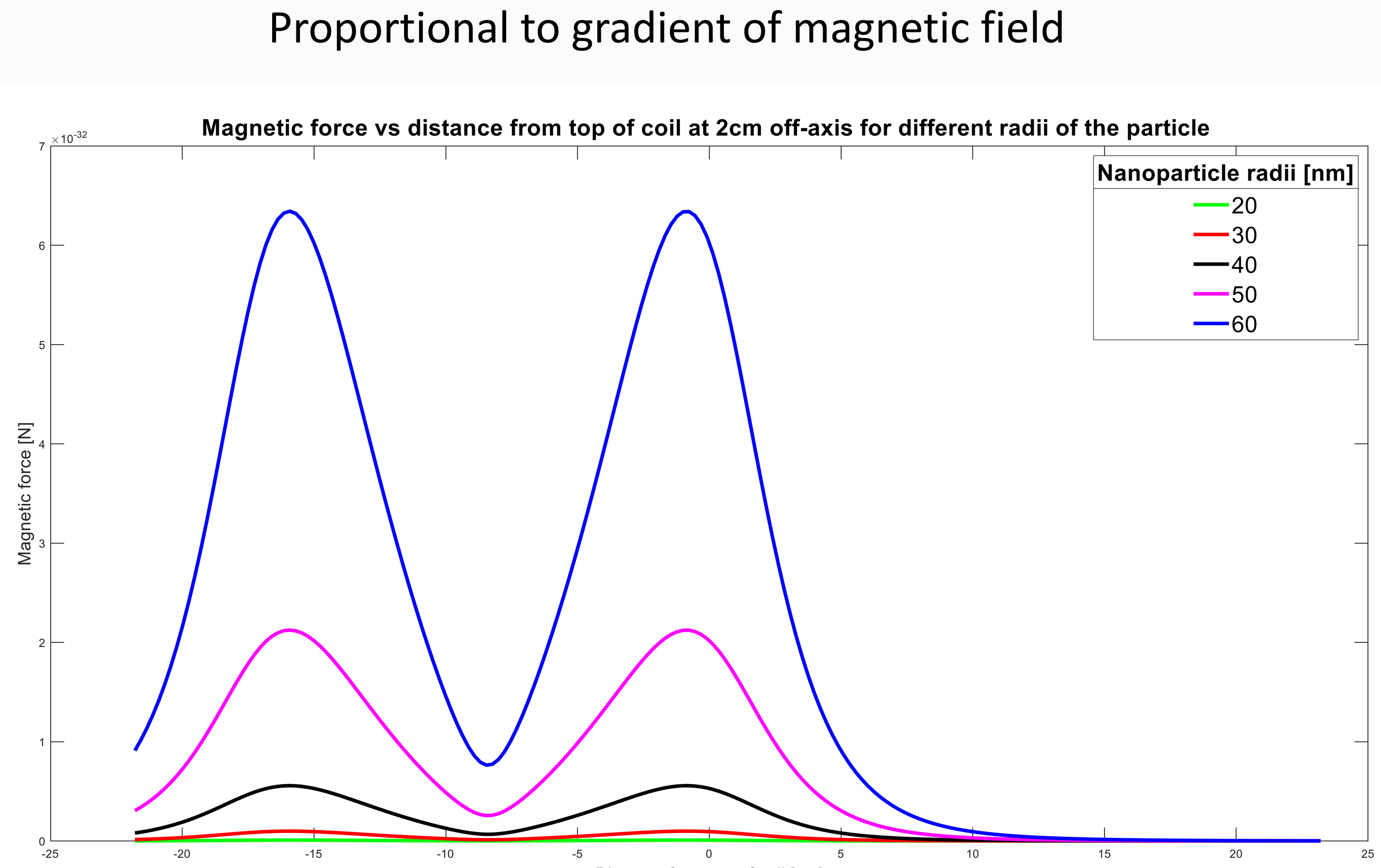


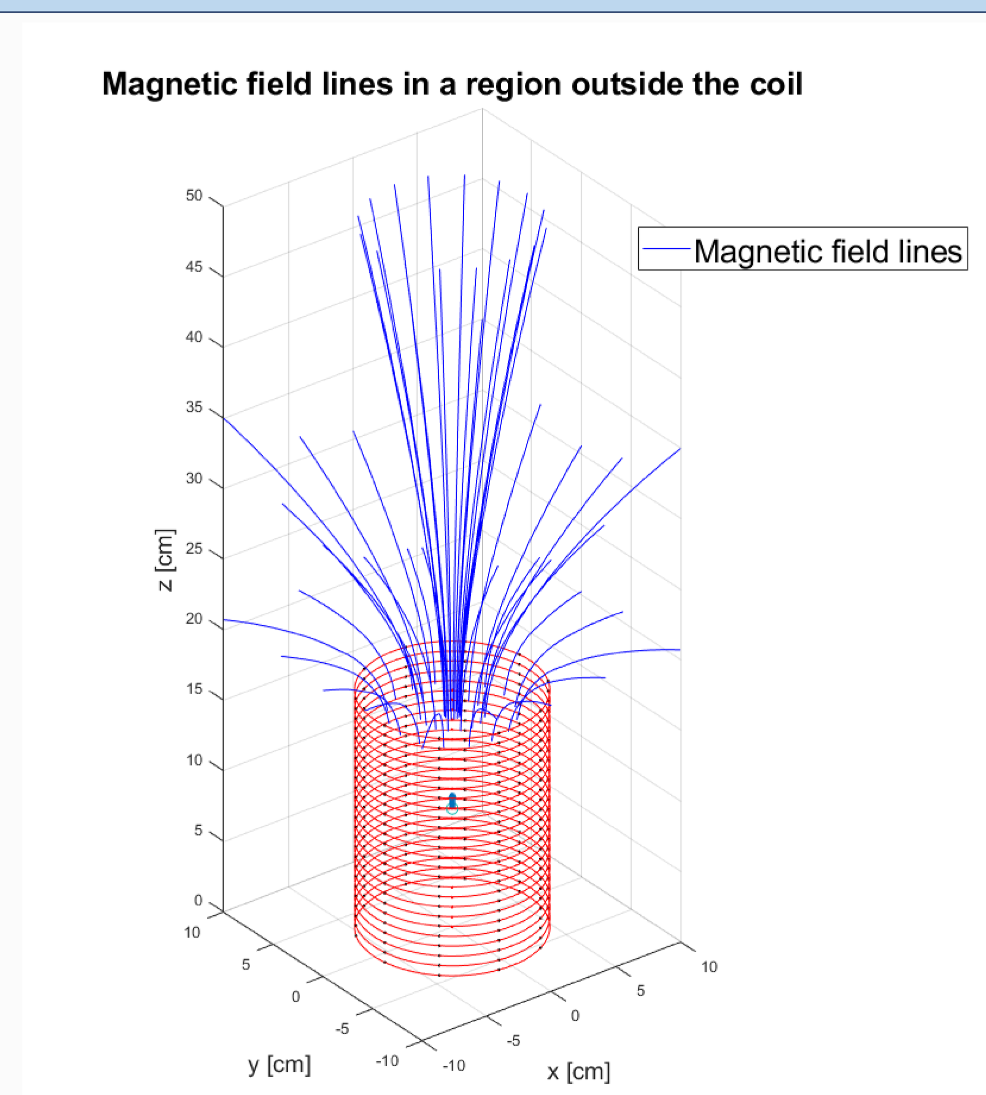


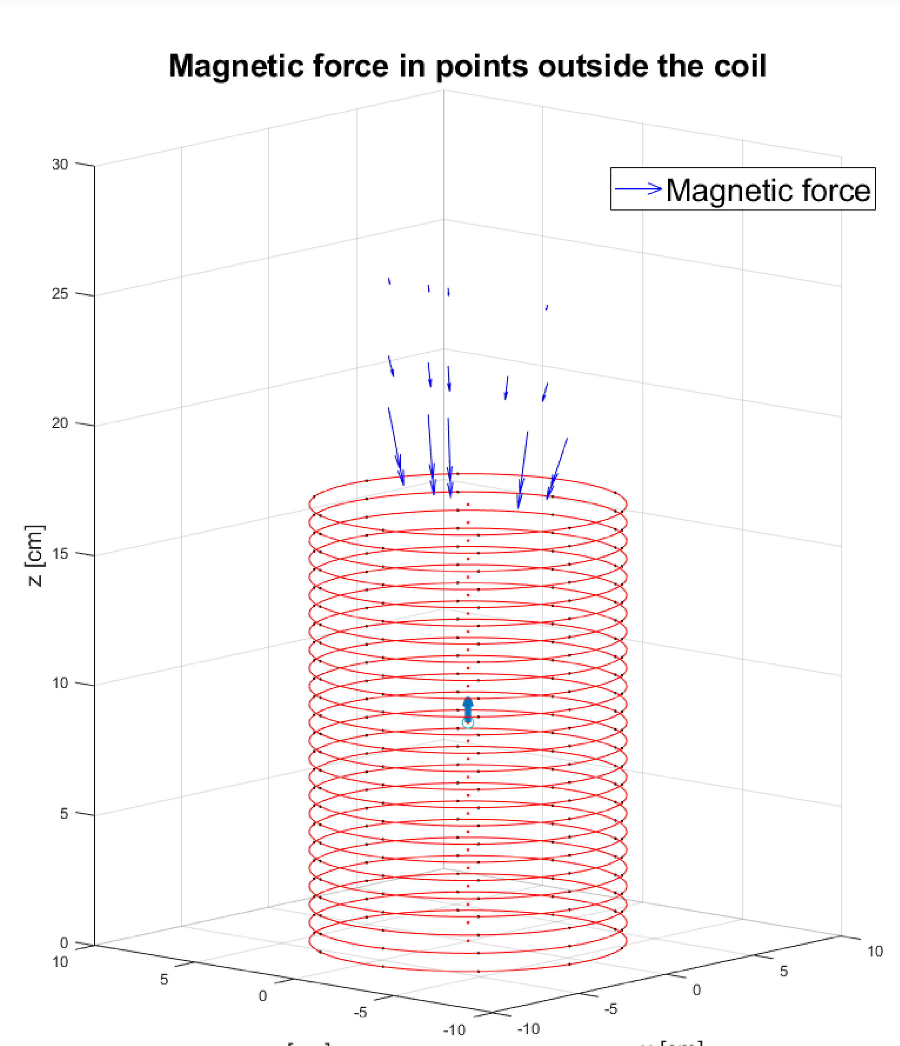



Robbe.Landuyt@ugent.be


Master of Science in Biomedical Engineering

# Development of a planning tool for robot assisted partial nephrectomy surgery based on 3D reconstructions of kidneys


GHENT UNIVERSITY

**Saar Vermijs**

prof. dr. ir. Charlotte Debbaut, prof. dr. ir. Patrick Segers, prof. dr. Karel Decaestecker

UZ Ghent & IBiTech-bioMMeda, Ghent University, Gent, Belgium

VUB VRIJE UNIVERSITEIT BRUSSEL


## PARTIAL NEPHRECTOMY SURGERY

**Personalizing patient care** is on the rise, making health care more effective than ever. In various hospital departments, an individual approach shows remarkable results, including in nephrology and urology.

For patients diagnosed with a **kidney tumor**, the recommended treatment is to remove this tumor. One approach is radical nephrectomy, but a better approach **safeguarding all functionalities**, is to remove only the tumor: a so-called partial nephrectomy. To **avoid healthy tissue ischemia**, the surgeon wants to clamp only the arteries that go to the tumor. Each kidney being different, the **clamping positions** need to be determined before surgery starts. For this, a **planning tool** is essential.

"A surgery that saves lives... and kidneys"

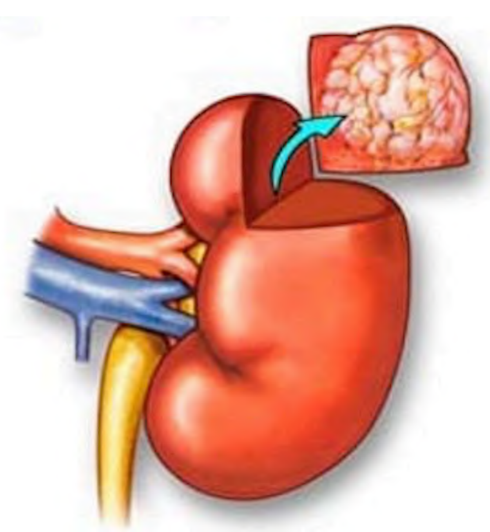

© Pace Hospital

## PLANNING TOOL

**1) Segmentation in Mimics** (Materialise)

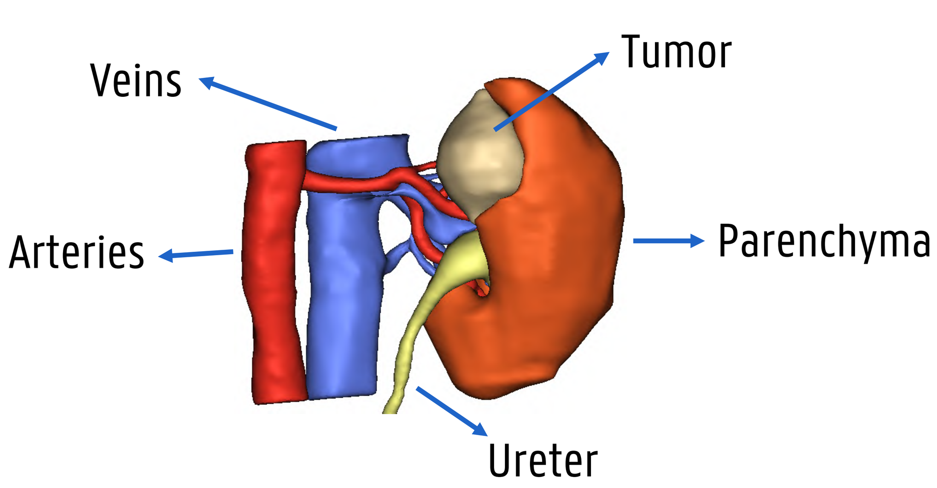


**2) Scripting in Mimics using Matlab**

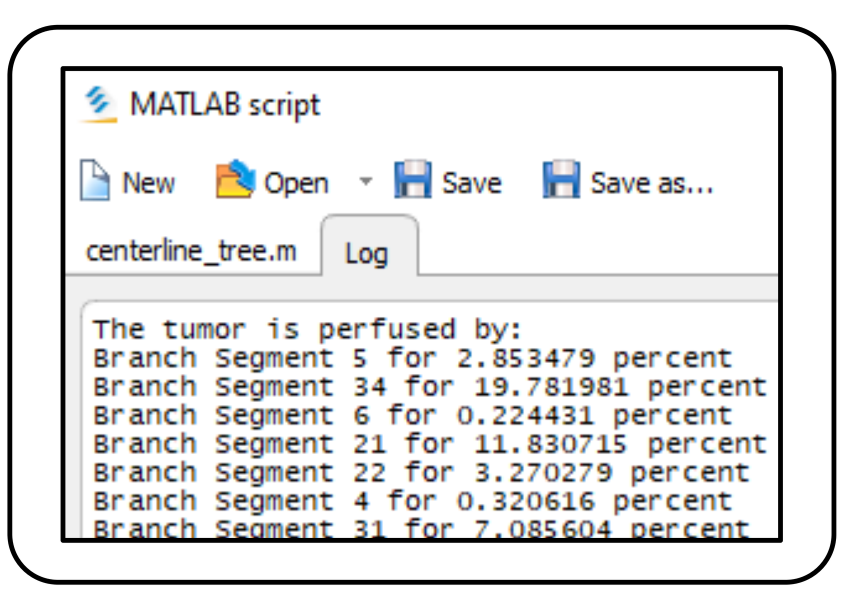

MATLAB script

New Open Save Save as...

centerline_tree.m Log

```
The tumor is perfused by:
Branch Segment 5 for 2.853479 percent
Branch Segment 34 for 19.781981 percent
Branch Segment 6 for 0.224431 percent
Branch Segment 21 for 11.830715 percent
Branch Segment 22 for 3.270279 percent
Branch Segment 4 for 0.320616 percent
Branch Segment 31 for 7.085604 percent
```

**3) Visualisation in Mimics** of the clipping areas

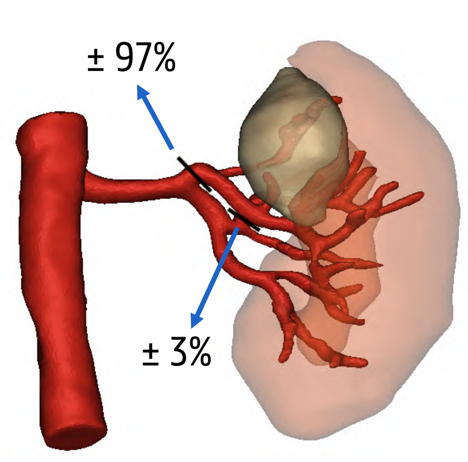


## THE ALGORITHM

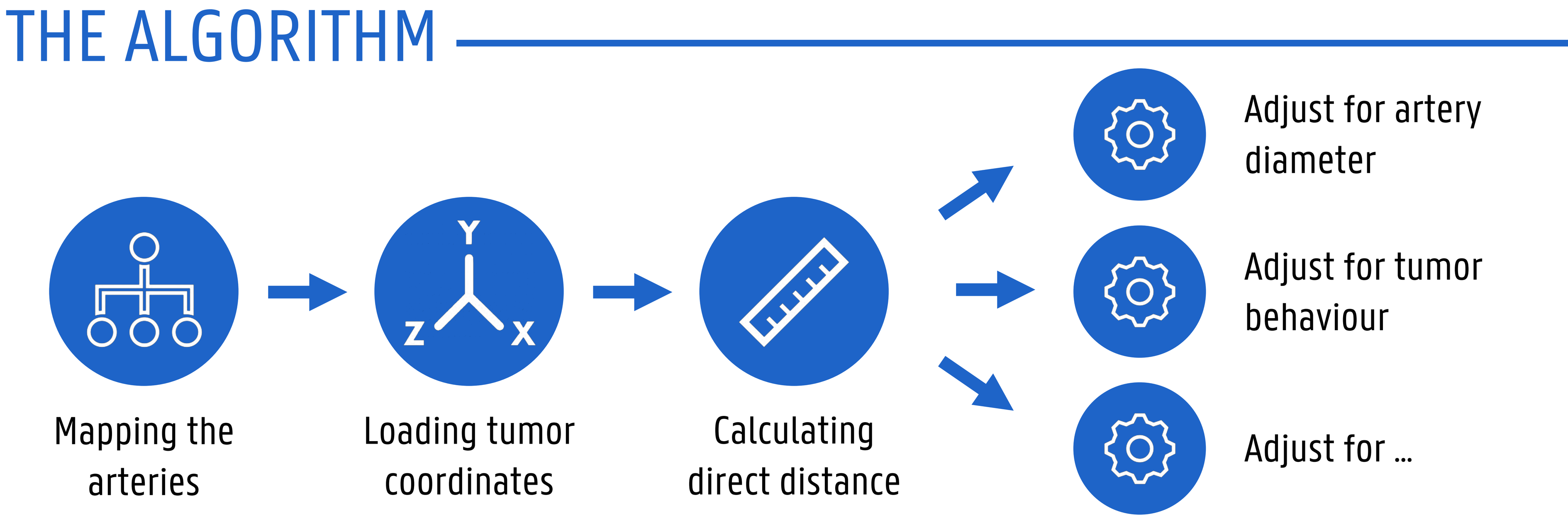


## FIRST RESULTS IN THE OR

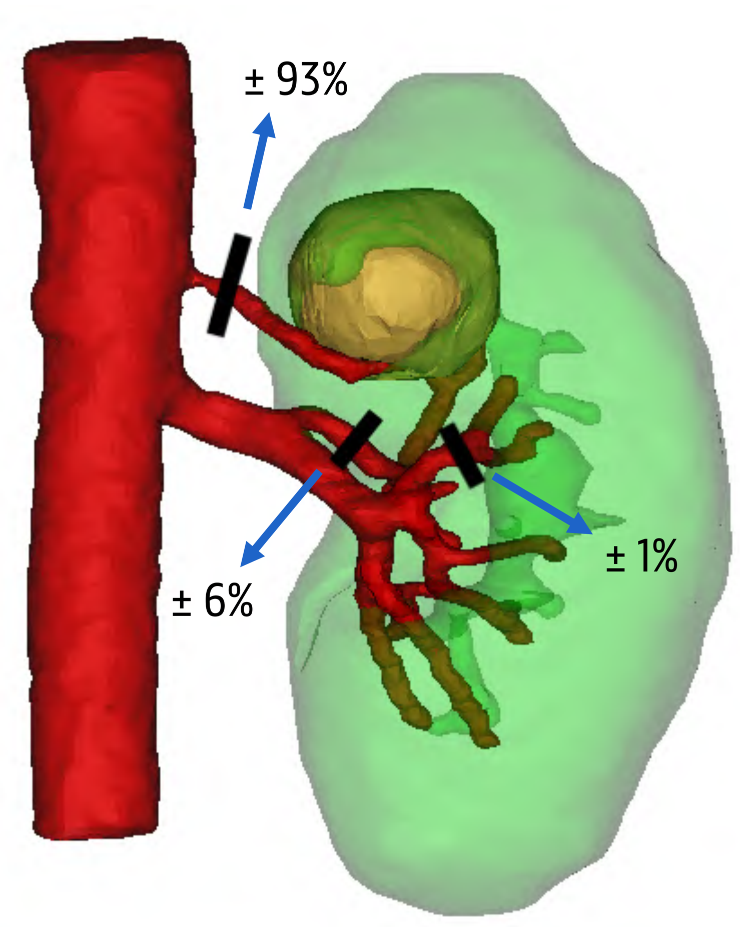


**Case:**
Patient with **renal cell carcinoma** & **polar renal artery** close to tumor

**Planning tool:**
Algorithm predicts tumor perfusion:

- 93% by polar artery
- 7% by two branches of renal hilum

**Robot assisted surgery:**
Decision to clamp only the polar artery & verification by injecting indocyanine green (ICG)
→ **Tumor succesfully ressected with acceptable blood loss**

**Conclusion:**

1) Direct distance calculation is almost accurate
2) Predictions can be optimized by refining the algorithm
3) Further validation is needed before it can be used in clinical practice

## VALIDATION

A **cast** is made by injecting a resin in the arteries of an ex vivo kidney. Scanning this cast with a **micro CT** gives us details from the smallest arteries. With this information, the perfusion zones obtained by the algorithm can be verified.

Injecting a contrast in one renal artery of a **pig's kidney**, will show, by means of a CT scanner, which segment is perfused by that artery. Doing this for each individual renal artery gives the perfusion map that is needed.

Once the kidney tests prove to be valuable, the next step is to repeat these tests with a **human cadaver kidney**. Based on the results of these tests, the algorithm can be refined to be more accurate.

## POSSIBILITIES OF MRI

| CT | MRI |
|---|---|
| + Current protocol<br>Detailed anatomical image | + No radiation<br>Different imaging modalities |
| − High radiation dose | − Poor resolution<br>High cost |

A test scan of healthy kidneys with the MRI arterial spin labeling (ASL) modality. With ASL, the oxygen perfusion can be visualized.


saar.vermijs@ugent.be


Master of Science in Biomedical Engineering

# Design and optimization of 3D printed titanium implants for mandibular reconstruction

**Stavros Chiotakis**

Prof. Wim Van Paepegem, Dr. Manuel da Silva Pinheiro

Mechanics of Materials and Structures, Ghent University, Gent, Belgium

## Mandibular defects and trauma plates

**Types of mandibular defects**

Mandibular defects are commonly caused due to tumor removal surgeries or traumatic injuries and lead to bone detachment or separation. Infections or inflammations can also lead to bone tissue devitalization. Different types of bone defects can include diverse parts of the mandible, like portion of the body, the angle or the ramus[1].

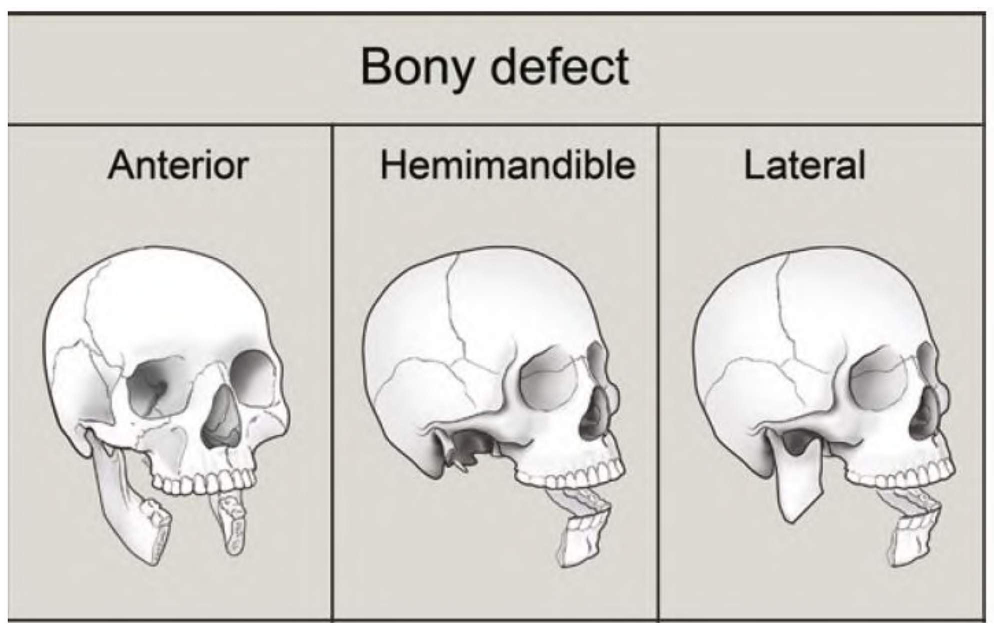


Figure 1: Different types of bone defects. Left picture illustrates a defect to the anterior part of the mandible, in the central figure part of the angle, the body and the ramus is dissected. The right figure illustrates a defect that includes one or two out of the three components (body, angle or ascending ramus) [1].

**Trauma plates in mandibular reconstruction**

Mandibular reconstruction trauma plates, usually made from titanium or stainless steel alloys, can be made conventionally by mass production and in predefined sizes and shapes, or can be 3D printed to provide custom patient benefits.

**Why Mandibular reconstruction plates?**

- Create a bridge across the resection area
- Restore patients masticatory function
- Maintain facial aesthetics
- Immediate functionalization after the surgery
- No post-operative morbidities, that could be caused in the case of fibula flap transplantation.

Figure 2: (left) Metal implants used for mandibular and facial reconstruction[2], (right) typical example of a mandibular metal plate [3].

## 3D printed trauma plates

**3D printed trauma plates offer a wide range of advantages over the conventional manufactured ones**

- 3D printing can provide complex structure implants for general purposes
- Patient specific implants which permanently solve any mismatch problem can be created with 3D printing
- 3D printing can wipe out the dense metal mismatch of stiffness and elastic modulus between implant and bone, by creating porous structures

**Workflow of the 3D printed implant design**

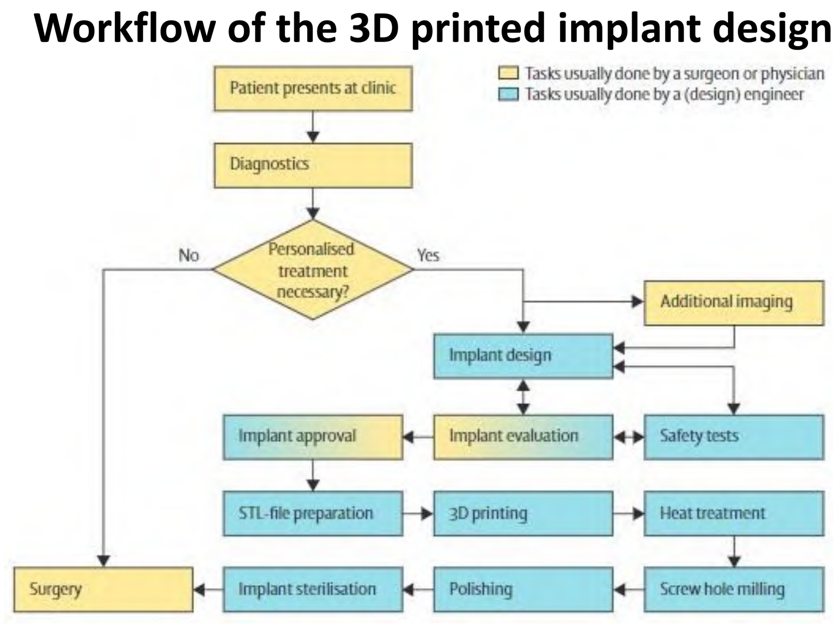


Figure 3: Diagram of the workflow behind the creation of a 3D printed implant as well as the contribution of the doctors and engineers in each step [4].

**Physical properties of biomaterial metals**

| Element / Properties | Aluminium | Magnesium | Titanium |
|---|---|---|---|
| Melting Point C$^0$ | 660 | 650 | 1678 |
| Boiling Point C$^0$ | 2520 | 1090 | 3289 |
| Density g cm$^{-3}$ | 2.700 | 1.740 | 4.512 |
| Elastic Modulus GPa | 70 | 45 | 120 |
| Thermal Conductivity Wm$^{-1}$k$^{-1}$ | 238 | 156 | 26 |
| Hardness HBW | 160 | 44 | 716 |

Figure 4: Table comparing the physical properties between different biomaterials [5].

**Titanium alloys used for 3D printing, offer superior properties to the implants, over other biomaterials, such as:**

- excellent biocompatibility
- Better osseointegration
- High wear and corrosion resistance
- Low compatibility issues
- High strength

**The most common causes where 3D printed may perform inadequately and fail are:**

- Reduced bone properties due to specific diseases and conditions, such as diabetes, osteoporosis and overweight patients
- Poor implant design
- Inaccurate manufacturing process
- Loosening or misplacement of the fixation screws

**Possible complications that may occur from implant failure:**

- Inability of the patient to masticate
- Facial deformations due to the lack of support from the affected side
- Soft tissue damage

## Thesis project in a glance

For this project, the data of a patient who underwent surgery due to mandible tumor and replaced the bone with a 3D printed titanium plate are used. 3D models of the skull and mandible were created from the CT data. With the help of a finite element simulations software, the conditions that need to be met for the implant to be fractured will be recreated and based on the results, an implant optimization will follow, in order to make it unbreakable in under any circumstances.

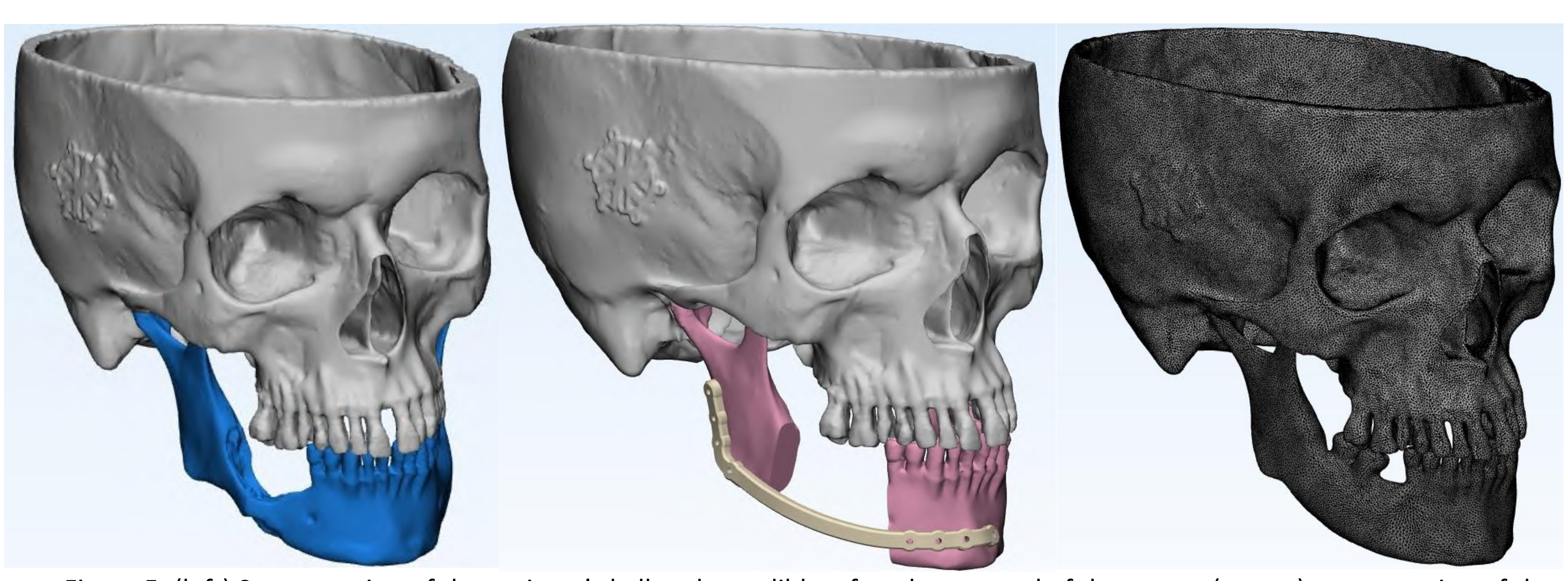

Figure 5: (left) Segmentation of the patients' skull and mandible, after the removal of the tumor, (center) segmentation of the skull and mandible with the implanted titanium plate, (right) mesh of the skull and mandible of a non-pathological subject.

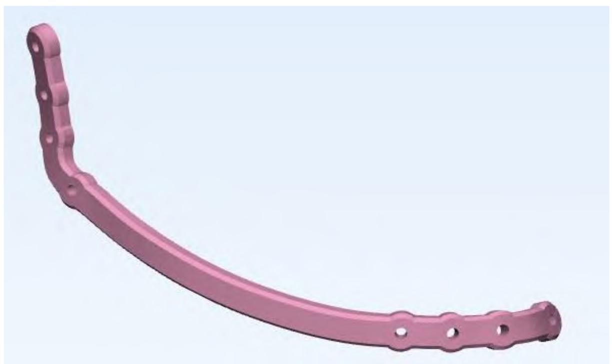

Figure 6: 3D Model of the titanium trauma plate

**The workload of the project, separated into parts:**

1. Segmentation of patients craniofacial anatomy from CT image data
2. Assignment of the appropriate material properties
3. Definition of muscle anatomy and bite forces
4. Validation of the boundary conditions (of the non-pathological model)
5. Meshing and FE analysis of the model with the titanium plate implanted
6. Recreate the implant fracture conditions in FE simulations, using the patients' 3D model and implant
7. Assessment of implant safety factors against fatigue failure
8. Implant improvement, topology and shape optimization

## Goals and future insights

1. The understanding of the biomechanics behind the loads during mastication on the titanium implants
2. Optimization of the implant in a manner that will render it unbreakable from any possible applied load patterns
3. Provide guidelines for improved 3D printing of titanium implants for future manufacturers

## References

1. Atlas of mandibular and maxillary reconstruction with the fibula flap, Giorgo De Santis et. al, 2019
2. Manual of operative maxillofacial trauma surgery, Michael Perry, Simon Holmes, 2014
3. Customized mandibular reconstruction plates improve mechanical performance in a mandibular reconstruction model, R. Gutwald et. al, 2016
4. Challenges on the design and regulatory approval of 3D-printed surgical implants: a 2 case series, K. Willemsen et. al, 2019
5. Titanium in biomedical Applications-Properties and Fabrication: a Review, A. Khorasani et. al, 2015

Stavros.chiotakis@ugent.be

Master of Science in Biomedical Engineering

# Development of a computational biomechanical framework to model the TEVAR treatment in type B aortic dissections

**Tjorben Billiet**

Prof. dr. ir. Patrick Segers, Prof. dr. ir. Nele Famaey

ir. Lise Gheysen, ir. Gerlinde Logghe

IBiTech-bioMMeda, Ghent University, Gent, Belgium

GHENT UNIVERSITY

VUB VRIJE UNIVERSITEIT BRUSSEL

## Background and objectives

### Type B aortic dissection

The aortic wall is composed out of three layers: the intima, the media and the adventitia. When there is a tear in the intima, blood can flow from the aortic lumen through this tear forcing the layers apart and creating a second channel within the wall (false lumen). This is illustrated in figure 1.

Type B suggests that only the descending part of the aorta is involved.

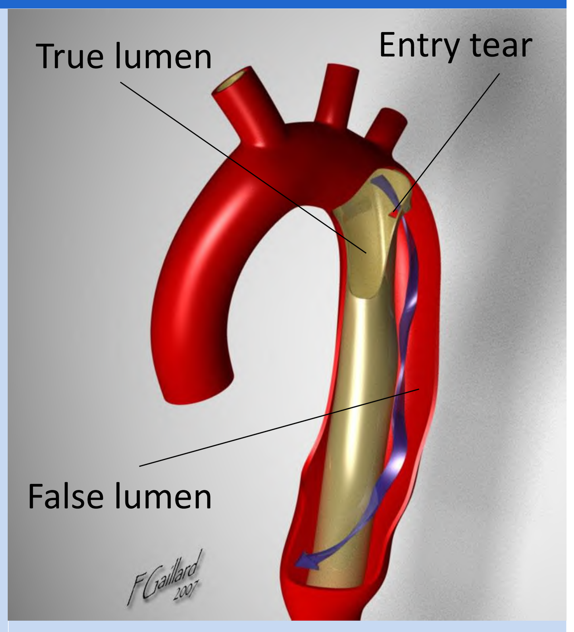


Figure 1 : Type B aortic dissection (Frank Gaillard, 2019)

### Thoracic Endovascular Aortic Repair (TEVAR)

In TEVAR, a stent-graft is inserted in the aorta at the site of the aortic dissection (as can be seen in figure 2).

The goal is to stop the flow in the false lumen, by sealing of the entry tear, resulting in clot formation of the blood inside the false lumen.

When the blood has clotted in the false lumen, the aorta can start to remodel.

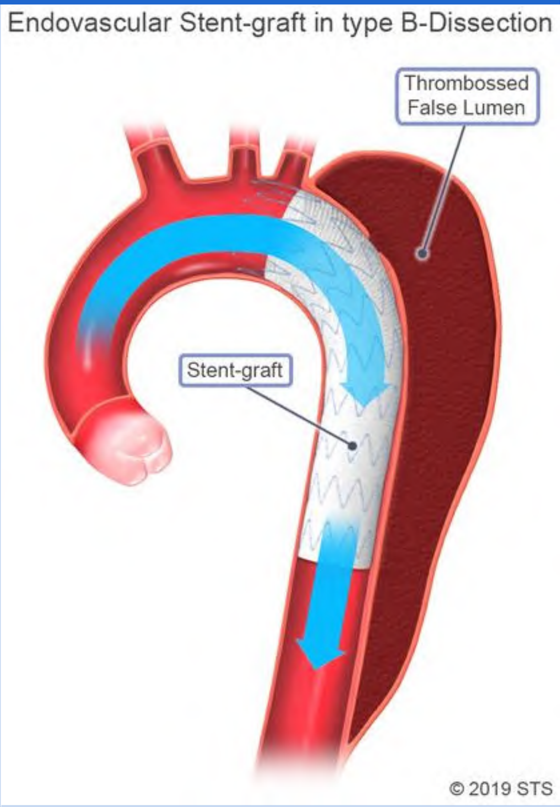


Figure 2: TEVAR (STS, 2019)

### Objectives

In a substantial amount of patients (29 %), however, TEVAR does not stop the progression of the disease, and the aorta continues to dilate posing a severe risk of rupture and death of the patient.

Another frequent (41 %) issue after TEVAR are endoleaks. (GEISBÜSCH, Philipp, et al., 2011)

Up to now, it is unclear which patients will benefit from the TEVAR treatment. Therefore, patient-specific computational models, able to predict the acute and longterm effect of the TEVAR procedure, could provide a large added value in the clinical decision process.

As a part of this longterm goal, it is the aim of this study to develop a computational model able to accurately mimic the TEVAR procedure.

## Methodology

### Stent-graft FE model

- Fully parametric model based on commercially available stent-grafts, used to treat type B aortic dissection in clinical practice
- Self-expanding stent-graft using Nitinol material properties
- Meshing using beam and solid elements, enabling to compare the result of both element types

Figure 3 : Parametric stent ring

### TEVAR procedure

The complete insertion process will be modeled :

1. Crimping of the stent-graft
2. Inserting the stent in the aorta (for aorta models with a curved centerline)
3. Expansion of the stent-graft in the aorta (with isotropic hyperelastic material properties)

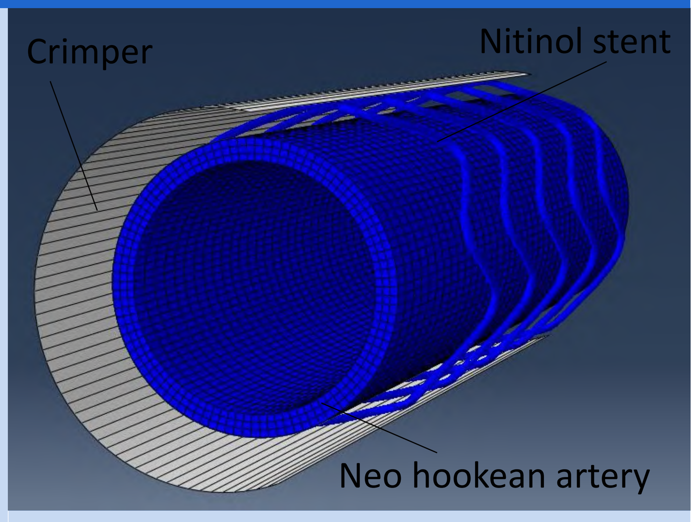


Figure 4: Set-up of the model

## Results

### Preliminary results

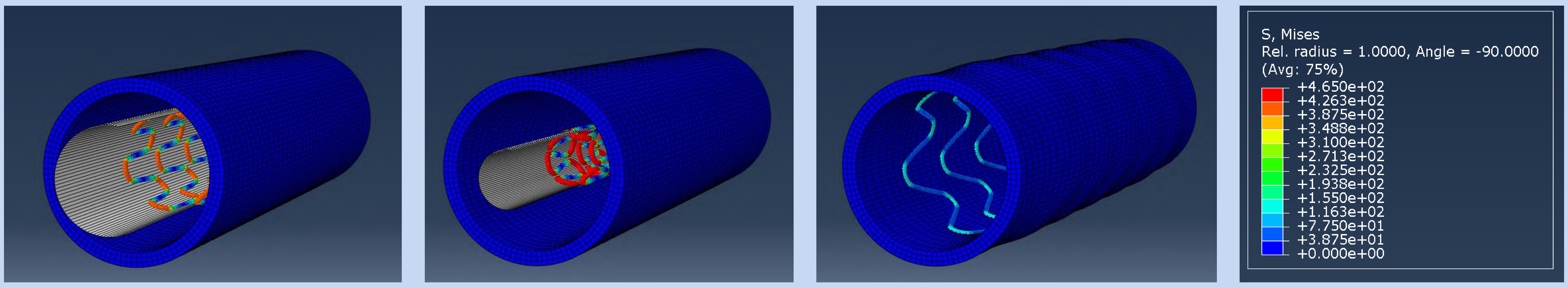


Figure 5: Von Mises stress of the stent during crimping (left), at the end of crimping (middle) and at the end of self-expansion (right) [MPa]

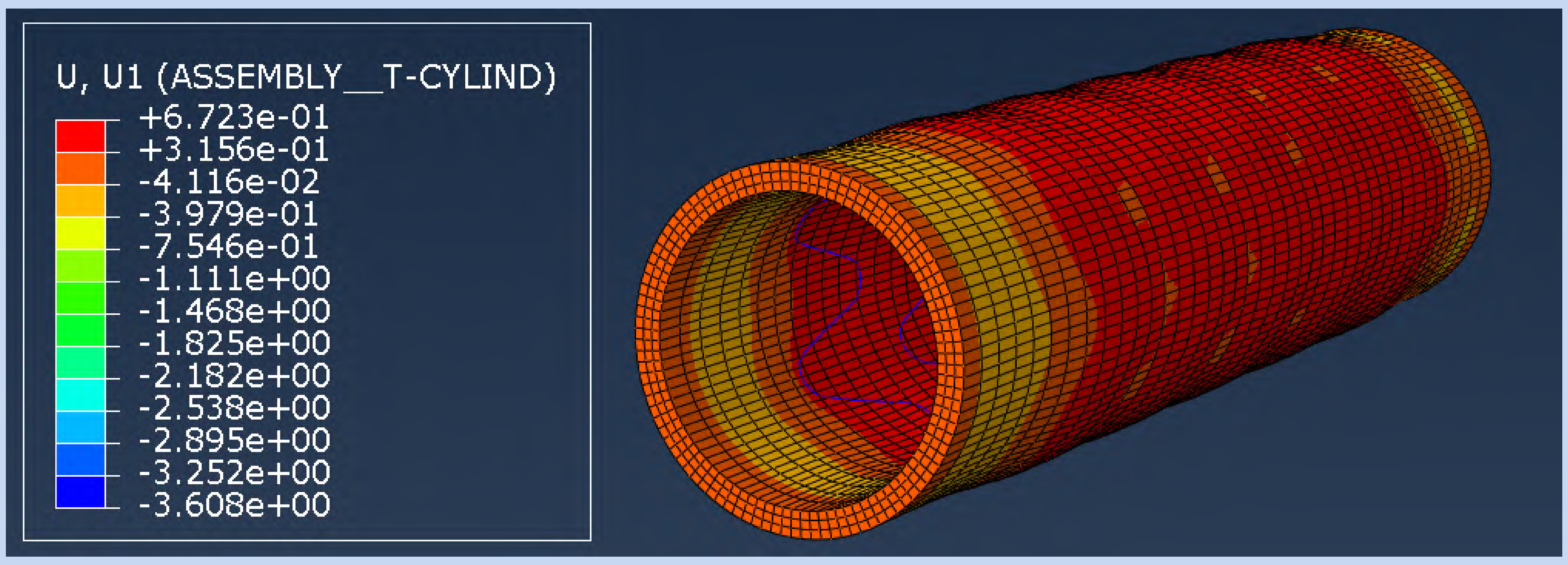


Figure 6: Radial displacements of the artery at the end of self-expansion [mm]

## Limitations and future work

### Towards a patient-inspired model

To get towards a more realistic model, the following changes will be made to the model above:

- Add graft material connecting the individual rings by using connector elements with a certain elasticity
- Add a patient-inspired curvature to get closer to a more realistic geometry
- Compare different element types based on accuracy and computational time

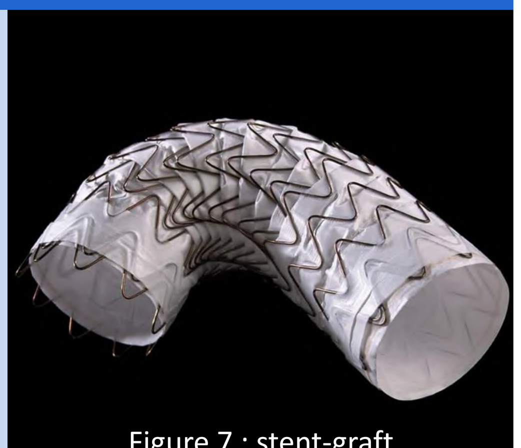

Figure 7 : stent-graft (Gore medical, 2020)

### Validation

In order to validate the model, crimping of a stent-graft will be performed, after which the stent-graft will be placed in a micro-CT.

Afterwards, this stent-graft will be deployed in a simple curved silicone model and placed again under the micro-CT.

The results of the computational method will be compared to the experimental results.

Tjorben.Billiet@UGent.be

Master of Science in Biomedical Engineering

# Effect of anti-epileptic drugs on functional brain connections

GHENT UNIVERSITY

**Wout Vanhenden**

Prof. dr. ir. Pieter van Mierlo, dr. ir. Gregor Strobbe and ir. Gert Vanhollebeke

IBiTech-bioMMeda, Ghent University, Ghent, Belgium
Epilog, Ghent, Belgium

VUB VRIJE UNIVERSITEIT BRUSSEL

## Anti-epileptic drug (AED) treatment

1% of the population is epileptic
Anti-epileptic drugs (AEDs) form the first-line treatment
2/3 of the patients become seizure-free thanks to AEDs

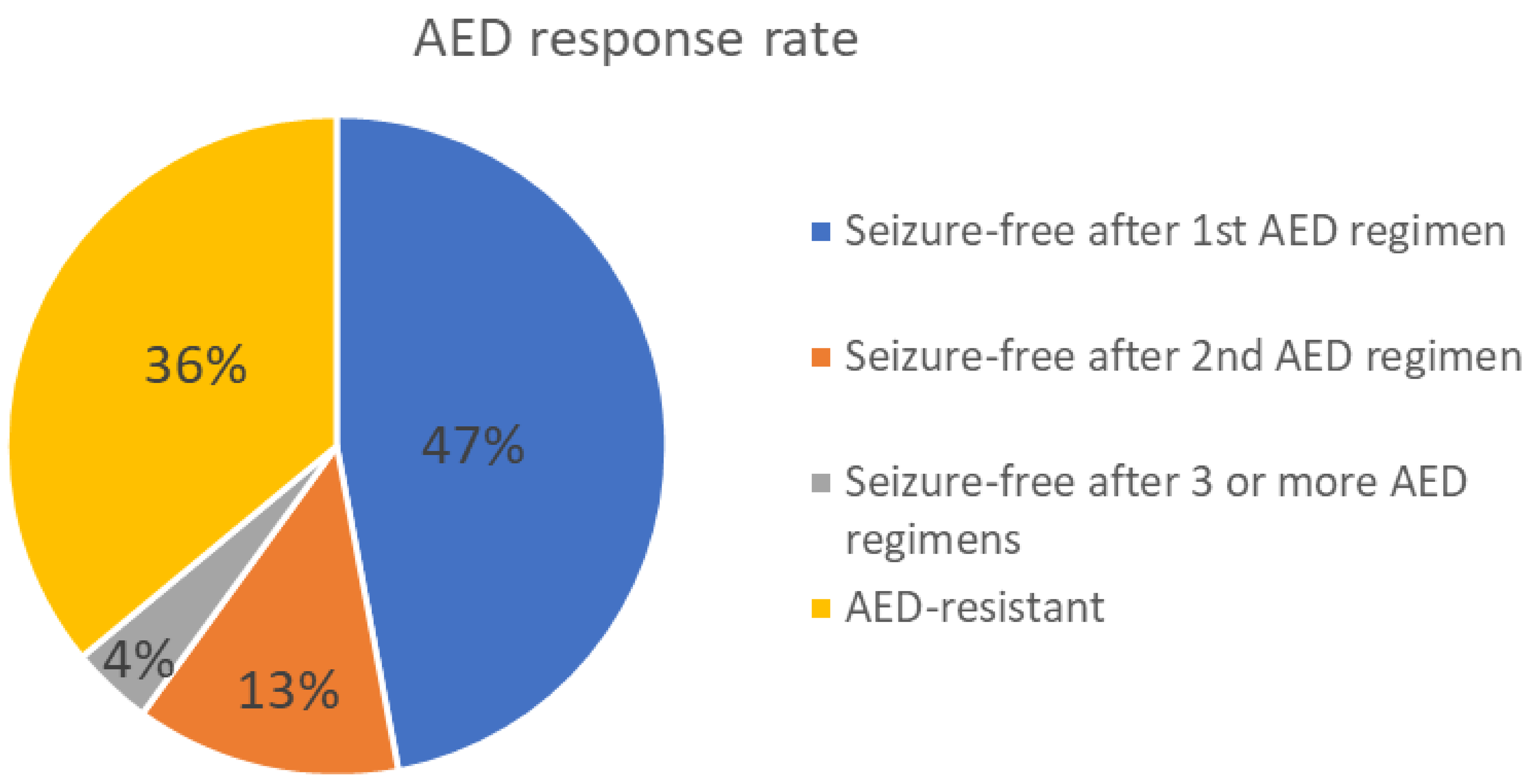


### Problem

Establishing the right AED treatment for a specific patient is a process of trial and error which can take years

### Possible solution

Features derived from routine EEG predict if a specific patient will respond to a certain AED

### Hypothesis of thesis

A short EEG-recording before and after AED (brivaracetam) administration can distinguish AED responders from non-responders

## Workflow

**Raw EEG**

50 patients from 2 different institutes

Pre- and post-AED (brivaracetam) EEG

31 non-responders

19 responders

→

**Pre-processing**

Select 20min EEG (awake)

Remove eye blink artefacts with independent component analysis

Band-pass filter [1Hz,70Hz]

Band-stop filter 50Hz

Amplitude filter [-85µV,85µV]

Divide in epochs of 3s

→

**Patient details**

Gender, age, amount of AEDs tried and levetiracetam (AED similar to brivaracetam) intake in the past

**Spectral analysis**

Mean Frequency: spectrum, δ, θ, α, β and ϒ

Spectral power fraction: δ, θ, α, β and ϒ

**Functional connectivity analysis**

Mutual information

→ **Feature selection** → **Machine learning**

## Spectral analysis

| AED = brivaracetam | | Non-responders | | Responders | |
|---|---|---|---|---|---|
| | | Pre-AED | Post-AED | Pre-AED | Post-AED |
| Mean frequency (Hz) | Spectrum [0Hz,35Hz] | 17.29 | 17.12 | 17.05 | 16.98 |
| | δ [0Hz,4Hz] | 3.07 | 3.05 | 3.11 | 3.09 |
| | θ [4Hz,8Hz] | 6.48 | 6.49 | 6.46 | 6.46 |
| | α [8Hz,14Hz] | 10.71 | 10.71 | 10.65 | 10.73 |
| | β [14Hz,30Hz] | 21.42 | 21.39 | 21.34 | 21.28 |
| | ϒ [30Hz,35Hz] | 32.48 | 32.51 | 32.43 | 32.46 |
| Power fraction | δ [0Hz,4Hz] | 0.02 | 0.02 | 0.02 | 0.02 |
| | θ [4Hz,8Hz] | 0.18 | 0.18 | 0.20 | 0.19 |
| | α [8Hz,14Hz] | 0.25 | 0.26 | 0.26 | 0.26 |
| | β [14Hz,30Hz] | 0.42 | 0.42 | 0.38 | 0.41 |
| | ϒ [30Hz,35Hz] | 0.13 | 0.12 | 0.14 | 0.12 |

Mean α frequency increases in responders after AED intake (p=0,14)

β power fraction increases in responders after AED intake (p=0,13)

Responders have a lower β power fraction than non-responders before AED intake (p=0,07)

## Functional connectivity analysis

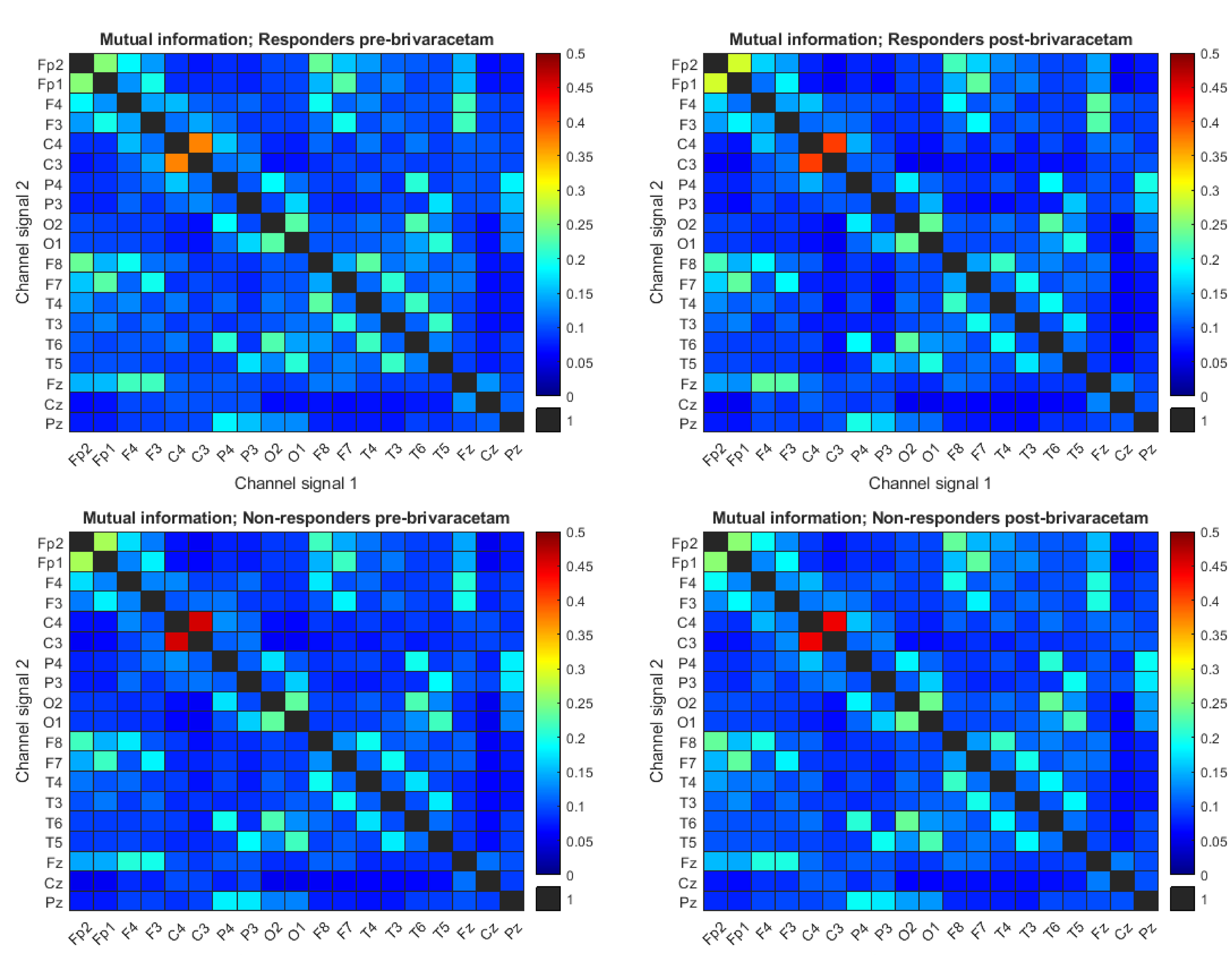


There are (small) differences in mutual information

- Between responders and non-responders
- Before and after AED intake

wout.vanhenden@ugent.be

Master of Science in Biomedical Engineering

# Construction of a conventional 12 lead ECG from a single self-recorded 3-lead RELF ECG

**Divya Joseph**

Prof. Peter Gheeraert, Prof. Patrick Segers

Department of Cardiology
Ghent University Hospital, Gent, Belgium

## INTRDUCTION and AIM

The time delay between onset of symptoms and seeking medical attendance is a major determinant of mortality and morbidity in patients with acute coronary artery occlusion. Response time might be reduced by reliable self detection with the RELF method[1]

We aim to reconstruct the 12- lead ECG from self recordings with the RELF device and validate the reconstruction by

- Face validation by experts
- Correlation coefficient & Root Mean Square Distance method

Ref: image- https://medium.com/researchfeatures/explaining-the-unexplained-the-link-between-panic-and-non-cardiac-chest-pain-8cbb5154b792, [1] Feasibility and performance of a device for automatic self-detection of symptomatic acute coronary artery occlusion in outpatients with coronary artery disease: a multicentre observational study, *Frederic Van Heuverswyn, Marc De Buyzere, Mathieu Coeman, Jan De Pooter, Benny Drieghe, Mattias Duytschaever, Sofie Gevaert, Peter Kayaert, Yves Vandekerckhove, Joeri Voet, Milad El Haddad, Peter Gheeraert, Lancet Digital Health* 2019; 1: e90–99

## METHODS (and expected results)

**Method part 1:** Reconstruction of 12 lead ECG from a 3 lead RELF recording

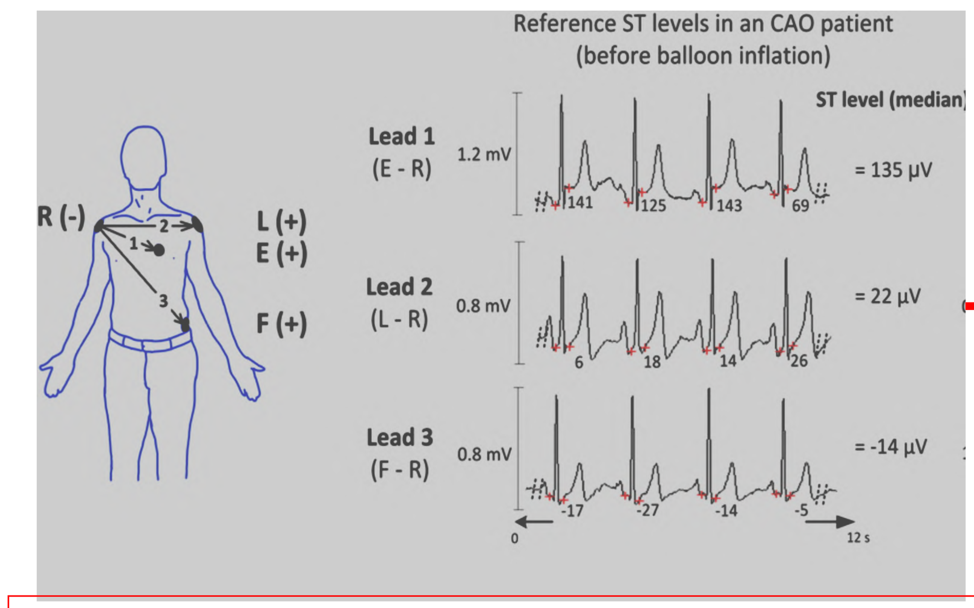


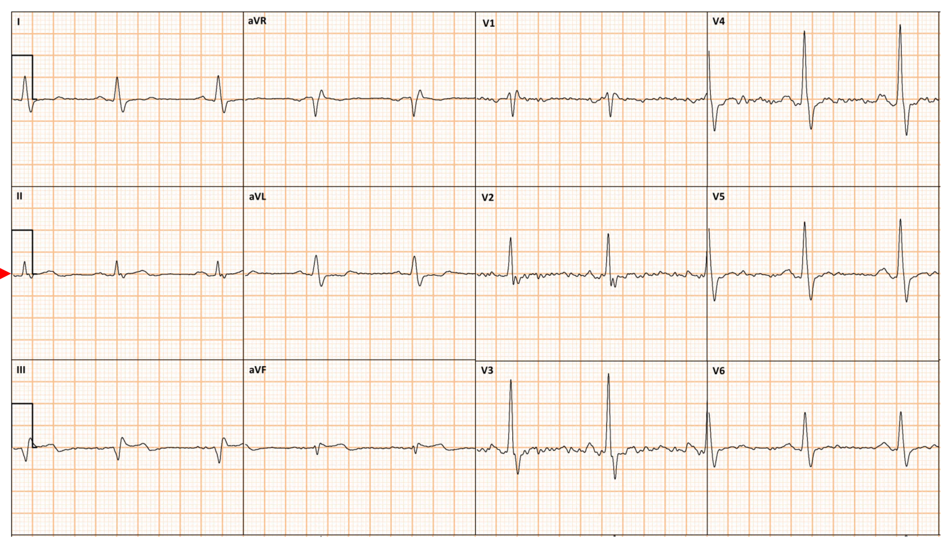

We used lead vectors for the reconstruction of the 12 lead ECG and derived three independent variables in horizontal (x), vertical (y) and sagittal (z) plane. Hence by linearity assumption the dipole $\hat{p}$ can be resolved into three orthogonal components

$$\hat{p} = px\hat{\imath} + py\hat{\jmath} + pz\hat{k}$$

Using the principle of superposition potential at the point $Q$ caused by the dipole $\bar{p}$ at the origin of the coordinate system is

$$\phi_Q = cxpx + cypy + czpz$$

$$\therefore \phi_Q = \hat{c} \cdot \hat{p}$$

Einthoven defined the potential differences between the three pairs of these three points to constitute the fundamental lead voltages in ECG. Thus the potential difference between any two points $p_i$ *and* $p_j$ *is*

$$V_{ij} = \phi_i - \phi_j$$

$$\therefore \quad V_I = \phi_L - \phi_R = \hat{c}_L \cdot \hat{p} - \hat{c}_R \cdot \hat{p} = (\hat{c}_L - \hat{c}_R) \cdot \hat{p} = \hat{c} \cdot \hat{p}_I$$

$$V_{II} = \phi_F - \phi_R = \hat{c}_F \cdot \hat{p} - \hat{c}_R \cdot \hat{p} = (\hat{c}_F - \hat{c}_R) \cdot \hat{p} = \hat{c} \cdot \hat{p}_{II}$$

$$V_{III} = \phi_F - \phi_L = \hat{c}_F \cdot \hat{p} - \hat{c}_L \cdot \hat{p} = (\hat{c}_F - \hat{c}_L) \cdot \hat{p} = \hat{c} \cdot \hat{p}_{III}$$

**Method part 2:** Validation reconstructed 12-lead ECG by testing the of diagnostic accuracy of for detection of acute coronary artery occlusion

60 patients with coronary artery disease and planned coronary angioplasty

↓

Before acute coronary occlusion: simultaneous test A and test B → (60 s coronary balloon occlusion) → During acute coronary occlusion: simultaneous test A and test B

Before acute coronary occlusion:

| | | Test A* Pos | Test A* Neg |
|---|---|---|---|
| Test B** | Pos | N = … | N = … |
| | Neg | N = … | N = … |

During acute coronary occlusion:

| | | Test A* Pos | Test A* Neg |
|---|---|---|---|
| Test B** | Pos | N = … | N = … |
| | Neg | N = … | N = … |

Hypothesis: test A and B have equal sensitivity and specificity for detection of acute coronary artery occlusion

* Test A : standard 12-lead ECG : ST elevation criteria: pos or neg

**Test B : 12-lead ECG constructed from 3-lead RELF device: ST elevation criteria: pos or neg

divya.joseph@ugent.be

# Application of Optical Surface Monitoring (OSM) in Image-Guided Radiotherapy (IGRT)

GHENT UNIVERSITY

**Ahmed Taieb Mokaddem**, Ir. Jennifer Dhont,
Prof.Dr.Ir. Jef Vandemeulebroucke, Prof.Dr. Dirk Verellen

VUB VRIJE UNIVERSITEIT BRUSSEL

ETRO, VUB, Brussels, Belgium
GZA, Antwerp, Belgium

## Introduction

Prostate motion during RT includes translation, …, in the order of … cm. To decrease geometrical treatment uncertainty, real-time monitoring using fiducial markers is routinely used.

## Purpose of Thesis

To evaluate if implanted fiducial markers (FM) in prostate can be replaced by non-invasive optical surface monitoring (OSM).

## Optical surface monitoring

- **Non-radiographic**, **non-invasive**, **continuous tracking** of patient surface.
- **Six degrees of freedom** ( 3 translation; 3 rotation)
- **Three main application areas:** inter-fraction setup, monitoring of intra-fraction motion and gating with breath-hold.
- **3D surface topography:** use of HD cameras.
- **Not representative** for accurate tumor positioning, tracks only the patient surface.

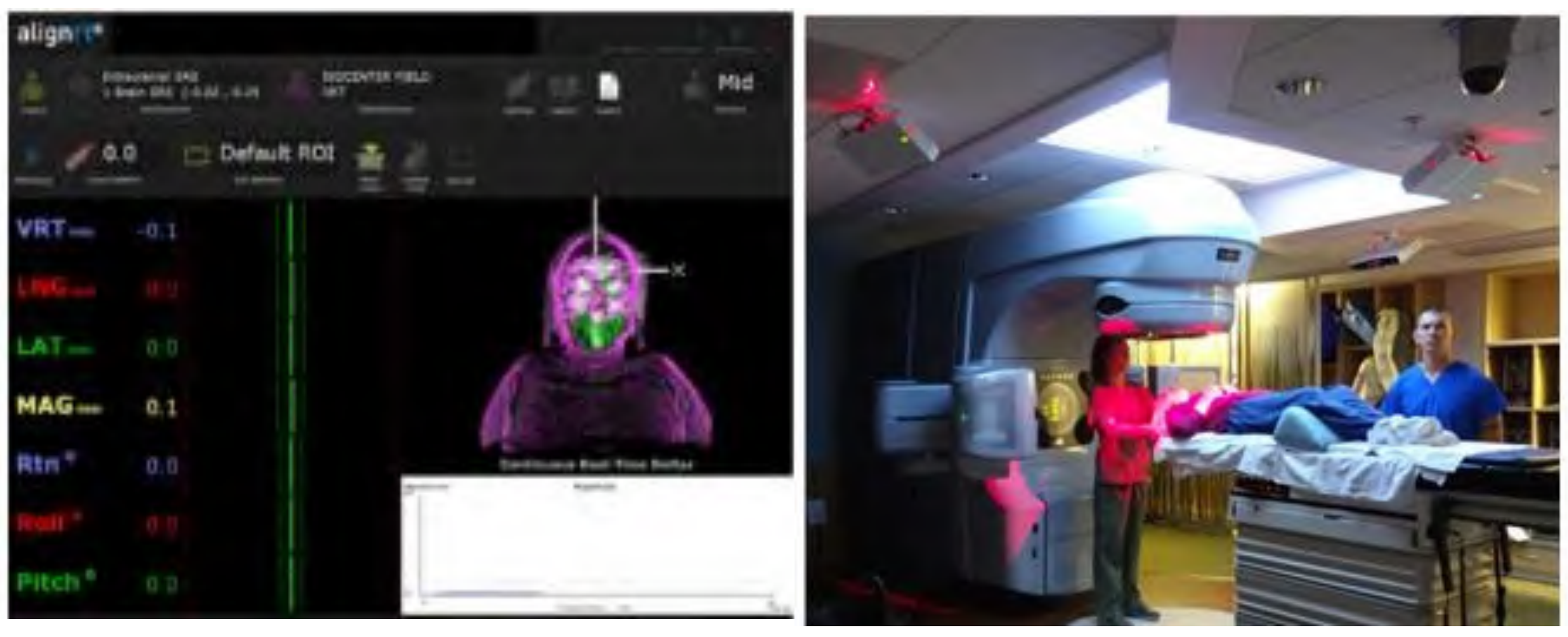

**Figure 1 (A)** AlignRT user interface showing reference surface (magenta) and live surface (green), along with displacements in 6 degrees of freedom and RMS magnitude displacement **(B)** in-room setup of AlignRT with ceiling-mounted cameras and light sources, and light projected onto the patient.

## Implanted fiducial markers

- **Real-time tracking of tumor** used for intra-fraction motion monitoring.
- Implanted in the prostate for **accurate patient positioning.**
- Markers must be **segmented automatically in real-time**, which is more difficult in **MV images** that have inherently **lower contrast** than **kV images.**
- FMs act as **surrogate** for the **tumor position, not the actual prostate**
- To avoid the **risk, cost, and uncertainty** related to the use of FMs, **markerless monitoring** (SGRT) are used.


**Figure 2.** Examples of FM. (a) 3 mm-long gold markers (civco, diameter between 0.8 and 1.2 mm) (top) can be implanted in any soft tissue (middle) for image guidance. The similar 5 × 1 mm CyberMark™ was developed specifically for use with CyberKnife® (bottom) (civco Radiotherapy, Coralville, IA)

## Signal analysis and comparison

- **Data:**
  2D kV images of FMs from minimal 5 patients:
  - Angle of 2D kV images
  - Frequency of images per data

  OSM Realtime data from minimal 5 patients:
  - Three translation positions (Lat, Vert, Long)
  - Three rotational positions (Pitch, Roll, Rot)
  - Root mean square

- **Method:**
  *Fiducial markers:*
  - Threshold Tracking of FMs.
  - Correct the images taken at a different angle to a reference angle.
  - For each image, estimate the mean position.
  - Create motion signal from the mean positions.

  *Optical Surface Monitoring:*
  - Create motion signal from Realtime data.

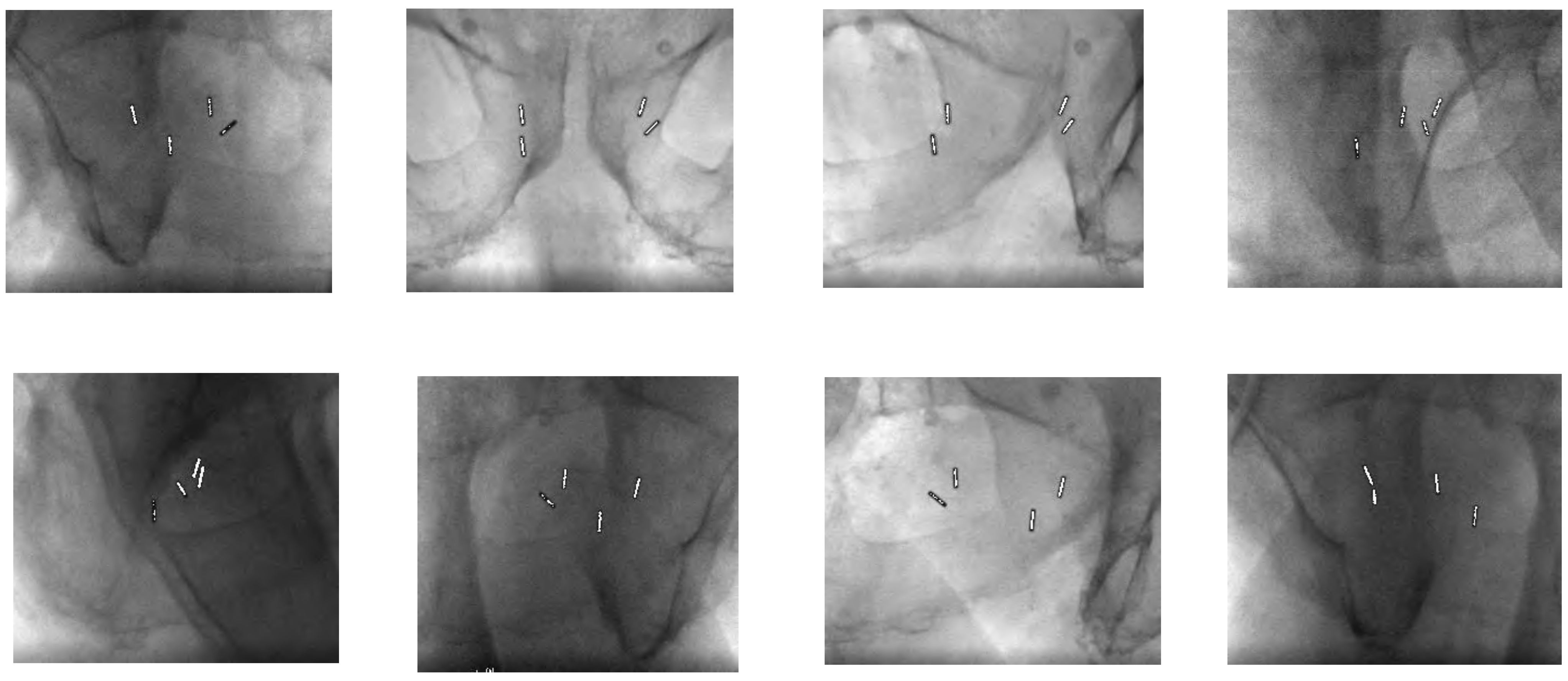

**Figure 3:** Treshold tracking of fiducial markers (in prostate cancer) based on Grayvalues

### Future work along the way:

Motion signal from Fiducial Markers → Comparing and analysing both signals
Motion signal from Surface Guidance → Comparing and analysing both signals

## References

Jeremy DP Hoisak and Todd Pawlicki. The role of optical surface imaging systems in radiation therapy". In: Seminars in radiation oncology. Vol. 28. 3. Elsevier. 2018, pp. 185- 193.
Jenny Bertholet et al. "Real-time intrafraction motion monitoring in external beam radiotherapy". In:Physics in Medicine & Biology64.15 (2019),15TR01.